EFFECT OF SOLAR RADIATION ON CETACEANS

Laura-Maria Madeleine Martinez

School of Biological and Chemical Sciences, Queen Mary University of London

&

Institute of Zoology, Zoological Society of London

A thesis submitted for the degree of doctor of philosophy at Queen Mary University of London

July 2011

Statement of originality

I certify that this dissertation is the result of my own research. Results obtained through collaboration are specifically indicated in the text. Samples were collected under permits SGPA/DGVS/00506/08, SGPA/DGVS/09760/08 and SGPA/DGVS/08021/06 issued by SEMARNAT. The total length of this dissertation does not exceed 100,000 words.

Acknowledgments

Lots of people have been part of this PhD adventure and in the following paragraphs I will try to thank as many tutors, collaborators, friends, family members and colleagues as possible.

I need to thank first two exceptional women, **Esther** and **Karina**, who made all this possible. Karina chose me to be part of her innovating and sexy "UV and whales" project, and my mother gave me the wings to jump without doubt and fear in that adventure.

I thank **Karina Acevedo-Whitehouse**, for being a SUPERvisor! *Gracias* for all your dedicated support, for pushing me to develop my own ideas, for always being available and ready for hours of meetings and for giving me my *"mini monstruo"* nickname. *Tu espíritu revolucionario y tu "nada es imposible" hacen parte de las armas que me trasmitiste para seguir en la investigación!*

I thank **Rob Knell**, my Queen Mary University supervisor, for his direction and support all along the thesis, for his valuable comments on the thesis' chapters and, above, all for his precious statistical guidance, *which ended up transforming me into an "R geek"*. For other statistical advices or "R tips", given during meetings, in pubs or during breakfast, I need to thank **Guillaume**, my housemate and friend; **Paddy**, my little PhD brother; **Daria**, my twin and officemate; and also **Nathalie, Marcus, Harry, Ben, Alienor, Aysiah, Thibault** and again, **Karina**. For their comments and encouragements, I thank my panel members **Caroline Brennan** and **Chris Faulkes**, and my IoZ co-supervisor **Alex Rogers**.

I thank **Diana Gendron**, the head of the Marine Mammal Ecology Laboratory of CICIMAR-IPN of La Paz in Baja California, Mexico, for introducing me to the fabulous world of whales and teaching me how to work with these giants of the oceans. *Gracias por tu confianza y tu ayuda durante esta fantástica aventura*

ballenera! BIG THANKS to the captains **Ciro Arista** (*alias "Ciruela" un gran capitán y cocinero*), **Manuel Zamarrón** y **Javier Álvarez**. Thanks to my whale fieldwork tutors **Cristian Ortega** *(y gracias por tu gran ayuda con la medición de ballenas)* **y Raúl Diaz** and to all who participated with the collection of data and samples: comrades **Fabiola Guerrero, Agnes Rocha, Marisol Rueda, Cristina Pinedo, Paula Costa, Natalia Espino, Geraldine Busquets** *(gracias por compartir tus datos de isotopos)***, Azucena Ugalde, Mario Pardo, Malie Lessard-Therrien, Edith Bertthiaume and Tiffany**. I thank **Azucena** for her help with the photoidentification of the whales. I also thank the Chemical laboratory technicians: **Silverio** and **Sonia**, and **Bárbara González-Acosta**, for offering advice and materials to set up the "Comet Assay" in the Marine Mammal Ecology Laboratory. Thanks to **Zamarrón** for setting up the dark room and finally, thanks to **Karina** for her great "vortex" idea.

I thank **Omar Garcia** for inviting me for a two week externship in the Laboratory of Radiobiology of the Centre for Radiation Protection and Hygiene (CPHR) of La Havana, Cuba. Big thanks to my "Comet Assay" tutor and my friend **Jorge Ernesto Gonzalez**. Thanks to all the CPHR lab members for being so amazingly friendly to me. And thanks to "**Pichon**" for sharing his house and CUBAN life with me. *Que fabuloso recuerdo este viaje a CUBA!*

I thank **Prof. Edel'O'Toole** and **Dr. Manuraj Singh** from the Centre for Cutaneous Research, Blizard Institute of Cell and Molecular Science (ICMS), Queen Mary University of London for their interest in collaborating with us in this project and for teaching me to run special skin-section stainings in the amazing laboratories of the ICMS. I thank **Prof. Mark Birch-Machin** and **Amy Bowman** from the Institute of cellular medicine of Newcastle University, who ran assays to detect and quantify UV-induced mitochondrial DNA damage. I thank **Prof. Rino Cerio** from the Institute of Pathology, Royal London Hospital, for the PAS/DPAS staining. I thank the **Molecular Genetics Laboratory of CICESE in Ensenada**, Mexico, who determined the sex of the blue whales sampled. I thank **Dr. Barbara Blacklaws** from Cambridge Infectious Disease Consortium, University of Cambridge, for running the pan-poxvirus PCR assays. I thank **Elizabeth Weatherhead**, **Paul**

Newman and **Eric Nash**, for the two graphs that showed total ozone and UV index over the Gulf of California between 2007 and 2009 (Chapter two, Fig. 2.6 and Fig. 2.7, respectively). I thank **Hal Whitehead** and **Manolo Alvarez-Torez** for inviting me on the field research vessel "*Balaena"* for a 10-day expedition in the middle of the Gulf of California, around San Pedro Martir, to work with the majestic sperm whales.

Thanks to **all IoZ members (Daria, Gabby, Judith, Janie, Frankie, Kate, Freya, Pete, Emma, Rebecca, Trenton_**thanks so much for sending me the bear attack records of the last six months, a wonderful first approach of Canada_**John**, etc without forgetting the Nuffield team with **Patricia, Nathalie, Alana and Ben, Amrit, Dave, Jo** etc etc etc), who through meetings or around beers, improved the project and helped shape the warm atmosphere in the Institute of Zoology, an ideal place to enter the world of investigation. Special thanks to **Matt** and **Belinda** (thanks to both of you for always being available for any lab issue and above all for teaching me unforgettable English songs). For other general lab advice, thanks to **Dada, Kate, Solenn, Amanda** (and her magic Trypsine) **and Rob** (*"la nutria gigante"*). BIG THANKS to **John**, **Kyunglee** and **Andres** for helping me with the melanocyte counts and DNA extractions. THANKS to **Kate, Solenn, Serian** and **Bill,** for the very useful "gene expression and Next Generation Sequencing" meetings. Thanks to **Paul Jepson** and **Rob Deaville** for offering me some porpoise skin tissue used for technique standardization. Special thanks to **Jim** and **Bill** who ran the Social Club, the ideal place to enjoy the great ZSL atmosphere.

And for following with great attention my adventures and for being the best anti-stress, I thank so much **my family and friends**. *Spécial merci à mon **JPapaLoutre** pour son éternelle curiosité et la porte ouverte de son petit coin de paradis Normand (où l'écriture de cette thèse fut un régal).* BIG THANK *a la banda Peruana de Londres, por aceptarme en su familia latina: **Ursula, Lucia, Caro, Jano** y **Edwin**. Gracias a mi familia adoptiva Mexicana, especialmente a mis hermanas Doris: **Agnes** (Super Doris o Gnegne), **Deni** (Doris-Deny) and **Clarissa** (Doris Mayor).* BIG THANK to ***ADRIAN** y su mama por alojarme a cada uno de mis viajes en la ciudad*

de México. Thanks to **my QMUL friends** (in particular **Helene**), who also survived the PhD journey. Thanks to **Siân** and **Charles** for inviting me to their lovely little cottage in Hereford, where I completed this thesis. *SUPER GRACIAS to my "**English Otter**", who transformed the last six months of my PhD into a joyful experience.* Thanks for all your advice and comments during this long process of writing up.

Finally, I thank my source of fundings: NERC (Studentship: NE/F00818X/1), IPN (Instituto Politecnico National de Mexico), CONACYT (CB-2006-61982), the Institute of Zoology (my case partner) and my mother, Esther. *Siempre conmigo ! Eres mi luz !*

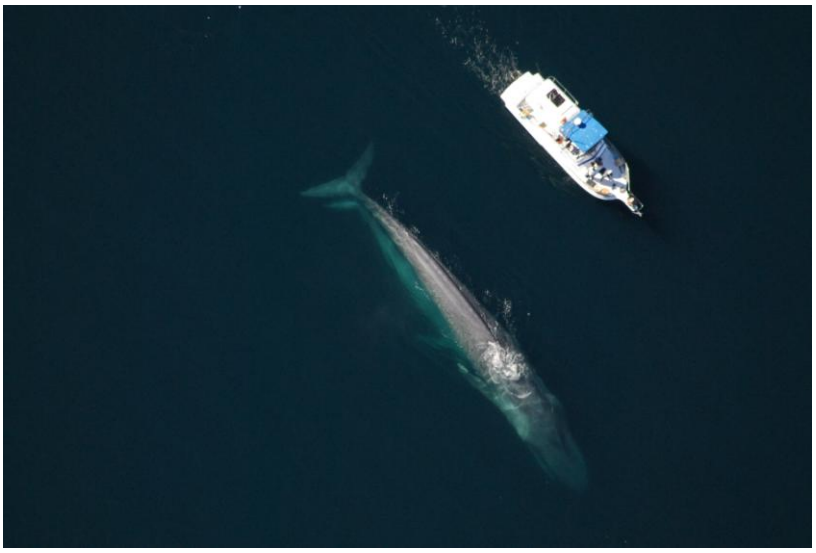

Abstract

Despite the marked deceleration in the amount of ozone lost at the poles each year, high levels of solar ultraviolet radiation (UVR) continue to reach our biosphere, potentially threatening living organisms, which owing to their life-histories and physiological constraints, are unable to avoid exposure to UVR. I aimed to demonstrate that cetaceans are affected by UVR and that they have adaptive mechanisms against exposure. Using histological analyses of skin biopsies and high-quality photographs, I characterized and quantified UVR-induced lesions in 184 blue, fin and sperm whales sampled in the Gulf of California, Mexico, and estimated indices of skin pigmentation for each individual. To examine the molecular pathways by which whales counteract UVR-induced damage, levels of expression of genes involved in genotoxic stress pathways (heat shock protein 70: *HSP70*, tumour protein 53: *P53*, and KIN protein genes: *KIN*) and melanogenesis (tyrosinase gene: *TYR*) were quantified. I not only detected evidence of sun-induced cellular and molecular damage but also showed that lesions were more prevalent in blue whales, the study species with lightest pigmentation, and sperm whales, the species that spends longest periods at the surface. Furthermore, within species, darker whales exhibited fewer lesions and more apoptotic cells, suggesting that darker pigmentation is advantageous. When accounting for interspecific differences in melanocyte abundance, sperm and blue whales presented similar amounts of melanin, although sperm whales overexpressed *HSP70* and *KIN*. This suggests that sperm whales may have limited melanin production capacity, but have molecular responses to counteract more sustained exposure to UVR. By contrast, increased UVR in the study area led to increases in melanin concentration and melanocyte abundance of blue whales, suggesting tanning capacity in this species. My study provides insights into the mechanisms with which cetaceans respond to UVR and reveals the central role played by pigmentation and DNA-repair mechanisms in cetaceans.

Table of contents

List of tables

List of figures

CHAPTER 1: Introduction

This thesis examines the effects of exposure to solar ultraviolet radiation (UVR) on cetacean skin at a cellular and molecular level (Chapter two and three, respectively) as well as the mechanisms used by cetaceans in response to such effects (Chapter three and four). The protective role of cetacean skin pigmentation against UVR is discussed in chapter four. Each chapter includes its own introduction and conclusion. The present chapter reviews the effects of UVR commonly observed in humans and laboratory animals. The few studies that have been conducted on wildlife, as well as their defence mechanisms against UVR, are discussed. The chapter then describes the present and future predictions of UVR trends on our planet, presents a general description of the three species included in this study, and enlists the aims of the thesis.

1.1 Solar ultraviolet radiation (UVR)

The solar radiation that enters the earth's atmosphere includes infrared, visible light and UVR (Gallagher and Lee, 2006). The latter is divided into three types according to their wavelengths: UVC (100-280 nm), being the most dangerous but fully absorbed by atmospheric ozone; UVB (280-315 nm), which represents only 0.8% of the total energy reaching the earth surface, but which causes the majority of damage observed in biological systems; and UVA (315-400 nm), the sun's predominant UVR source (Andrady et al., 2007; Pattison and Davies, 2006; Vernet et al., 2009).

The amount of UVR reaching the earth's surface is not only influenced by atmospheric ozone levels but also by complex interactions amongst temporal, geographical and meteorological factors (Vernet et al., 2009). These natural factors are directly or indirectly associated with the angle at which the sun' rays incise on the earth (McKenzie et al., 2007). This angle, formed between the zenith and the solar disc, is known as the solar zenith angle (SZA). When the SZA is small, absorption from the atmosphere is small and consequently the quantity of UVR

reaching the earth's surface is high. Therefore, the highest quantity of UVR received by the planet is at the equator when the sun is directly overhead (Fig. 1.1).

Another important factor that influences the amount of UVR that reaches the planet's surface is cloud cover (McKenzie et al., 2007; Vernet et al., 2009). Clouds can reflect part of the UVR but reflection will vary according to the type and amount of cloud. Other factors that affect surface UVR include the seasonal variation in distance between the earth and the sun, altitude and surface reflectance (albedo) (McKenzie et al., 2007). To help humans protect themselves from the harmful effect of UVR, an international standard measurement called the UV index has been standardized by the World Health Organization (Fig. 1.1).

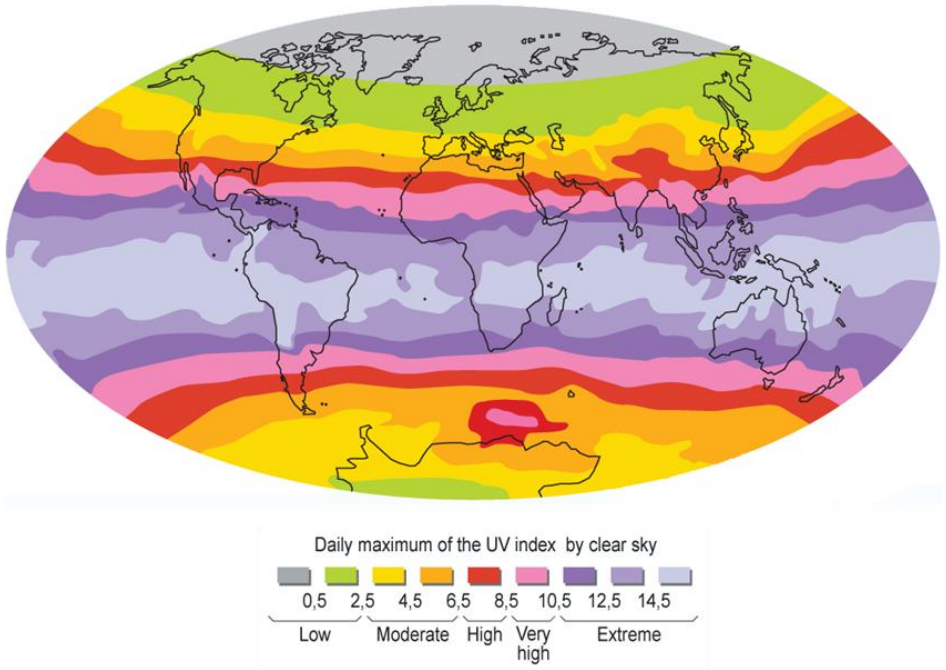

Figure 1.1. Global solar UV index. The UV index is a simple measurement of level of UVR reaching the surface of the globe. Index values are directly related to levels of UVR-induced damage. The highest values are observed near the equator where the solar zenith angle is the smallest. This map corresponds to the UV index values recorded on 28 October 2004. *Source: http://maps.grida.no/go/graphic/the-global-solar-uv-index (UNEP-DTIE and GRID-Arendal, 2007).*

1.2 Effects of UVR

The atmosphere absorbs most of the harmful UVR that reach the earth's surface. Without the formation of the atmosphere millions of years ago, direct exposure to sunlight would be lethal to all living organisms on our planet. However, unabsorbed UVR, particularly UVB rays, continue to cause adverse effects to living organisms and are now recognized as one of the most injurious environmental factors for human health (De la Coba et al., 2009). These effects can be observed at different levels including molecular, cellular and organismal levels and have been studied mostly in humans and laboratory animals.

1.2.1 Molecular effects

At the molecular level, DNA is the main target of UV radiations. This is because DNA absorbs UVR wavelengths between 245 and 290 nm, which correspond to UVC and UVB wavelength ranges (Tornaletti and Pfeifer, 1996). As UVC are completely screened out by the atmosphere, the main natural cause of genetic damage is the direct DNA absorption of UVB (Schuch and Menck, 2010), which can induce the formation of photoproducts including pyrimidine dimers, pyrimidine monoadducts, purine dimers and photoproducts between adjacent A and T bases (Tornaletti and Pfeifer, 1996). Photoproducts are formed by bonding between adjacent pyrimidine bases; the two most important being cyclobutane pyrimidine dimers (CPD) and pyrimidine [6, 4] pyrimidone photoproducts [(6-4)PP] (Schuch and Menck, 2010; Tornaletti and Pfeifer, 1996) (Fig. 1.2). The bond most frequently seen in CPDs is 5'-TpT, but bonds can be formed between any adjacent pyrimidine base including 5'-TpC, 5'-CpT or 5'-CpC. Contrastingly, (6-4)PPs are most commonly seen at 5'-TpC and 5'-CpC . While formation of CPDs is nearly 30% higher than (6-4)PPs, (6-4)PPs are repaired faster than CPDs in mammalian cells (De Cock et al., 1992; Tornaletti and Pfeifer, 1996). Formation of pyrimidine dimers depends on different factors such as the nucleotide sequence, UVR wavelength, DNA methylation, chromatid structure and presence of DNA proteins (Tornaletti and Pfeifer, 1996). The formation of photoproducts can incite DNA helix distortion,

inhibit cellular replication or create mutations, for example by mis-incorporation of the adenine during replication (Schuch and Menck, 2010; You et al., 2001). The most frequent mutations (C-T and CC-TT transitions) have been termed "UVR-signature mutations" and can lead to oncogenic processes (Schuch and Menck, 2010).

Although UVB has been shown to be the main cause of direct DNA damage, UVA can also indirectly damage DNA by inducing the formation of reactive oxygen species (ROS) such as singlet oxygen ($^1O_2$), superoxide radical ($O_2^{\bullet -}$), hydrogen peroxide (H_2O_2) and hydroxyl radical ($OH^{\bullet}$) (De la Coba et al., 2009; Finkel and Holbrook, 2000; Schuch and Menck, 2010). A marker described for oxidative DNA damage is the 7,8-dihydro-8-oxoguanine obtained by the oxidation of single bases in the DNA (De Gruijl 1997; Schuch and Menck, 2010). UVA-oxidation can also affect other cellular components such as RNA, lipid and protein and form DNA-strand breaks (De Gruijl 1997; De la Coba et al., 2009; Finkel and Holbrook, 2000; Peterson and Côté, 2004).

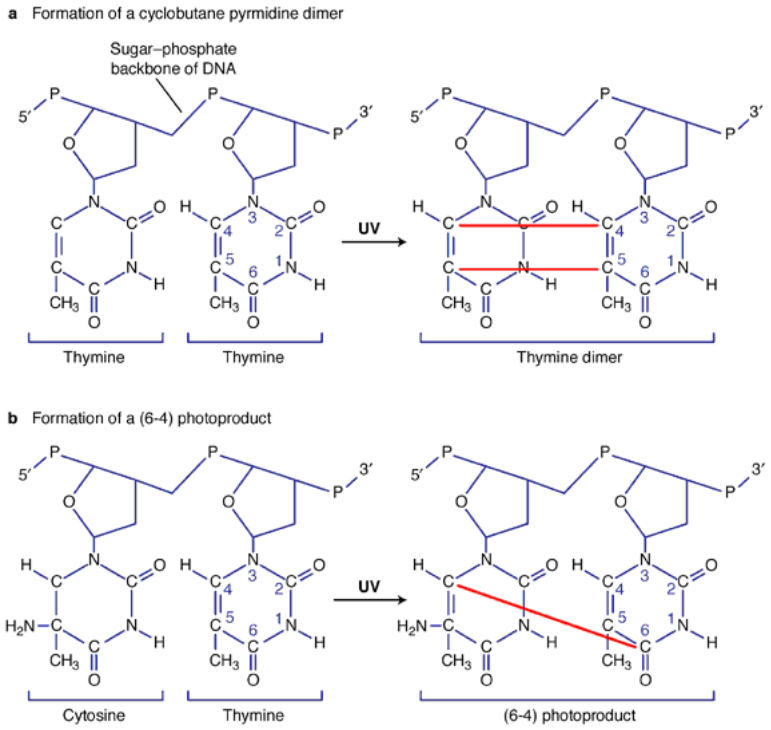

Figure 1.2. Structure of the two major UVR-induced photoproducts in DNA. a) formation of cyclobutane pyrimidine dimer b) formation of a (6-4) photoproduct. *Source: Ultraviolet light as a carcinogen (Ananthaswamy, 1997).*

1.2.2 Cellular effects

Well-known effects of acute exposure to UVR in humans include sunburn and photoallergy (De la Coba et al., 2009), while chronic exposure often leads to photoimmunosuppression, photoaging and photocarcinogenesis (De la Coba et al., 2009; Finkel and Holbrook, 2000; Martens et al., 1996).

Sunburn can be formed by either UVB or UVA and be observed a few hours after exposure depending on the intensity of irradiance and the sensitivity of the skin (De la Coba et al., 2009). Following overexposure, the epidermis becomes reddened (erythema) and oedematous (De la Coba et al., 2009) when melanin exceeds its capacity to absorb UVR (see section 1.3.2). Epidermal lesions commonly associated with sunburn and generally observed 24h after UVR-exposure include gross blistering, infiltration of inflammatory cells (lymphocytes and neutrophils), cytoplasmic vacuolation, intracellular and intercellular oedema, glycogen deposition and microvesicles (De la Coba et al., 2009; Nakaseko et al., 2003; Ohkawara et al., 1972). UVR-exposure also induces epidermal thickening and the appearance of "sunburn cells" (eosinophilic keratinocytes with or without pyknotic nuclei, which are undergoing apoptosis) (De la Coba et al., 2009; Nakaseko et al., 2003; Yamaguchi et al., 2008).

The absorption of UVR by different chromophores such as DNA-generated photoproducts, urocanic acid (UCA) transformed in cis-UCA or membrane components that lead to oxidative stress (Halliday et al., 2008; Nghiem et al., 2002) can induce stimulation of immunosuppressive cytokines (e.g. IL4 and IL10), alteration of the function of epidermal dendritic Langerhans cells and mast cells, thus leading to defects in antigen presentation and suppression of IL12 production (an immunoproliferative cytokine) (Halliday et al., 2008). The net result is suppression of cell-mediated immunity. In turn, UVR-induced immunosuppression can further impact on critical stages of specific diseases, as occurs in herpes-virus infections or skin cancer (Halliday et al., 2008).

1.2.3 Organismal effects

Cumulative UVR effects such as mutagenesis, stimulation of cell division and immunosuppression engender an environment favourable for skin neoplasia development (Halliday et al., 2008). For instance, DNA mutations, which can occur on different regions, including the *P53* tumour suppressor gene (Giglia-Mari and Sarasin, 2003; Kucab et al., 2010), can lead to abnormal proliferation of cells. Depending on the type of cell that is damaged, malignant neoplasias are classified as malignant melanoma skin cancer (MSC; originating from melanocytes), and non-melanoma skin cancer (NMSC; originating from keratinocytes) (Giglia-Mari and Sarasin, 2003). To date, UVR-induced skin cancer has mainly been studied and recorded in humans, laboratory and domestic animals (Martens et al., 1996; Noonan et al., 2003; Spradbrow et al., 1987). In contrast, published studies on the effects of UVR on wildlife are very scarce and essentially restricted to amphibians, fishes and marine invertebrates.

Increased UVR exposure in interaction with other stressors such as contaminants has been proven to lead to severe mortality in amphibian populations (Blaustein et al., 2003; Kiesecker et al., 2001). Sublethal UVR effects have also been observed in amphibians including decreased hatching success, behavioural modifications, impaired development and malformations (Blaustein et al., 1998; Blaustein et al., 2003). Marine invertebrates such as sea urchins and fishes present similar UVR-induced damages particularly during early life stages (Dahms and Lee, 2010). Indeed, the most dangerous solar radiations in the water column are found near the surface (Tedetti and Sempere, 2006) where many primary and secondary consumers, including zooplankton, fish eggs and larvae, reside. Kouwenberg *et al.* (1999) evaluated that after 42 h of UVR exposure, 50% of Atlantic cod eggs concentrated in the first 10 cm of the water column will die. In Antarctic zooplankton, during periods of high UVB, significant levels of DNA damage have been observed (Malloy et al., 1997). In addition, increased UVB irradiance can reduce primary production by inhibiting photosynthesis (Karentz and Bosch, 2001), having a cascading effect in the entire food chain.

1.2.4 Beneficial effects

Although intense exposure to the sun can have detrimental effects on human health, low levels of UVR are essential for the production of the biologically active form of vitamin D (Webb, 2006; Zittermann and Gummert, 2010). Through the action of UVB, the 7-dehydrocholesterol (7DHC) present in the skin is transformed into the active form of vitamin D, the 1, 25-dihydroxyvitamin D_3 (Webb, 2006), of which only a small percentage can be supplied through the diet (Zittermann and Gummert, 2010). In Europe and North America, where sun irradiance is low, it is common for vitamin D deficiency to occur, a condition that has been associated with an increased risk of cardiovascular disease (Zittermann and Gummert, 2010). Indeed, vitamin D plays an important role in calcium regulation and thus is involved in homeostasis, muscle and bone function (Halliday et al., 2008). Vitamin D can also reduce UVR-induced DNA damage via the upregulation of *P53* (Halliday et al., 2008).

1.3 Animal defences against UVR

Over time, many living organisms have been able to adapt to solar UVR exposure by the evolution of a number of behavioural, physiological and molecular mechanisms. Such UVR-defense adaptive mechanisms vary widely between and within species, and some examples are explained below.

1.3.1 Behavioural mechanisms

Changes in behaviour, such as remaining in shady areas during the hours of highest solar radiation, wearing protective clothing, sun shades and using sunscreen significantly help avoid detrimental effects from UV irradiation in humans (Gies et al., 1998). Shelter-seeking behaviour is commonly observed in horses (Heleskia and Murtazashvili, 2010), amphibians (Han et al., 2007) or arthropods (Barcelo and Calkins, 1980) and zooplankton day-time downward migration is at least partly explained as UVR avoidance (Rhode et al., 2001). It is also possible that night-time spawning of corals and other reef animals is an adaptation to avoid high levels of

UVR, which considerably reduces sperm mobility (Dahms and Lee, 2010). Finally, some species of salamander wrap leaves around their eggs to protect them from UVB (Marco et al., 2001).

1.3.2 Physiological mechanisms: melanin a photoprotective pigment

Melanin is a pigment found across a wide range of organisms including mammals, amphibians, birds, fishes and, even, plant species. Melanin gives colour to the skin, hair, iris, feathers and scales. Dermal melanin is produced in specialized cells called melanocytes (Fig. 1.3), found in the basal layer of the epidermis (Lin and Fisher, 2007). In humans, there are two different types of dermal melanin: eumelanin, seen as black to brown pigments and found in dark skin, and pheomelanin, seen as reddish-brown pigments, found in all skin types (Lin and Fisher, 2007). The skin type, genetically determined, results in the combination of concentration, type and epidermal distribution of the melanin (Lin and Fisher, 2007).

Melanin plays an important role in photoprotection by absorbing most of the UVR and thus protecting the epidermis from lesions such as DNA damage and sunburn (Lin and Fisher, 2007). Melanin can also inhibit conversion of 7DHC to vitamin D_3, implying that darker skin produces less vitamin D_3 per equal dose of UVB than lighter skin (Webb, 2006). These mechanisms explain how natural selection has promoted darker skin near the equator, where UVR intensity is higher, and lighter skin towards the poles where sunlight is low and absorption necessary for fixing vitamin D (Jablonski and Chaplin, 2010) (Fig. 1.4).

The increase in skin pigmentation over the basal constitutive level is called tanning (Costin and Hearing, 2007). Immediate tanning occurs within 1-2h of sun exposure and is based on the photoxidation of pre-existing melanin and/or modification in their distribution (Costin and Hearing, 2007). Delayed tanning is induced by repeated UVR exposure generally after 48-72h of exposure and can remain up to 8-10 months (Costin and Hearing, 2007). Both UVA and UVB are involved in the process of tanning; however UVA-induced skin pigmentation is less protective against further acute UVR damage than tanning produced by UVB (Costin and Hearing, 2007).

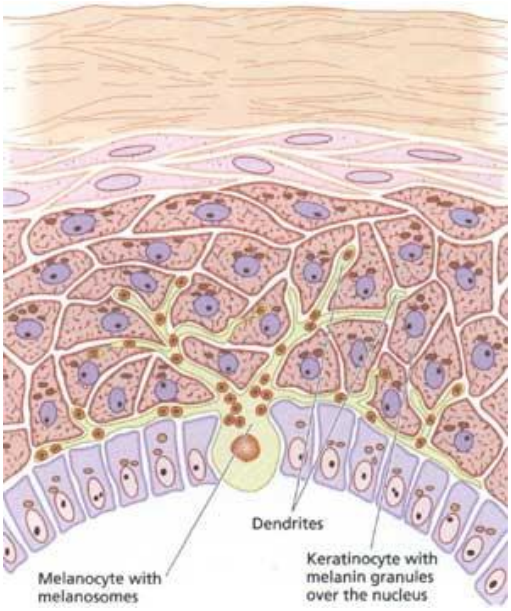

Figure 1.3. Distribution of melanin in the epidermis. Melanocytes produce melanin granules and distribute them in the epidermal cells using specialized organelles called melanosomes. From the bottom to the top of the figure, the epidermal layers are the *stratum basal, the stratum spinosum, the stratum granulosum and the stratum corneum*. *Source: P&G Skin Care Research Center- www.pg.com.*

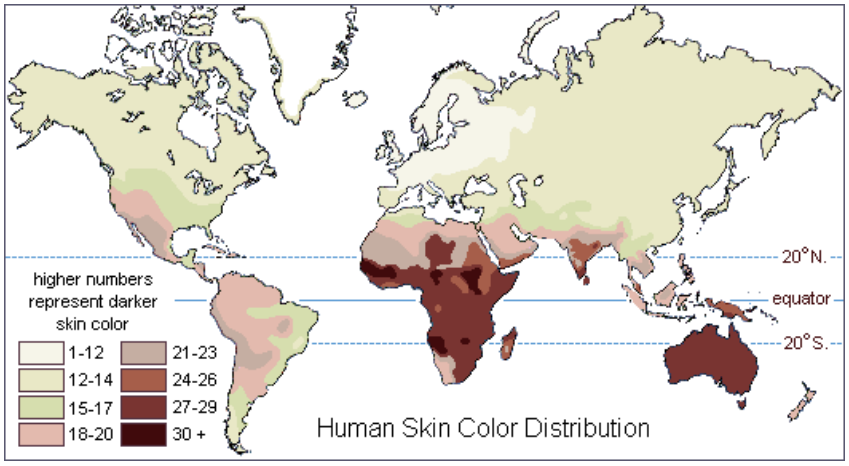

Figure 1.4. Geographic distribution of human skin colour. In latitudes where intensity of UVR is higher, human skin colour is darker as a result of adaptation. *Source: What controls variation in human skin color (Barsh, 2003).*

Changes in skin coloration as a consequence of UVR have also been observed in wild animals such as sharks (Lowe and Goodman-Lowe, 1996) and zooplankton (Hansson, 2000). Other important natural sunscreen compounds found in marine organisms include carotenoids and mycosporine-like amino acids (MAAs) (Cockell and Knowland, 1999; Karentz et al., 1991). Only microorganisms can produce MAAs so those are mainly obtained via feeding (Riemer et al., 2007) or symbiosis (Sommaruga et al., 2006). Finally, it has been proposed that hippopotamus sweat, which rapidly turns the skin red and then brown, plays the role of a natural sunscreen (Saikawa et al., 2004). When UVR levels are too high to be absorbed by sunscreen compounds, DNA photoproducts are formed and consequently activate specific DNA repair mechanisms, the second most important defence that protects skin from UVR (Zittermann and Gummert, 2010).

1.3.3 Molecular mechanisms: DNA repair

Regardless of the cause, damage to DNA can lead to lethal mutations, genomic instability and cell death (Peterson and Côté, 2004). However, most of the ~10,000 DNA lesions that occur in a human cell per day are quickly repaired by DNA-repair

mechanisms (Lindahl and Wood, 1999). These mechanisms include direct reversal, base excision repair, nucleotide excision repair, mismatch repair and double strand break repair (Peterson and Côté, 2004). Generally, prior to the initiation of these mechanisms, the cell-cycle is arrested to allow DNA repair (Nakanishi et al., 2009). When DNA damage exceeds repair capacity, cells enter apoptosis or senescence (Nakanishi et al., 2009). These mechanisms are complex and generally require overlapping sets of enzymatic machineries. One of the most important proteins involved in these mechanisms is P53, that activates expression of a set of target genes, which facilitate DNA repair and enable cell-cycle arrest or apoptosis (Helton and Chen, 2007; Ikehata et al., 2010). For UVR-induced damage, nucleotide excision and direct reversal repair are the mechanisms directly used for DNA repair (Peterson and Côté, 2004).

Nucleotide excision repair (NER) plays an important role in the elimination of pyrimidine dimers (Peterson and Côté, 2004). The mechanism is controlled by a complex protein machinery and involves four steps: DNA damage recognition and distortion; DNA unwinding; DNA excision using endonucleases and DNA synthesis by copying the undamaged strand using DNA polymerase I and DNA ligase (Peterson and Côté, 2004).

A second repair mechanism, direct reversal DNA repair, also called photoreactivation, uses the energy of the sun to activate photolyase. This enzyme binds complementary DNA strands and breaks the pyrimidine dimers. There are two types of photolyases, one specific for cyclobutane pyrimidine dimers (CPD photolyase) and one specific for pyrimidine (6-4) pyrimidone photoproducts [(6-4) photolyase] (Todo et al., 1996). CPD photolyase is widely distributed among species, while (6-4) photolyase has only been described for *Drosophila melanogaster* (Todo et al., 1996).

Defects in NER can engender photosensitive genetic diseases like Xeroderma pigmentosum, Cockayne's syndrome and trichothiodystrophy (Rass and Reichrath, 2008; Tornaletti and Pfeifer, 1996), all well described in humans. These diseases are mostly induced by genetic mutations in DNA repair genes (Rass and Reichrath, 2008).

1.4 Global environmental change

Environmental change is occurring globally at an unprecedented rate. Physical effects of such changes in the marine environment vary across latitudes, but include augmented sea-surface temperatures, extreme weather and increased solar ultraviolet radiation, which are likely to be a major threat to living organisms, by affecting their habitat or individuals. For example today, 3649 species are threatened as a consequence of climate change and extreme weather (IUCN Red List: www.iucnredlist.org, 04/03/11), and it is likely that this number is a vast underrepresentation due to often incomplete or unavailable data for many species.

1.4.1 Ozone depletion

The ozone layer is a small part of our atmosphere, vital for life on earth. Ozone is a natural gas composed of three oxygen atoms (O_3). The ozone layer, composed by 90 % of the total atmospheric ozone, is found in the upper atmosphere called stratosphere, around 50 km from the earth' surface. The remaining 10 % is found in the troposphere (Andrady et al., 2007). Ozone molecules from the stratosphere are formed by the action of UVR on the atom of oxygen (O_2), which breaks it into two molecules. Each oxygen atom then combines with an oxygen molecule to produce an ozone molecule (Equation 1.1) (Andrady et al., 2007).

$$O_2 + \text{solar radiation} \rightarrow O + O \text{ and } O + O_2 \rightarrow O_3 \qquad \text{(Eq. 1.1)}$$

The first evidence of ozone depletion was recorded in 1985, when Joseph Farman, Brian Gardiner, and Jonathan Shanklin from the British Antarctic Survey reported a "hole" in the ozone layer above the Antarctic (Farman et al., 1985). The ozone layer was thinning dramatically, falling 40% from 1975 to 1984 in mid-October during Antarctic spring. This decline has been linked mainly to the increase in human-made chlorofluorocarbons (CFCs) and bromofluorocarbons (BFC) that occurred during the middle of the 20th century. These compounds were part of various domestic or industrial appliances such as refrigerator coolants, air conditioners or spray cans

(Farman et al., 1985). The halogen atoms (chlorine and bromide) destroy ozone by photocatalytic decomposition in the stratosphere. This process is observed in both poles but is dramatically amplified over the Antarctic due to the very cold conditions (Solomon, 2004; Solomon et al., 2007). The holes are observed only in springtime (largest hole observed in October for the Antarctic and in March for the Arctic) when there is sunlight, a key aspect for the ozone destroying reactions (Solomon, 2004). The evidence of the association between CFC accumulation and ozone depletion was unequivocal, as were the consequences of increased UVR for human skin cancer. Consequently, in 1987, the Montreal Protocol banished the use of most ozone depleting substances (ODSs). The report, written and review by 300 scientists and published in September 2010 by the World Meteorological Organization (WMO) and the United Nations Environment Programme (UNEP) states that the Montreal protocol was a success, as global production and consumption of ODSs has been controlled and consequently the ozone layer stopped decreasing (WMO-UNEP, 2011). Nevertheless, the report admitted that it would take several decades for the ozone layer to recover. Effectively, the long atmospheric lifetime (50-100 years) of the megatonnes of the CFCs released in the atmosphere before the application of the Montreal protocol (Solomon, 2004) continue to destroy the ozone today and each year the poles continue to suffer from a large loss of ozone (WMO-UNEP, 2011).

1.4.2 Present and future levels of UVR

In the Northern Hemisphere, average total ozone values recorded in 2006-2009 remained below the 1964-1980 averages of roughly 3.5% at mid-latitudes (35°-60°), whereas in the Southern Hemisphere mid-latitude levels were 6% lower than the 1964-1980 averages (WMO-UNEP, 2011). While clear-sky UVR levels have been consistent with ozone column observations, UVR levels are also significantly influenced by clouds and aerosols. For example, in Europe, erythemal irradiance has continued to increase due to the net reduction effect of clouds and aerosols whereas in southern mid-latitude these effects had increased (WMO-UNEP, 2011). Although the projected increase of ozone thickness is expected to lead to a 10% reduction of surface erythemal by the year 2100, changes in cloud coverage may lead to decreases or increases of up to 15% in surface erythemal irradiance (WMO-UNEP, 2011). Ozone thickness also depends on other factors such as the detection of new ozone

depleting substances as sulphur dioxide (SO_2) and nitrogen dioxide (NO_2) (WMO-UNEP, 2011). Besides, changes in global and local climate might have significant effects on some of these factors. For instance, the ozone layer above the Arctic is projected to be more sensitive to climate change than in the Antarctic as the increasing levels of greenhouse gases could lead to changes in stratospheric temperatures and circulation that could in turn have important consequences for the ozone column, particularly in mid-latitudes (WMO-UNEP, 2011). In this sense, it is a huge challenge for atmospheric science to provide reliable mid to long-term predictions of UVR trends in our planet.

1.5 Cetaceans

1.5.1 Biology, ecology and conservation status of cetaceans

1.5.1.1 Generalities

The order Cetacea includes whales, dolphins and porpoises and is divided into two suborders: Mysticeti or baleen whales, and Odontoceti or toothed whales (Wandrey, 1997). As all mammals, cetaceans are placentated homoeothermic animals that breathe air through their lungs. However, in stark contrast to other mammals, cetaceans have a number of evolutionary adaptations that allow them to survive in a marine environment, dive for prolonged periods and to great depths and tolerate high salinity and low temperatures (Wandrey, 1997).

1.5.1.2 Conservation status

To date, at least 18 species of the 85 extant cetacean species are threatened as a result of different anthropogenic activities including the XIX century's intensive hunting, ship strikes, disturbance from increasing whale watch activity, entanglement in fishing net, pollution and global environmental change (IUCN Red List, 04/03/11). Of these 18 species, two are considered critically endangered; six, including the blue whale and the fin whale, are listed as endangered; and five, including the sperm whale, are considered vulnerable (IUCN Red List, 04/03/11).

1.5.1.3 Cetacean's skin

The first physical barrier that protects animals from the environment is their skin. Nearly 95% of the epidermal cells are keratinocytes, whose morphology varies distinctly amongst epidermal layers (Costin and Hearing, 2007). While there are some disagreements about the number of layers that compose cetacean skin (Geraci et al., 1986), three layers are generally recognized: *stratum basale* or *germinativum* (junction with the dermis), *stratum spinosum* and *stratum corneum*. The *stratum granulosum* seems to be absent in cetaceans whereas it is generally present in other mammals (Reeb et al., 2007). A peculiarity of cetacean integument is the presence of long epidermal extensions (called ridges) that anchor the dermis. Epidermal ridges (Er) are generally oriented parallel to the body axis (Reeb et al., 2007; Geraci et al., 1986). One of the roles of the Er is to increase the surface of the basal layer (Reeb et al., 2007; Geraci et al., 1986). The basal layer is a single layer formed by two types of cells; columnar keratinocytes and melanocytes, at a ratio of 12:1. In that layer, keratinocyte stem cells divide and granules of melanin are formed (Geraci et al., 1986). New epidermal cells differentiate as they are pushed up to the *stratum corneum* where they form a layer of enucleated and keratinized cells called squamous cells. The time of skin regeneration has so far only been studied in dolphins and is around 70 days (Geraci et al., 1986).

1.5.2 Study species

This study focused on three species, the blue whale, the fin whale and the sperm whale. These species were selected due to their different skin pigmentation and diving behaviour (Fig. 1.5), which makes them ideal for interspecies comparisons in UV-induced damage and repair capacity. Besides, the three species are seasonally sympatric within the Gulf of California, Mexico, which is the present thesis' study site (see Chapter two).

1.5.2.1 The blue whale: Balaenoptera musculus (Linnaeus, 1758)

Blue whales, *Balaenoptera musculus*, are the biggest animals to have ever lived on earth, with a body length of up to 30 metres (Wandrey, 1997). Blue whales' integument is characteristically light grey (Fig. 1.5) which appears blue from the water's surface, thus giving them their common name. They generally dive during 10 minutes and surface to breath for few minutes (Croll et al., 2001). Sexual maturity is reached at 8-10 years and adult females give birth every 2-3 years after a 10-11 month long gestation (Wandrey, 1997). Each year, blue whales migrate from sub-polar cold waters rich in zooplankton to the warmers tropical waters where they reproduce (Calambokidis et al., 2009).

Blue whales were abundant in all the oceans until the intense whaling industry killed more than 90% of the entire population during the first half of the 20th century (Sears and Calambokidis, 2002). The last estimation, conducted in 2002, suggested 5000 to 12000 blue whales worldwide (Sears and Calambokidis, 2002), and at present the species is considered endangered by the IUCN (IUCN Red List, 04/03/11). Blue whales are present in all the oceans and are separated into three distinct populations: the North Atlantic, North Pacific and Southern Hemisphere population (Sears and Calambokidis, 2002), with the largest subpopulation found in the coasts of California (United States) and Baja California including the Gulf of California (Mexico). The minimum population estimate in California, Oregon, and Washington waters is 1136 blue whales (Carretta et al., 2009), of which around 600 are found in the Gulf of California (Diane Gendron, pers. comm.).

1.5.2.2 The fin whale: Balaenoptera physalus (Linnaeus, 1758)

Fin whales, *B. physalus*, are the second largest cetacean in the world, measuring up to 25 metres in body length (Wandrey, 1997). Their pigmentation differs markedly from the blue whale, as their skin is dorsally dark grey-brown. Diving and surfacing times are similar to blue whales, as are gestational periods and reproductive behaviour. After a long migration of thousands of kilometres from the poles, females

give birth in warm low latitude waters (Wandrey, 1997). Fin whales currently are widespread and are mostly pelagic.

B. physalus was also heavily exploited by the modern whaling industry and is now listed as endangered by the IUCN (IUCN Red List, 04/03/11). In 1973, the fin whale north Pacific population was estimated to have been reduced by 62% (26,875 out of 43,500 whales) and the eastern Pacific stock was estimated to range between 8,520 and 10,970 whales (Carretta et al., 2009). Today, the minimum population estimate of fin whale abundance in California, Oregon, and Washington waters is 2,316 (Carretta et al., 2009), of which a minimum of 148 individuals are found in the Gulf of California, where they are believed to be year-round residents (Carretta et al., 2009). Genetic studies have shown that the population in the Gulf of California is an evolutionarily unique population (Bérubé et al., 2002).

1.5.2.3 The Sperm whale: Physeter macrocephalus (Linnaeus, 1758)

Sperm whales, *Physeter macrocephalus*, are the largest of all odontocetes (Whitehead, 2003). Sexual dimorphism in sperm whales is extreme, with males measuring twice as long as females and reaching up to 20 metres in body length and growing up to at least 57 tonnes, more than four times the weight of the females (Whitehead, 2003). Sexual maturity is reached around 20 years for the males and 10 years for the females. Adult females give birth every 4 to 6 years with a gestation period that lasts between 14 and 15 months. Females are extremely social individuals, spending all their life in the same social group of approximately ten adults and their calves. In contrast, adult males are less gregarious and are normally found near the herds during mating season (Whitehead, 2003). Sperm whale skin is dark grey in colour and has a smooth rubbery texture, which is 10 to 20 times thicker than that of terrestrial mammals (Geraci et al., 1986). Their diving patterns are unique as they are able to dive up to 1000 metres and remain underwater for up to an hour (Teloni et al., 2008; Whitehead, 2003). During these deep dives they hunt squid to satiate their daily need for several hundred to several thousand kilograms of food (Whitehead, 2003). Sperm whales spend around 7-10 minutes breathing at the surface between foraging dives. They also aggregate during hours at the surface during socialization, remaining for periods of up to six hours at a time at the sea surface (Whitehead, 2003).

Sperm whales are found in all the oceans. No clear population structure has been recorded, at least in the South Pacific Ocean (Whitehead et al., 1998). Social groups of females and immature males are generally found between the 40°N and 40°S, whereas mature males are normally found in the higher latitudes of both hemispheres (Whitehead, 2003). Global population size has been estimated at 360,000 individuals, 32% of its original level (1,110,000 individuals) before the whaling industry (Whitehead, 2002). Off the west coast of Baja California, sperm whales have been estimated at around 1,640 individuals (Carretta et al., 2009). However, there is no evidence for genetic exchange between these animals and those in the Gulf of California. It has been suggested that if not a year-round residency for sperm whales, the Gulf of California, might be an important breeding ground for this species (Jaquet and Gendron, 2002).

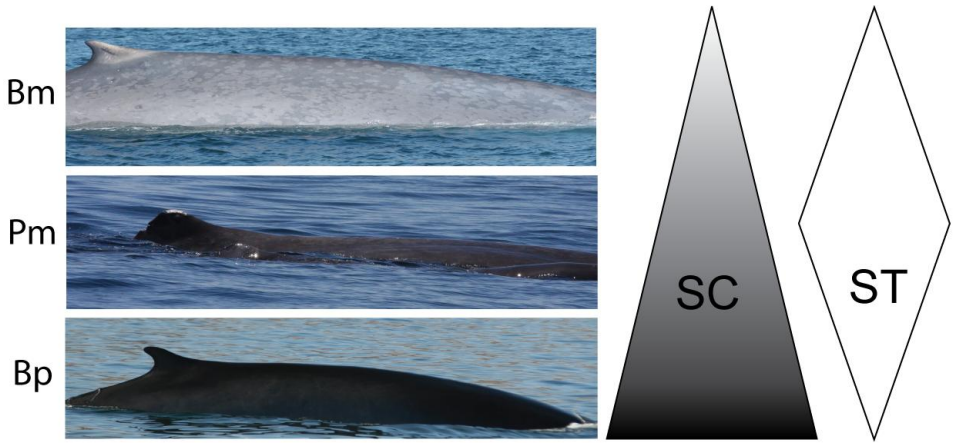

Figure 1.5. Differences in skin colour (SC) and time spent at the surface (ST) among blue (Bm), sperm (Pm) and fin whales (Bp).

1.6 Thesis aim

The aim of this thesis is to investigate the effects of solar ultraviolet radiation (UVR) on cetaceans. Using a combination of fieldwork, pathology and molecular techniques, the thesis addresses the following questions:

1) What is the extent of molecular and cellular damage on cetacean epidermis caused by UVR exposure?

2) How do intra- and interspecies variations in skin pigmentation, surface behaviour and migration patterns influence exposure to UVR and sensibility to UVR-induced damage?

3) What mechanisms do cetaceans employ to defend themselves from daily UVR exposure and how do cetaceans respond to seasonal increases in UVR intensity?

CHAPTER 2: General materials and methods

This chapter describes the general materials and methods used throughout the thesis. It includes a detailed description of the fieldwork, the general statistical analysis used in the thesis, the standardization of individual measurements of skin pigmentation and a brief account of solar ultraviolet radiation (UVR) data available for this study. Each results chapter describes in detail the specific methodologies relevant to that section. Appendix 2.1 contains a general overview of the different methods used and their relevance for this study.

2.1 Samples and data collection

2.1.1 Study site: the Gulf of California, Mexico

The Gulf of California is located in the Pacific Ocean in the north-western region of Mexico, between the peninsula of Baja California and the mainland (Fig. 2.1). The Gulf of California, also known as the sea of Cortes, is one of the richest seas in the world. The prolific phytoplankton at the base of food chain sustains a huge number of species that includes more than 2000 invertebrate-, 800 fish- and 30 mammal species of which one, the vaquita (*Phocoena sinus*), is endemic (Lluch-Cota et al., 2007).

Figure 2.1. Study sites (areas encircled by red lines) in the Gulf of California, Mexico. Blue whales were sampled along the coastline between La Paz (24°21.9' N, 110°23.5' W) and Loreto (25°39.1' N, 111°7.0' W), and fin whales between La Paz and Santa Rosalia (27°20.2' N, 112°16.0' W). Sperm whales were sampled along the coastline between La Paz and Santa Rosalia and also within the area of San Pedro Martir Island (28°22.3' N, 112°20.15' W).

The Gulf of California was chosen as the site to conduct my research for a number of reasons. Firstly, the three study species are located in this area: fin and sperm whales reside in the area year-long (Bérubé et al., 2002; Jaquet and Gendron, 2002), while the blue whale is found between January and June (Gendron, 2002). Secondly, the

Marine Mammal Ecology Laboratory (MMEL) of CICIMAR in La Paz, Mexico, has studied the species' populations in this area for the past 15 years and has kindly made available a vast blue whale photo-identification catalogue of around 460 individuals, for which various types of information are available including sex and minimum age. Finally, Mexico represents an ideal site to study the effects of UVR on marine life as UVR is high during most of the year (see Fig. 1.1 in Chapter one) with a UV index at clear sky values (a measure of the potential human exposure to UVR) between 6 (high) and 15 (extreme) (Lemus-Deschamps et al., 2002).

2.1.2 Fieldwork: sea-expeditions and sample collection

Cetacean surveys were conducted in the Gulf of California (Fig. 2.1) between January and June of 2007, 2008 and 2009, in collaboration with the MMEL of CICIMAR of La Paz (Baja California, Mexico). Each trip was conducted in a motorized vessel, and lasted between five days and three weeks.

Field expeditions followed a well-established protocol. Briefly, when cetaceans were located at sea using visual survey (blue and fin whales, Fig. 2.2.a) or acoustic (sperm whales) technique consisting of detecting whale song using an omni-directional hydrophone, we recorded the sighting's GPS position, the whale's individual behaviour and dive duration (Fig. 2.2.c). Once these data were recorded, the whale was photographed from a distance of approximately 100 metres using a digital camera (Canon EOS D1) with a 100 to 300 mm zoom lens (Fig. 2.2.b). Each whale was photo-identified based on skin patterns and scars on the back and dorsal fin (Hammond, 1990) and the ventral side of the flukes (Whitehead, 2003) and cross-referenced with the MMEL catalogue. Once photo-identified, we approached the whale at a slow but constant speed in order to collect a skin biopsy. When at approximately 20 metres from the whale the sample was collected using a stainless steel dart (7 mm) fired from a crossbow to the whale's flank, behind the dorsal fin (Fig. 2.2d). Immediately after collection, the epidermal sample was divided in five sections and conserved in 500µl of different reagents depending on the subsequent analysis (Appendix 2.1). One section was preserved in 10% buffered formaldehyde solution for histology, one in ethanol 96% for genetic analyses, a third was preserved in RNA later (Qiagen, UK) for gene expression assays and the fourth section was

immersed in a cryogenic solution (Recovery™Cell Culture Freezing Medium, Invitrogen GIBCO, UK) for the comet assay. RNA-later and Recovery-cell preserved samples were immediately frozen in a liquid nitrogen container and kept at less than -80°C until processing. The final section was conserved in liquid nitrogen and transferred to a -80°C freezer at CICIMAR where it was archived in the whale tissue bank of MMEL.

Twenty-six sea expeditions, of which I participated in 17, were conducted, during which a total of 184 skin biopsies were collected from 106 blue whales, 55 fin whales and 23 sperm whales (details of sample size for each method are described in the appropriate chapters). The identity of each whale was confirmed in the laboratory using visual method as described in the last paragraph. To reduce disturbance to individuals, we aimed to only sample each individual once in its lifetime. When an individual was sampled twice, recaptures were excluded from the analyses. Information related to blue whale observations such as GPS position, time and duration of the sighting and type of sample collected was collated in the MMEL database. The information contained in this database allowed us to estimate the minimum age for each blue whale sampled. This parameter was calculated by taking into account the first year of observation reported for a particular individual in the Gulf of California. Data on age category (1 = juvenile, 2 = youth, 3 = subadult, 4 = sexually mature adult, and 5 = morphologically mature adult) were available for 31 of the whales included in this thesis (Ortega Ortiz, 2009). The sex of the sampled blue whales was determined by molecular amplification of cetacean sex markers (Berube and Palsboll, 1996), work that was conducted at the Molecular Genetics Laboratory of CICESE in Ensenada, Mexico, and was made available for this study.

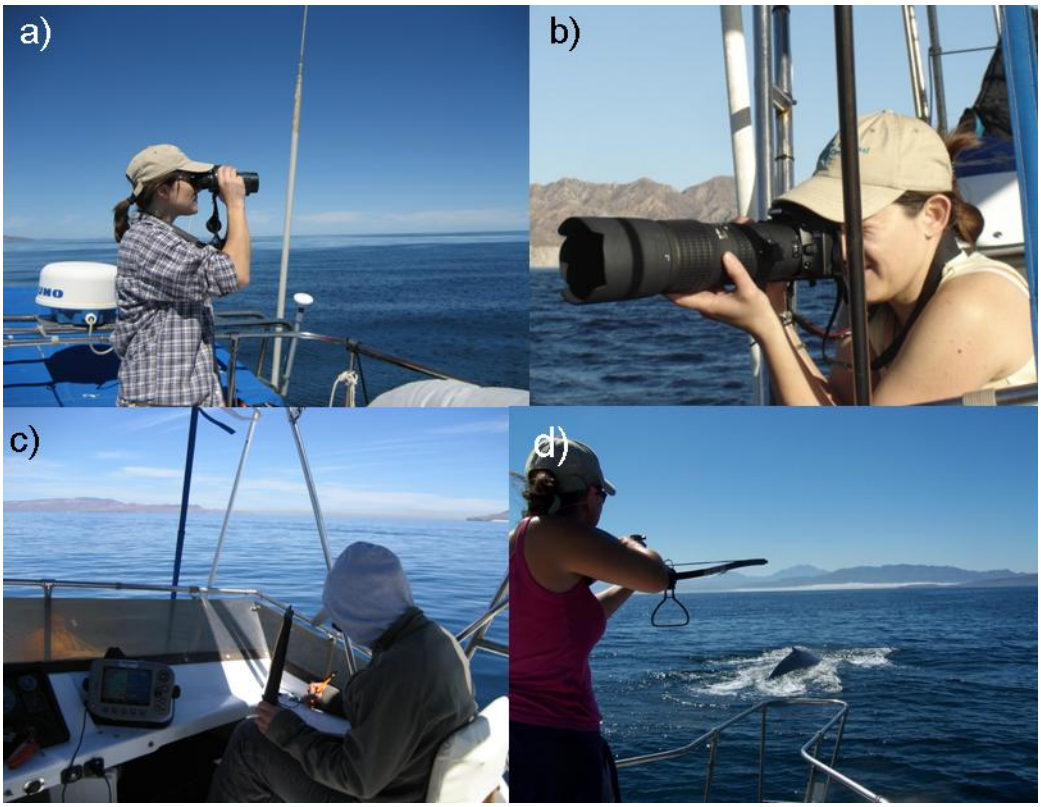

Figure 2.2. Main tasks conducted during the sea expeditions. a) Observation b) Photo-identification c) Data collection d) Biopsy collection.

2.2 General statistical analysis

The statistical analyses were conducted in R (Ihaka and Gentleman, 1996; R Development Core Team, 2008). Specific analyses, which varied between research questions, are described in detail in each chapter. Before conducting any analysis, the data distribution was examined. In general, when comparing groups of independent observations, I used two-sample t-test (for two groups) or one-way ANOVA test (for more than two groups). Wilcoxon and Kruskal-Wallis tests were used for non parametric data. The Bonferroni correction was applied when appropriate. To compare proportions, Chi-squared or Fisher-exact tests (for frequency lower than 5%) were used. When looking for correlations between two groups of continuous data, I used linear regression or spearman tests (for non parametric data).

Generalized linear models (GLMs) were constructed to investigate interspecies differences in epidermal lesions, and temporal trends in lesion prevalence (Chapter three). When appropriate, response variables were defined as bimodal and the

model's error structure was defined accordingly. Linear models were constructed to investigate interspecific, intraspecific and temporal variation in levels of gene expression (Chapter five and six) and quantity of melanocytes and melanin pigments (used as skin pigmentation indices; Chapter six). In some cases, linear mixed effect models (Zuur et al., 2009) were constructed. Models were built in R (Ihaka and Gentleman, 1996; R Development Core Team, 2008). To construct mixed effect models I used the *lme* function in the *nlme* package (Pinheiro et al., 2008).

To build the models (including simple linear model and mixed effect model, Chapters five and six), I used a top-down strategy, which begins with the most complete model, also called the maximal model (fitted with all of the explanatory variables, interaction terms and random factors of interest) and ends, through a series of simplifications, with a "minimal adequate model". In other words, the best model needs to have as few parameters as possible and yet describes a significant fraction of the data (Crawley, 2007). A variable was retained in the model only if it caused a significant increase in deviance when removed from the current model (Crawley, 2007), which was assessed using deletion tests (F-tests for linear models with normal errors and Likelihood ratio tests (LRT) for GLMs with error structures other than normal and for mixed-effects models) (Crawley, 2007). Differences were considered to be significant for values of $p<0.05$. When comparing mixed effect models, those were fitted by the Maximum Likelihood method (ML), whereas final models were fitted with the Restricted Maximum Likelihood method (REML). ML and REML are the two available functions of the log likelihood function used in defining the measure of fit. They are mathematical techniques that estimate the parameters that make the observed results the most probable. REML is used to correct the estimator of the variance and estimates the standard deviations of the random effects better than ML does. However it is inappropriate to construct likelihood ratio tests with REML because REML requires identical fixed-effects specifications for both models, consequently when comparing models, an ML estimator was used (Ruppert et al., 2003). When the random effect was not retained in the final model, the *gls* function (generalized least squares function corresponding to an *lme* function without the argument random in the *nlme* package) was used (Zuur et al., 2009). The final models were validated by visual inspection of the plotted residuals (residuals = observed values – fitted values) (Zuur et al., 2009). To check for heteroscedasticity,

the residuals were plotted against the fitted values and to look for non-normality, the residuals were plotted against the standard normal deviates. Minor violations of normality and/or homogeneity were corrected by logarithmic transformation of the response variable.

2.3 Melanocyte counts

Epidermal melanocytes play a central part in protecting the skin from UVR exposure (Costin and Hearing, 2007). In response to UVR, melanocytes stimulate the synthesis of melanin, a pigment that gives colour to the skin and has an important role in photo-protection (Lin and Fisher, 2007). Periodic changes in skin colour, which reflects the quantity and distribution of melanin throughout the epidermis, can occur in response to UVR exposure (Lin and Fisher, 2007). Thus, I used melanocyte counts as a surrogate measure of constitutive pigmentation (Costin and Hearing, 2007). As mentioned earlier (see Introduction, section 1.5.1.3), cetacean epidermis has elongations that appear as ridges and enter the dermis (Fig. 2.3a) called *rete* ridges or epidermal ridges (Geraci et al., 1986). Melanocytes are located in the basal layer of the epidermis, at the junction with the dermis (Fig. 2.3d) (Geraci et al., 1986). I measured the quantity of melanocytes using skin sections stained with hematoxylin and eosin (H&E) after establishing a standardized counting area. To determine the counting area, for each individual I calculated the number of melanocytes per 100 arbitrary units along the epidermal ridges (Er). Melanocyte distribution was examined along the Er and the association between number of melanocytes and Er perimeter was tested. In all cases, melanocytes were counted in triplicate using a cell counter, and the mean of these repeated measures was used for analysis.

The distribution of melanocytes along the epidermal ridges was determined by dividing each Er into three layers (Fig. 2.3b), each of 100 arbitrary units (AU), corresponding to 40 µm (magnification 250 X). This was done using a microscope-crossed graticule (10 mm long with 100 subdivisions of 0.1 mm). In each layer, melanocytes were quantified along the entire Er perimeter. Results were expressed as the number of melanocytes per 100 AU.

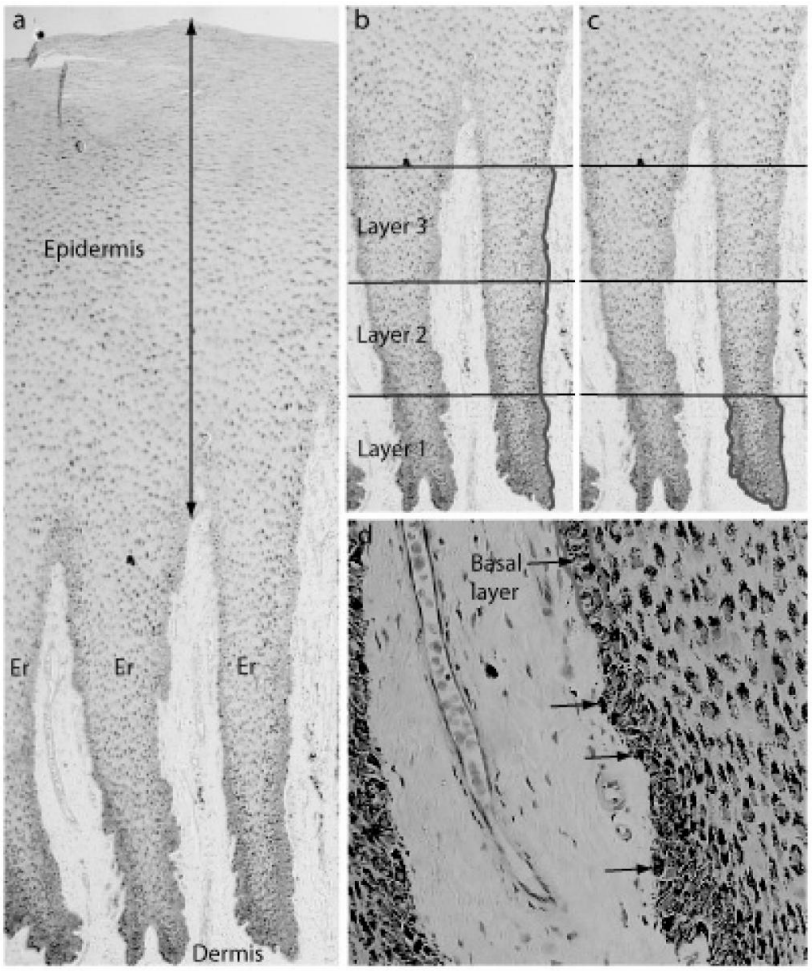

Figure 2.3. Haematoxylin & Eosin-stained (H&E) sections of fin whale epidermis. a) Skin section showing epidermis, dermis and several epidermal ridges (Er). b) Three layers of 100 AU are dividing the Er along which the melanocytes were counted (grey line) to describe their distribution. c) Melanocytes were quantified in the first layer (grey line). d) Melanocyte location in the basal layer (examples showed by arrows).

I counted melanocytes in 116 Er (see details in Table 2.1) and found significant differences amongst layers in blue whale sections (Kruskal-Wallis, $\chi^2 = 29.76$, df = 2, $p = 3.45 \times 10^{-7}$), fin whale sections (Kruskal-Wallis, $\chi^2 = 50.16$, df=2, $p = 1.28 \times 10^{-11}$) and sperm whale sections (Kruskal-Wallis, $\chi^2 = 38.06$, df = 2, $p = 5.44 \times 10^{-9}$). Melanocyte counts decreased significantly between the first, second and third layers ($p < 0.02$ for all species; Figs. 2.4a-c), and were highest deeper in the epidermis;

consequently, melanocyte counts were conducted in the first (deepest) layer of 100 AU (Fig. 2.3c).

Table 2.1. Number of epidermal ridges in each layer (L) used for melanocyte counting.

Species	Number of individuals	L1	L2	L3
Blue whale	3	38	38	14
Fin whale	2	35	35	19
Sperm whale	2	43	43	20

To assess the relationship between the quantity of melanocytes and the perimeter of Er, I counted melanocytes in the first layer of five individuals (Bm = 2, Bp = 2 and Pm = 1) and calculated the Er perimeter for that layer using a crossed graticule. Melanocyte counts and Er perimeter were significantly correlated in blue whales (Spearman's correlation; $n = 34$; $p = 2.4 \times 10^{-4}$; Fig. 2.4d), sperm whales ($n = 33$; $p = 9.0 \times 10^{-10}$; Fig. 2.4e) and fin whales ($n = 38$; $p = 2.7 \times 10^{-3}$; Fig. 2.4f).

In order to estimate how many Er were necessary to obtain a representative mean of the melanocytes in each section, I counted melanocytes in the first layer of each Er and calculated the cumulative running mean on the randomized data (melanocyte count obtained for each Er). A total of 108 Er of two blue whales, two fin whales and a sperm whale were used for counting (details in Table 2.2). The mean number of melanocytes (±1) stabilised when more than three Er were analysed (Table 2.2; Figs. 2.4g-i).

Table 2.2. Cumulative running mean tests to determine the minimum number of epidermal ridge (Er) required for accurate melanocyte quantitation

Er	Blue whale		Fin whale		Sperm whale
n*	15	18	38	13	24
R1	1	1	1	2	1
R2	3	2	2	3	1
R3	1	1	2	2	2

* n: number of Er counted in each individual. R1 to R3: cumulative running tests after different data randomization.

Melanocyte counts varied significantly between species, being lowest for blue whales (14.1 M ± 0.77), and highest for fin whales (30.8 M ± 1.71; Kruskall-Wallis, $\chi 2 = 54.1$, df = 2, $p = 1.8 \times 10^{-12}$) as predicted.

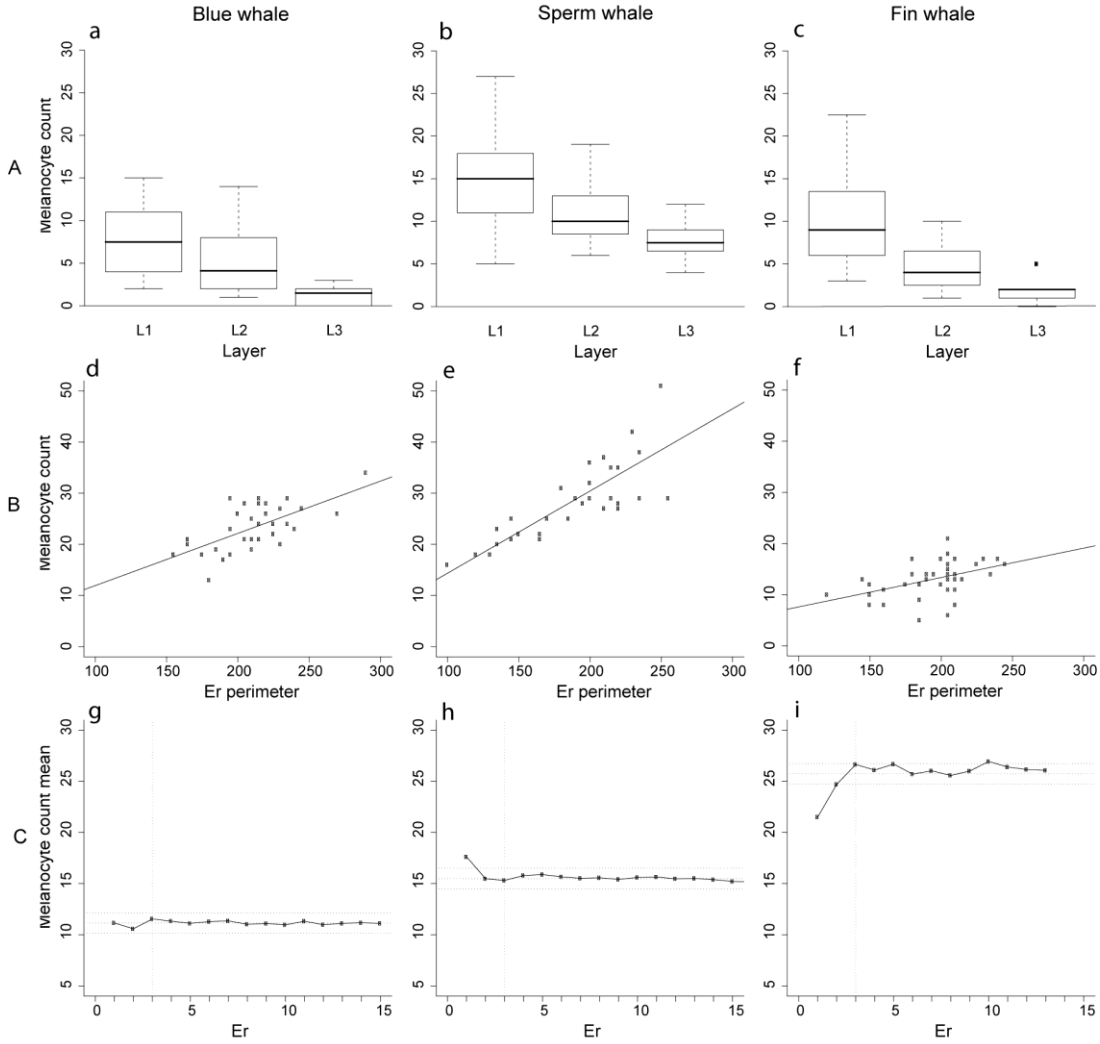

Figure 2.4. Plots describing standardization of epidermal melanocyte counts using skin sections of three cetacean species (blue whale, Bm; sperm whale, Pm and fin whale, Bp). **A.** Boxplots of melanocyte counts showing significant differences amongst the three skin layers (L1-L3). Melanocyte numbers were highest when deeper in the epidermis (L3). **B.** The quantity of melanocytes was directly correlated with the perimeter of epidermal ridges (Er). **C.** Cumulative running mean of melanocyte counts shows that three Er are sufficient to obtain a representative melanocyte count per individual.

2.4 Solar ultraviolet radiation data

The amount of solar ultraviolet radiation (UVR) that reaches the biosphere depends on the interaction of several variables such as the time of day, latitude, meteorological conditions (e.g. cloud coverage) and pollution (Vernet et al., 2009). An element that greatly influences the quantities of UVR reaching the earth is the thickness of the ozone layer (McKenzie et al., 2007; Vernet et al., 2009). Although several electronic maps on ozone layer thickness around the globe are freely obtainable, at the time of conducting the present study, such information was not available for the study areas within the Gulf of California.

I was able to procure data on ozone measurements over Mexico City between 2007 and 2009 on the Total Ozone Mapping Spectrometer (TOMS) website (http://avdc.gsfc.nasa.gov; OMI overpass file for Mexico City kindly sent by Prof. McPeters on 26/10/2010). These data were measured by the Ozone Monitoring Instrument (OMI) launched aboard the EOS-Aura satellite in late 2004. However, Mexico City is at a different latitude from the Gulf of California and has dissimilar climatological conditions. Consequently such data could not be used reliably.

Via collaboration with NASA scientists Elizabeth Weatherhead and Paul Newman, I had access to plots on total ozone (Fig. 2.6) and UV index (Fig. 2.7) over the Gulf of California (data of records for 26°-28°N and 109°-112°W) between 2007 and 2009. These plots had been constructed using total ozone observations from the Total Ozone Mapping Spectrometer (TOMS) and Ozone Monitoring Instrument (OMI).

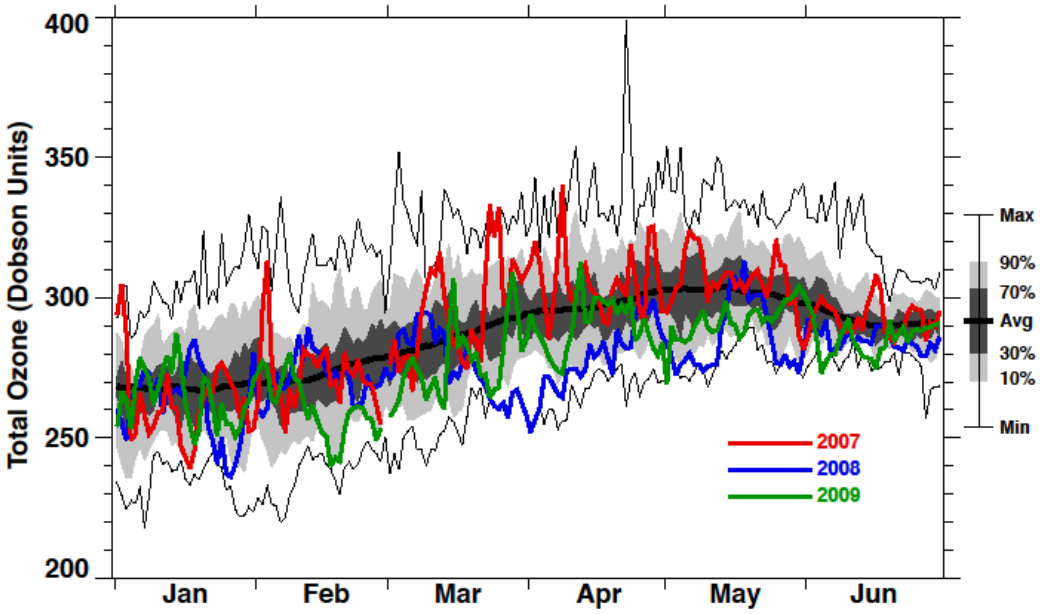

Figure 2.6. Total ozone levels recorded between January and June over the Gulf of California (data average records for 26°-28°N and 109°-112°W) for the years 2007 (red), 2008 (blue) and 2009 (green). The years of observations extend from 1979-2010 (32-year running average shown by a thick black line). The lower (upper) thin black line shows the minimum (maximum) value observed. The grey shading shows the pdf distribution (probability distribution function, i.e., 80% of the observations are within the light grey shading, while 40% are within the dark shading). Plot obtained using total ozone observations from the Total Ozone Mapping Spectrometer (TOMS) and Ozone Monitoring Instrument (OMI). Figure kindly made available by Paul Newman and Eric Nash.

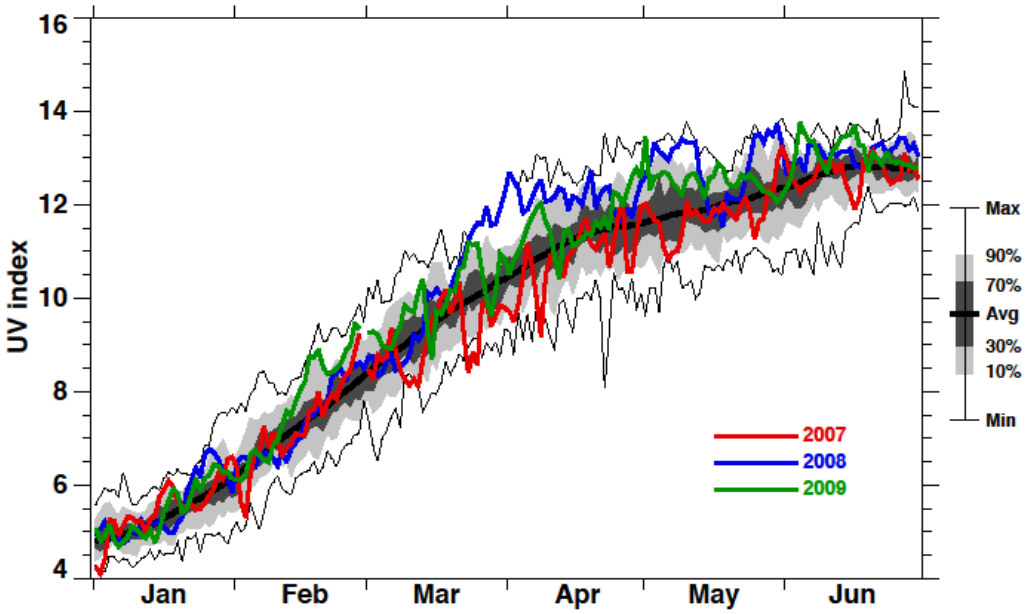

Figure 2.7. UV index recorded between January and June over the Gulf of California (data average records for 26°-28°N and 109°-112°W) for the years 2007 (red), 2008 (blue) and 2009 (green). This calculation (a simply function of total column ozone and the solar zenith angle) was realized under local noon and clear sky conditions and does not include cloud or aerosol effects. The years of observations extend from 1979-2010 (32-year running average shown by a thick black line). The lower (upper) thin black line shows the minimum (maximum) value observed. The grey shading shows the pdf distribution (probability distribution function, i.e., 80% of the observations are within the light grey shading, while 40% are within the dark shading). Plot obtained using total ozone observations from the Total Ozone Mapping Spectrometer (TOMS) and Ozone Monitoring Instrument (OMI). Figure kindly made available by Paul Newman and Eric Nash.

Although I was unable to obtain ozone and UVR measurements for the dates the whales were sampled, the information shed from the above plots was valuable for my study. The plots showed that, as expected for Northern mid-latitudes, ozone increases from mid-winter to spring, and then decreases over the course of the summer into early fall (Fig. 2.6). Interestingly, day-to-day ozone fluctuations of around 10 DU (see Fig. 2.6) were higher than the average decreasing rate of 0.3 DU per year (Paul Newman, pers. comm.). Noteworthy, there is an important increase of the UV index by almost a factor of three between January and April, months at which the values plateau (Fig. 2.7).

CHAPTER 3: UVR-induced cetacean skin lesions – macroscopic and microscopic evidence of damage

This chapter has been published as an original manuscript in the journal Proceedings of the Royal Society: B (Appendix 3.1). The discussion of this chapter differed slightly from the discussion of the manuscript as it has now been adapted to comments and collegial criticisms received after publication.

3.1 Introduction

The skin is a barrier against the environment, essential for survival, and has been adapted to protect the organism from harmful agents, including ultraviolet radiation (UVR), which does not penetrate any deeper than the epidermis and the dermis (De Gruijl, 1997; D'Errico et al., 2007). The absorption of UVR by skin chromophores such as DNA induces a cascade of responses that includes occurrence of skin sunburn. This generally appears a few hours following UVR exposition and is typically described as redness (erythema) and swelling of the skin (oedema) (Ishii et al., 1997; De la Coba et al., 2009). When UVR exposure is intense, large blisters can appear on the surface of the epidermis (Ishii et al., 1997; De la Coba et al., 2009), especially in light skinned individuals that produce less melanin, a "natural sunscreen" (Lin and Fisher, 2007; Brenner and Hearing, 2008). UVR-induced lesions can also be observed deep within the epidermis using common histology stains such as haematoxylin–eosine (H&E) or specific stains such as TUNEL, which detects apoptotic cells (Nakaseko et al., 2003; Yamaguchi et al., 2008). Characteristic microscopic lesions include cytoplasmic vacuoles, intracellular and intercellular oedema, glycogen deposits and microvesicles (Ohkawara et al., 1972; Nakaseko et al., 2003; De la Coba et al., 2009). It is also common to observe the infiltration of inflammatory cells surrounding the lesions (De la Coba et al., 2009). Interestingly, while many studies on the effects that UVR exposure can exert on the skin have been conducted in humans and laboratory animals, similar studies in wildlife species are still rare. However, the effects of UVR are unlikely to be negligible, particularly for

species such as cetaceans, which by anatomical (e.g. lack of fur, feathers or keratinized plates) or life-history constraints (e.g. obligate air-breathing physiology, lactation or socialization at the sea surface) are unable to avoid continuous exposure to UVR (Geraci et al., 1986; Acevedo-Whitehouse and Duffus, 2009).

In recent years, skin lesions in cetaceans from various regions around the globe have increasingly been reported (Wilson et al., 1999; Van Bressem et al., 2009). The aetiologies of some of these lesions that show distinct patterns have already been characterized (e.g. lobomycosis, caused by the fungus *Lacazia loboi* (Taborda et al 1999) and poxvirus tattoo skin disease; Van Bressem et al., 2009), but many other types of lesions (e.g. blistering lesions) have not (Flach et al., 2008). It is possible that uncharacterized cetacean skin lesions are linked to mounting levels of UVR, given that for each percentage of stratospheric ozone lost, erythemal (skin damaging) radiation increases 1.2% (McKenzie et al., 2007). Studies in humans and laboratory animals have shown that individuals with relatively lower concentrations of melanin (lighter-skinned) are more sensitive to UVR (Lin and Fisher, 2007; Yamaguchi et al., 2008). Furthermore, when controlling for skin pigmentation, longer periods of exposure to the sun influence the severity of skin damage (Chang et al., 2009). If this knowledge were extrapolated to cetaceans, it would be expected that cetaceans with paler skin pigmentation and those spending longer periods on the sea surface will be more severely exposed and consequently develop more skin lesions.

I tested these predictions by examining gross skin lesions using high-quality photographs, and microscopic lesions using skin sections stained with routine and specialized staining to detect apoptotic cells in three seasonally sympatric cetacean species (blue, fin and sperm whales) from the Gulf of California. Marked differences in skin pigmentation among these species, as well as distinct surface behaviours (section 1.5.2, Chapter one), made it possible to investigate the potential photoprotective role of cetacean skin pigmentation and the significance of duration of exposure on the development of lesions.

3.2 Material and Methods

Using 156 high-quality photographs and 142 skin biopsies collected from blue whales, fin whales and sperm whales in the Gulf of California, Mexico (details in Table 3.1), I characterized and quantified the number of gross skin lesions and microscopic epidermal abnormalities and investigated their relationship with individual skin pigmentation estimated as number of melanocytes (method described in detail in Chapter two). To avoid any bias, I examined all photographs and histology sections from all three seasons at the end of the 2009 sampling season.

Table 3.1. Number of cetacean skin samples and photographs collected per year included in this chapter.

	Photographs				Skin sections			
Species	2007	2008	2009	TOTAL	2007	2008	2009	TOTAL
Blue whale	48	28	22	98	40	25	6	71
Fin whale	6	11	17	34	12	12	26	50
Sperm whale	ns	ns	24	24	ns	21	ns	21

* ns: No sample collected

3.2.1 Analysis of gross skin lesions

Gross skin lesions were determined in a standardized area on each whale using high-quality photographs as described in the paragraph below. Photos were included only when the whale's flank was perpendicular to the camera and focus was sharp.

3.2.1.1 Defining a standardized area from high-quality photographs

The few published studies on cetacean skin lesions have counted abnormalities on the entire body surface that appears on a photograph (Hamilton and Marx, 2005; Brownell et al., 2008; Bearzi et al., 2009). However, as species and individuals do

not expose the same proportion of their total body when surfacing, comparing the number of lesions between species and/or individuals might be misleading. To circumvent this problem, I defined a standardized area of the whale dorsal surface in which to count lesions. First, I demonstrated that a linear relationship exists between the dorsal fin length (DFL) and the whale body length. Thus, the DFL was used as a reference unit to draw an area in which to count the lesions.

I investigated the relationship between the dorsal fin length and the body length (defined and measured from the nasal holes to the top of the fin). To achieve this, I first drew two lines that followed the animal's body curvature. The segment obtained by joining the dorsal fin to the point where both lines intersected was defined as the base of the dorsal fin (Fig. 3.1). The length of the base of dorsal fin (LDF) was measured three times using SigmaScanPro (version 4.0) and the mean obtained was used as the final measure. I determined the LDF for 30 blue whales (LDF mean = 0.60 m ± 0.14 SD) and compared these values to their body length obtained by Ortega Ortiz (Ortega-Ortiz, 2009). I used a Spearman test to examine the correlation between both measures. All analyses were conducted in R (Ihaka and Gentleman, 1996).

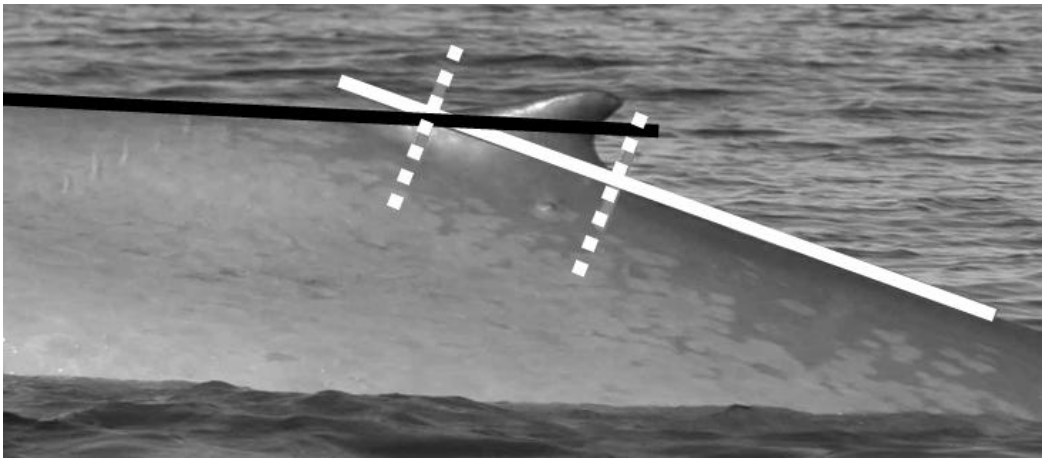

Figure 3.1. Method to define the base of the dorsal fin. Two lines (black and white) that followed the animal's body curvature are first drawn. The segment obtained (between doted lines) is defined as the base of the dorsal fin. This image shows a blue whale dorsal fin.

Blue whale body length was linearly related to LDF (Fig. 3.2a; Spearman test: $p = 4.53x10^{-4}$, rho = 0.60). As blue and fin whales have the same morphology (size and shape), I made the assumption that an equivalent relationship existed for fin whales. For sperm whales, which have different body characteristics, I conducted the same analysis in five individuals and confirmed a similar positive linear relationship (Fig. 3.2b; Spearman test: p = 0.02, rho = 1). Sperm whale body length and total dorsal fin height were also significantly correlated (Fig. 3.2c; Spearman test: p = 0.02, rho = 1).

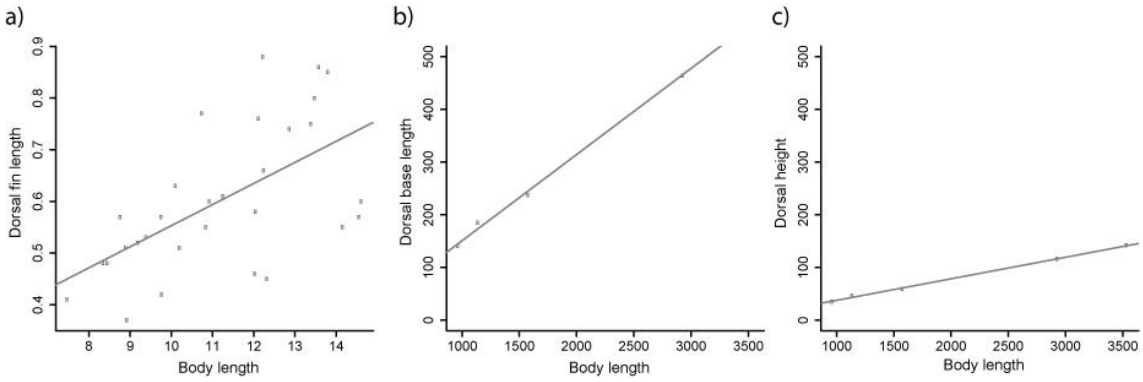

Figure 3.2. Relationship between whale body length and dorsal fin base length in the three species a) blue whales (n=30; measured in metres), b) sperm whales (n=5; measured in pixels); dorsal fin height in c) sperm whales (n=5; measured in pixels).

For blue whales, body length was 19.2-fold longer than LDF. For sperm whales, body length was 6.4-fold longer than LDF (see details in Table 3.2). LDF:body length ratio was 3-fold higher in blue whales than sperm whales. Thus, if I was to use LDF as a reference unit with which to define the counting area in sperm whales, this area would be impractically large. Instead, I used the height of the dorsal fin (HDF) to standardize the counting area as it was 3.8-fold smaller than its base (see details in Table 3.2).

Table 3.2. Cetacean morphometric ratios.

Ratio	Species	n	Mean	SE
B:b	Blue whale	30	19.2	0.7
B:b	Sperm whale	5	6.4	0.1
b:h	Sperm whale	14	3.8	0.1

*B:b: Body length:dorsal fin base length.

*b:h: dorsal fin base length:dorsal fin height.

Having defined LDF as a reference unit for blue and fin whales and HDF for sperm whales, I drew four to six squares, each measuring one reference unit per side, on the dorsal surface of the whale (Fig. 3.3) using Adobe Photoshop (version 7.0). The

number of lesions per individual was defined as the number of lesions counted in the previously established area (corresponding to six squares).

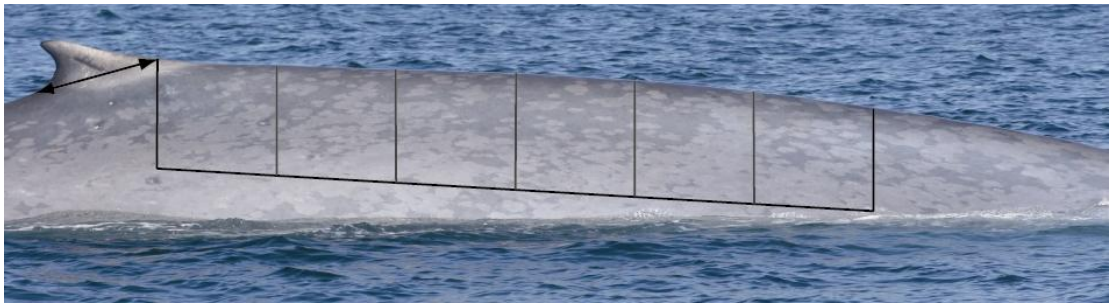

Figure 3.3. Photograph of a blue whale showing the area where skin lesions were recorded. The length of the dorsal fin was used as a reference unit to draw the six squares.

3.2.1.2 Gross skin lesions

Occurrence, prevalence (%) and intensity (number of lesions/individual) of gross skin lesions were determined in the previously-defined area. I recorded gross blisters similar to those observed after severe sun exposure in laboratory animals (Ishii et al., 1997; De la Coba et al., 2009) (Fig. 3.4). Bite marks (Fig. 3.4) were used as an environmental control as it would not be sensible to expect a trend related to environmental changes in the prevalence of these predation marks. To ensure that the blistering observed was not related to poxvirus infection, DNA extracted from a subset of individuals that had blisters was sent for pan-poxvirus PCR assays to Dr. Barbara Blacklaws, Cambridge Infectious Disease Consortium, University of Cambridge. No evidence of poxviral infection was found (Barbara Blacklaws, unpublished data).

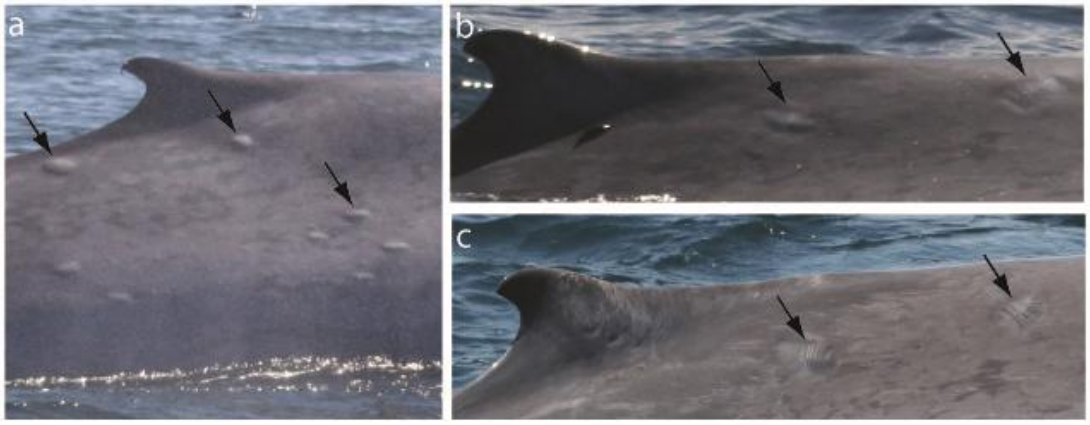

Figure 3.4. High-resolution photographs of blue whale gross lesions. a) Gross blistering (examples indicated by arrows), b) Bite marks seen as oval-shaped lesions with sunken perimeters (arrows), c) Bite marks seen as parallel teeth marks (arrows).

3.2.2 Analysis of microscopic lesions

In humans, evidence of microscopic sunburn lesions include skin inflammation characterised by leukocyte infiltration, oedema and microvesicule formation (Nakaseko et al., 2003; De la Coba et al., 2009). Other characteristic UVR-induced lesions comprise the presence of cytoplasmic vacuolation, keratinocyte glycogen deposition and apoptotic cell also called sunburn cells (Ohkawara et al., 1972; Nakaseko et al., 2003; De la Coba et al., 2009). I searched for evidence of these lesions in the whale skin sections.

3.2.2.1 Skin inflammation and cytoplasmic vacuolation

Skin inflammation and cytoplasmic vacuolation were assessed using routine H&E staining (Nakaseko et al., 2003; De la Coba et al., 2009). Each whale skin section (in total 142, details in Table 3.1) was cut longitudinally (~ 3 mm), placed in a histocassette and sent to Abbey Veterinary Services for processing (http://www.abbeyvetservices.co.uk). Briefly, the skin sections were embedded in paraffin and sliced longitudinally with a microtome. The sections were deparaffinized and rehydrated before staining with hematoxylin and counterstaining with eosin. Finally, the skin sections were dehydrated and coverslips were mounted

over them. With this procedure basophilic structures appeared blue (e.g. nuclei) and acidophilic appeared pink (e.g. cytoplasm, collagen) (Fig. 3.5abc).

3.2.2.2 Apoptosis

The presence of apoptotic cells was investigated in a subset of 43 individuals (18 blue whales, 14 fin whales and 11 sperm whales) using the terminal deoxynucleotidyl transferase-mediated deoxyuridine triphosphate-biotine nick end labelling method (DeadEnd^{TM} Colorimetric TUNEL system, Promega), which detects DNA fragmentation, the final stage of apoptosis (Nakaseko et al., 2003; Lo et al., 2005; Yamaguchi et al., 2006). I used this technique in a subset of individuals due to time and financial constraints. To ensure that the TUNEL staining correctly reflected apoptosis, six of the skin sections were selected at random (two blue whales, two fin whales and two sperm whales) and stained using cleaved caspase-3 (a specific indicator of apoptosis) antibodies (Nakaseko et al., 2003; Yamaguchi et al., 2006). The procedures were conducted at the Centre for Cutaneous Research, Blizard Institute of Cell and Molecular Science, Queen Mary University of London, in collaboration with Prof. Edel A. O'Tool and Dr. Manuraj Singh. For this, I cut new sections from the original paraffin blocks containing the whales' skin samples. The blocks were first cooled in an ice water bath before cutting 5-µm sections with a microtome. The sections were placed in a 45ºC water bath and set on a frosted microscope slide. The slides were kept at 40ºC for 12-20h. To deparaffinise the sections, the slides were immersed twice in a fresh xylene solution for 5 min and washed with 100% ethanol for 3 min. For re-hydration, slides were immersed in graded ethanol (twice in 100% ethanol, once in 90% ethanol, and once in 70% ethanol) during 3 min each and finally immersed in distilled water.

Between each following protocol step involving the use of a new solution, slides were washed three times in PBS-1X for 5 min. So first, slides were placed in a 0.85% NaCl solution during 5 min. Firstly, the sections were fixed in a 4% formaldehyde solution for 15 min. After removing the liquid from the sections, 100 µl of proteinase K solution (20 µg/ml) was added to each section and incubated for 10 min. The tissue sections were fixed again in a 4% formaldehyde solution for 5 min and incubated for 10 min with 100 µl of equilibration buffer (200 mM potassium

cacodylate, 25 mM Tris-HCl, 0.2 mM Dithiothreitol, 0.25 mg/ml Bovine Serum Albumin, 2.5 mM cobalt chloride). After paper blotting excess buffer, 100µl of rTdT reaction mix (98µl of equilibration buffer, 1µl of biotinylated nucleotide mix, 1µl of rTdT enzyme) were added. The sections were covered with plastic coverslips and incubated at 37ºC for 1h in a chamber (humidity was maintained with humidified paper). This step allowed the end-labelling reaction to occur. To terminate the nucleotide incorporation of biotinylated deoxyuridine triphosphate, slides were immersed in 2X SSC (0.075M NaCl and 0.1M sodium citrate) for 15 min. Endogenous peroxidases were blocked by immersing slides in 0.3% hydrogen peroxide for 5 min. The sections were incubated with 100µl of streptadivin HRP solution (1:500 in PBS-1X) for 30 min. DAB (3,3'-Diaminobenzidine) staining solution was added as needed until the stain developed. The skin sections were rinsed several times in deionised water and then mounted with permanent mounting medium. When observed under the microscope, the nuclei of apoptotic cells appeared brown (e.g. Fig. 3.5def).

A parallel procedure, immunohistochemical apoptotic cell detection (using antibodies for caspase-3), was conducted as follows. After rehydrating the slides (described in the first paragraph of this section), those were placed in a 1X sodium citrate buffer (pH=6), brought to boil and maintained at sub-boiling temperature for 10 min. This step, called antigen unmasking, breaks the protein cross-links produced by formalin fixation and thus uncovers hidden antigenic sites (MacIntyre, 2001). The slides were then cooled on the bench for 20 min, washed three times by pipetting PBS-1X over the sections and after that, incubated in a fresh 3% H_2O_2 solution for 5 min. After washing the slides as explained above, each skin section was incubated with 100 µl of 5% horse serum (blocking solution) during 30 min. After removing the blocking solution, 100 µl of caspase antibody [cleaved caspase-3 (Asp175) antibody] were added on each skin section and the slides were incubated overnight at 4ºC. The following day, the antibody solution was removed and sections were washed five times during 2 min in PBS-1X. After that, 100 µl of secondary antibody (universal anti-mouse/rabbit Ig) were added onto each section and left for 30 min. I used a purple staining (Vector® VIP Peroxidase Substrate; Vector Laboratories, UK) and controlled the level of staining under the microscope. As soon as the sections were correctly stained, the slides were immersed in distilled water for 5 min twice.

The sections were then dehydrated and coverslips were mounted as described previously. The nuclei of apoptotic cells stained dark purple when observed under the microscope.

3.2.2.3 Keratinocyte glycogen deposition

Periodic Acid Schiff (PAS) and diastase-resistant (DPAS) staining were used to verify whether the "cell swelling lesions" observed in the skin sections were in fact an accumulation of glycogen, which can be seen after UVR exposure (Ohkawara et al., 1972). For that, six duplicate paraffin-embedded skin sections of 11 individuals (5 blue whales, 2 sperm whales and 4 fin whales) presenting different levels of cell swelling were sent for PAS/DPAS staining to Prof. Rino Cerio from the Institute of Pathology, Royal London Hospital. Briefly, as described previously, the skin sections were first deparaffinized and rehydrated. They were subsequently stained through a series of immersion baths (5 min in a 0.5% periodic acid solution, 15 min in Schiff reagent, and 1 min in Mayer's hematoxylin). Between each immersion, slides were washed for 5 min in distilled water. Finally, sections were dehydrated and coverslips were mounted. In the end, glycogen was observed in magenta tones under the microscope. Each duplicate skin section was stained with DPAS, which digests glycogen. This slide was used as negative control. The difference in the intensities between the two stains (PAS and DPAS) was used to determine the presence of glycogen in whale skin sections. I failed to show a correlation between "cell swelling lesions" and accumulation of glycogen.

3.2.2.4 Microscopic lesion counts

The occurrence (presence/absence in an individual) and prevalence (% of individuals) of microscopic skin lesions were determined. The lesions recorded were leukocyte infiltrate, oedema, microvesicule, cytoplasmic vacuoles, glycogen deposition and apoptotic cells. I evaluated the intensity (number per individual) of microvesicules in a full skin section, whose area was measured on digital photographs using Sigma Scan Pro. For each individual, the number of microvesicules per 100 squared arbitrary units was obtained. Apoptotic cell counts and cytoplasmic vacuoles were categorized in four, from 0 (absence) to 3 (high level)

(Fig. 3.5) and semi-quantitative results were obtained. As a further confirmation of the nature of the observed lesions, all slides were examined by dermopathologists Prof. Edel'O'Toole and Dr. Manuraj Singh from the Centre for Cutaneous Research, Blizard Institute of Cell and Molecular Science, Queen Mary University of London.

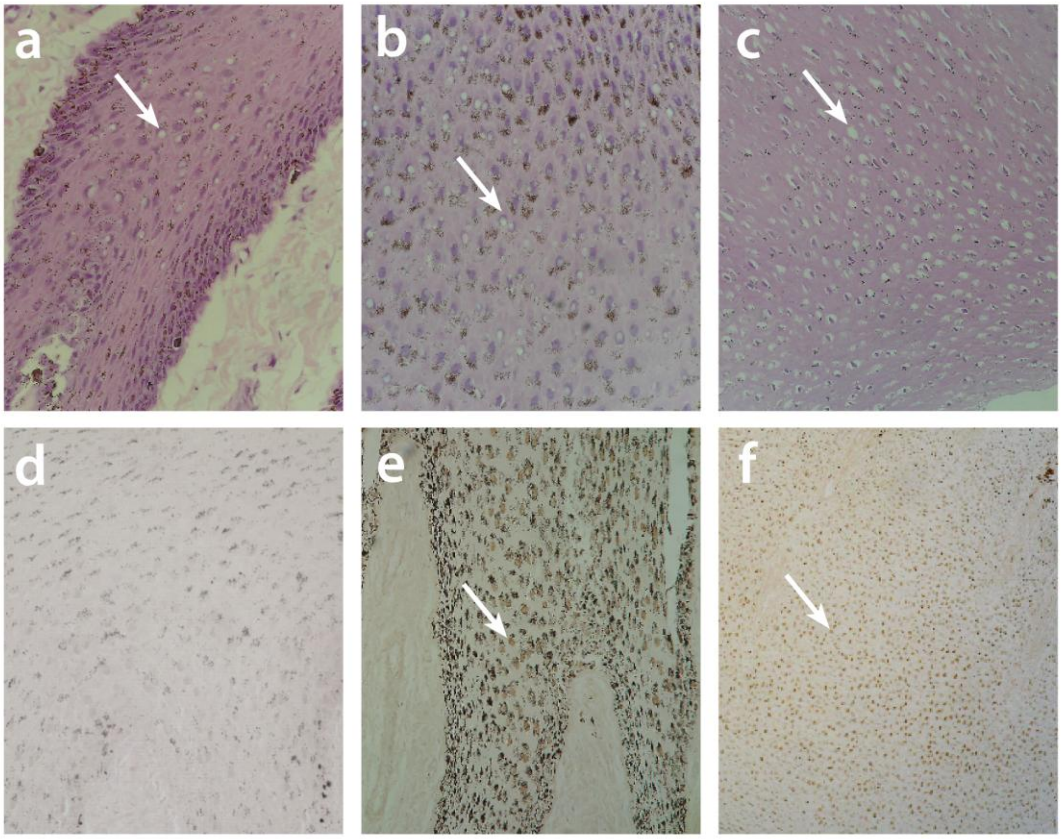

Figure 3.5. Graded levels of acute sun-induced damage in whales. Four categories were defined for cytoplasmic vacuolation and apoptosis, from 0 (absence) to 3 (high level). The top half of the figure (images a, b, and c) shows three categories (1, 2 and 3, respectively) of cytoplasmic vacuolation (see arrows) in fin whales (a and b) and blue whale (c) H&E stained skin sections. The bottom half of the figure (images d, e, and f) shows different categories of apoptotic cells (see arrows) detected with TUNEL staining. d) Absence of apoptotic cells in a blue whale skin section. e) Moderate (category 2) apoptotic cells (cells with light brown nucleus) in a fin whale skin section. f) High counts of apoptotic cells in a sperm whale skin section. (All images are seen at 250 X magnification except for the bottom right image, which corresponds to 60 X).

3.2.3 Statistical methods

Differences in lesion prevalence between species were examined with Fisher-exact tests. Non-parametric Kruskal-Wallis tests were used to compare the intensity of lesions between species. Generalized linear models (GLMs) were constructed to investigate interspecies differences in melanocyte counts and epidermal lesions, and temporal trends in lesion prevalence. Length of time spent at the surface (ST) and skin colour (SC) were defined as bimodal factors (short=1, long=2; light=1; dark=2). Binary data on cytoplasmic vacuolation were collapsed to generate response categories (0-2=absent or low, 3=high), as I was interested in examining differences in the frequency of highly-damaged skin between species. A similar method was used to analyse apoptotic cells (0-2=absent or low and 3=high and widespread distributed). Where appropriate, explanatory variables were indicated as bimodal responses and the model's error structure defined accordingly. Analyses were conducted in R (Ihaka and Gentleman, 1996). All recaptured individuals were excluded from the analyses to avoid pseudoreplication.

3.3 Results

3.3.1 Skin lesions, overall prevalence and intensity

Blister-type lesions (hereafter blisters; Fig. 3.4a) were present in 28% of the individuals, and the number of blisters recorded per individual ranged between 1 and 60. This number is likely to underestimate the total number of blisters present in an individual as counts were conducted within a standardized area (section 3.2.1.1). Microscopic examination revealed a range of abnormalities, including intracellular oedema, cytoplasmic vacuolation, glycogen deposition, microvesicles and leukocyte infiltration. While more than 90% of the whales presented cytoplasmic vacuoles, almost none showed leukocyte infiltration (<1%). The overall prevalence of intracellular oedema and microscopic vesicles was similar, being 66% and 68%, respectively. For each skin section, I recorded between 1 and 73 microvesicles, which after correction (section 3.2.2.4) ranged from 2 to 324. Apoptotic cells (those that stain positive to TUNEL), were observed and confirmed by using antibodies for

cleaved caspase-3 (Yamaguchi et al., 2006). These cells were present in nearly all (95%) of the skin sections analyzed, and in more than half (56%) of the whales were distributed throughout the epidermis (category three, see Fig. 3.5f and Fig. 3.6), including the basal layer. Basal dendritic melanocytes, and basal and suprabasal perinuclear melanin pigments were common findings.

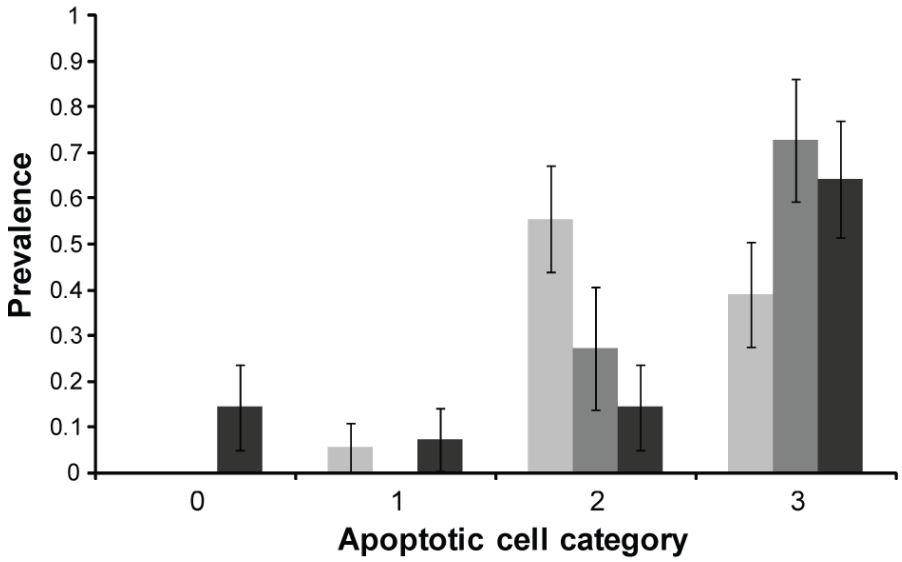

Figure 3.6. Prevalence of the different categories of apoptotic cells (AC) found in cetacean skin. Blue whales in pale grey bars (n = 18), sperm whales in grey bars (n = 11) and fin whales in dark grey bars (n = 14). Bars = ± SE.

No significant differences were observed between sex or age category for any of the lesions recorded in blue whales, the species for which this information was available. As these variables, including minimum age, did not appear to play a significant role in the prevalence of lesions, they were excluded from the rest of the analyses.

3.3.2 Interspecies differences

The prevalence of gross blisters, cytoplasmic vacuolation, intracellular oedema and glycogen deposition varied amongst species, being lowest for the fin whale and equally highest for blue and sperm whales (Fig. 3.7). Prevalence of apoptotic cells did not differ amongst species. However, differences in the frequency of apoptotic

cell categories (AC) present in each species were observed (Fig. 3.6). Both sperm whales and fin whales showed high levels and a widespread distribution of apoptotic cells (AC 3 significantly higher compared to the other categories; Fisher tests: $p<0.04$, $\chi^2>4$ overall; Fig. 3.6). This was not seen for blue whales (Fig. 3.6). The prevalence of microscopic vesicles differed amongst species (GLM, df=2, $\chi^2=4.57$, p=0.01) with the lowest value recorded for sperm whales. The intensity of blister-type lesions was not different amongst species (Kruskall-Wallis: df=2, $\chi^2= 0.62$, p=0.73).

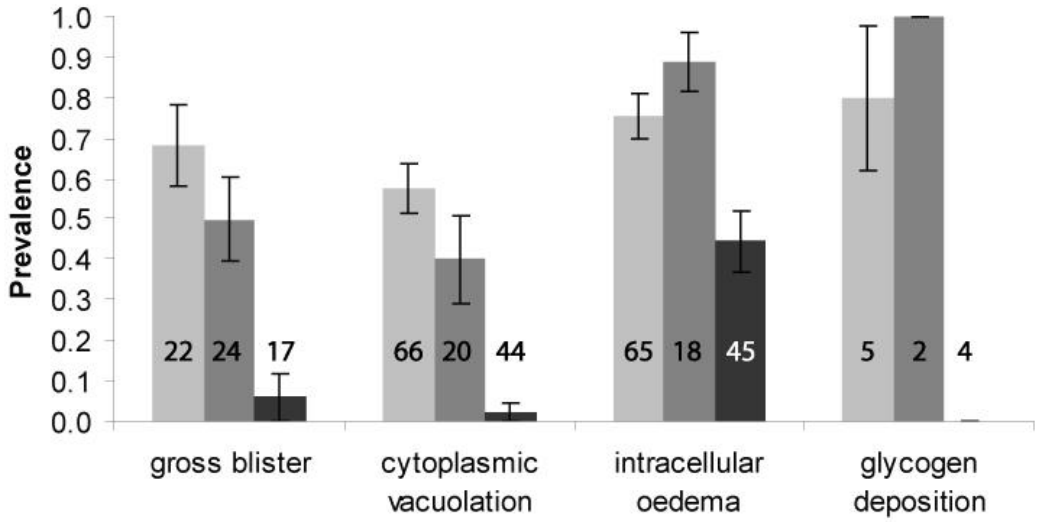

Figure 3.7. Prevalence of gross blisters and microscopic epidermal abnormalities in blue whales (pale grey bars), sperm whales (grey bars) and fin whales (dark grey bars). The prevalence of blisters was calculated for 2009, the only year ID-photographs for sperm whales were obtained. Estimates of cytoplasmic vacuolation were transformed to binary data (categories 0-2=absent or low, category 3=high). Sample sizes are indicated in the figure. Bars = ± SE.

3.3.3 Skin colour and surface time implication

For each species, cytoplasmic vacuolation and intracellular oedema were both inversely predicted by melanocyte counts ($p < 0.02$ for all responses; full model details in Table 3.3). A positive relationship was found between individual

melanocyte counts and apoptosis for all three species (Table 3.3). Gross blisters were not significantly related to melanocyte counts (Table 3.3).

Table 3.3. Effect of melanocyte counts (M) and species (sp) on the prevalence of epidermal lesions and apoptotic cells. Data presented is the summary of four independent GLMs (binomial error distribution; logit link). Categorical data on cytoplasmic vacuolation and apoptotic cells were collapsed to generate two response categories (0-2=absent or low, 3=high), as I was interested in examining differences in the frequency of highly-damaged skin between species. Bold text indicates $p \leq 0.05$.

Response terms	Term	df	Likelihood ratio	p
Cytoplasmic vacuolation	M	1	13.65	**2.20×10^{-4}**
	sp	2	17.94	**1.27×10^{-4}**
Intracellular oedema	M	1	22.82	**1.78×10^{-6}**
	sp	2	9.90	**7.09×10^{-3}**
Gross blisters	M	1	0.38	0.54
	sp	1	5	**0.02**
	M:sp	1	4.98	**0.03**
Apoptotic cells	M	1	5.92	**0.01**
	sp	2	0.52	0.77

A fitted generalized linear model (GLM) showed that the length of sun exposure (i.e. time remaining on the sea surface) significantly predicted epidermal lesions, although skin pigmentation remained the most important explanatory factor for all lesions (see Table 3.4 for model details).

Table 3.4. Effect of length of time spent at the surface (ST) and skin colour (SC) on the prevalence of skin lesions and apoptotic cells. Data presented is the summary of four independent GLMs (binomial error distribution; logit link). ST and SC were defined as bimodal responses (short=1, long=2; light=1; dark=2). Bold text indicates $p \leq 0.05$.

Response terms	Term	df	Likelihood ratio	p
Gross blisters	ST	1	6.53	**0.011**
	SC	1	9.64	**0.002**
Intracellular oedema	ST	1	6.15	**0.013**
	SC	1	10.91	**0.001**
Cytoplasmic vacuolation	ST	1	0.17	0.68
	SC	1	44.35	**2.7×10^{-11}**
Apoptotic cells	ST	1	0.84	0.36
	SC	1	4.78	**0.03**

3.3.4 Temporal variation

Blue whales sampled at the beginning of each sampling season (February) showed a higher prevalence of microscopic lesions than those sampled at the end of each sampling season (May-June) (see Fig. 3.8; full GLM and model details in Table 3.5).

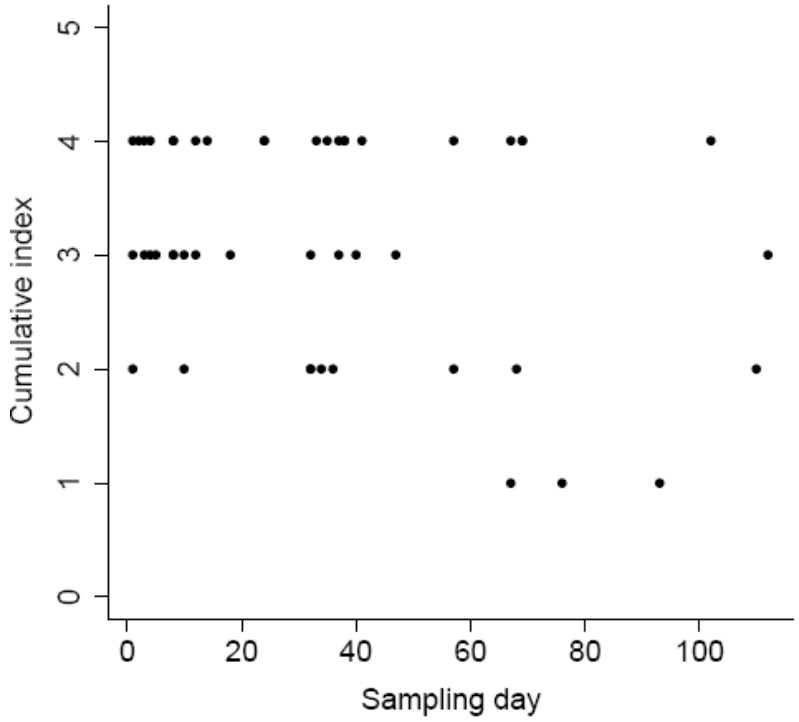

Figure 3.8. Changes in occurrence of microscopic skin lesions of blue whales between February and June. Sampling day indicates the moment the biopsy was taken (day 0 through 20 = February, 21 through 50 = March, 51 through 80 = April and more than 81 = May and June). I included only individuals that were seen for the first time in that season when sampling. Lesion cumulative index takes into account the presence (1) or absence (0) of intracellular oedema and the category of cytoplasmic vacuolation (0 to 3). Each dot represents a different individual.

Table 3.5. Effect of sampling day and year on the presence of blue whale microscopic skin lesions. The cumulative index takes into account the presence (1) or absence (0) of intracellular oedema and the category of cytoplasmic vacuolation (0 to 3). Sampling day corresponds to the moment the biopsy was taken, and includes only individuals which were seen for the first time in that season at the time of sampling. Bold text indicates $p \leq 0.05$.

Response term	Term	df	Likelihood ratio	p
Cumulative index	Sampling day	1	37.99	**0.04**
	Year	2	34.13	0.09

In blue whales, the species for which I had data and samples spanning the study's three-year period, I found that while bite marks were constant (GLM: LR = 110.33, df = 2, p = 0.18), the prevalence of gross blisters rose significantly over time (GLM: LR = 90.50, df = 2, $p = 5.24 \times 10^{-5}$; Fig. 3.9), being markedly higher in 2009. A similar, but statistically non-significant, upwards trend was observed for cytoplasmic vacuolation (GLM: LR = 5.44, df = 2, p = 0.07; Fig. 3.9). Blue whale epidermal apoptotic cells and melanocyte counts also expanded in time (GLM: LR = 16.00, df = 2, p = 0.04; ANOVA: F = 4.33, df = 2, p = 0.02, respectively), a trend that was consistent in fin whales, the darkest species studied (GLM: LR = 5.00, df = 1, $p = 3.6 \times 10^{-3}$; ANOVA : F = 11.20, df = 2, $p = 1.74 \times 10^{-4}$). Intensity did not vary between years for both types of macroscopic lesions (Kruskal-Wallis: χ^2=0.30, df=2, p=0.86 for blisters; χ^2=1.67, df=2, p=0.43 for bite marks).

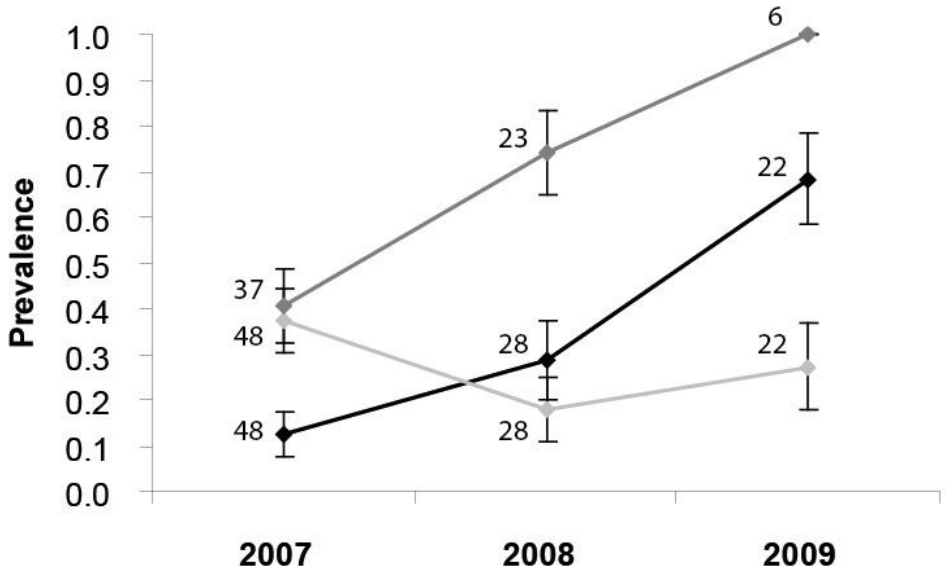

Figure 3.9. Temporal changes in the prevalence of blue whale skin lesions (blisters: black line; bite marks: pale grey line; cytoplasmic vacuolation: dark grey line). Sample sizes are indicated in the figure. Bars = ± SE.

3.4 Discussion

Photographs and histological analyses of whale skin biopsies revealed a range of abnormalities, including gross blisters, intracellular oedema, cytoplasmic vacuolation, glycogen deposition, microvesicles and leukocyte infiltration, all considered typical of acute sunburn and generally observed 24h after exposure (Ohkawara et al., 1972; Nakaseko et al., 2003). Basal dendritic melanocytes, and basal and suprabasal perinuclear melanin pigments (supranuclear caps) were common findings. These phenomena arise as protective responses following UVR exposure in humans (Stierner et al., 1989; Kobayashi et al., 1998).

As predicted under the assumption that pigmentation plays a significant photoprotective role (Yamaguchi et al., 2006; Lin and Fisher, 2007), the prevalence of blisters and microscopic abnormalities differed between species being lowest for fin whales, the darkest of the three study species. Moreover, for each species, melanocyte counts inversely predicted cytoplasmic vacuolation and intracellular oedema, providing further evidence of melanin-dependent photoprotection in

cetaceans. Interestingly, despite their different average melanocyte counts (section 2.4, Chapter two), prevalence of blisters and microscopic abnormalities was equal for blue and sperm whales. This finding might reflect their markedly dissimilar sea-surfacing behaviours. Sperm whales spend approximately 7 to 10 minutes breathing at the surface between foraging dives, whereas both blue and fin whales tend to surface for less than 2 minutes at a time (Croll et al., 2001). Moreover, although all species remain at the surface while resting, sperm whales also aggregate during daylight hours at the surface for socialization, remaining there for up to six hours at a time (Whitehead, 2003). Skin pigmentation and surface time both independently predicted epidermal lesions, although pigmentation remained the most important explanatory factor for all lesions examined.

A further non-exclusive factor that might explain the higher prevalence of lesions observed in blue whales compared to fin whales is the differences in their migration patterns. This is because UVR (and consequently, skin radiation dosage) varies across latitudes, being five times higher at lower latitudes compared to mid-latitudes (Ilyas, 2007). Across Mexico, UVR is high during most of the year, and the UV index at clear sky values (a measure of the potential human exposure to UVR) is normally 6 (high) to 15 (extreme) (Lemus-Deschamps et al., 2002). Blue whales from the north-east pacific population migrate annually from the feeding areas between Alaska and California (Calambokidis et al., 2009) to the Gulf of California, where most remain for at least two months (arriving in January/February and leaving in April/May) (Gendron, 2002), meaning that they will be abruptly exposed to higher UVR. Conversely, fin whales are year-round residents of the Gulf of California (Bérubé et al., 2002) and thus are constantly exposed to high UVR. If, as occurs in humans, sun-induced damage is most critical at first exposure to higher levels of UVR, it is possible that the observed variations in lesions, melanocytes and apoptotic cells between species reflects differences in migration. Interestingly, blue whales sampled at the beginning of each sampling season had a higher prevalence of microscopic lesions than those sampled at the end of each sampling season, suggesting that some acclimatization might occur, as is known to happen in humans (Sayre et al., 1981).

Exposure to UVR produces numerous effects on keratinocytes, including the formation of 'sunburn cells', namely keratinocytes showing eosinophilic cytoplasm with or without remnants of shrunken and condensed nuclei (Nakaseko et al., 2003; Takeuchi et al., 2004). These are apoptotic cells resulting from UVR-induced DNA damage (Takeuchi et al., 2004). I found that sunburn cells were present in nearly all of the skin sections, and in more than half of all whales these cells were distributed throughout the epidermis, including the basal layer. Such high levels and widespread distribution of apoptotic cells are uncommon in clinically-healthy mouse skin, and are associated with acute responses to UVR exposure, which peak between 24h and 48h (De la Coba et al., 2009). Highly pigmented skin is better able to prevent damage and remove potentially precancerous UVR-damaged cells via melanin-mediated apoptosis (Yamaguchi et al., 2008). Thus, whales with more pigmentation would be predicted to have higher epidermal apoptotic rates than less-pigmented whales when exposed to damaging levels of UVR. The positive relationship between melanocyte counts and apoptosis found for all species is consistent with this, implying that darker pigmentation confers an advantage for the elimination of UVR-induced damage in whales. Geographic variation in pigmentation has been described for Southern right whales, *Eubalena australis* (Schaeff et al., 1999) and humpback whales, *Megaptera novaeangliae* (Rosenbaum et al., 1995), and there is evidence that dorsal skin gradually darkens with age in right whales (Schaeff et al., 1999). To my knowledge, the evolutionary significance of whale skin pigmentation patterns has not been discussed in terms of photoprotection, but it is tempting to speculate, based on these findings, that selection might operate at this level.

Compared to previous years, 2009 showed markedly high levels of gross blisters prevalence for blue whales, the species for which I had data and samples spanning a three-year period. A similar trend was observed for cytoplasmic vacuolation. These patterns raise the possibility that 2009 might have been a particularly intense year in terms of UVR exposure. As levels of UVR are directly related to ozone thickness under clear sky conditions, it is tempting to speculate that the high prevalence of lesions observed in 2009 was due to intense exposure to UVR consequential to ozone-layer thinning. However, there is no evidence of reduction in the ozone layer between 2007 and 2009 (WMO-UNEP 2011). A more parsimonious explanation might be that regional cloud coverage was lower in 2009 than in the other two study

years. It is also possible that the observed trend reflects day-to-day variations in ozone levels (see Chapter two, section 2.5).

It is worth mentioning that I found no evidence that the population is aging (section 3.3.1), thus suggesting that the results do not reflect an age-related decrease in repair mechanisms (Matts and Fink, 2010). The obvious question to arise from these results is: if whales are historically adapted to daily UVR exposure, are their photoprotection and damage-repair mechanisms able to respond to increasing average radiation? When addressing this question I found that blue whale epidermal apoptotic cells and melanocytes also increased in time, a trend that also occurred in fin whales, the darkest species studied. If, as occurs in humans and laboratory animals, exposure to UVR increases the number of melanocytes (Stierner et al., 1989), stimulates the synthesis of melanin and leads to augmented apoptosis (Takeuchi et al., 2004), it is possible that our results indicate that cetaceans are able to elicit quick responses to high levels of UVR.

3.5 Conclusions

In this chapter, I provide evidence that epidermal lesions commonly associated with acute and severe sunburn are widespread in cetaceans and that as predicted, species with lighter pigmentation and those spending longer time at the sea surface are more severely affected. I demonstrated that, for all species, individuals with higher melanocyte counts tend to have fewer lesions and higher numbers of apoptotic cells. This suggests that the pathways used to limit and resolve UVR-induced damage in humans are shared by whales and that darker pigmentation is advantageous to them. Finally, I observed an increase over time of both lesions and indicators of UVR protection, suggesting evidence of cetacean quick photoprotection responses.

CHAPTER 4: UVR-induced DNA damage

The last chapter provides evidence that cetaceans develop macro and microscopic skin lesions as a consequence of exposure to solar ultraviolet radiation (UVR). It is likely that UVR can also induce molecular alterations. However, as most studies have been conducted in humans and laboratory animals, tools need to be developed and optimized in order to detect and quantify UVR-induced DNA damage in cetacean skin. This chapter presents the standardization and preliminary results of the single cell gel electrophoresis assay, which detects DNA damage at a nuclear level, and the use of real time quantitative PCR to detect and quantify UVR-induced DNA alterations of mitochondria.

4.1 Introduction

DNA is one of the main cellular structures affected by ultraviolet radiation (UVR) (Tornaletti and Pfeifer, 1996). DNA absorption of UVR, mainly between 245 and 290 nm of wavelength provokes the formation of photoproducts such as pyrimidine dimers (Fig. 4.1) (Burren et al., 1998). Cyclobutane pyrimidine dimers and pyrimidine [6, 4] pyrimidone photoproducts are the two most important photoproducts (Schuch and Menck, 2010; Tornaletti and Pfeifer, 1996). When not repaired, these can lead to mutations such as C-T and CC-TT transitions, which are considered signature mutations for UVR-induced damage (Schuch and Menck, 2010). Due to the implication of these mutations for the development of skin cancer, particularly when they occur in genes involved in DNA repair such as the tumor suppressor *P53* (Daya-Grosjean et al., 1995), it has become of growing importance to investigate and understand UVR-induced DNA damage in human. For this purpose, several techniques have been developed, including single cell gel electrophoresis, and detection of point mutations.

Single cell gel electrophoresis, also known as comet assay, can assess nuclear DNA single-strand breaks in a single cell (Olive and Banath, 2006). Due to its sensitivity,

relatively low cost and simplicity, the comet assay has gained popularity for investigating UVR-induced DNA damage in humans (Al-Baker et al., 2005; Olive et al., 1999). The technique has also been used in a number of non-model species, such as cnidarians (Baruch et al., 2005), molluscs and fish (Lee and Steinert, 2003). There are few published studies that use the comet assay to examine the genotoxic effect of pollutants on marine mammal leukocytes and lymphocytes (Betti and Nigro, 1996; Diaz et al., 2009; El-Zein et al., 2006; Taddei et al., 2001). However, this technique has not been standardized in marine mammal keratinocytes. Such standardization would allow its use to quantify UVR-induced DNA strand breaks in cetacean skin cells, which due to the species' physiological and anatomical constraints are likely to be particularly sensitive to UVR exposure.

A recently developed method to measure cumulative damage caused by exposure to UVR involves the use of mtDNA (Birch-Machin and Swalwell, 2010; Birch-Machin et al., 1998). Indeed, mtDNA has a higher rate of mutation than nuclear DNA and reduced capacity to repair damage, mainly due to the absence of nucleotide excision repair mechanisms (Birch-Machin and Swalwell, 2010). Consequently UVR-induced mtDNA lesions accumulate throughout the life of an individual and offer an excellent biomarker for cumulative exposure to UVR (Birch-Machin, 2000; Birch-Machin and Swalwell, 2010; Birch-Machin et al., 1998). Although the use of mtDNA as a biomarker of cumulative exposure has only been tested in humans, this method might prove to be useful to evaluate damage induced by UVR in cetaceans as well as other wildlife species.

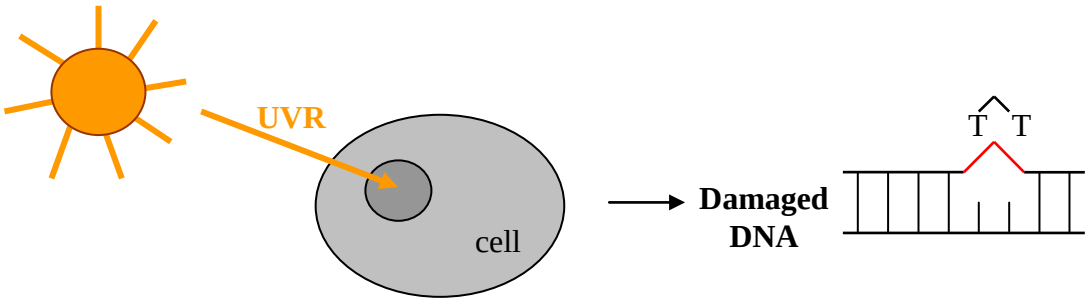

Figure 4.1. Schematic representation of the UVR-induced pyrimidine dimer formation. The absorption of UV irradiation by DNA induces the formation of a bond between two adjacent pyrimidines (for example two thymines).

4.2 Nuclear DNA damage

4.2.1 The single cell gel electrophoresis assay

The principle of the comet assay consists of processing cells in order to observe the presence of a "comet" with a head (intact DNA) and a tail (damaged or broken pieces of DNA) (Fig. 4.2) (Garcia et al., 2007). After obtaining a suspension of 1 x 10^5 cells per ml of a specific cell type, cells are embedded in a thin agarose gel on a microscope slide. The cell suspension is lysed and treated with an alkaline solution to unwind and denature the DNA and hydrolyze sites of damage. During electrophoresis, broken DNA fragments (damaged DNA) migrate away from the nucleus. The extent of DNA that is liberated from the head is directly proportional to the damage. The comets are stained with silver or fluorescent dyes and observed under a standard light microscope (200 X). The advantage of using silver is that staining is permanent and allows archiving of the slides for later analyses.

To reduce the time of sample preservation prior to their analysis, I ran the comet assay in the Marine Mammal Laboratory of CICIMAR (Mexico) at the end of each sea-expedition. However, although the commercial kit CometAssay™ Silver Kit (Trevigen, UK) was used, in order to reduce potential methodological errors, the lack of specialized equipment and suboptimal working conditions in the laboratory meant that the protocol needed to be optimized before analyses could be conducted.

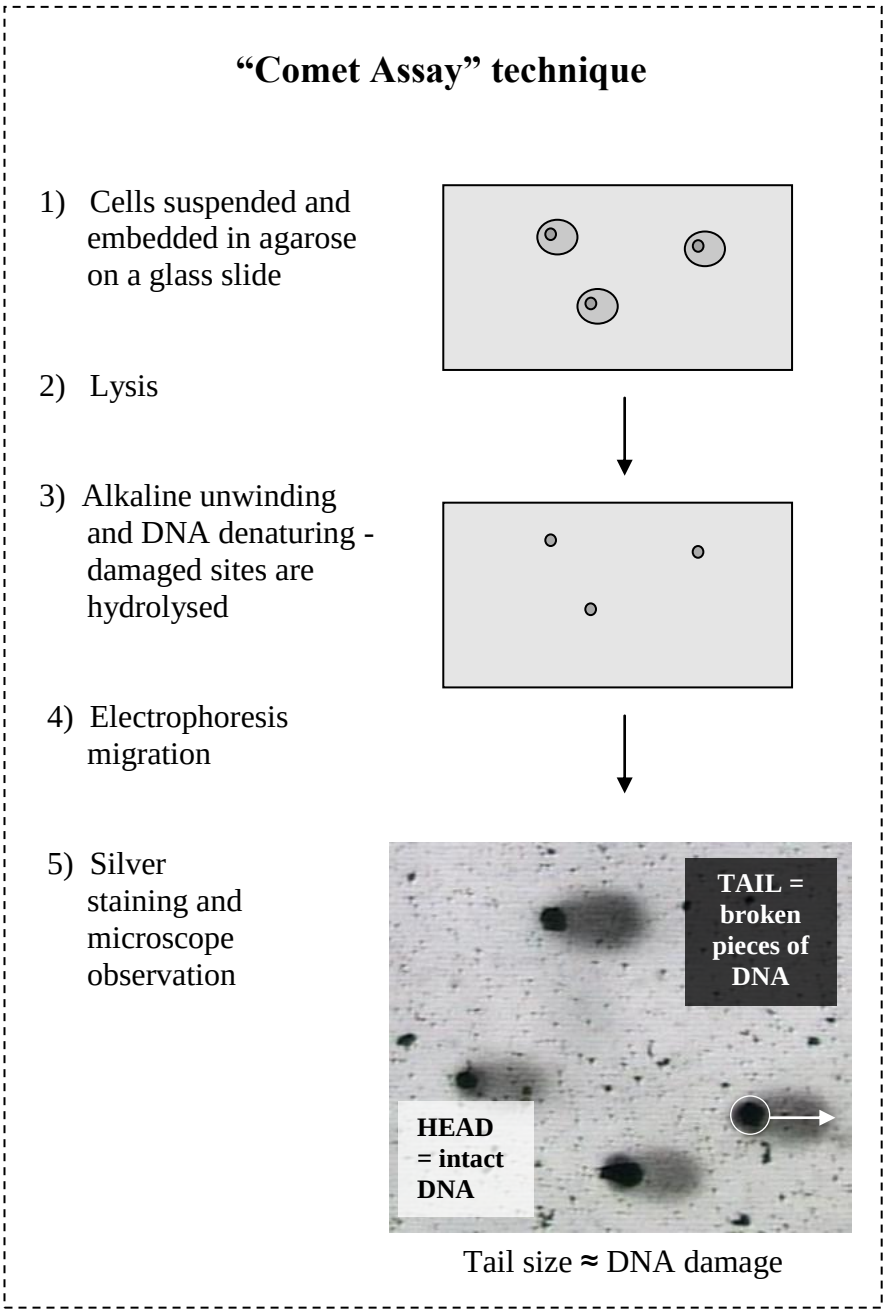

Figure 4.2. Schematic representation of the main steps of the Comet Assay technique.

4.2.2 Standardization of the Comet Assay technique

To gain the skills necessary to set up the comet assay technique in the field laboratory**,** I completed a two week externship in the Laboratory of Radiobiology of the Centre for Radiation Protection and Hygiene (CPHR) of La Havana, Cuba. The next sections describe the steps followed for optimization.

4.2.2.1 Optimization of the CometAssay protocol

Briefly, the first step of the protocol using the CometAssay™ Silver Kit is to combine the cell solution ($1x10^5$ cells per ml of PBS-1X) at a ratio 1:10 with low melting point agarose (LMA agarose) previously boiled and cooled to 37°C for 20 min. Immediately, 75 µl of the solution is pipetted onto the sample area of a CometSlide™ and placed at 4°C in the dark for 10 min. The slides are then immersed in prechilled lysis solution (2.5 M NaCl, 10 mM Tris Base, 100 mM EDTA pH 10, 1% sodium lauryl sarcosinate, 1% triton X-100) and maintained at 4°C during 30 min. After removing the excess of lysis buffer, slides are immersed in freshly-prepared alkaline unwinding solution (0.3 NaOH, 1mM EDTA) for 30 min at room temperature and kept in the dark. Slides are then transferred to a horizontal electrophoresis chamber, where alkaline solution (0.3 NaOH, 1mM EDTA) is added. Electrophoresis needs to be performed during 30 min at 1 Volt/cm, maintaining amperage of approximately 300 mA. Deionised water (dH_2O) is used to rinse the slide, which is then immersed in 70% ethanol for 5 min. When the gel is dry, the sample area is covered with fixation solution and incubated for 20 min at room temperature. After a 30 min wash in dH_2O, the sample is covered with staining solution and incubated at room temperature until the comets are visible under the microscope. At that moment, the reaction is stopped with 5% acetic acid during 15 min. The slide is rinsed with H_2O, air dried and stored in the dark.

One of the main problems that I faced when using the Kit was the accumulation of debris in the background that was produced during staining, which did not allow adequate examination of the comets. During my externship in Cuba, I used a solution of isolated lymphocytes to compare the effectiveness of the CometAssay™ Silver Trevigen Kit staining (hereafter KIT stain) with the silver staining protocol published by Garcia *et al.* (2007) used in the radiobiology laboratory in Cuba (hereafter RB staining protocol; see details in Appendix 4.1). I found that the RB staining protocol produced comets of higher quality and allowed the use of the software CASP, a computer image-analysis program that can calculate comet parameters such as tail length (Koñca et al., 2003) which was not possible to do when using the KIT stain.

To conclude, the RB staining protocol gave better results, partly because in this protocol, slides are placed vertically during staining, thus avoiding silver residue to accumulate on the gel as occurs with the KIT stain.

In addition, due to the hydrophobic barrier of the kit-supplied comet slide (see Fig. 4.3), the resulting gel was too thick and led to overlapping of comets. This phenomenon occurred despite various repeated attempts to follow the manufacturer's protocol. Consequently, I abandoned the use of the commercial kit and used self-prepared comet slides consisting of a conventional microscope slide covered with a thin agarose layer (see protocol in Appendix 4.1). I modified the protocol to cover the cell solution embedded in LMA agarose with a glass coverslip, which help spread of the gel uniformly on the slide. The use of the self-prepared slides and high quality glass coverslip also helped to decrease the percentage of gel lost, one of the most common problems faced when conducting comet assays (Tice et al., 2000). To aid gel adherence, the prepared slides were pre-warmed at 37°C before use.

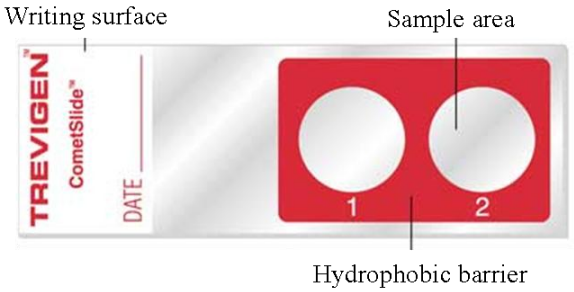

Figure 4.3. Kit supplied comet slide (Treviden, UK) with two wells corresponding to the sample areas.

4.2.2.2 Adaptation of the comet assay to the field laboratory conditions

To standardize the comet assay to work in the available working conditions of the field laboratory, I used leukocytes obtained by finger puncture (see details in Appendix 4.1). These blood samples were used to both set up the technique and to serve as an internal control in the experiments. Due to the high ambient temperature in La Paz (22 ºC and 40 ºC minimal and maximal average temperature, respectively), it was essential to maintain all reagents cool and to run most of the protocol steps at

4°C. Temperature control was critical during electrophoresis when the majority of the gels were lost. This was achieved running the electrophoresis inside a freezer, where the alkaline buffer could be maintained at below 10ºC.

The low resistance of the power supply available did not allow the standard 1V/cm migration and 300 mA needed during electrophoresis (Tice et al., 2000). However, good results were obtained using 0.8V/cm. With these modifications, comets observed for undamaged leukocytes were adequate (Fig. 4.4). The comets were classified as class 0 (i.e. without a tail and consequently lacking DNA damage) (Fig. 4.4). These samples were used as negative controls in all experiments. During optimization, I also tested epidermal cells from human oral mucosa. However, the comets obtained were highly damaged, likely due to the cell collection method, and consequently were not useful as a negative control.

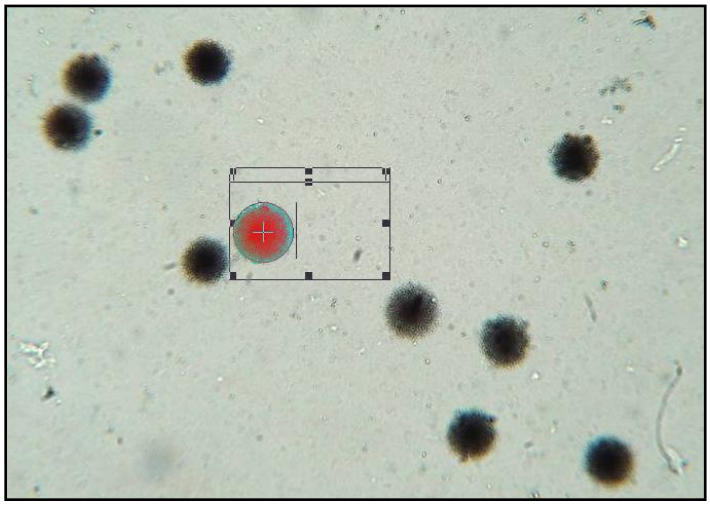

Figure 4.4. Image of silver-stained comets of human leukocytes without DNA damage. The frame observed around the comet, generated by CASP software, limits the comet's full area. A circle identifies the comet head and the end of the tail is recognized by a line. The small rectangle above corresponds to the background reference. The comets observed are class 0 with no tail.

To obtain a positive internal control that accounted for correct DNA migration during electrophoresis, I tried different approaches, including exposing leukocytes to 312 nm UVR using a spectrophotometer. The best control was obtained by exposing

the leukocytes to 3.8 mM hydrogen peroxide (H2O2) solution at 4ºC during 10 min in the dark right before lysis. In this way, I managed to obtain comets with various degrees of DNA damage (Fig. 4.5).

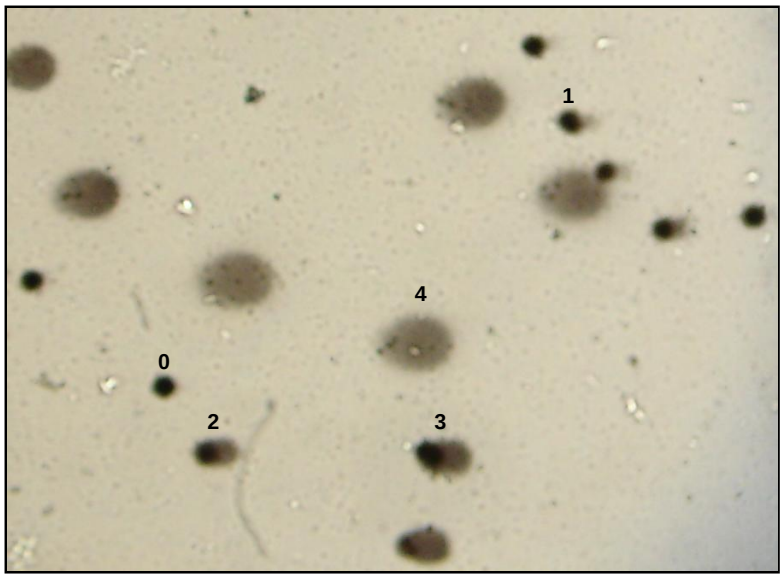

Figure 4.5. Image of silver stained comets of human leukocytes damaged with a 3.8 mM solution of H2O2. The comets observed show the five degrees of DNA damage, class 0 representing undamaged DNA and class 4 the most damaged DNA.

Before running the comet assay on cetacean skin, I wanted to ensure that the preservation of the samples in liquid nitrogen following their collection in the field had no effect on the level of DNA damage. To test this, I collected human leukocytes and immersed them in a cryogenic solution before preserving them in liquid nitrogen for different time lengths (1 day, 2 days, 1 week, 2 weeks, 3 weeks and 4 weeks) before analysis. The majority of comets observed were class 0 reflecting that cryopreservation did not cause DNA damage. The experiment was repeated two times obtaining the same results, confirming that cryopreservation for up to 4 weeks prior to analysis does not interfere with the comet assay results.

4.2.2.3 Standardization of the comet assay using cetacean skin samples

The first step of the comet assay was to obtain a cell solution without causing damage to the DNA. I tested different methods, including mechanic disruption (Hartmann et al., 2003) such as mincing, smashing or pushing the tissue through a mesh nylon membrane, and enzymatic lysis (Hartmann et al., 2003). The best results were obtained using trypsin. Briefly, the skin samples were first cleaned with PBS-1X and cut into small fragments which were incubated trypsin solution (0.25% trypsin, 1mM EDTA-4Na) at 4ºC during 12h. Samples were transferred to a microcentrifuge tube containing 500 µl of fresh trypsin solution and placed in a rotor for 45 min at 37ºC. The reaction was stopped by adding 500 µl of cell culture medium (Recovery™Cell Culture Freezing Medium, Invitrogen, UK). Samples were centrifuged at 250 G for 1min and the supernatant was collected before mixing with 0.4 % trypan blue (V/V) in order to test the viability of the cells in a hemocytometer.

To increase assay sensitivity, an additional lysis was conducted on the cell samples by using a solution containing sodium dodecyl sulphate (0.5%) and proteinase K (0.1 mg/ml) (see details in Appendix 4.1), and incubating the samples at 37 ºC for 1h (Decome et al., 2005). Using this method comets were observed, although the shapes of the heads were not as round as would normally be expected (Fig. 4.6). It is possible that the DNA obtained by the process described above was not entirely devoid of cell products due to incomplete lysis. Consequently, I tested the use of an additional 2h incubation at room temperature and a third lysis with trypsin solution at 4ºC during 30 min. This procedure allowed visualization of comets of the expected shape (Fig. 4.7). However, despite modifications to the technique, reproducibility was low. Furthermore, gel loss (up to 50 %) remained a problem during the assays regardless of other slight modifications such as the addition of a third layer of LMA agarose (see Appendix 4.1).

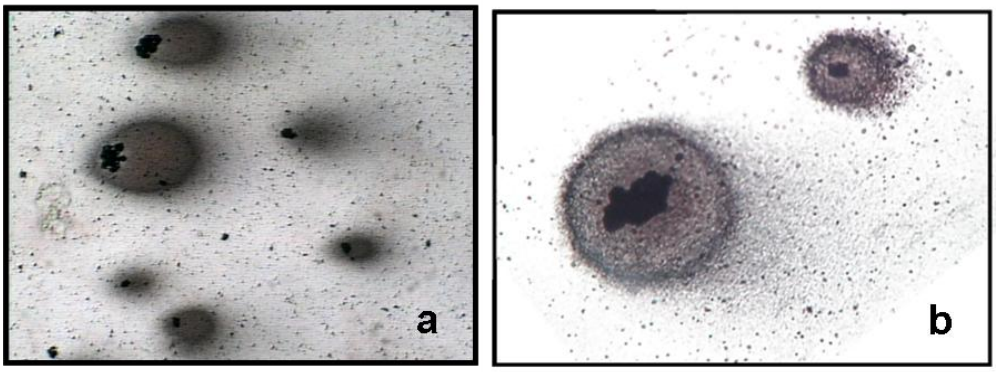

Figure 4.6. Silver-stained comets of whale epidermal cells. a) Comets that appear highly damaged. b) Comets with a clear head showing low levels of damage.

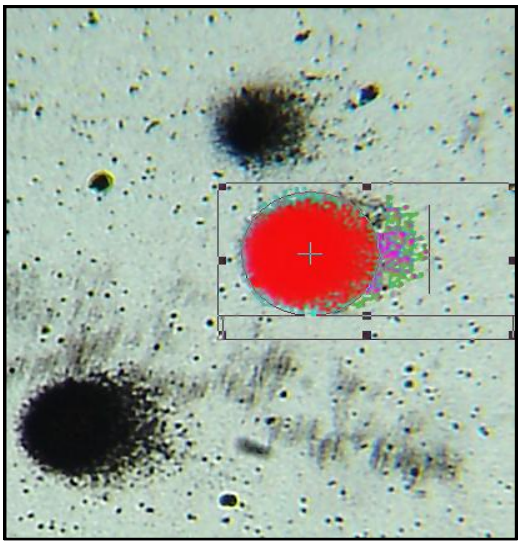

Figure 4.7. Silver stained comets of whale epidermal cells showing low levels of damage to the DNA. The frame observed around the comet was generated by the CASP software. The circle identifies the comet head and the end of the tail is recognized by a line.

4.2.3 Feasibility of using the comet assay to detect DNA damage in cetacean epithelial cells

I was able to standardize the comet assay on leukocytes and adequately use them as internal test controls, and the percentage of gel loss was diminished by preparing my own slides, using high-quality glass coverslips and maintaining the temperature below 10ºC, particularly during electrophoresis. However, although I managed to prepare successfully cetacean epithelial cell DNA samples by modifying the protocol's disruption-lysis steps, reproducibility was low and gel loss remained an issue. It is likely that the high gel loss ratio was due to high ambient temperatures recorded in La Paz, which significantly altered the environment within the laboratory where I ran the assays. It is likely that further trials would have allowed me to optimize the technique, but I was constrained in time during my field work. Running the assays back in the laboratory at the Institute of Zoology was not an option as, having remained in cryopreservation for much more than 4 weeks before analysis, cell viability would have undoubtedly been compromised (see section 4.2.2.2). For this reason, I desisted from using the comet assay in my thesis and explored other methods to evaluate UVR-induced DNA damage.

4.3 Mitochondrial DNA damage

The following section was conducted in collaboration with Prof. Mark Birch-Machin and Amy Bowman from the Institute of cellular medicine of Newcastle University, who kindly agreed to run assays to detect and quantify UVR-induced mitochondrial DNA damage. I prepared the samples in terms of DNA extraction and selection, but the assays were conducted by M. Birch-Machin and A. Bowman. They have agreed for me to include details on the experiments that they conducted (details in section 4.3.1.2) and to use the results for analyses and future publications.

4.3.1 Material and method

4.3.1.1 DNA extraction

To isolate DNA for assessment of mitochondrial DNA damage, I used phenol chloroform extraction followed by ethanol precipitation (Sambrook et al., 1989). Briefly, skin samples were minced and placed in a sterile microcentrifuge tube with 20 µl of 20% SDS, 315 µl of 5 % Chelex (BioRad, UK) and 20 µl of proteinase K (20mg/ml) before incubating at 56°C during 12h. The digested sample was centrifuged at 11000 G for 1 min and the supernatant was transferred to a new tube. One volume of phenol:chloroform:isoamyl alcohol mixture (25:24:1) was added (V/V) and the mixture was vigorously mixed for 1 min prior to a 5 min centrifugation at 11000 G. This step separated the DNA-containing aqueous phase, which was transferred into a fresh tube. To purify the DNA sample, 75 µl of 8M ammonium acetate and 250 µl of 95% ethanol were added. The solution was mixed gently by repeatedly inverting the tube and maintained at -20°C for 30 min, before a 15 min centrifugation at 16000 G. The liquid was discarded and after adding 250 µl of 70% ethanol to the microcentrifuge tube, the sample was centrifuged for 2 min at 16000 G. Finally, the ethanol was discarded carefully and the uncapped tube was kept at room temperature until residual ethanol was evaporated. DNA was resuspended in 30 µl of sterile nuclease-free water.

4.3.1.2 mtDNA damage detection using quantitative real-time PCR

UVR-induced mtDNA lesions were detected and quantified in blue and fin whale skin DNA samples using quantitative real-time PCR (qPCR). Taking into account that this was the first time that mtDNA lesions were to be quantified in whale skin, it was important to first ensure that the right size of mtDNA fragment was amplified. Indeed a too small fragment would decrease the probability of detecting any lesion, whereas too long a fragment would reduce DNA polymerase efficiency and thus under-estimate the amount of lesions. To determine the ideal size to amplify, the first step was to align blue and fin whale mtDNA sequences (NCBI GenBank database; www.ncbi.nlm.nih.gov). Several primer pairs, each amplifying different fragment

sizes and regions, were designed using the free software Primer3 (Rozen and Skaletsky, 2000) in order to cover the whole mitochondrial genome. During primer design, occurrence of nuclear pseudogenes was checked for on NCBI GenBank database. Two sets of primers were designed to amplify two regions of around 8.5kb. However, the efficiency of DNA polymerase was very low to the (large) size of the fragments. The ideal fragment length was found to be around 4.4kb and four new sets of primers were designed to amplify independent fragments of that size (Fig. 4.8). The primer pairs selected were analyzed with the Basic Local Alignment Tool (BLAST, www.ncbi.nlm.nih.gov/BLAST) to confirm their specificity to the blue and fin whale mitochondrial regions where they were expected to bind (details on Fig. 4.8; primers details in Table 4.1). Following the same method, a final primer pair was designed to amplify a 99 bp fragment of mtDNA. These primers were used to quantify the amount of mtDNA in each whale sample and correct for differences in initial mtDNA concentration before running qPCR (primer details in Table 4.1).

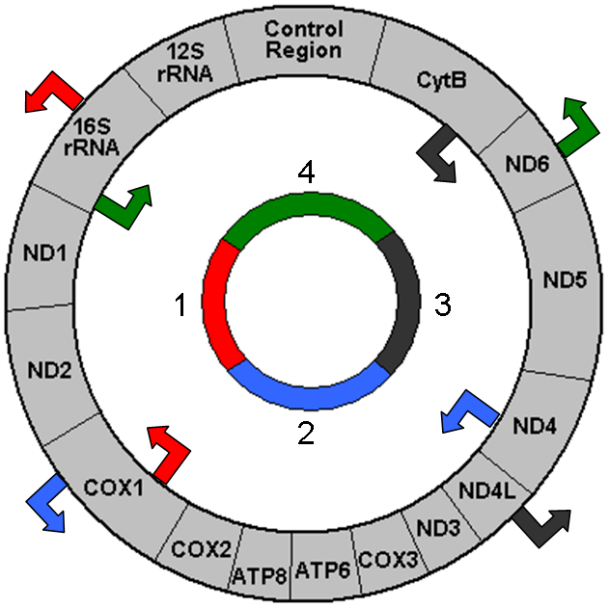

Figure 4.8. The four regions of mitochondrial DNA used to evaluate UVR-induced mtDNA damage in the whole whale mtDNA genome. Four pairs of primers (red, blue, back and green) were used to amplify the corresponding four regions. Figure drawn by Amy Bowman and kindly made available for this thesis.

Table 4.1. Primer sequences. The first four primer pairs were designed to cover the entire whale mtDNA genome. The last pair was designed to amplify a small fragment of mtDNA in order to quantify the initial amount of mtDNA present in each whale sample. Primer sets 3 and 4 had low specificity and were excluded from further analyses.

Primer	Sequence (5' to 3')	Product size
4kb Forward 1	GAA CTC GGC AAA CAC AAA CC	4489bp
4kb Reverse 1	CCG CCT ACT GTG AAA AGG AA	
4kb Forward 2	TCA AAC TCC CCT TTT CGT ATG	4400bp
4kb Reverse 2	TGG GCT GTG GAG TTA ATT CAG	
4kb Forward 3	TCC CAC CTA ATA TCC GCA TT	4329bp
4kb Reverse 3	TTA AGC AGA GGC CGA GTA GG	
4kb Forward 4	TTT GAA GAA ACC CCC ACA AA	4405bp
4kb Reverse 4	CTA CCT TTG CAC GGT CAG GA	
99bp Forward	CTT TGA AGA AAC CCC CAC AA	99bp
99bp Reverse	TTG GTC ATG GTT GAA GTC CA	

All qPCRs were performed in a Chromo4 Real-Time PCR detection System (BioRad, UK) using SYBR Green dye (Qiagen, UK). This method is based on the principle that, at each cycle, the thermalcycler detects the fluorescence emitted by SYBR Green which is intercalated between each newly generated double-stranded DNA and the corresponding curve is drawn to represent the quantity of PCR product per cycle number (e.g. Fig. 4.9). The crossing threshold (Ct) is defined automatically by the machine as the cycle number at which the curve crosses the inflexion point of the exponential curve, signalling the end of exponential growth (Fig. 4.2) (Schmittgen and Livak, 2008). Damaged mtDNA will amplify at a lower efficiency rate than undamaged mtDNA and thus the Ct value obtained will be directly proportional to the level of damage (Meyer, 2010).

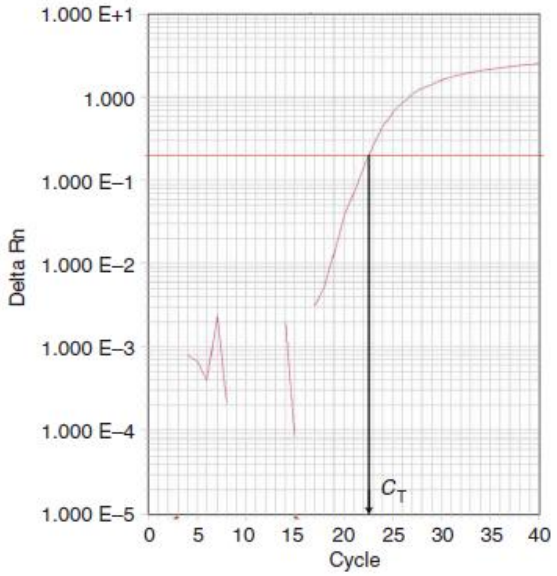

Figure 4.9. Real-time PCR output, calculation of the crossing threshold (Ct) (Schmittgen and Livak, 2008)**.** At each cycle, the qPCR machine detects the fluorescence (Delta Rn) and draws the corresponding amplification plot. The point at which the curve intersects the threshold (horizontal line) is the Ct (Ct = 22.5 on the figure).

To ensure that the same amount of mtDNA was used to evaluate UVR-induced mtDNA lesions in each sample, it was necessary to measure accurately the quantity of mtDNA per sample. For this, total DNA was determined by measuring optical density in a Nanodrop® ND-1000 UV-Vis (Thermo Scientific, UK) spectrophotometer. Once titrated, samples were diluted with deionized water to a final concentration of 50 ng/µl. The total volume of each qPCR reaction was 25 µl (containing 1X JumpStart SYBR Green Kit (Sigma, UK), 0.4 µM forward and reverse primers and 1µl of the DNA sample). Each sample was run in triplicate. Cycling conditions were an initial step of 2 min at 94°C, followed by 35 cycles of 15 sec at 94°C, 45 sec at 60°C and 45 sec at 72°C. The samples were finally incubated 2 min at 72°C. A melting curve analysis (from 60°C to 95°C) was added at the end to detect non-specific amplifications. The results were viewed in Opticon Monitor 3

(BioRad, UK). The mean mtDNA amount of the thrice-run reactions was calculated for each sample (Lin et al., 2008).

The final volume of each qPCR reaction was 20µl, which included 1X Phusion HF Buffer (Finnzymes, Thermo Fisher Scientific, UK), 0.4 mM dNTPs, forward and reverse primers (0.3 µM), 0.1X SYBR Green (Sigma, UK), 0.02U/µl Phusion DNA Polymerase (Finnzymes, Thermo Fisher Scientific, UK) and the DNA sample (2µl). Each sample was run in triplicate. Cycling conditions were an initial 30 sec at 98°C, followed by 30 cycles of 8 sec at 98°C, 20 sec at 57°C and 135 sec at 72°C. The samples were finally incubated at 72°C during 8 min. A melting curve analysis (from 55°C to 95°C) was added at the end to detect non-specific amplifications. The results were viewed using Opticon Monitor 3 (BioRad, UK) and the mean of the triplicate reactions were calculated for each sample (Lin et al., 2008). For each sample, the levels of mtDNA lesions in region 1 and in region 2 (Fig. 4.8) were quantified on the same plate.

4.3.1.3 Statistical analysis

Eleven samples, from seven blue and four fin whales were analysed successfully. The limited number of samples processed was due to the fact that the method needed to be standardized and optimized for cetaceans, as it had not been used previously in species other than humans. Thus, we were restricted in terms of budget and time. Owing to the small sample size I used simple statistical tests such as t-tests and Spearman tests which do not allow controlling for other variables.

4.3.2 Results

Significant levels of mtDNA lesions were detectable in all samples (Fig. 4.10). The amount of mtDNA lesions varied amongst individuals (Fig. 4.10).

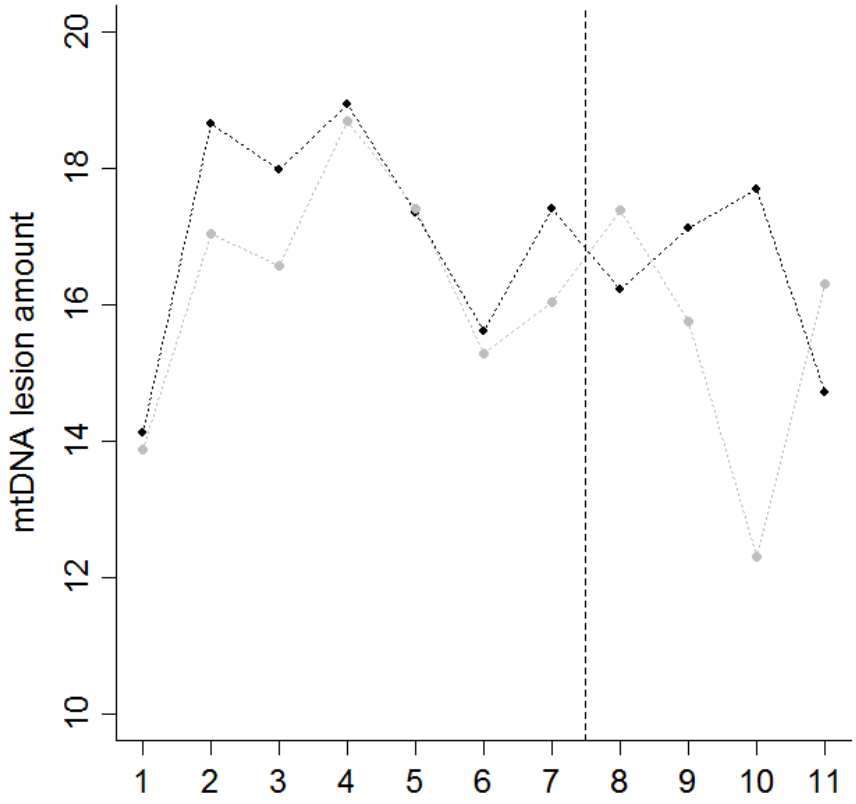

Figure 4.10. Mitochondrial DNA lesions quantified using qPCR in 11 whale samples (Lanes 1-7 correspond to blue whales and 8-10 to fin whales; mtDNA lesion amount is expressed as Ct). The black dots show damage detected in mtDNA region 1 whereas grey dots show damage detected in region 2.

As expected, the amount of damage detected in mtDNA region 1 was highly and significantly correlated with those quantified in region 2 of blue whales (Spearman test: rho = 0.79 and p = 0. 05; Fig. 4.11) implying that UVR-induced damage might occur in more than one region of the mitochondrial genome. However, it might be possible that some regions are more affected than others. Indeed, for both species there is slight evidence that lesions were more prevalent in region 1 than in region 2 (Fig. 4.12), but power was insufficient to detect any significance (Wilcoxon tests; p = 0.38 and p = 0.69 for blue and fin whales, respectively).

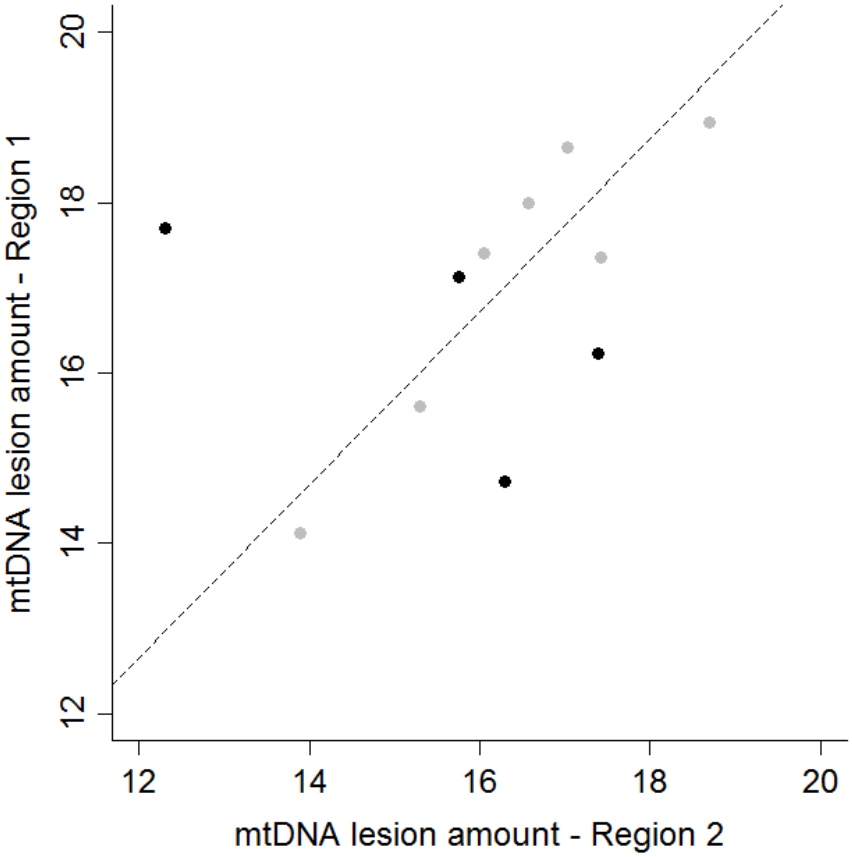

Figure 4.11. Correlation between whale mtDNA lesions between region 1 and 2. mtDNA lesions were quantified using qPCR (mtDNA lesion amount in Ct). Grey dots correspond to blue whales and black dots to fin whales. The dotted line shows the positive relationship of blue whale mtDNA lesions between genomic regions (Spearman test: rho = 0.79 and p = 0. 05). The low number of fin whale samples (n = 4) did not allow sufficient power to detect a potential correlation of the lesions quantified in the two regions (Spearman test: rho = - 0.80 and p = 0. 33).

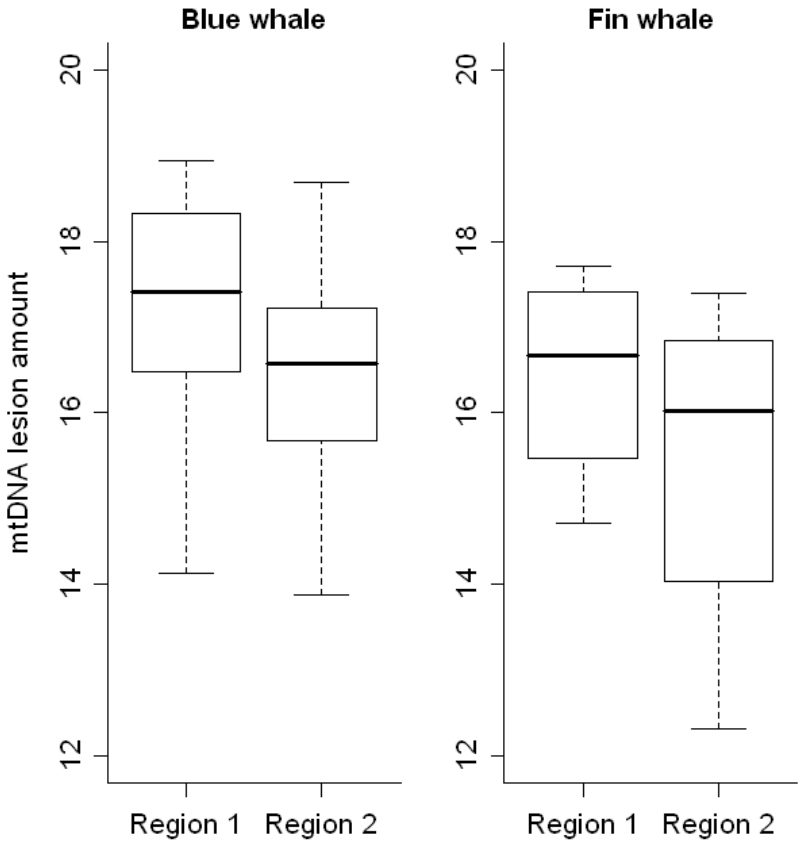

Figure 4.12. mtDNA lesions detected in regions 1 and 2 of blue and fin whale skin samples. Lesions were quantified using qPCR (mtDNA lesion amount in Ct).

Studies conducted in humans show that individuals with less pigmented skin tend to have more UVR-induced DNA lesions than those with darker skin (Tadokoro et al., 2003; Yamaguchi et al., 2006). Thus, it would be predicted that, similarly, levels of damage would be higher in blue whales than in fin whales, due to the differences in their pigmentation (Fig 1.5 in Chapter one). As expected, damage in mtDNA region 1 and 2 appeared to be higher in blue whales (Fig. 4.13), although the differences were not statistically significant (t-tests: $p = 0.46$, $p = 0.47$ and $p = 0.23$ for regions 1, 2 and region [1+2], respectively), most likely due to the reduced sample size, particularly for fin whales ($n = 4$) which did not allow sufficient power to detect potential differences between the two species.

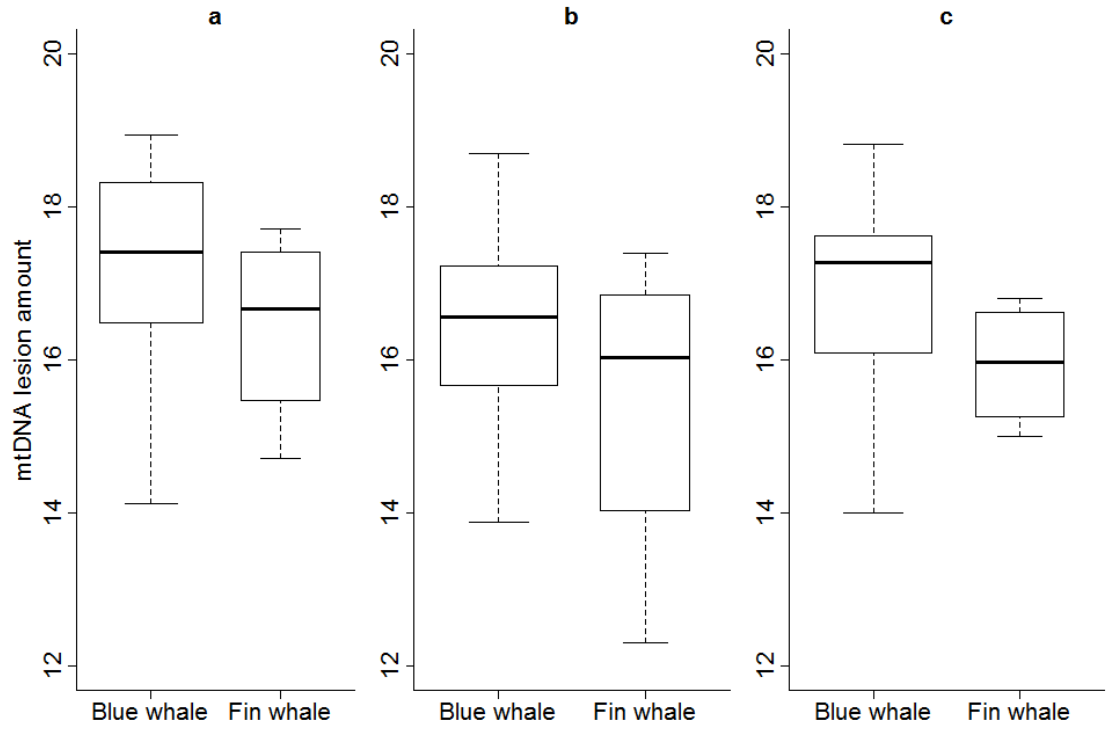

Figure 4.13. Amount of mtDNA lesions (regions 1 (a), 2 (b) and 1 + 2 (c) in blue and fin whales. Lesions were quantified using qPCR and values are expressed in Ct. Differences in mtDNA lesion abundance between blue and fin whales were not statistically significant (t-tests: p = 0.46, p = 0.47 and p = 0.23 for regions 1, 2 and region [1+2], respectively).

For the remaining analyses I used the amount of mtDNA damage recorded in region 1 because this region presented the highest level of lesions and lowest variation within data (Fig. 4.12).

Higher levels of mtDNA damage occurred in whales with dermal oedema (t-test: p = 0.02; Fig. 4.14a). A similar, although statistically insignificant, trend was observed for whales presenting apoptosis (Fig. 4.14b; t-test: p = 0.24). No difference in levels of mtDNA damage was observed between whales with low and high levels of vacuolation (t-test: p = 0.88; Fig. 4.14c).

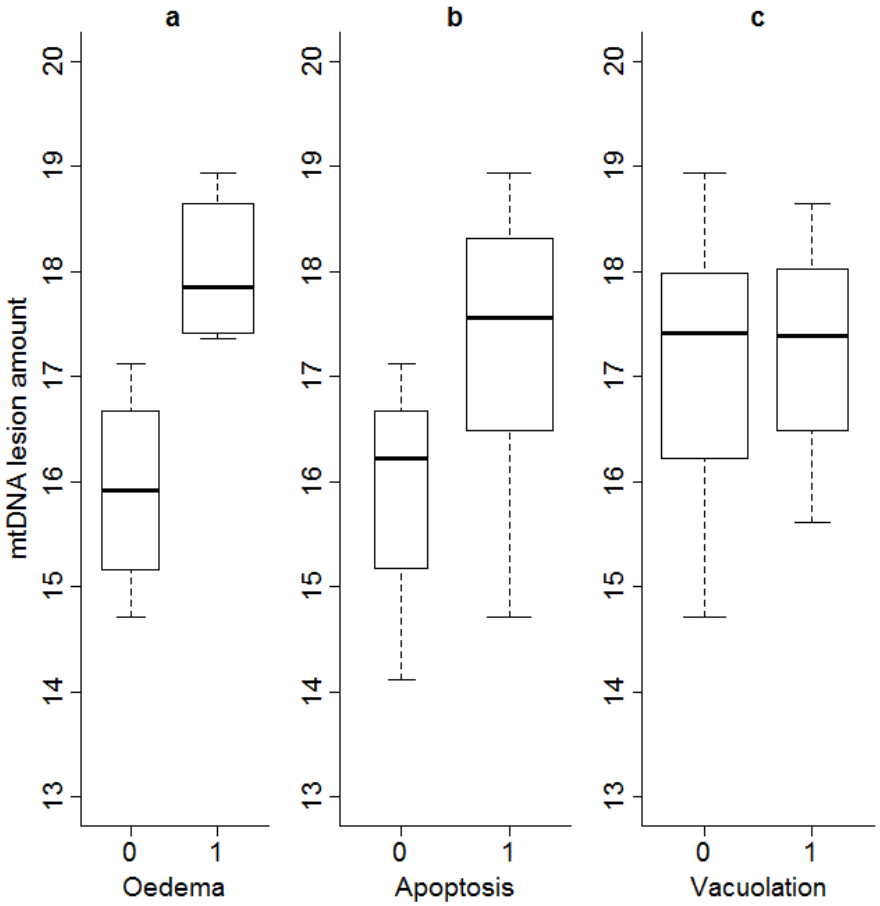

Figure 4.14. Relationship between microscopic lesions and mtDNA damage. a) oedema (n = 4 and n = 6 respectively for absence and presence): t -test: p = 0.02 b) apoptosis (n = 3 and n = 8 respectively for absence and presence): t-test: p = 0.24 c) vacuolation (n = 6 and n = 4 respectively for low level and high level): t-test: p = 0.88. mtDNA damage was quantified within region 1 of whale mtDNA using qPCR and is expressed in Ct. The width of the boxes is proportional to the sample size.

Skin pigmentation was inversely proportional to the amount of mtDNA damage (Spearman test: rho = - 0.73 and p = 0. 03; Fig. 4.15). The same pattern was maintained when looking only at blue whales (Spearman test: rho = - 0.83 and p = 0. 06; Fig. 4.15).

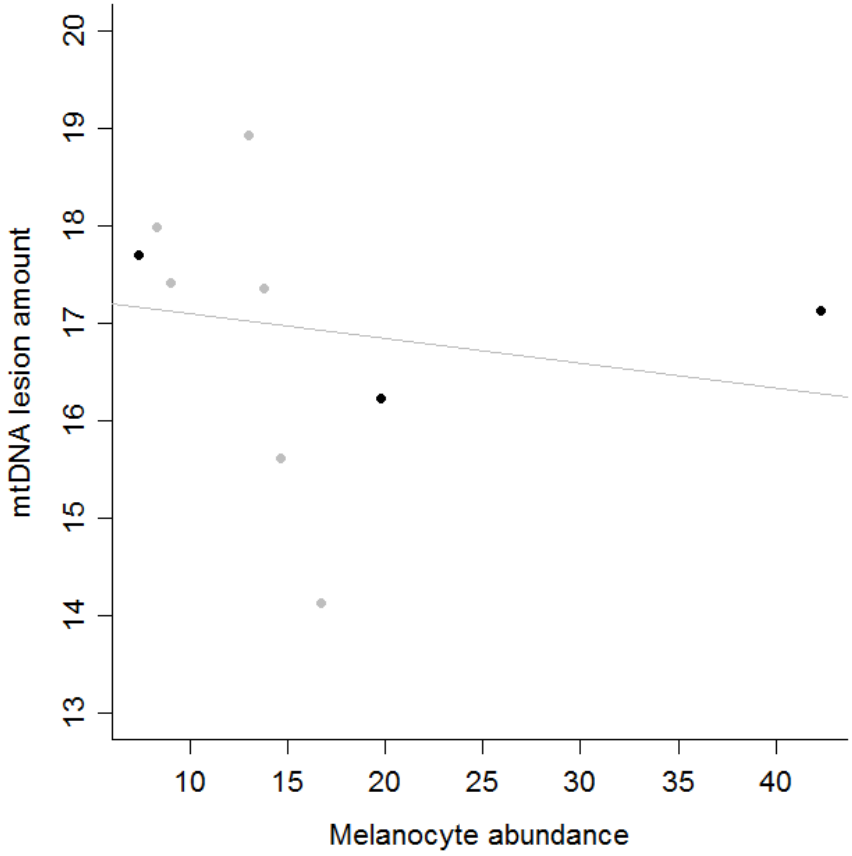

Figure 4.15. Association between mtDNA damage and skin pigmentation (measured as melanocyte abundance). mtDNA lesions were quantified using qPCR (expressed as Ct) within region 1. Black dots represent fin whales, grey dots represent blue whales. The line shows the inverse relationship between whale mtDNA lesions and melanocyte counts (Spearman test: rho = - 0.73 and p = 0. 03).

4.3.3 Discussion

The use of quantitative real-time PCR to detect and measure UVR-induced mtDNA lesions was successfully standardized for cetaceans, a taxonomic group for which the technique has not been attempted previously. Although it could be argued that nuclear copies of mtDNA genes ("nuMTs") might exist and affect the amplification efficiency, considering the size of the fragments used in the assays (4.4Kb), it is unlikely that this is the case. Significant levels of mtDNA damage were detected in most of the samples, and the observed association between damage and aspects of

pigmentation and lesions is promising, although the small sample size, determined mostly by financial restrictions, limits statistical power and makes interpretation of the results rather difficult. There appears to be some evidence that mtDNA damage is higher in blue whales than in fin whales, as would be expected if darker pigmentation confers higher protection against exposure to UVR (Del Bino et al., 2006), however, a larger sample set would have to be analysed in order to address this question unequivocally. Nevertheless, it was interesting to observe an inverse relationship between the quantity of mtDNA lesions and melanocyte abundance (used as a surrogate measure of individual skin pigmentation) of blue whales. As far as I am aware no other study has been done on mtDNA damage occurrence and skin pigmentation. However a study on nuclear DNA damage showed that humans with paler skin tend to have higher amounts of UVR-induced DNA damage than darker (more pigmented) individuals (Tadokoro et al., 2003; Yamaguchi et al., 2006). It is possible that cetacean pigmentation acts as a protective barrier against UVR (Yamaguchi et al., 2006) and, thus helps explain why lower mtDNA damage was observed in darker whales.

Excessive or unrelenting exposure to UVR can lead to cellular and molecular changes which, if unresolved, can lead to chromosomal aberrations and harmful mutations (Chipchase and Melton, 2002; Schuch and Menck, 2010). These effects are well documented for humans and laboratory mammals, but have rarely been explored in wild mammals. The quantitative real-time PCRs showed that higher levels of mtDNA lesions were more frequent in whales with cellular damage associated with exposure to UVR, such as intracellular oedema (Ishii et al., 1997). These findings suggest that in whales there is a link between cytotoxic and genotoxic damage induced by exposure to the sun.

Earlier I showed that melanocyte counts inversely predict oedema (see Chapter three). Thus, it is also possible that oedema and mtDNA damage are independent, but both predicted by constitutive skin pigmentation. Analysing a larger set of samples and investigating the relationship between these two types of UVR-induced lesions while controlling for variations in individual skin pigmentation would help answer this question in the future.

While nuclear DNA lesions induced by UVR can be efficiently removed (Peterson and Côté, 2004; Tadokoro et al., 2003), mtDNA has a reduced capacity to repair damage, mainly due to the absence of nucleotide excision repair mechanisms (Birch-Machin and Swalwell, 2010). Due to the importance of mitochondria in energy production, mitochondrial disorders secondary to either nuclear or mtDNA mutations can have dramatic consequences for cell function (Birch-Machin, 2000). Indeed, if the ratio of mutated:wild-type mtDNA exceeds a certain threshold level, cellular dysfunction can occur (reviewed in Birch-Machin, 2000). Recent studies demonstrated the role of mitochondria in the regulation of apoptosis (Susin et al., 1998) and showed a link between mtDNA disorders and skin diseases, including cancer (Birch-Machin, 2000; Jakupciak et al., 2005). It is likely that, in cetaceans, as seen in humans, mtDNA lesions can engender cell dysfunction or skin disease, particularly in light skin individuals, which present lower level of apoptosis (see Chapter three).

4.3.4 Conclusions

The use of quantitative real-time PCR to detect and quantify UVR-induced mtDNA lesions was standardized and successfully optimized in cetaceans. Lesions were quantified across 8.8 Kb, representing half the whale mtDNA genome. I not only found significant levels of mtDNA lesions but also demonstrated that individuals with darker pigmentation have fewer mtDNA lesions than lighter-skinned individuals. Regardless of the limitations imposed by a small sample size, the results obtained here constitute preliminary evidence of UVR-induced mtDNA damage and of the role that skin pigmentation has in protecting whales from such damage. Taking these results and their implications into account, I propose using mtDNA as a biomarker for measuring the effect of cumulative UVR exposure in cetaceans.

CHAPTER 5: Expression of genes involved in genotoxic stress response pathways

In order to evaluate the capacity of cetaceans to cope with UVR-induced genotoxic stress, I screened the expression of three relevant genes: the gene coding for the heat shock protein 70 (*HSP70*), the gene coding for the tumour protein P53 (*P53*) and the gene coding for the KIN17 protein (*KIN*). As observed for lesion prevalence (Chapter three), it is likely that gene expression will vary amongst the three study species due to their markedly different skin colour and surface behaviour. It is also possible that the level of transcription of these genes will mimick the seasonal increase in UVR levels reported for the Gulf of California. To investigate these predictions, I used real-time quantitative PCR (qPCR) to study interspecies and temporal variations in the expression of the three selected genes. Abbreviations for genes are written, throughout the thesis, in italicized capital letters.

5.1 Introduction

Extrinsic insults such as solar ultraviolet radiation (UVR) activate a complex network of interacting pathways that together will execute cellular responses (Peterson and Côté, 2004; Zhou and Elledge, 2000). Such response mechanisms involve the coordinated action of hundreds of genes that may have multiple functions depending on the different response pathways activated (Zhou and Elledge, 2000). Important genes involved in the complex network of the UVR response pathway are those encoding the heat shock proteins (HSPs), also called stress proteins. HSPs are involved in the recovery of proteins that can unfold under stress (Hightower, 1991). HSPs can either repair the damaged proteins by refolding their structure, or can degrade them if damage is too extensive. The HSPs are also involved in intracellular protein transport between compartments and disposal of old proteins as well as in generating an immune response as they participate in the presentation of abnormal peptides (i.e. antigens) to immune effectors on the surface of abnormal cells (Helmbrecht et al., 2000; Stangl et al., 2011; Wheeler et al., 2011). The different

families of HSPs, classified according to their structure, function and weight (in kilodaltons), include HSP100, HSP90, HSP70, HSP60, HSP40 and the small heat shock proteins family. One of the most studied HSPs is HSP70, which is the major stress-induced member of the family, specifically involved in protein-folding and protein membrane transport. Most studies, mainly done in humans and laboratory animals, showed that under severe UV irradiance, the gene coding for HSP70 is over-expressed and helps to protect against UVR-induced epidermal damage, including apoptosis and DNA damage (Matsuda et al., 2010). However, when UVR insults exceed HSP70's capacity, DNA damage can occur, leading to mutations.

To minimize the number of heritable mutations transferred from one cell to its daughters, the structure of chromosomes is continuously under surveillance. When damage is detected, repair and cell-cycle progression are coordinated (Zhou and Elledge, 2000). Thus, the DNA damage response acts as a network of interactive pathways (Fig. 5.1), with the participation of sensors of aberrant DNA, signal transducers and effectors that execute the appropriate responses (Zhou and Elledge, 2000). Although the identities of the sensors are still unclear, transducers include four sets of conserved proteins (phospho-inositide kinase such as ATM and ATR, check point kinases 1 and 2 and BCRT). Effectors, involved in DNA repair, transcription regulation and cell cycle control, comprise proteins such as BCRA1, Nbs1 and P53 (Zhou and Elledge, 2000).

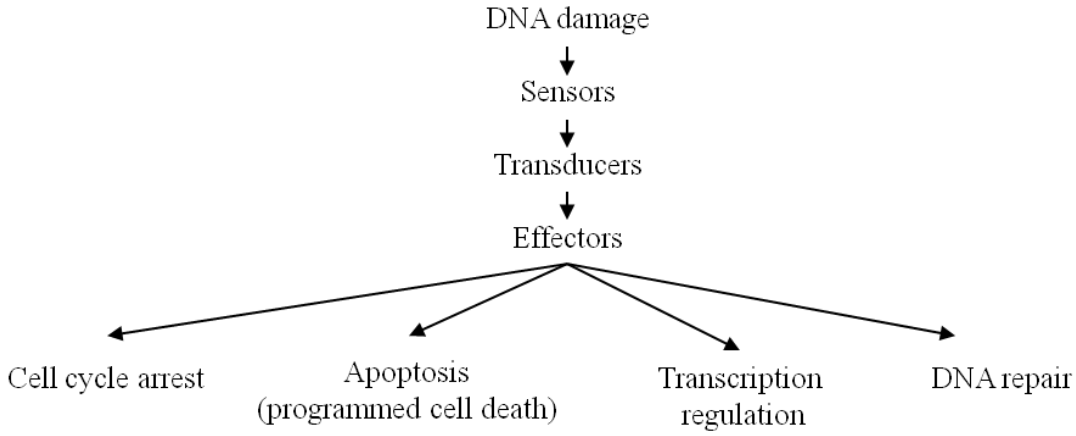

Figure 5.1. General network of interacting response pathways (From Zhou and Elledge, 2000).

Protein P53, also called tumour suppressor protein because mutations of this gene can promote cancer (Giglia-Mari and Sarasin, 2003; Hollstein et al., 1991; Kucab et al., 2010), is actively involved in different response pathways including cell cycle arrest, DNA repair and, in case of non repairable damage, apoptosis (Amundson et al., 1998; Bhana and Lloyd, 2008; Burren et al., 1998; Ikehata et al., 2010; Porter et al., 2006). P53 is a central transcription factor in cellular stress responses and its synthesis is controlled by dozens of other proteins (Latonen and Laiho, 2005). One of P53's most important transcriptional targets is the cyclin-dependent kinase inhibitor p21, which can provoke the arrest of the cell cycle at G1 phase (Latonen and Laiho, 2005). P53 also participates, via transcriptional regulation and direct interaction, in DNA repair mechanisms such as nucleotide excision repair (NER; the main P53 target is repair factor P48), although it has been shown that P53 is not always essential to NER (Latonen and Laiho, 2005). P53 also induces the expression of *DDB2* and *XPC* genes, which encode factors of the global genome repair mechanism (GGR) (Bhana and Lloyd, 2008; Ikehata et al., 2010). While programmed cell death can occur independently of P53, this protein is involved, via various routes, with apoptosis, its most important suppressive function (Latonen and Laiho, 2005; Ikehata et al., 2010). Finally, P53 is also involved in the tanning response (Murase et al., 2009; Oren and Bartek, 2007).

A gene recently found to be implicated in cellular responses to UVR-induced damage is the gene coding for KIN17 protein (hereafter KIN). The *KIN* gene is expressed in all tissues and its expression significantly increases after UVR exposure (Biard et al., 1997; Kannouche et al., 2000; Masson et al., 2003). Experimental trials have shown that DNA-bound KIN protein accumulates 24h after irradiation and that KIN can arrest the cell cycle prior to DNA replication (Biard et al., 2002; Kannouche and Angulo, 1999; Masson et al., 2003; Miccoli et al., 2005). It has been proposed that the KIN protein helps to overcome the perturbation of DNA replication in unrepaired DNA sites (Angulo et al., 2005; Biard et al., 2002).

5.2 Material and Methods

A schematic representation of the general methods used in this chapter is provided in Appendix 5.1.

5.2.1 RNA extraction and cDNA transformation

5.2.1.1 RNA extraction

All section skin samples were stabilised in RNA later (Qiagen, UK) and kept at -80 ºC until processing. Total RNA was extracted using the RNeasy® Mini Kit (Qiagen, UK) according to the manufacturer's instructions. Briefly, 20-30 mg of tissue were cut on a sterile Petri dish and lysed with a solution containing buffer RLT with 1% of 2-Mercaptoethanol. The tissue was disrupted using a sterile plastic pestle. To reduce the viscosity, the cell lysate was homogenized by five consecutive passes through a blunt 18 gauge needle fitted on a 10 ml syringe. After centrifugation (3 min at 11300 G), the supernatant was decanted and one volume of 70 % ethanol was added. The solution was then applied onto the membrane of an RNeasy mini column (Qiagen, UK) and centrifuged for 15 sec at 6700 G, during which the RNA was bound to the membrane. To efficiently remove potential contaminants, columns were washed three times using simple wash-spins with ethanol-containing buffers RW1 and RPE according to the manufacturer's protocol. Finally, RNA was eluted with 30 µl of RNAse free water after 1 min centrifugation at 9500 G.

5.2.1.2 Assessing quantity, quality and integrity of RNA

The quantity of RNA obtained was determined for each sample by optical density (OD) measurement using the Nanodrop® ND-1000 UV-Vis spectrophotometer (Thermo Scientific, UK). OD 260/280 and 260/230 ratios were used to evaluate RNA purity. Presence of intact RNA subunits 28S and 18S were checked in an automated capillary-electrophoresis system, the QIAxcel system (Qiagen,UK). All

samples were diluted to a final concentration of 50 ng/µl before performing reverse transcription.

I selected 60 RNA samples extracted from whale skin biopsies (22 blue whales, 22 fin whales and 16 sperm whales; details in Appendix 5.2). The maximum and minimum concentrations obtained for these samples were 634 ng/µl and 51 ng/µl, respectively (mean for all samples: 233 ng/µl ± 42.38 SE). The samples showed an absorbance ratio at 260/280 nm between 2.1 and 1.81, and an absorbance ratio at 260/230 nm greater than 0.95 except for four samples that showed an absorbance ratio of 0.85, 0.75, 0.74 and 0.59. All samples selected showed one or two intact bands at visual examination in the QIAxcel system (Qiagen, UK; see example on Appendix 5.3).

5.2.1.3 Reverse transcription polymerase chain reaction

Complementary DNA (cDNA) was obtained by reverse transcription using the QuantiTect® Reverse Transcription Kit (Qiagen, UK). This procedure includes a first step of DNA digestion. Briefly, the genomic DNA elimination reaction (14 µl total volume containing 1X gDNA wipeout buffer and 12 µl of the diluted RNA sample) was incubated for 2 min at 42°C and immediately placed on ice. The reverse transcription master mix (total volume of 20 µl) included quantiscript reverse transcriptase, 1X quantiscript RT buffer (containing dNTPs), 0.7 µM RT primer mix (including oligo-dT, random primers, dNTPs and Mg^{2+}) and the genomic DNA elimination reaction. Three samples were prepared without the quantiscript reverse transcriptase, to act as RT negative controls and confirm absence of DNA in the samples. The reverse transcription (RT-) reaction included two steps: 20 min at 42°C and 3 min at 95°C. RT reactions were performed on a GenAmp® PCR System 9700 (Applied Biosystems, UK) thermalcycler. Prior to use, cDNA was diluted 1:25 with nuclease free water and conserved at -20°C.

5.2.2 Primer design and validation

5.2.2.1 Primer design

Primers were designed for the three selected genes. First, for each gene, cDNA sequences listed for other species were searched for in the NCBI GenBank database (www.ncbi.nlm.nih.gov). Sequences were aligned using the free Multiple Alignment software ClustalW (www.ebi.ac.uk/Tools/msa/clustalw). Primer pairs were designed within conserved regions, ideally spanning two exons to avoid DNA amplification. The primers were targeted to amplify a small region (100-200 nucleotides) in order to reduce the effect of possible RNA degradation and maintain good standards during the quantitative PCR (qPCR) procedure. In addition, each primer was 18-24 bp length, containing between 50-55 % of guanine (G) and cytosine (C) nucleotide bases, had a melting temperature (Tm) of 60°C and ended with a G or C at the 3' end. Occurrence of hairpins, homodimers and heterodimers were checked in the Integrated DNA technology freeware (IDT, http://eu.idtdna.com/analyzer/Applications/OligoAnalyzer/Default.aspx). Finally, primers were analysed in the Basic Local Alignment Tool (BLAST, www.ncbi.nlm.nih.gov/BLAST/) to confirm their specificity.

5.2.2.2 PCR validation

Each primer pair was tested in two samples of each species by independent PCRs. The total volume per reaction was 12.5 µl and contained 1X PCR buffer (Tris-Cl, KCl, $(NH_4)_2SO_4$ and $MgCl_2$; Qiagen, UK), 0.2 mM dNTPs (Bioline, UK), 0.4 µM of each primer, 0.325 U of HotStarTaq®Plus DNA polymerase (Qiagen, UK) and 1 µl of cDNA. The PCR conditions were 95°C for 5 min, 35 cycles of 94°C for 1 min, 60°C for 45 s, 72°C for 30 s, and a final extension at 72°C for 10 min. Amplification products were run on a 2 % agarose gel stained with 2.5X SYBR® Safe DNA stain gel (corresponding to 0.1 µl per ml; Invitrogen, USA). Fragments were excised and cleaned using the QIAquick® gel extraction kit (Qiagen, UK) before being sent for bi-directional Sanger sequencing (Cogenics, UK). Each sequence obtained was

analysed using BLAST to confirm that the PCR product amplified corresponded to the gene targeted.

5.2.2.3 Final primers

Five primer pairs were designed for *KIN* by aligning highly conserved exonic regions of this gene in cow, horse, chimpanzee, mouse and human genomes. Three primer pairs were designed for *P53* by aligning dolphin, cow, pig and human sequences, while one pair was designed for *HSP70* using the cDNA sequence reported for a north Atlantic Right whale (Ierardi et al., 2009). Most of the primers successfully amplified in the three whale species. For each gene, I selected the set of primers that best generated a single and well-defined band and a unique qPCR dissociation curve (Appendix 5.4). Finally, the specificity of the selected primers was confirmed via bi-directional sequencing as described previously (complete sequences provided in Appendix 5.5). The primers selected for the rest of the analyses are described in Appendix 5.6.

5.2.3 Normalization of real-time quantitative PCR

5.2.3.1 Internal control gene candidates

I selected internal control genes as those whose levels of expression are known to not be affected by exposure to UVR in humans and that have been shown to be "stable" in other marine mammal species. The primer sets of the four control genes that fitted these criteria were obtained from a previous study conducted on striped dolphins (Spinsanti et al., 2006), being the genes coding for the ribosomal proteins S18 (*RSP18*), ribosomal proteins L4 (*RPL4*), succinate dehydrogenase complex subunit A (*SDHA*) and phosphoglycerate kinase 1 (*PGK1*). Although the genes coding for the Glyceraldehyde-3P-dehydrogenase (*GAPDH*) and tyrosine 3-monoxygenase (*YWHAZ*) have been reported as reliable control genes in dolphins (Spinsanti et al., 2006), these were not included in the present study because *GAPDH* expression is known to fluctuate during epithelial differentiation (Steele et al., 2002) and *YWHAZ* interacts with the process of apoptosis (Li et al., 2010), both being processes that are

affected by exposure to UVR (Costin and Hearing, 2007; De la Coba et al., 2009). Instead, I selected *RSP18* and *RPL4*, the next most stable genes in dolphin skin (Spinsanti et al., 2006) and not biologically related to UVR exposure and epithelial proliferation nor apoptosis. Furthermore, although *PGK1* appeared to be less suitable as a control gene in striped dolphin skin (Spinsanti et al., 2006), I selected it for our study because in humans it is, together with *SDHA*, the most reliable control gene when studying the effects of exposure to UV-B radiation on keratinocytes (Balogh et al., 2008). The selected primer pairs were synthesized and tested for specificity in the three whale species as described above (section 5.2.3.2).

5.2.3.2 Standard curve and amplification efficiency

PCR products were used as a template for the construction of standard curves for each of the genes tested. For this, three amplified products of each gene were run on a 2% agarose gel, excised and cleaned using the QIAquick® gel extraction kit (Qiagen, UK). PCR quantity was measured with the Nanodrop® ND-1000 UV-Vis spectrophotometer (Thermo Scientific, UK) and seven dilutions were made to obtain stocks containing 10^2 to 10^8 copies of PCR product per µl. The seven dilutions were run in triplicate in a 7300 Real-Time PCR System (Applied Biosystems, UK) as described below (section 5.2.4.3.). The logarithm of the product quantity obtained for each threshold value (Ct) was plotted against the Ct values to obtain the linear correlation coefficient (R^2) for each gene. The slope of the curve was used to calculate qPCR amplification efficiencies ($E=10^{1/-slope}-1$) for each set of primers (Schmittgen and Livak, 2008). The R^2 and amplification efficiency of all genes tested ranged from 0.991 to 1 and 0.92 to 1.01, respectively.

5.2.3.3 Real-time quantitative PCR using SYBR green

All qPCRs were performed in a 7300 Real-Time PCR System (Applied Biosystems, UK) using Power SYBR Green PCR Master Mix (Applied Biosystems, UK) following the same principle as described in Chapter four (section 4.3.1.2; Fig. 4.9). The total volume of each qPCR reaction was 10µl, which included forward and reverse primers (500 nM), 1X Power SYBR Green PCR Master Mix (Applied

Biosystems, UK) and the cDNA sample (2µl of a 1:25 cDNA dilution). 96-well reaction plates were set up to include sample triplicates and three no-template controls (NTC) to control for inadvertent contamination. Three RT-negative controls were run in the first plate to confirm that DNA elimination was successful.

Cycling conditions were an initial 2 min at 50°C, followed by 15 min at 95°C, and 40 cycles of 15 s at 95°C, 1 min at 60°C and 1min at 72°C. A melting curve analysis (95ºC/15sec; 60ºC/1min; 95ºC/15sec; 60ºC/15sec) was added at the end of the final cycle to detect non-specific amplifications. The 7300 Real-Time PCR System software (Applied Biosystems, UK) was used to determine each Ct. The mean of the triplicate reactions were calculated for each sample (standard deviation = ± 10 % of the mean).

5.2.4 Statistical analysis

5.2.4.1 Stability of Internal control gene expression

To examine the stability of the selected control genes, I randomly selected 20 cDNA samples (7 blue whales, 7 fin whales and 6 sperm whales). Gene expression values were analyzed using the packages BestKeeper, geNorm and NormFinder (freely available at http://gene-quantification.com/bestkeeper.html, http://medgen.ugent.be/~jvdesomp/genorm and http://www.mdl.dk/publicationsnormfinder.htm, respectively).

Briefly, the Excel-based program BestKeeper ranks the control gene candidates according to the standard deviation of their Ct-value ($SD_{Ct\ value}$). The correlation (Pearson correlation coefficient and probability) between each gene and the index was calculated in order to determine the best suited genes (Pfaffl et al., 2004). For this, BestKeeper assumes that the Ct-value for each gene is normally distributed, an assumption that was confirmed by a Shapiro test. The software geNorm ranks the candidate genes according to their average expression stability M. Briefly, a variation parameter V_{jk} is calculated for every combination of two internal control genes *j* and *k*. V_{jk} is equal to the standard deviation (SD) of the sum of the logarithmic

transformed level expression ratio of the two tested genes measured for each sample *i* (see Equation 5.1) (Vandesompele et al., 2002).

$$(\forall j,k \in [1,n] \text{ and } j \neq k) : V_{jk} = SD\left[\log_2\left(\frac{a_{ij}}{a_{ik}}\right)_{i=1\rightarrow m}\right] \quad \text{(Eq. 5.1)}$$

M_j is determined for each gene *j* as the arithmetic mean of all V_{jk} (Vandesompele et al., 2002). Ideally, the expression ratio of two tested genes is identical in all samples. Increasing variation in ratio corresponds to decreasing expression stability (Vandesompele et al., 2002). Finally, normFinder ranks the control gene candidates according to their expression stability and allows the estimation of intra- and intergroup expression variation, which makes this software analysis more robust when using co-expressed genes (Andersen et al., 2004).

For geNorm and NormFinder, I used transformed Ct values corresponding to the quantities obtained with the standard curve (Andersen et al., 2004; Vandesompele et al., 2002), whereas raw Ct values were used for BestKeeper (Pfaffl et al., 2004).

5.2.4.2 Target gene expression

Gene expression levels were analysed using the relative quantification method (level of expression of the target gene relative to internal control genes) that is based on the ΔCt method ($Ct_{\text{target gene}}$- geometric mean $Ct_{\text{control genes}}$) (Schmittgen and Livak, 2008; Vandesompele et al., 2002). In order to control for a possible effect of the qPCR plate on the level of gene expression (each of the 15 qPCR plates prepared might reflect some grouping of the data that could hide a potential effect of interest; see Appendix 5.2 for details on the data used in the analyses), I used linear mixed effect modelling (for method details see section 2.2 in Chapter two) (Zuur et al., 2009) to investigate inter-, intra-species and temporal variations in gene expression.

Instead of building a full model that included all explanatory variables of interest, a series of independent models, each one answering a specific question, were fitted. Indeed, the limited number of observations per group (60 observations in total;

sample size detail per group in Appendix 5.2), did not allow including more than six explanatory variables including interaction terms and a random factor) as too many degrees of freedom would have been lost and thus the power of the analysis considerably reduced. Thus, it was not always possible to control for a potential effect of 'species' and/or 'sampling month' on the variation of the data. Potential effects of 'year' were not controlled for as some species were only sampled in a specific month/year and thus yearly variation data would be biased by a month effect. However, as levels of solar ultraviolet radiation differ more between months than between years in the Gulf of California (see section 2.5 in Chapter two), it was more parsimonious to include month and not year as a variable in the models.

Violation of normality or homoscedasticity assumption (see section 2.3 in Chapter two) was corrected by logarithmic transformation of the response variable. As lower ΔCt values represent higher levels of expression, it was easier for the interpretation of the results to negatively transform the response variable. The transformed values used were: - log (ΔCt_{gene}).

5.3 Results

The first part of this section describes the results of the analyses used to select the two best internal control genes, an essential step when wishing to study the variation in levels of expression of target genes.

5.3.1 Stability of internal control gene expression

The expression stabilities of the genes RPS18, RPL4, PGK1 and SDHA were analysed using the freeware packages BestKeeper, geNorm and NormFinder.

5.3.1.1 Bestkeeper analysis

All the candidate genes were stably expressed ($SD_{Ct\ value} \leq 1$; Table 5.1; Fig. 5.2) and thus were considered as suitable control genes (Pfaffl et al., 2004). When considering all study species together, the two most stables genes, according to their $SD_{Ct\ value}$,

were *RPL4*, and *RPS18* followed by *SDHA* and *PGK1* (Table 5.1). Thus, all candidate genes were used for the calculation of the BestKeeper index, which corresponds to the geometric mean of the Ct-value of all suitable candidate genes (Pfaffl et al., 2004). When pooling samples from the three species, the most suitable genes, according to their coefficient of correlation, were in order: *RPS18*, *RPL4* or *PGK1* and *SDHA* (Table 5.1). When looking at each species separately, *RPS18* had the highest correlation coefficient in all cases, while the second best candidate gene differed amongst species, being *RPL4* for fin and sperm whales and *PGK1* for blue whales. Sample integrity was of high quality, as all intrinsic variances (InVar [±x-fold]) ranged between 0.05 and 0.97. One sample showed a higher InVar value (2.43) but was still within the range of acceptance (Pfaffl et al., 2004).

Table 5.1. Descriptive statistics of gene expression values obtained with the Bestkeeper software.

	RPS18	**SDHA**	**PGK1**	**RPL4**
n	20	20	20	20
GM	19.23	26.91	23.44	19.10
AM	19.25	26.93	23.47	19.12
Min	17.92	25.19	21.51	17.55
Max	22.11	28.89	26.60	21.18
SD	0.84	0.84	1.00	0.70
CV	4.35	3.12	4.26	3.66
Corr. coeff.	**0.97**	0.648	0.94	0.94
p-value	0.001	0.002	0.001	0.001

Gm (Geometric Mean), Min (Minimum), Max (Maximum), SD (Standard Deviation), CV (Coefficient of variance) of the Ct-value of the 20 samples (n) for each candidate gene. The last two rows show the coefficient of correlation (Corr.coeff.) and its p-value between the BestKeeper index and each of the candidate genes. The most reliable candidate gene is the one showing the highest correlation coefficient with the BestKeeper index (in bold).

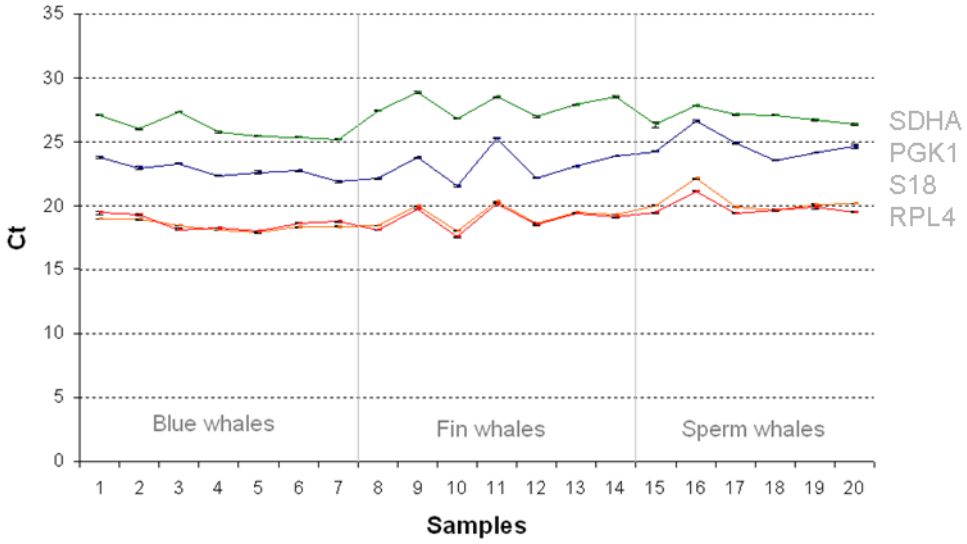

Figure 5.2. Expression levels of the internal control gene candidates. Mean Ct-values (left axis) for 20 blue, fin and sperm whales (n = 7, 7 and 6, respectively). RPS18 = 19.25 ± 0.23 SE, RPL4 = 19.12 ± 0.19 SE, PGK1 = 23.47 ±0.28 SE, SDHA = 26.93 ±0.24 SE. Bars ± SE.

5.3.1.2 geNorm analysis

The expression of the four tested genes showed strong stability; the highest M value (0.98) detected (*SDHA*) being lower than the program's default limit of M=1.5. The two most stable genes for the three species were *RPS18* and *RPL4* (Fig. 5.3). When looking at each species separately, the best candidate genes for blue and fin whales were *RPS18* and *RPL4* whereas for sperm whales *RPS18* and *PGK1* were better suited in terms of stability. The optimal number of control genes needed for qPCR normalization was higher than four genes when comparing the three species ($V_{3/4}$ = 0.237 > 0.15 default cut-off value), whereas when looking at each species separately, less than three genes were needed.

5.3.1.3 NormFinder analysis

Analysing the three species together, the gene with the lowest (best) stability value was *RPL4* (stability value: 0.184; Fig. 5.3) and the most suitable gene combination was *RPS18* with *RPL4*, having a stability value of 0.184. When analysing the three

species separately, the best gene in all cases was *RPS18*, concurring with the results generated with the other software (Table 5.2). To find which genes were sufficiently stable to compare expression levels between the three species, I drew a bar plot of the intergroup variation (Fig. 5.4). The top-ranked candidates were *RPS18* and *RPL4*, those with an inter-group variation closest to zero and smallest error bars (Fig. 5.4).

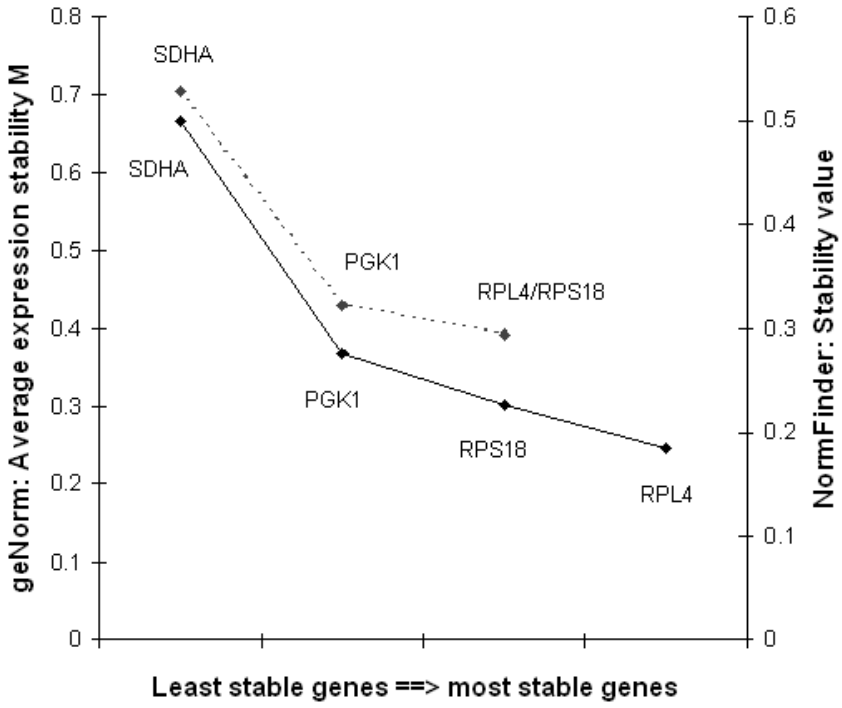

Figure 5.3. Gene expression stability of the internal control gene candidates. The average expression stability (M) values of the candidate genes were calculated with geNorm after stepwise exclusion of the least stable gene (left axis; M value from the least stable on the left to the most stable on the right: 0.705, 0.430 and 0.392; plain line). The right axis corresponds to the stability values calculated with NormFinder (stability value from left, least stable, to right, most stable: 0.501, 0.275, 0.227 and 0.184; dotted line).

Table 5.2. Best internal control genes for each whale species calculated with BestKeeper, geNorm and NormFinder.

	Blue whale	Fin whale	Sperm whale
BestKeeper	RPS18 / PGK1	RPS18 / RPL4	RPS18 / RPL4
geNorm	RPS18 / RPL4	RPS18 / RPL4	RPS18 / PGK1
NormFinder	RPS18 / PGK1	RPS18 / RPL4	RPS18 / RPL4

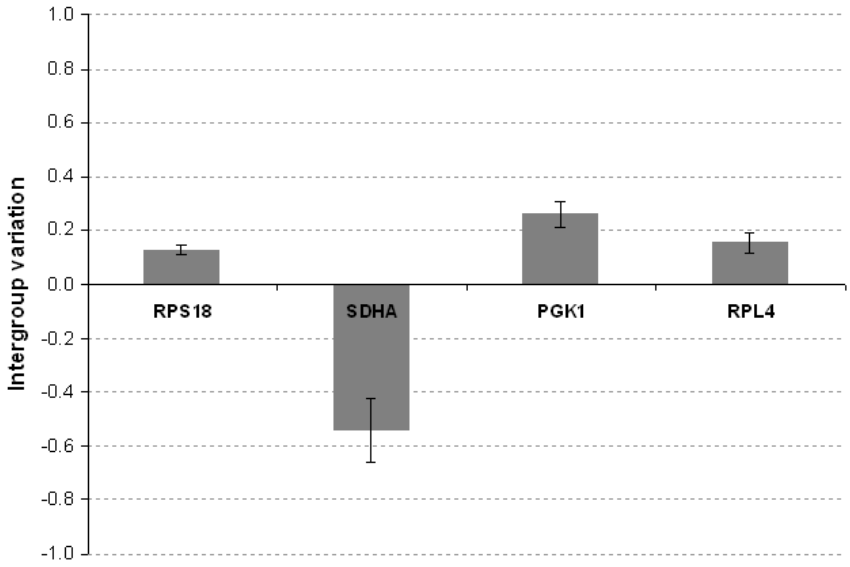

Figure 5.4. Inter-species variations of the internal gene candidates. The top ranked internal control gene candidates were *RPS18* and *RPL4*, having an inter-group variation close to zero and small error bars (average of intra-group variance). Blue whales = group 1, fin whales = group 2 and sperm whales = group 3. Bars ± SE.

To conclude, all software packages concurred in selecting *RPL4* and *RPS18* as best intra- and interspecies control genes. Thus, I used them for subsequent expression analyses of target genes.

5.3.2 Variation of gene expression levels

5.3.2.1 Levels of gene expression

The gene with the highest expression level was the gene coding for the heat shock protein 70 (*HSP70*; ΔCt mean = 5.22 ± 0.21 SE, n = 60). Expression levels for *HSP70* were 1.31 times the levels observed for the tumour protein *P53* gene (ΔCt mean = 6.72 ± 0.12 SE, n = 59) and 1.69 times that of the gene coding for the KIN protein (ΔCt mean = 8.85 ± 0.11 SE, n = 60) (Fig. 5.5).

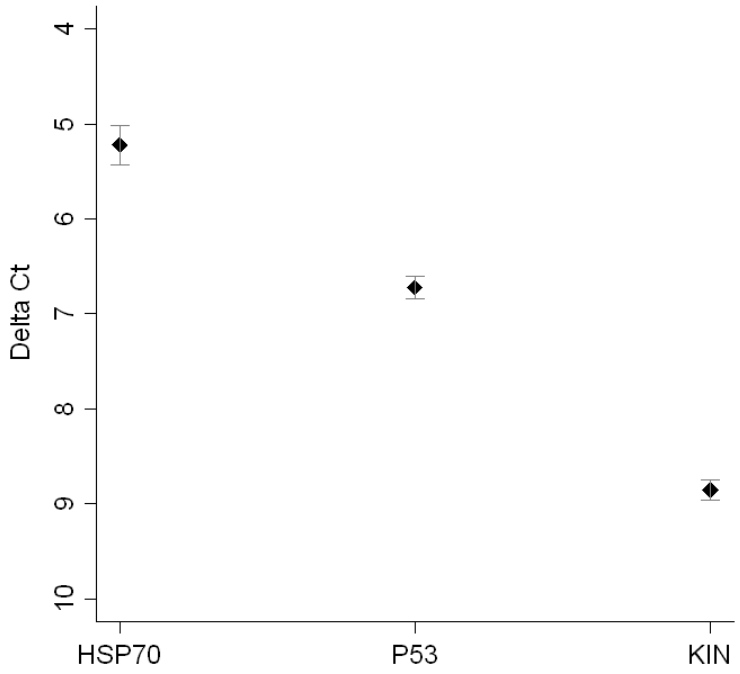

Figure 5.5. Means of the level of expression of the genes (in ΔCt, y axis inverted) *HSP70* (n=60)**, *P53*** (n=59) **and *KIN*** (n=60) **amongst species.** Lower ΔCt values represent higher levels of expression. Bars = ± SE.

To investigate whether gene expression levels were correlated, I fitted three mixed effects models, one for each of the target genes (Table 5.3). Direct relationships were observed between the expressions of *KIN* and H*SP70* and the expression of *P53* and

HSP70 (Table 5.3; Fig. 5.6). No correlation was observed between *P53* and *KIN* expression levels (Table 5.3).

Table 5.3. Likelihood ratio tests (left half of the table) used for constructing the three independent minimal adequate models (right half of the table) showing relationships between the expressions of the genes. The left part of the table provides the explanatory variables (Expl) included in the full model and their corresponding likelihood ratios (LR) and p-value (p). The factors plate (15 levels), species (3 levels) and month (four levels) were fitted as explanatory variables to control for their potential effect on the variation of gene expression. The right part of the table presents the value and standard error (SE) of the estimated coefficients (intercept and slope), the t- and p-values obtained using the Student's t-test (Ho: value of the estimated parameter equals zero) and degrees of freedom (df). Bold text indicates $p \leq 0.05$. The retained variable of interest is highlighted in grey. Transformed values used: - log (ΔCt_{gene}).

Gene	***Expl***	***LR***	***p***	***Param***	***value***	***SE***	***df***	***t***	***p***
KIN	*P53 : HSP70*	3.56	0.06	*Intercept*	-2.02	0.06	55	-32.89	0.00
	Months	1.14	0.77	*HSP70*	0.12	0.04	55	3.37	**0.001**
	P53	0.98	0.32	*fin*	0.04	0.02	55	1.70	0.09
	Species	7.50	**0.02**	*sperm*	0.05	0.03	55	1.60	0.11
	HSP70	7.26	**0.01**						
	plate-random	2.55	0.11						
P53	*KIN : HSP70*	1.54	0.21	*Intercept*	-1.63	0.10	52	-16.49	0.00
	KIN	0.07	0.78	*HSP70*	0.21	0.05	52	3.86	**0.0003**
	Species	8.42	**0.01**	*fin*	-0.01	0.03	52	-0.41	0.68
	Months	15.46	**0.002**	*sperm*	-0.16	0.06	52	-2.69	**0.01**
	HSP70	14.60	**0.0001**	*March*	0.12	0.04	52	2.98	**0.004**
	plate-random	0.20	0.65	*April*	0.17	0.04	52	4.02	**0.0002**
				May	0.11	0.05	52	2.10	**0.04**
HSP70	*P53 : KIN*	0.75	0.39	*Intercept*	1.41	1.36	38	1.03	0.31
	KIN	2.35	0.13	*P53*	0.59	0.18	38	3.25	**0.002**
	Months	11.52	**0.01**	*fin*	0.10	0.30	38	0.35	0.73
	Species	39.70	**<0.0001**	*sperm*	-2.98	0.48	38	-6.15	**<0.0001**
	P53	10.59	**0.001**	*March*	-0.30	0.43	38	-0.68	0.50
	plate-random	10.43	**0.001**	*April*	0.28	0.47	38	0.60	0.55
				May	1.28	0.51	38	2.52	**0.02**

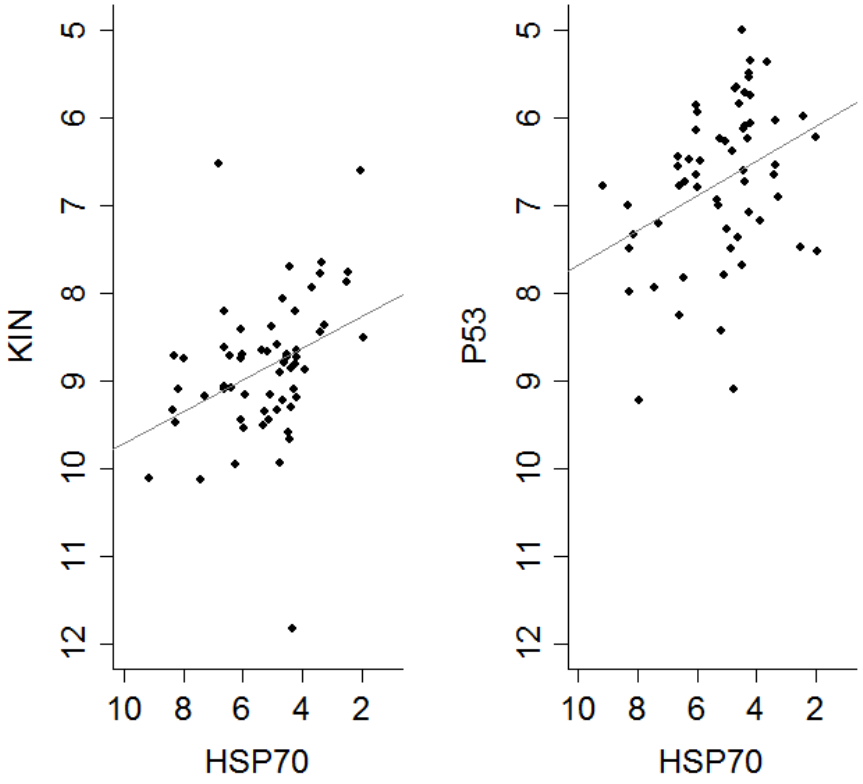

Figure 5.6. Correlation of gene expression levels (in ΔCt) between DNA repair genes (*KIN* left, *P53* right) and the gene coding for the heat shock protein (*HSP70*). Lower ΔCt values represent higher levels of expression. The lines show regression lines.

5.3.2.2 Interspecies variation

To investigate whether gene expression varied between species and whether individual skin pigmentation (measured as the quantity of melanocytes) had an effect on the level of expression of the genes, I fitted three independent mixed effects models, one for each of the target genes (Table 5.4).

In all cases, the model with the random effect provided a significantly better fit to the data (Table 5.4) (Zuur et al., 2009). For both *KIN* and *HSP70* genes, the interaction terms (interaction between species and the quantity of melanocytes) and the main effects of the quantity of melanocytes were not retained in the final models (Table 5.4) suggesting that the expression of *KIN* and *HSP70* genes does not depend on

individual skin pigmentation. The final fitted models showed that there was a significant difference between species in the levels of expression of these two genes, with the sperm whales, the species spending the longest time at the surface, showing the highest levels (Table 5.4; Fig. 5.7). No differences were observed between blue and fin whales (Table 5.4; Fig 5.7), the two species with similar surface behaviour but different skin colour, confirming that skin pigmentation differences between species does not have an effect on the *HSP70* and *KIN* gene expression. Interestingly, the fitted model that examined variation in *P53* expression levels included a significant interaction between melanocyte abundance and species on the expression of *P53* (Table 5.4).

Table 5.4. Likelihood ratio tests (left half of the table) used to obtain the estimated values of the three independent minimal adequate models (right half of the table) showing differences between species in gene expression. The explanatory variables included in the full model were species, the quantity of melanocytes (Qm) and the interaction between the two (species:Qm), while 'plate' was fitted as a random factor. Bold text indicates $p \leq 0.05$. The transformed response variable was: - log (ΔCt_{gene}).

Gene	*Expl*	*LR*	*P*	*Param*	*value*	*SE*	*df*	*t*	*p*
KIN	*species:Qm*	1.76	0.41	*Intercept*	-2.22	0.02	35	-108.04	0.00
	Qm	0.44	0.51	*fin*	0.02	0.02	35	1.10	0.28
	species	13.87	**0.003**	*sperm*	0.11	0.03	35	4.08	<**0.0005**
	plate-random	5.11	**0.02**						
HSP70	*species:Qm*	1.21	0.55	*Intercept*	-1.67	0.07	35	-25.49	0.00
	Qm	0.82	0.37	*fin*	-0.04	0.06	35	-0.71	0.48
	species	10.59	**0.005**	*sperm*	0.25	0.07	35	3.34	**0.002**
	plate-random	10.99	<**0.001**						
P53	*species:Qm*	10.14	<**0.001**	*Intercept*	-1.86	0.07	30	-26.28	0.00
	Qm	na*	na*	*fin*	-0.15	0.09	30	-1.61	0.12
	species	na*	na*	*sperm*	0.10	0.10	30	1.00	0.33
	plate-random	9.00	**0.003**	*Qm*	0.00	0.00	30	-0.17	0.87
				fin:Qm	0.01	0.01	30	1.28	0.21
				sperm:Qm	-0.01	0.01	30	-1.34	0.19

*na : not applicable

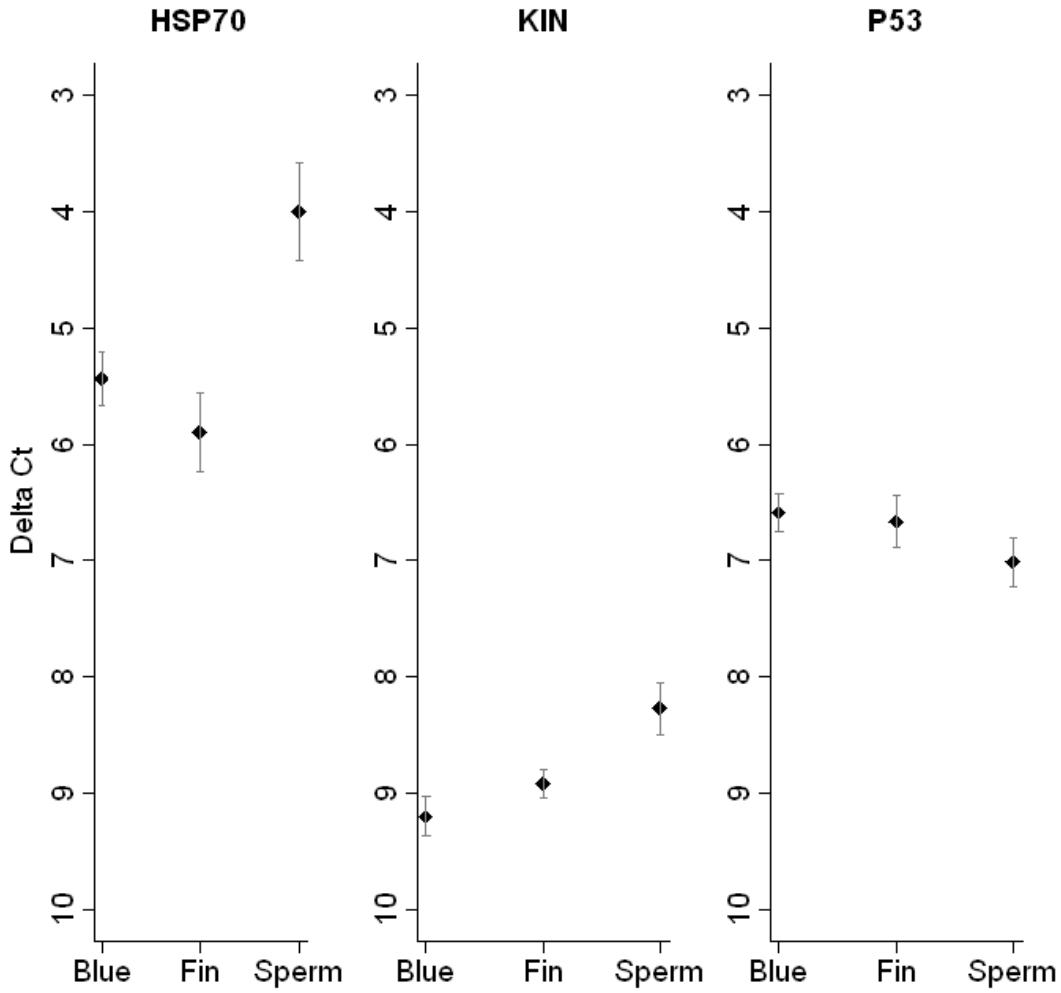

Figure 5.7. Mean level of expression of *HSP70, KIN* and *P53* genes (in ΔCt) in blue whales (n = 22), fin whales (n = 22) and sperm whales (n = 16). Lower ΔCt values represent higher levels of expression. This figure includes all years. Bars = ± SE.

To confirm that the differences observed between species were not biased by the month of sampling, particularly because sperm whales were only sampled in April/May (details in Appendix 5.2), the same analyses were run only for the period including the months of April and May. Although the sample size was reduced (n = 6, 13, 16 respectively for blue, fin and sperm whales), comparable results were obtained showing the significance of the factor species for *HSP70*, *KIN* and *P53* (Table 5.5). Analyses were repeated for samples collected during the year 2008 (all months included) and, again, results were similar (Table 5.5). Interestingly, an

inverse relationship was observed between melanocyte abundance and expression of *P53* (Table 5.5).

Table 5.5. Likelihood ratio tests (left half of the table) used for estimating values of six independent minimal adequate models (right half of the table) of the effect of species and skin pigmentation on the expression of *KIN*, *HSP70* and *P53* genes during April/May sampling period and for 2008. The explanatory variables included in the full models were species, the quantity of melanocytes (Qm) and the interaction between the two (species:Qm), while 'plate' was fitted as a random factor. Bold text indicates $p \leq 0.05$. In all cases, the response variable transformed was: - log (ΔCt_{gene}).

Gene	*Expl*	*LR*	*p*	*Param*	*value*	*SE*	*df*	*t*	*p*
KIN	*species:Qm*	1.39	0.50	*Intercept*	-2.20	0.04	26	-51.05	0.00
Apr/May	*Qm*	1.47	0.23	*fin*	0.01	0.05	26	0.12	0.91
	species	7.32	**0.03**	*sperm*	0.08	0.05	26	1.61	0.12
	plate-random	1.94	0.16						
KIN	*species:Qm*	2.01	0.37	*Intercept*	-2.20	0.03	22	-63.55	0.00
in 2008	*Qm*	1.37	0.24	*fin*	0.01	0.05	22	0.26	0.79
	species	5.78	**0.05**	*sperm*	0.08	0.04	22	1.90	**0.07**
	plate-random	1.60	0.21						
HSP70	*species:Qm*	0.36	0.84	*Intercept*	-1.85	0.13	13	-14.60	0.00
Apr/May	*Qm*	0.22	0.64	*fin*	0.14	0.12	13	1.11	0.29
	species	10.98	**0.004**	*sperm*	0.44	0.12	13	3.68	**0.003**
	plate-random	6.27	**0.01**						
HSP70	*species:Qm*	1.95	0.38	*Intercept*	-1.75	0.10	13	-17.70	0.00
in 2008	*Qm*	0.01	0.91	*fin*	-0.08	0.10	9	-0.83	0.43
	species	15.66	<**0.0005**	*sperm*	0.33	0.09	9	3.56	<**0.01**
	plate-random	6.03	**0.01**						
P53	*species:Qm*	19.31	**0.0001**	*Intercept*	-1.70	0.08	13	-21.30	0.00
Apr/May	*Qm*	na*	na*	*fin*	-0.26	0.09	9	-2.78	**0.02**
	species	7.89	**0.02**	*sperm*	-0.08	0.09	9	-0.85	0.42
	plate-random	7.92	**0.005**	*Qm*	-0.02	0.01	9	-3.05	**0.01**
				fin:Qm	0.02	0.01	9	3.89	**0.004**
				sperm:Qm	0.01	0.01	9	1.48	0.17
P53	*species:Qm*	5.14	0.0764	*Intercept*	-1.88	0.05	12	-37.16	0.00
in 2008	*Qm*	6.84	<**0.01**	*fin*	0.00	0.05	8	0.03	0.98
	species	6.85	**0.03**	*sperm*	0.11	0.05	8	2.18	0.06
	plate-random	3.89	**0.05**	*Qm*	-0.01	0.00	8	-2.85	**0.02**

*na = not applicable

5.3.2.3 Association of gene expression with epidermal damage

The unequal number of observations per level of apoptotic cells (n = 1, 1, 8, 16 for level 0, 1, 2, 3 respectively; level 0 corresponding to absence of apoptotic cells and level 3 to high level of apoptotic cells; Fig. 5.8) did not allow a test for a relationship between level of *P53* expression and apoptosis. However, it is interesting to see that the variance of the measures of *P53* expression in level three (high abundance of apoptotic cells) is six times higher than the one in level two (variance = 0.21 and 1.26 respectively for levels 2 and 3). Measures of apoptosis were not included in the rest of the analyses on gene expression.

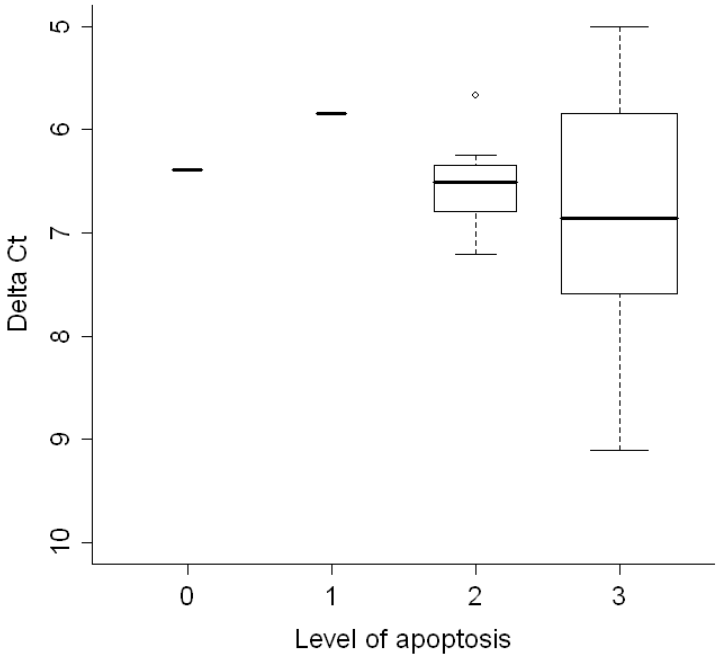

Figure 5.8. Box plot of *P53* expression (in ΔCt, y axis inverted) per level of apoptosis (level 0 indicates absence and level 3 indicates high abundance; n = 1, 1, 8, 16 for level 0, 1, 2, 3, respectively; box width is proportional to sample size).

To investigate whether the presence of oedema and cytoplasmic vacuolation was related to the level of the expression of the genes, I constructed three mixed effect models, one for each of the target genes (Table 5.6). Interestingly, the models

showed that expression of *P53* and *HSP70* was lower when oedema was present (Table 5.6; Fig. 5.9). The same trend was observed for the melanogenesis-related gene encoding tyrosinase protein (Fig. 6.12 in Chapter six). Surprisingly, species was not a significant explanatory factor in the *P53* model (Table 5.6). It is possible that the differences observed amongst species in the final *P53* models (Tables 5.3 and 5.5) were actually due to interspecies differences in the level of oedema (see Chapter three).

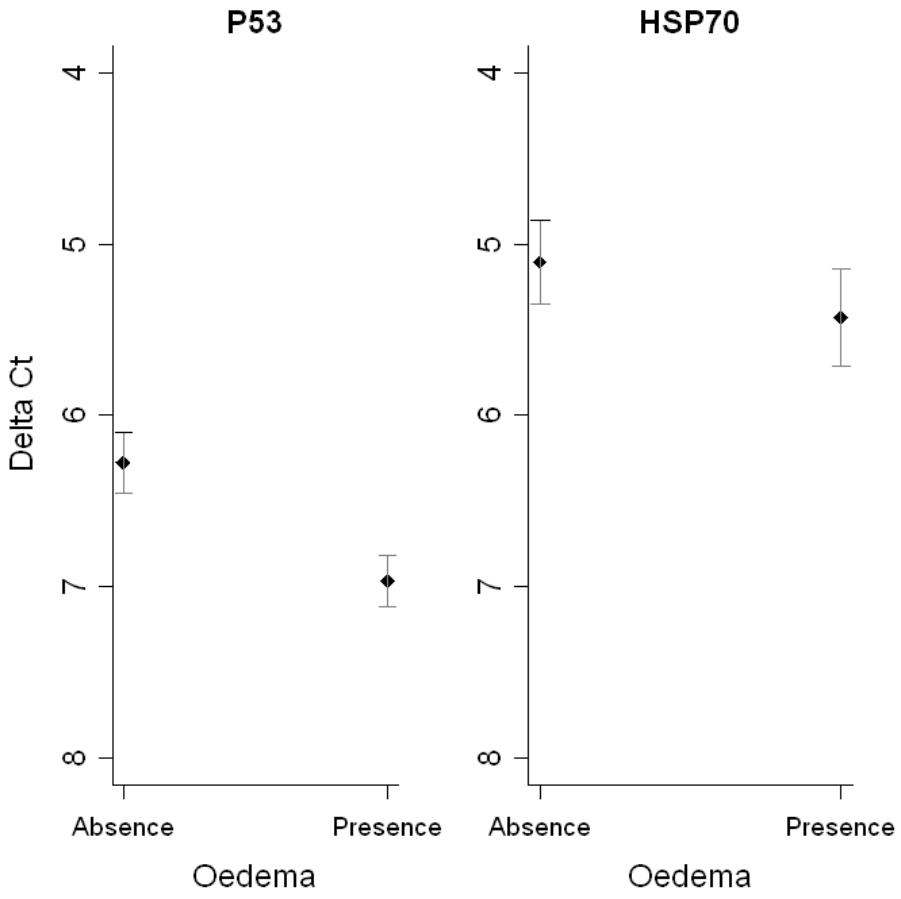

Figure 5.9. Relationship between mean expression levels of *P53* and *HSP70* genes (in ΔCt, y axis is inverted) and the presence of intracellular oedema (absence: n = 20; 1; presence: n = 37). Bars = ± SE.

Unexpectedly, vacuolation did not significantly predict gene expression and thus was not retained in the final models (Table 5.6). However, when observed graphically, there appears to be a slight trend where higher levels of gene expression, particularly for *HSP70*, tend to be observed when vacuoles are present (Fig. 5.10). *KIN*

expression was not significantly correlated with any of the epidermal lesions included in the full model (Table 5.6).

Table 5.6. Likelihood ratio tests (left half of the table) used for determining the three minimal adequate models (right half of the table) constructed to analyse the relation between gene expression and the presence of epidermal lesions. The explanatory variables included in the full model were the factor oedema (with two levels: absence=intercept, presence=oed), the factor vacuolation (vac with four levels including absence=intercept) and the interaction between the two. To control for potential effects of species and sampling month, I included these as explanatory variables. "Plate" was fitted as a random factor. Bold text indicates $p \leq 0.05$. The retained variable of interest is highlighted in grey. In all cases, the response variable transformed was: - log (ΔCt_{gene}).

Gene	***Expl***	***LR***	***P***	***Param***	***value***	***SE***	***df***	***t***	***p***
P53	*oed:vac*	1.21	0.75	*Intercept*	-7.03	0.26	51	-26.88	0.00
	species	0.60	0.74	*oed*	-0.60	0.21	51	-2.82	**0.01**
	vac	2.52	0.47	*March*	0.96	0.31	51	3.13	**0.003**
	oed	8.04	**0.005**	*April*	1.31	0.30	51	4.40	**0.0001**
	months	18.24	**0.0004**	*May*	0.46	0.29	51	1.60	0.12
	plate-random	2.32	0.13						
HSP70	*oed:vac*	3.01	0.39	*Intercept*	-1.66	0.09	36	-19.49	0.00
	vac	2.04	0.56	*oed*	-0.14	0.06	36	-2.20	**0.03**
	months	11.62	**0.01**	*Fin*	-0.02	0.06	36	-0.35	0.73
	oed	6.90	**0.01**	*Sperm*	0.51	0.10	36	4.88	**<0.0001**
	species	26.92	**<0.0001**	*March*	0.13	0.08	36	1.54	0.13
	plate-random	10.49	**0.001**	*April*	0.10	0.09	36	1.14	0.26
				May	-0.12	0.10	36	-1.20	0.24
KIN	*oed:vac*	2.63	0.45						
	months	5.22	0.16						
	vac	3.21	0.36						
	oed	0.79	0.37						
	species	13.05	**0.002**						
	plate-random	2.68	0.10						

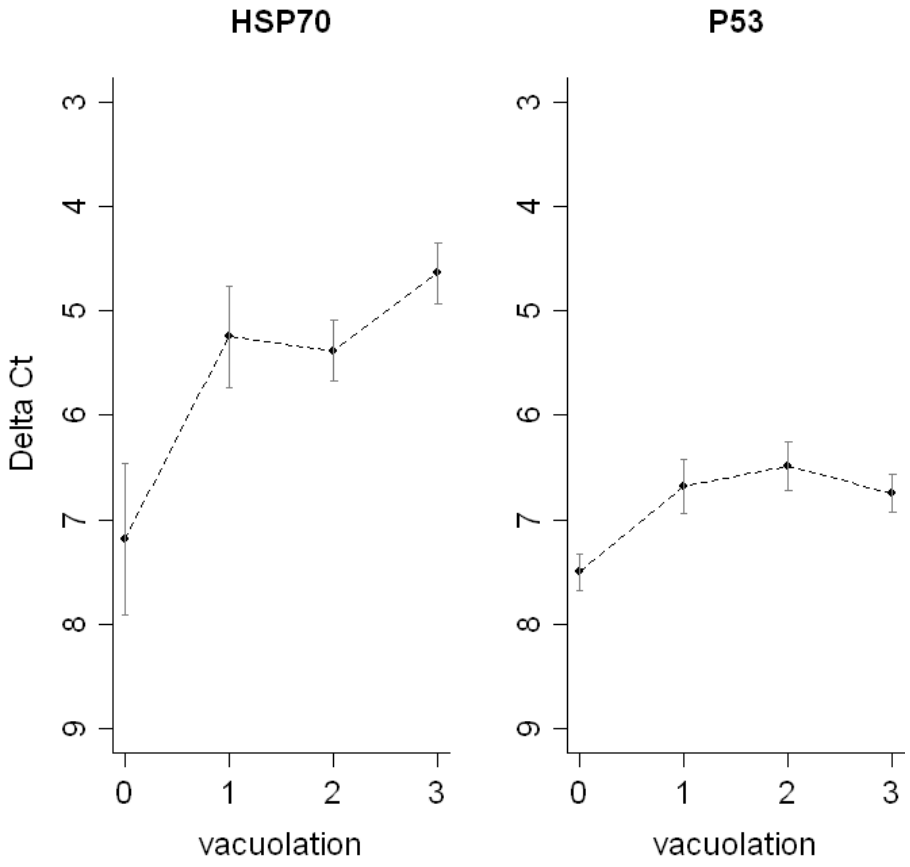

Figure 5.10. Relationship between *HSP70* and *P53* gene expression (in ΔCt, y axis inverted) and occurrence of cytoplasmic vacuolation (level 0 corresponding to absence and level 3 to high abundance; n = 5, 14, 20, 18 for level 0, 1, 2, 3 respectively). Bars ± SE.

5.3.2.4 Temporal variation

Data on sperm whales were excluded from this analysis as this species was mainly sampled during May 2008. Species was not a significant factor (Table 5.7), a result which is concordant with those presented in section 5.3.4.2, where no differences in gene expression levels between blue and fin whales were observed. *P53* and *HSP70* gene expression was significantly higher in March than in February (Table 5.7; Fig. 5.11). Significant differences in gene expression were also observed between April and February for *P53* (Table 5.7; Fig. 5.11). Nevertheless, May and February both showed similar levels of *P53* and *HSP70* expression. Although results need to be interpreted carefully due to the relatively small sample size per month, it seems that the expression of *P53* and *HSP70* follow a normal curve with a peak in March/April

(Fig. 5.11). No monthly differences were observed for *KIN* expression (minimal adequate model = null model; Table 5.7; Fig. 5.11).

Table 5.7. Likelihood ratio tests (left half of the table) used for constructing three minimal adequate models (right half of the table) that investigated variation in gene expression levels amongst months. The fixed explanatory variable is the factor month (with four levels including February as the intercept). To control for a potential effect of species, I included this factor (two levels: blue and fin whales) as an explanatory variable. "Plate" was fitted as a random factor. Bold text indicates $p \leq 0.05$. In all cases, the response variable was transformed: - log (ΔCt_{gene}).

Gene	***Expl***	***LR***	***P***	***Param***	***value***	***SE***	***df***	***t***	***p***
P53	*species*	1.07	0.30	*Intercept*	-2.00	0.03	40	-57.16	0.00
	month	13.39	**<0.005**	*March*	0.15	0.05	40	3.24	**<0.005**
	plate-random	2.43	0.12	*April*	0.19	0.05	40	4.07	**<0.0005**
				May	0.07	0.06	40	1.26	0.21
HSP70	*species*	0.44	0.51	*Intercept*	-1.73	0.07	26	-26.39	0.00
	month	15.02	**0.002**	*March*	0.16	0.07	26	2.34	**0.03**
	plate-random	10.53	**0.002**	*April*	0.08	0.07	26	1.12	0.27
				May	-0.12	0.09	26	-1.41	0.17
KIN	*species*	3.15	0.08						
	month	3.73	0.29						
	plate-random	1.52	0.22						

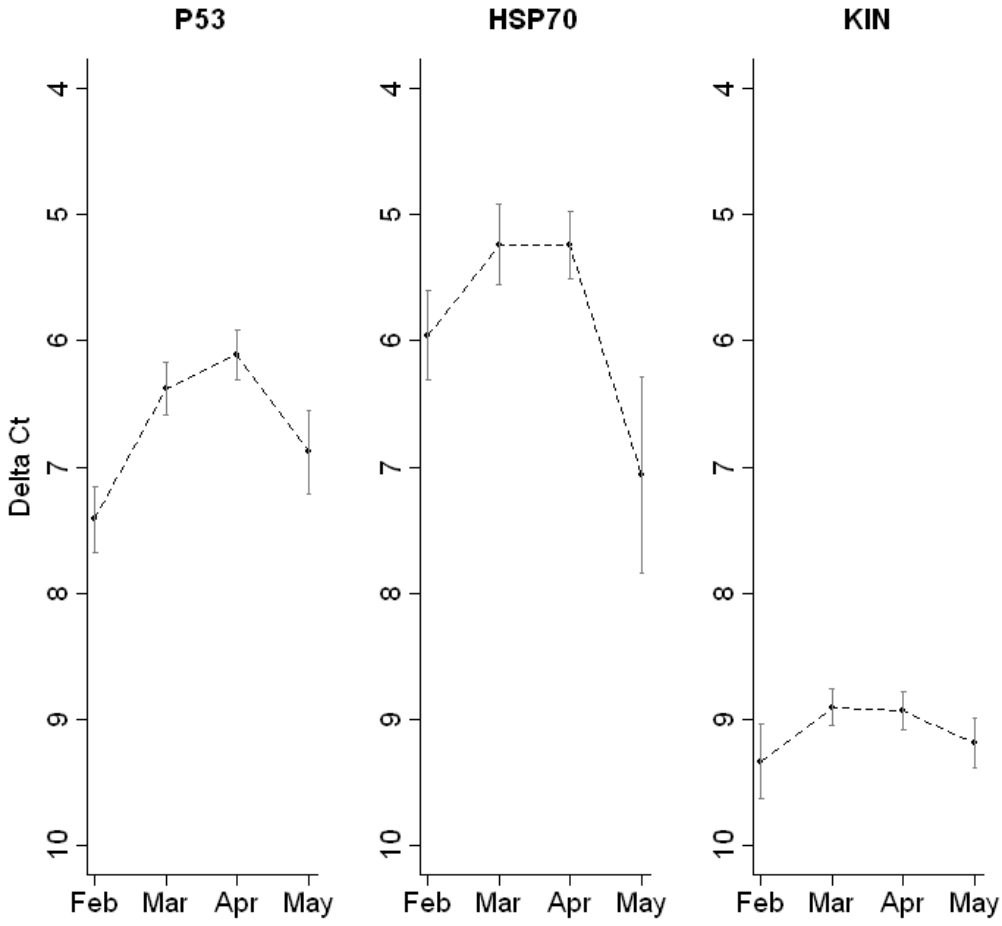

Figure 5.11. Monthly differences in mean expression levels of *P53, HSP70* and *KIN* genes (in ΔCt, y axis inverted). n = 11, 14, 12 and 6 for February, March, April and May, respectively. Bars ± SE.

5.4 Discussion

To study the genotoxic stress pathways develop by cetaceans as a response to sun exposure, I quantified changes in the expression of the genes encoding heat shock protein 70 (*HSP70*), an indicator of cell stress (Hightower, 1991), tumour protein 53 (*P53*), involved in most of the UVR-induced gene transcription (Latonen and Laiho, 2005), and KIN17 protein (*KIN*), a cell cycle control protein up-regulated by UVR (Kannouche and Angulo, 1999; Masson et al., 2003; Miccoli et al., 2005). qPCR was used for the analyses because of its accuracy, sensitivity and ability to produce results rapidly (Taylor et al., 2010). However, despite its apparent simplicity, normalization of the technique, including selection of suitable internal control genes,

is vital (Vandesompele et al., 2002). This is particularly true when working in field conditions, as it is extremely difficult to ensure that RNA quality will be equal for all samples. Here, qPCR was successfully standardized for each target gene and the genes encoding the ribosomal proteins S18 (*RSP18*) and L4 (*RPL4*) proved to be adequate for their use as internal controls.

HSP70 was found to be the gene with the highest level of expression (1.3 and 1.7 times more than *P53* and *KIN*, respectively). Similar results have been observed in human melanocytes, where *HSP70* was expressed at least 2.2 fold higher than the other 11 genes involved in different pathways of DNA repair mechanisms when under UV irradiance (Jean et al., 2001). Over-expression of *HSP70* might help initially to restore unstable or denatured proteins affected by UVR stress (Hightower, 1991). It might also protect the cells against UV-induced damage, including apoptosis and DNA lesions (Matsuda et al., 2010).

Expression of *P53* and *KIN* was directly related to expression of *HSP70*. It is possible that *HSP70* induces the expression of *P53* and *KIN* in whales. Alternatively, *P53* and/or *KIN* might induce expression of *HSP70*. In humans, *HSP70* closely interacts with cell-cycle arrest proteins such as P53 protein (Helmbrecht et al., 2000; Zylicz et al., 2001). Although no studies on the association between *HSP70* and *KIN* have been published, it is possible that, as *KIN* participates in the cell-cycle arrest, *HSP70* may regulate its expression. Chaperones from the HSP70 family are known to recognize and bind mutant P53 proteins and thus regulate their accumulation and localization in the cell (Helmbrecht et al., 2000; Zylicz et al., 2001). Furthermore, when *P53* is mutated, its tertiary structure is modified liberating a binding domain, where *HSP70* can bind (Fourie et al., 1997). Although *HSP70-P53* complexes have been observed in carcinoma cell lines, their biological significance is still unclear (Fourie et al., 1997).

Interestingly, sperm whales, which spend up to six hours at a time at the sea surface (Whitehead, 2003), showed significantly higher expression of *HSP70* than the two other species. *HSP70* expression is considered an early and sensitive indicator of UVR-induced skin damage (De la Coba et al., 2009). Thus it is possible that the high

levels of *HSP70* expression observed in sperm whales reflect high levels of UVR-induced molecular damage, such as proteins unfolding (Hightower, 1991), that occur in a time-dependent manner (Yoshida et al., 2003). The relatively higher expression of HSP70 could be explained by the presence of paralogs. However, considering the close evolutionary relationship between the study species, it is unlikely that the interspecies differences in HSP70 expression reflect the presence of paralogs for this gene. Investigating this possibility in more depth was beyond the scope of this thesis. Besides, sperm whales also presented comparatively higher expression of *KIN*. In humans, up-regulation of *KIN* begins 8h after UVR exposure (Masson et al., 2003), by which time the nucleotide excision repair (NER) mechanism had resolved 50-75 % of the UVR-induced DNA lesions (Jensen and Smerdon, 1990). As proposed for humans, it is possible that in cetaceans, *KIN* plays a role in late phases of UVR response by helping to repair those lesions not eliminated by NER (Angulo et al., 2005; Masson et al., 2003). Knowing that *KIN* and *HSP70* play a central role in cell and DNA protection against UVR (Biard et al., 2002; Calini et al., 2003; Simon et al., 1995), it is possible to interpret my results as an indication that sperm whales respond to excessive UVR exposures by activating molecular pathways that involve *HSP70* and *KIN* expression, thus counteracting UVR-induced skin lesions.

Interestingly, *KIN* and *HSP70* expression levels were not related to individual melanocyte abundance. This result strengthens the prior suggestion that duration of exposure to UVR might be more important than skin pigmentation in the activation of early stress response pathways of cetaceans. However, *P53* expression was inversely correlated with melanocyte abundance, suggesting that lighter-skinned whales express this tumour suppressor protein gene comparatively more than darker individuals. A study that investigated skin colour variation and protective responses to UVR, including dermal accumulation of P53 protein, found that after 24h of exposure, P53 deposition was evident in all skin types but in darker skins this protein accumulated only in the suprabasal layer (Del Bino et al., 2006). It is possible that the lower levels of *P53* expression detected in more pigmented whales might reflect differential *P53* expression between skin layers. On the other hand, *P53* is known to be involved in melanogenesis (Oren and Bartek, 2007), thus the higher levels of expression observed in lighter whales might be an early step of the response

pathways that include activation of DNA repair mechanisms as well as the tanning response (see Chapter six).

Although results need to be interpreted carefully due to the relatively small sample size, it appears that expression of *P53* and *HSP70* increased between February and March and then declined in May. Interestingly, in the Gulf of California, where the samples were collected, the levels of UVR increase between January and March and reached a plateau in April (Chapter two, section 2.5). It is possible that between February and March over-expression of DNA repair genes occurs in a UVR dose-dependent manner, as observed in humans and laboratory animals (De la Coba et al., 2009; Masson et al., 2003) and that the decrease in gene expression levels recorded in May reflects the ability to acclimatize to sustained UVR (Sayre et al., 1981).

5.5 Conclusions

In this chapter, I have shown that sperm whales exhibit significantly higher expression levels of *HSP70* and *KIN* than what is observed for the two other species. I also showed that expression of *P53* and *HSP70* mimicked the changes in UVR observed between February and March in the Gulf of California, the study site. In May, when UVR levels reach a plateau, levels of gene expression decreased. These results suggest that whales can acclimatize to counteract UVR exposure. To conclude, this chapter suggests that gene-products involved in genotoxic stress pathways accumulate in cetacean skin in time and dose-dependent manners.

CHAPTER 6: Cetacean skin pigmentation and UVR protection

I previously showed that skin lesions were inversely predicted by melanocyte counts used as a surrogate measure of individual pigmentation. To explore in detail the photoprotective role of cetacean pigmentation that was proposed in chapter three, I measured the abundance of melanin in each individual and assessed expression levels of the tyrosinase gene (*TYR*; gene abbreviation in italicized capital letters), a key player of melanogenesis.

6.1 Introduction

The variability of skin colour amongst and within species has fascinated scientists since the nineteenth century, when Charles Darwin and Alfred Wallace proposed the idea of natural selection (Stevens and Merilaita, 2009). Various reasons for such variability have been proposed, such as camouflage, thermoregulation and protection against solar ultraviolet radiation (UVR) (Stevens and Merilaita, 2009; Stuart-Fox and Moussalli, 2009). The best known example of variation in skin colour is the pronounced latitudinal gradient in pigmentation seen in humans, which tend to be darker near the equator and lighter towards the poles (Jablonski and Chaplin, 2010). Natural selection has promoted darker skin near the equator to protect from constant exposure to harmful UVR while lighter skin tends to be found approaching higher latitudes where sunlight is comparatively lower but absorbance of those low levels are necessary to synthesize vitamin D (Jablonski and Chaplin, 2010).

Primarily, skin pigmentation is determined by the type, amount and distribution of melanin, a pigment produced by melanocytes, specialized cells located in the basal layer of the epidermis (Costin and Hearing, 2007; Lin and Fisher, 2007). Melanocyte number and activity play a key role in the amount of melanin produced deep within the epidermis. Melanin is derived from the oxidation of tyrosine and can be of two types, eumelanin (black or brown pigment) and pheomelanin (red or yellow pigment)

(Ito and Wakamatsu, 2003; Lin and Fisher, 2007). These pigments are combined within the melanocytes into granules, termed melanosomes, which are transferred via dentrites to the surrounding keratinocytes (Costin and Hearing, 2007). Melanogenesis occurs within melanosomes through complex molecular pathways that involve the expression of several genes called pigmentation genes (Sturm et al., 2001). The genetic basis of skin pigmentation has been identified through studies of phenotypic variation seen in mouse coat colours and studies of human hypopigmentary disorders (Oetting, 2000; Sturm et al., 2001; Lin and Fisher, 2007).

Of the 125 distinct genes known to be directly or indirectly involved in melanogenesis, critical genes include the tyrosinase genes, *TYR*, *TYRP1* and *TYRP2*, which form the tyrosinase enzyme complex (Sturm et al., 2001). *TYR* mediates the first two steps in melanin synthesis, which involve hydroxylation of tyrosine to DOPA (3-4-dihydroxyphenylalanine) and the subsequent oxidation to dopaquinone (Hearing and Ekel, 1976; Land and Riley, 2000). *TYR* is expressed in both eumelanosomes and pheomelanosomes whereas *TYRP* is only present in eumelanosomes (Sturm et al., 2001; Lin and Fisher, 2007). Human TYR protein activity has been shown to be 10-fold higher in darker skin types (Sturm et al., 2001). Mutations in *TYR* can induce human albinism (Oetting, 2000; Sturm et al., 2001). Another gene with a key role in pigmentation is melanocortin 1 receptor (*MC1R*), located on the membrane of melanocytes, whose function is the regulation of melanin synthesis (Rouzaud et al., 2006; Lin and Fisher, 2007; Lightner, 2008). *MC1R* has a critical role in switching between eumelanin and pheomelanin during synthesis. The gene is highly polymorphic with over 30 variant alleles (Rana et al., 1999; Sturm et al., 2001). Variation in *MC1R* has been proposed to have functional consequences on skin colouration. For instance, unique amino acid substitutions within conserved regions of MC1R were reported for various species within the Cetartiodactyla clade, including belugas and sperm whales (Ayoub et al., 2009). Other important genes include the keratinocyte receptor *PAR2* involved in melanosome transfer and P-protein, which governs intramelanosomal pH (Sturm et al., 2001).

Skin responds to UVR by inducing proliferation of keratinocytes and increasing pigmentation over the basal constitutive level, a phenomenon known as tanning

(Costin and Hearing, 2007; Lin and Fisher, 2007). Repeated exposure to UVB leads to delayed tanning, generally observed after 48-72h of exposure. Delayed tanning can remain visible between 8 and 10 months, in contrast to immediate tanning that occurs within 1-2h of exposure and generally disappears rapidly (Costin and Hearing, 2007). Immediate tanning depends on photoxidation of preexisting melanin as well as on changes in their distribution. In contrast, delayed tanning is due to increased number and dendricity of melanocytes and to melanogenesis, via up-regulation of *TYR* activity (Costin and Hearing, 2007). Melanin plays a major photoprotective role by absorbing free-radicals, neutralizing them and preventing DNA damage, among other mechanisms by supranuclear capsule formation (Costin and Hearing, 2007). The survival and genome integrity of melanocytes is essential for photoprotection (Kadekaro et al., 2003; Costin and Hearing, 2007) and to maintain melanin's proper function as a "natural sunscreen".

6.2 Material and Methods

6.2.1 Melanocyte and melanin pigment quantification

6.2.1.1 Melanocyte count

Melanocyte density, used as a surrogate measure of constitutive pigmentation (Costin and Hearing, 2007), was calculated for each individual within a standardized area using digital photographs of H&E stained skin sections (for method details see section 2.4 in Chapter two).

6.2.1.2 Melanin pigment count

To calculate individual melanin abundance, I used the same photographs as were used for melanocyte quantification and analyzed them using the freely available image processing program Image J (http://rsbweb.nih.gov/ij/index.html; (Abramoff et al., 2004). Each image was first transformed into a greyscale image (Image>Type>8-bit; Fig. 6.1a). The amount of melanin was determined by establishing a threshold (Image>Adjust>Threshold) and transforming the image into

binary format (black = presence of melanin, white = absence of melanin, Fig. 6.1b). An area corresponding to the surface of the first layer of 100 AU (measured with a microscope-crossed graticule; see Fig. 6.1) of the epidermal ridge (area of selection in square pixels; Fig. 6.1) was selected. The average grey value within the selection was measured as the sum of grey values of the pixels in the selected area divided by the total number of pixels. To increase accuracy, I subtracted the grey value of the ruler to the average grey value obtained for each image (see Fig. 6.1).

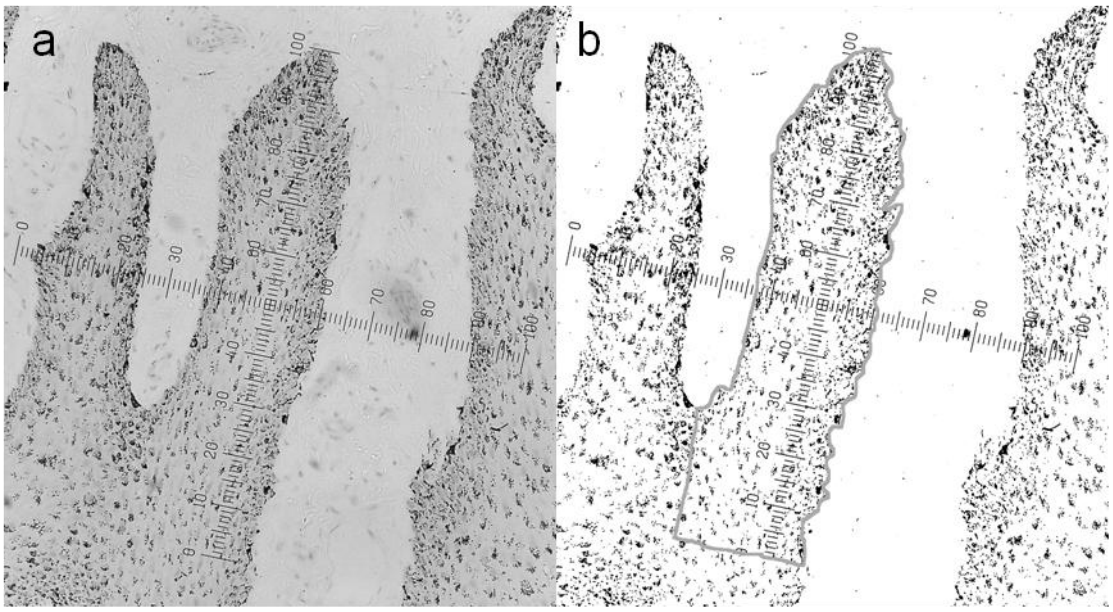

Figure 6.1. Determination of melanin pigments in an epidermal ridge using image J. a) Microphotograph of the deepest layer (100 AU) measured using a microscope-crossed graticule (10 mm long with 100 subdivisions of 0.1 mm). Image transformed into greyscales. b) Detection of melanin using the threshold option for binary transformation of the image. The area was selected to measure total grey pixels. The grey values of the microscope-cross graticule (ruler) within the selected area were substracted from the total grey values, yielding total melanin.

In total, I measured the quantities of melanocyte and melanin in 357 epidermal ridges corresponding to 119 different individuals. I used these data to relate the abundance of melanin pigments to the quantity of melanocytes in order to investigate melanin-producing capacity of melanocytes.

6.2.2 Expression levels of the tyrosinase pigmentation gene

To detect and measure the capacity of cetaceans to produce melanin, I estimated the level of expression of the tyrosinase gene (*TYR*) using the same methods described in Chapter five (section 5.2). A schematic representation of the general methods is provided in Appendix 5.1.

Eight primer pairs were designed (see method in section 5.2.2, Chapter 5) for analysis of *TYR* expression. This was done by aligning highly conserved exonic regions of *TYR* sequences reported for cows, pigs and humans. Of the eight pairs, those that successfully amplified a single band of the expected size in the three study species and that generated a single dissociation curve during real-time PCR (Appendix 5.4) were selected. Finally, primer specificity was confirmed by direct sequencing (Appendix 5.5). The primer sequences are listed in Appendix 5.6.

6.2.3 Statistical analysis

TYR expression levels were analyzed using the relative quantification method (level of expression of the target gene relative to internal control genes) that is based on the ΔCt method ($Ct_{\text{target gene}}$- geometric mean $Ct_{\text{control genes}}$) (Vandesompele et al., 2002; Schmittgen and Livak, 2008). In order to control for possible effects of the qPCR plate (inter-experimental variations) on the level of gene expression, I used linear mixed effect modelling (Zuur et al., 2009). This is because it is possible that each of the 15 qPCR plates prepared might group data in a way that could hide or exacerbate a potential effect of interest; see Appendix 5.2 for details on the data used in the *TYR* expression analyses. Thus, *P53* expression level was included in the models built to investigate the importance of transcription levels on melanin production as this gene is known to be involved in the activation of melanogenesis in humans (Khlgatian et al., 2002). As lower ΔCt values represent higher levels of expression, the response variable (i.e. level of gene expression = - ΔCt_{gene}) was negatively transformed to aid interpretation of results.

Linear models were constructed in R (details in Chapter two, section 2.3) (Ihaka and Gentleman, 1996; R Development Core Team, 2008) to investigate inter- and intra-species, and temporal variation in skin pigmentation. Mixed effect models were constructed using the *lme* function in the *nlme* package (Pinheiro et al., 2008).

6.3 Results

6.3.1 Melanocytes, melanin and pigmentation gene expression

The skin sections examination revealed a thick epidermis with a high number of elongated epidermal ridges that penetrated deep into the dermis (Fig. 2.3 in Chapter two) and an elevated concentration of dark brown melanin in the epidermis. Melanocytes were concentrated in the basal layer (Fig. 2.3 in Chapter two). It was common to observe melanocytes with dendritic expansion and accumulation of melanin above the keratinocyte nucleus (Fig. 6.2), particularly when in the deepest epidermal layers.

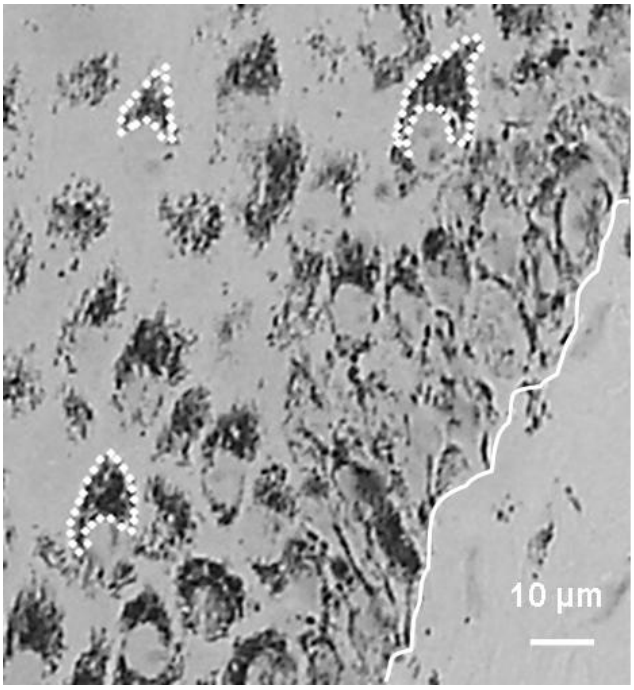

Figure 6.2. Accumulation of melanin above the keratinocyte nucleus forming supranuclear caps (fin whale H&E stained skin section). Examples of melanin caps are delimited with dotted lines. The line represents the limit between epidermis and dermis.

A total of 357 epidermal ridges from 119 individual samples were used to investigate melanin producing capacity of melanocytes (details in section 6.2.1). There was a high correlation between melanin pigment and melanocyte abundance (details in Table 6.1 and Fig. 6.3). Differences between species were evident and will be addressed below. No differences in melanocyte and melanin abundance between sexes were observed in blue whales (Fig. 6.4), the only species for which there is data on sex available (see Chapter two).

Table 6.1. Likelihood ratio tests (left half of the table) used to obtain the minimal adequate model (right half of the table) looking at the correlation between melanin abundance (response variable = Resp) and quantity of melanocytes (Qm). The left part of the table provides the explanatory variables (Expl) included in the full model and their corresponding likelihood ratios (LR) and p-values (p). Individual was fitted as a random factor (Ind-random with 119 levels). The right part of the table presents the value and standard error (SE) of the estimated coefficients (intercept and slope), the t- and p-values obtained using the Student's t-test (Ho: value of the estimated coefficients equals zero) and degrees of freedom (df). Bold text indicates $p \leq 0.05$.

Resp	***Expl***	***LR***	***p***	***Param***	***value***	***SE***	***df***	***t***	***p***
Melanin	*Qm:species*	0.99	0.61	*Intercept*	18.46	1.72	237	10.72	0.00
	species	37.99	**<0.0001**	*fin*	9.72	2.36	116	4.12	**0.0001**
	Qm	60.89	**<0.0001**	*sperm*	-8.07	2.75	116	-2.93	**0.004**
	Ind-random	104.75	**<0.0001**	*Qm*	0.70	0.08	237	8.59	**<0.0001**

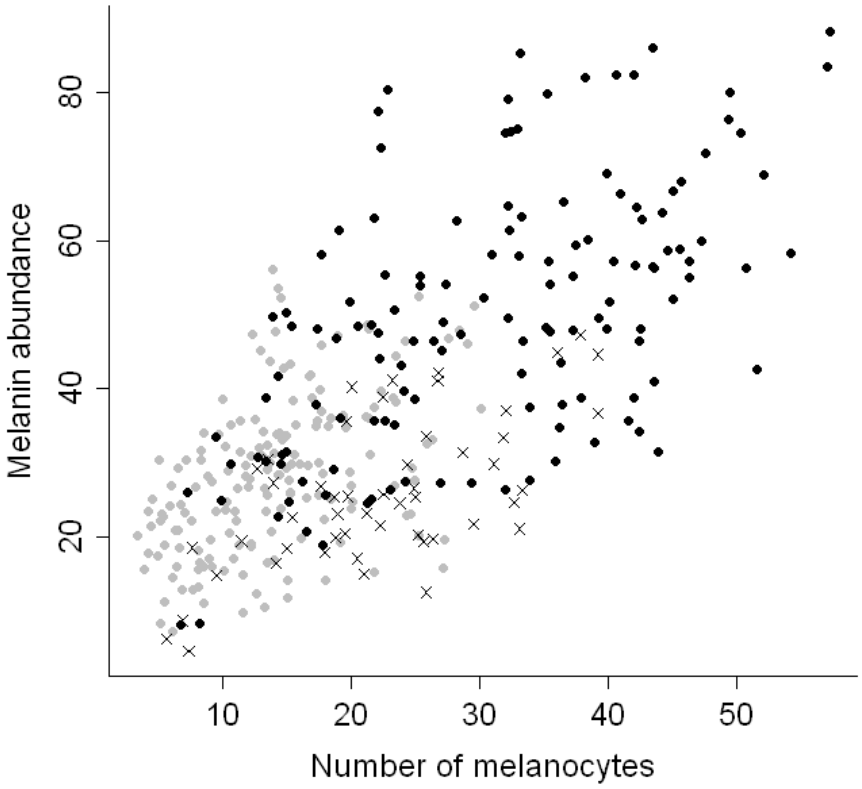

Figure 6.3. Association between melanin abundance and melanocyte counts in the three species. Grey dots correspond to blue whales, black dots to fin whales and the cross to sperm whales. Three measures (corresponding to three epidermal ridges) per individual were included (total number of individuals examined = 119).

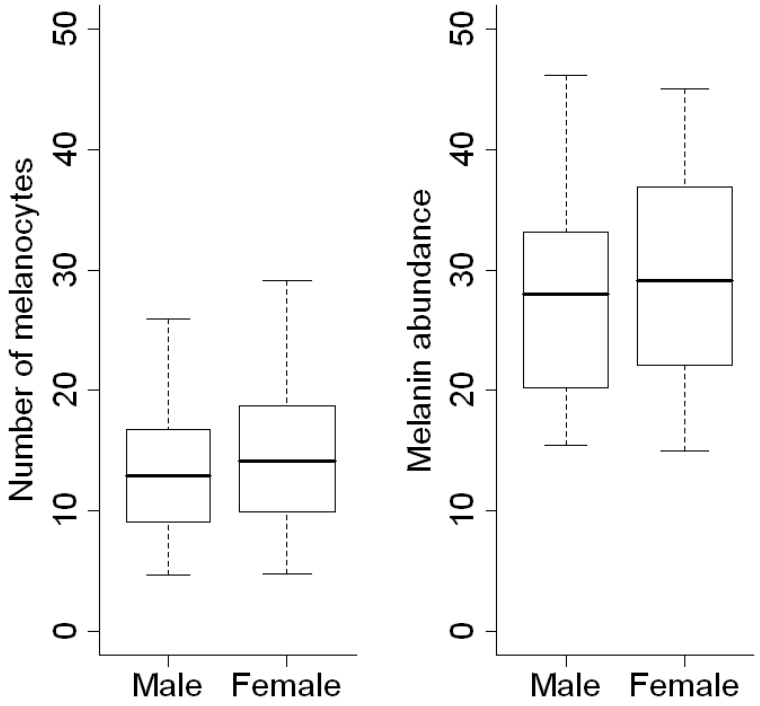

Figure 6.4. Differences between sexes in blue whale abundance of melanocytes and melanin. n = 37 males and 47 females.

When evaluating melanin-production capacity in terms of gene expression analysis, I found that *TYR* expression directly predicted melanin abundance (Table 6.2; Fig. 6.5).

Table 6.2. Deletion steps (left half of the table) used to obtain the minimal adequate model (right half of the table) fitting the data on melanin abundance (response variable = Resp). The left part of the table provides the explanatory variables (Expl) included in the full model and their corresponding Fisher value (F) and p-value (p). The right part of the table presents the value and standard error (SE) of the estimated parameters (intercept and slope) and the t- and p-values obtained using the Student's t-test. Bold text indicates $p \leq 0.05$.

Resp	***Expl***	***F***	***p***	***Param***	***value***	***SE***	**df**	***t***	***p***
Melanin	*P53*	3.83	**0.05**	*Intercept*	24.73	15.44	42	1.60	0.12
	TYR	4.87	**0.03**	*Qm*	0.86	0.17	42	5.00	**<0.0001**
	species	6.30	**<0.005**	*TYR*	3.12	1.41	42	2.21	**0.03**
	Qm	24.97	**<0.0001**	*fin*	4.39	3.78	42	1.16	0.25
				sperm	-10.34	4.35	42	-2.38	**0.02**
				P53	-3.84	1.96	42	-1.96	**0.05**

To address the question from a different angle, I fitted a mixed effect model to the *TYR* expression data. *P53* expression and melanin abundance were both directly associated to *TYR* expression (Table 6.2; Fig. 6.5). Melanocyte abundance and species were not retained in the final model (Table 6.2).

Table 6.3. Likelihood ratio tests (LR; left half of the table) used to obtain the minimal adequate model, with estimated coefficients showing the direct correlation between *TYR* expression and *P53* expression and *TYR* expression and melanin abundance (right half of the table). In the full model, the explanatory variables included were quantity of melanocyte (Qm), melanin abundance (melanin), the factor species (three levels) and *P53* expression. Plate was fitted as a random factor (14 levels). Bold text indicates $p \leq 0.05$.

Resp	***Expl***	***LR***	***p***	***Param***	***value***	***SE***	***df***	***t***	***p***
TYR	*species*	1.36	0.51	*Intercept*	-5.77	1.12	32	-5.16	0.00
	Qm	1.22	0.27	*melanin*	0.03	0.01	32	3.32	**0.002**
	melanin	10.07	**0.002**	*P53*	0.84	0.16	32	5.20	**<0.0001**
	P53	21.22	**<0.0001**						
	plate-random	8.10	**0.004**						

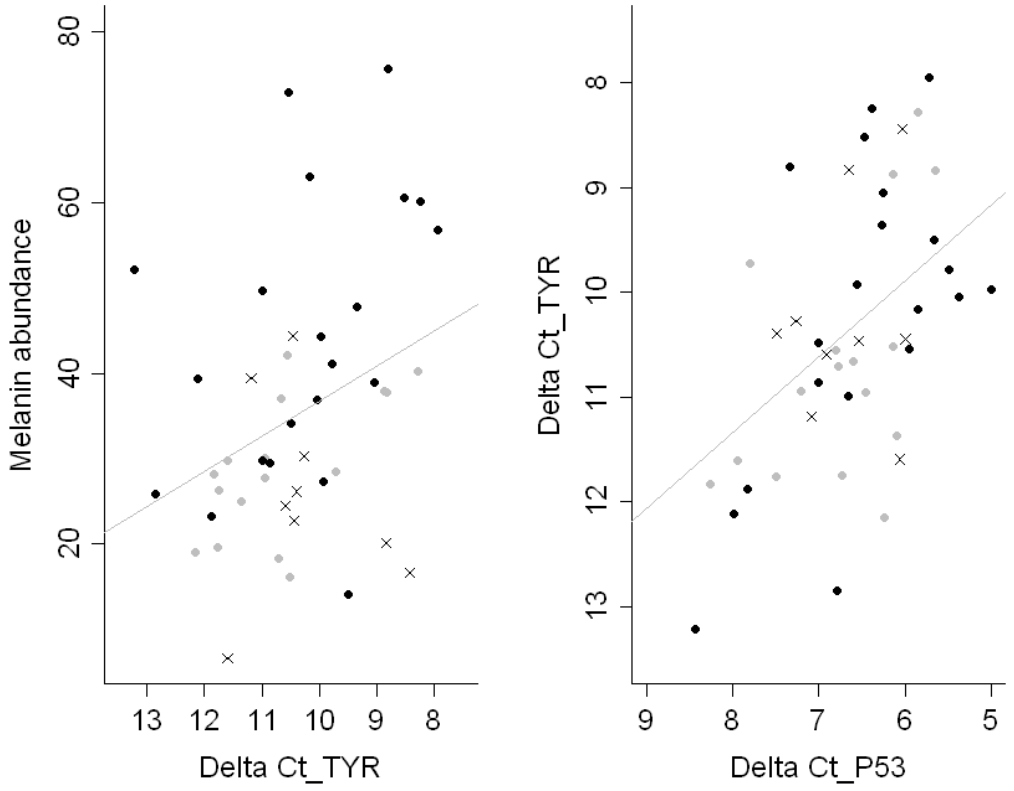

Figure 6.5. Association between melanin abundance and *TYR* expression levels and between *TYR* and *P53* transcription (expression showed as ΔCt, y axis inverted). Grey dots correspond to blue whales, black dots to fin whales and crosses to sperm whales. The grey line represents the regression line.

6.3.2 Inter-species variation

As mentioned above, variation in melanin abundance were partially explained by the species to which the sample belonged (see Table 6.1 and 6.2). However, interspecies variation in expression of *TYR* was not significant (see Table 6.3). To explore these results further, three independent models controlling for potential temporal grouping effects were constructed. The models sought to explain variation amongst species in melanocyte abundance, melanin abundance and *TYR* expression, respectively. To control for the possibility that interspecific variation was biased by the month of sampling, particularly because sperm whales were only sampled in April/May (details in Appendix 5.2), the same analyses were initially carried including only samples collected during the months of April and May. Analyses were then repeated for samples collected during the entire 2008 field period.

Melanocyte counts were significantly lower in blue whales than in sperm and fin whales (Table 6.4; Fig. 6.6). Unexpectedly, although significant differences in melanocyte abundance were observed between blue and sperm whales, melanin abundance did not differ significantly; the highest levels of melanin being recorded in fin whales (Table 6.5; Fig. 6.6). With respect to *TYR*, sperm whales showed the highest level of expression (Table 6.6; Fig. 6.6). This trend remained in 2008 (Table 6.6).

Table 6.4. Deletion tests (Fisher; left half of the table) used to obtain the estimated values of the minimal adequate model describing variation in melanocyte abundance amongst species (right half of the table). Bold text indicates $p \leq 0.05$.

Resp	***Expl***	***F***	***p***	***Param***	***value***	***SE***	***df***	***t***	***p***
Qm	*month*	0.97	0.41	*Intercept*	12.40	1.31	109	9.48	0.00
	year	26.36	**<0.0001**	*fin*	11.23	1.68	109	6.67	**<0.0001**
	species	25.06	**<0.0001**	*sperm*	9.10	2.28	109	3.99	**0.0001**
				2008	0.93	1.78	109	0.52	0.60
				2009	13.86	2.04	109	6.79	**<0.0001**
Qm	*year*	15.48	**<0.0001**	*Intercept*	13.91	2.08	56	6.70	0.00
Apr/May	*species*	5.39	**<0.01**	*fin*	8.86	2.79	56	3.17	**0.002**
				sperm	7.80	4.22	56	1.85	0.07
				2008	0.72	4.02	56	0.18	0.86
				2009	14.65	2.76	56	5.30	**<0.0001**
Qm	*month*	0.67	0.58	*Intercept*	14.43	1.53	46	9.40	0.00
in 2008	*species*	4.61	**0.02**	*fin*	8.04	2.62	46	3.07	**0.004**
				sperm	8.00	2.29	46	3.49	**0.001**

Table 6.5. Deletion tests (Fisher; left half of the table) used to estimate values of the minimal adequate model describing variation in melanin abundance amongst species (right half of the table). Bold text indicates $p \leq 0.05$.

Resp	***Expl***	***F***	***p***	***Param***	***value***	***SE***	***df***	***t***	***p***
Melanin	*month*	0.45	0.72	*Intercept*	28.38	1.70	111	16.68	0.00
	year	0.16	0.85	*fin*	21.33	2.50	111	8.54	**<0.0001**
	species	29.58	**<0.0001**	*sperm*	-2.38	3.43	111	-0.69	0.49
Melanin	*year*	0.22	0.80	*Intercept*	31.057	3.064	58	10.135	0.00
Apr/May	*species*	7.8753	**<0.001**	*fin*	17.503	3.711	58	4.716	**<0.0001**
				sperm	-5.06	4.138	58	-1.223	0.226
Melanin	*month*	0.06	0.98	*Intercept*	29.96	2.37	46	12.63	0.00
in 2008	*species*	7.36	**0.002**	*fin*	15.47	4.05	46	3.82	**<0.0005**
				sperm	-3.96	3.55	46	-1.12	0.27

Table 6.6. Deletion tests (Likelihood Ratio; left half of the table) used to obtain the estimated values of the minimal adequate model describing variation in *TYR* expression amongst species (right half of the table). Bold text indicates $p \leq 0.05$.

Resp	***Expl***	***LR***	***p***	***Param***	***value***	***SE***	***df***	***t***	***p***
TYR	*month*	1.26	0.74	*Intercept*	-2.32	0.03	50	-72.20	0.00
	year	13.92	**0.001**	*fin*	0.05	0.03	50	1.37	0.18
	species	11.62	**0.003**	*sperm*	0.16	0.05	50	3.29	**0.002**
	plate-random	1.90	0.17	*2008*	-0.14	0.04	50	-3.43	**0.001**
				2009	-0.03	0.04	50	-0.68	0.50
TYR	*month*	5.52	0.14	*Intercept*	-11.64	0.38	23	-30.83	0.00
in 2008	*species*	12.62	**0.002**	*fin*	0.43	0.53	23	0.80	0.43
	plate-random	0.99	0.32	*sperm*	1.62	0.47	23	3.42	**0.002**
TYR	*year*	0.05	0.98						
Apr/May	*species*	0.93	0.63						
	plate-random	0.25	0.62						

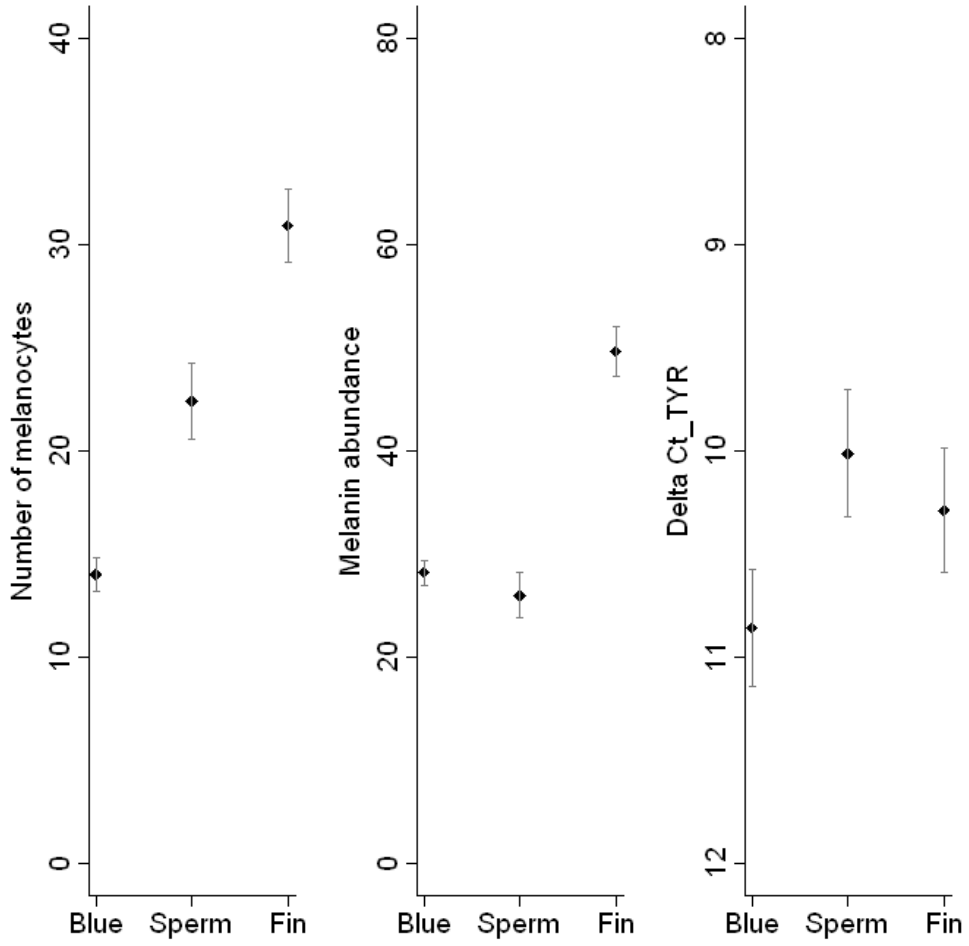

Figure 6.6. Abundance of melanocytes, melanin and *TYR* expression in whales. Figure shows values for blue whales (n = 53 for melanocytes and melanin analyses, and 19 for *TYR* expression), sperm whales (n = 45 and 22) and fin whales (n = 17 and 12). Bars = ± SE.

6.3.3 Temporal variation

If as occurs in humans, different skin colour types engender different responses to UVR exposure (Yamaguchi et al., 2006), it is possible that the blue whale will increase melanogenic activity (measured here as the increase in number of melanocytes, melanin abundance and levels of *TYR* expression) as the season advances, in contrast to darker species. Regrettably, sperm whales were mostly sampled during May, and thus could not be included in the temporal analyses, so the comparison was limited to blue and fin whales.

For both species, melanocyte abundance was partly explained by yearly variations (Table 6.7). Although the observed effect was limited to the sample population and not to individual variation (each individual only being sampled once, see section 2.2 in Chapter two for details), both species showed similar changes in melanocyte abundance amongst years, with highest levels observed in 2009 (Table 6.7; Fig. 6.7). Blue whale melanocyte abundance increased between February and April (right half part of Table 6.7; Fig 6.8).

Table 6.7. Deletion tests (Fisher; left half of the table) used to obtain the estimated values of the final model looking at temporal variation in quantity of melanocytes (Qm; right half of the table). Bold text indicates $p \leq 0.05$.

Resp	***Expl***	***F***	***p***	***Param***	***value***	***SE***	***df***	***t***	***p***
Qm	*month*	2.49	0.07	*Intercept*	8.34	1.94	46	4.30	0.00
blue	*year*	6.86	**0.002**	*2008*	4.62	1.88	46	2.46	**0.02**
				2009	9.29	2.70	46	3.44	**0.001**
				Mar	3.97	1.97	46	2.01	**0.05**
				Apr	5.40	2.25	46	2.40	**0.02**
				May	7.12	3.64	46	1.96	0.06
Qm	*month*	1.72	0.19	*Intercept*	6.35	3.30	22	1.93	0.07
blue				*Mar*	5.99	3.66	22	1.64	0.12
2007				*Apr*	8.18	3.94	22	2.08	**0.05**
				May	9.11	4.67	22	1.95	0.06
Qm	*month*	0.73	0.54	*Intercept*	23.15	2.62	42	8.85	0.00
fin	*year*	18.93	**<0.0001**	*2008*	-0.69	3.70	42	-0.19	0.85
				2009	15.57	3.18	42	4.90	**<0.0001**
Qm	*month*	0.06	0.94	*Intercept*	23.32	3.98	8	5.86	0.00
fin				*Mar*	-2.29	6.90	8	-0.33	0.75
2008				*Apr*	-1.26	7.97	8	-0.16	0.88

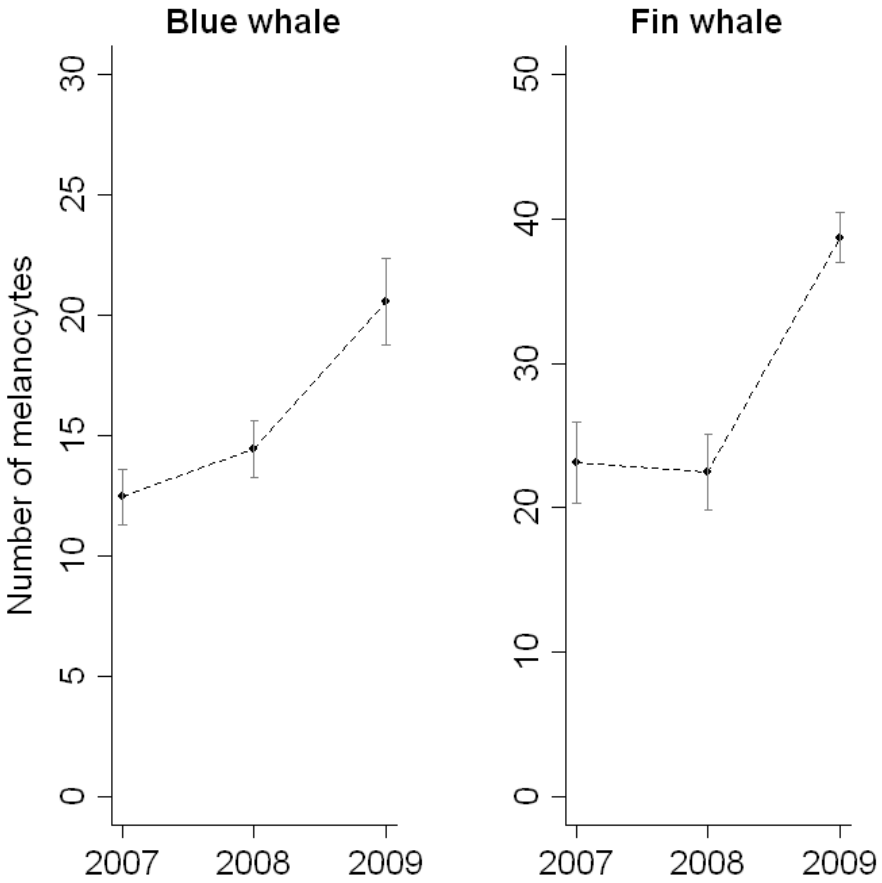

Figure 6.7. Yearly increase in whale melanocyte abundance. Figure shows blue whales (n = 27, 21 and 5 for 2007, 2008 and 2009, respectively) and fin whales (n = 11, 11 and 23). Bars = ± SE.

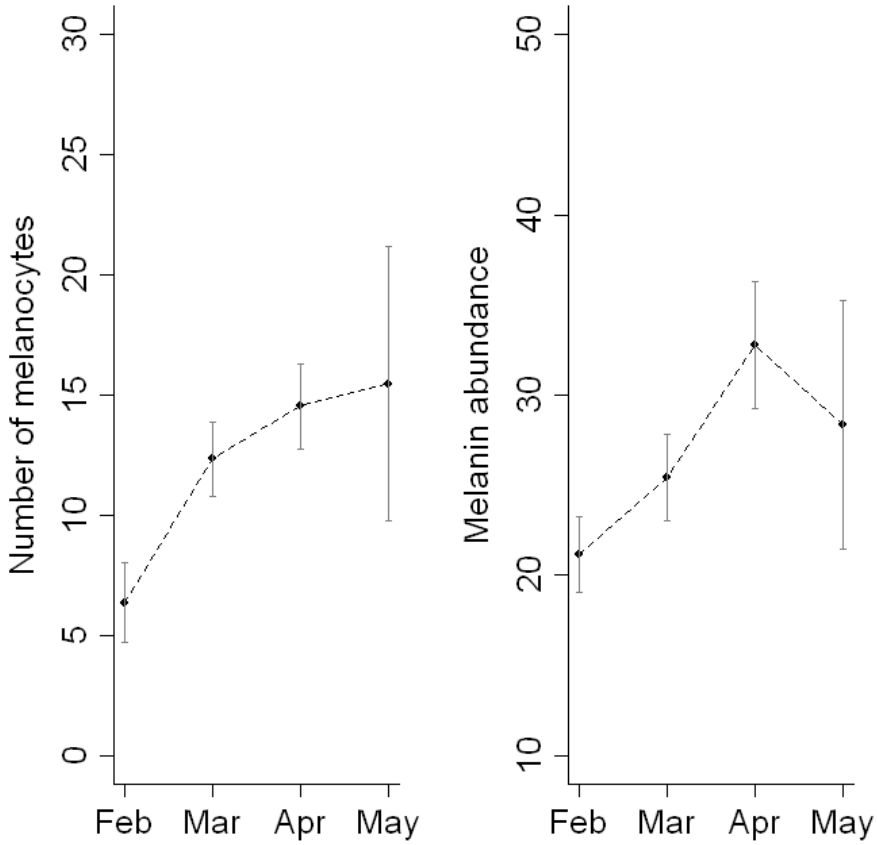

Figure 6.8. Monthly variation in blue whale melanocyte and melanin abundance during 2007. (n = 3, 13, 7 and 3 for February, March, April and May, respectively). Bars = ± SE.

Melanin abundance of blue whales remained stable between 2007 and 2009 (Table 6.8). Higher levels of melanin were observed in fin whales in 2009 compared to 2007 (Table 6.8). Similarly to what was observed for melanocytes, fin whale melanin abundance did not reflect monthly variations whereas blue whales showed an increase between February and April (Table 6.8; Fig. 6.8). No significant differences in *TYR* expression were detected amongst months (Table 6.9; Fig. 6.9).

Table 6.8. Deletion tests (Fisher; left half of the table) used to obtain the estimated values of the final model looking at temporal variation in melanin abundance (right half of the table). Bold text indicates $p \leq 0.05$.

Resp	***Expl***	***F***	***p***	***Param***	***value***	***SE***	***df***	***t***	***p***
Melanin	*year*	2.12	0.13	*Intercept*	22.07	3.08	46	7.17	0.00
blue	*month*	0.82	0.49	*Mar*	4.36	3.13	46	1.39	0.17
				Apr	8.37	3.57	46	2.34	**0.02**
				May	6.28	5.77	46	1.09	0.28
				2008	6.06	2.99	46	2.03	**0.05**
				2009	1.43	4.29	46	0.33	0.74
Melanin	*month*	1.72	0.19	*Intercept*	6.35	3.30	22	1.93	0.07
blue				*Mar*	5.99	3.66	22	1.64	0.12
2007				*Apr*	8.18	3.94	22	2.08	**0.05**
				May	9.11	4.67	22	1.95	0.06
Melanin	*month*	0.73	0.54	*Intercept*	23.15	2.62	42	8.85	0.00
fin	*year*	18.93	**<0.0001**	*2008*	-0.69	3.70	42	-0.19	0.85
				2009	15.57	3.18	42	4.90	**<0.0001**
Melanin	*month*	0.06	0.94	*Intercept*	23.32	3.98	8	5.86	0.00
fin				*Mar*	-2.29	6.90	8	-0.33	0.75
2008				*Apr*	-1.26	7.97	8	-0.16	0.88

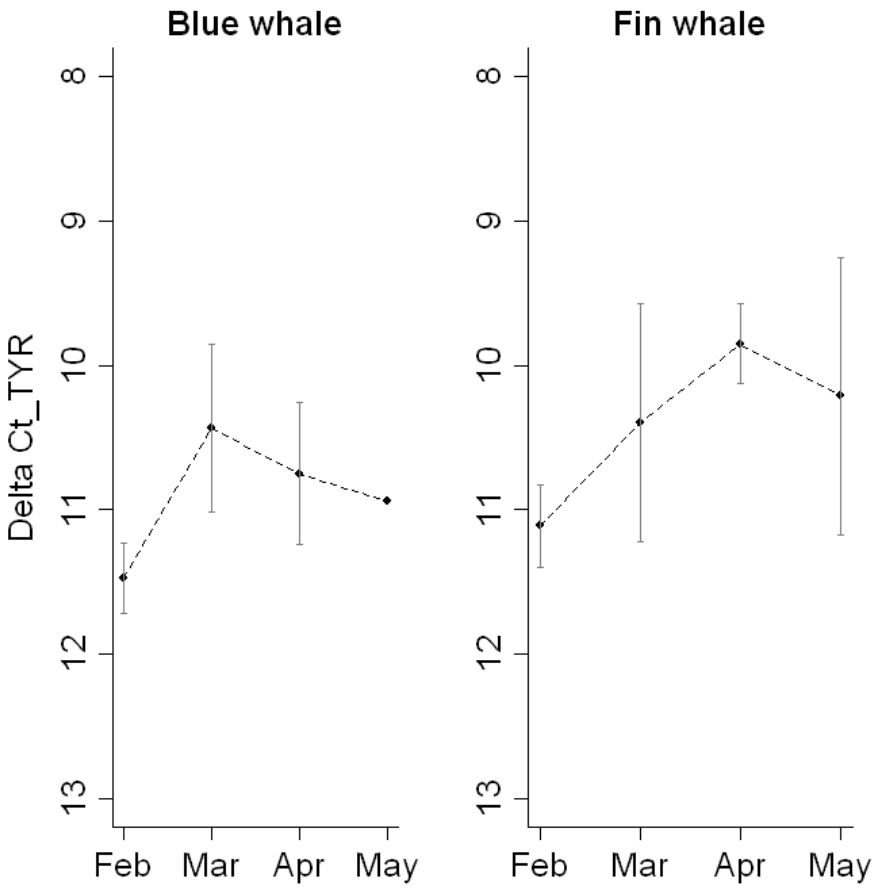

Figure 6.9. Monthly variations in *TYR* expression of blue and fin whales. Blue whales: n = 6, 8, 4 and 1 for February, March, April and May, respectively. Fin whales: n = 4, 5, 8, 5 for February, March, April and May, respectively). Bars = ± SE.

Table 6.9. Deletion tests (Fisher; left half of the table) used to obtain the estimated values of the final model looking at temporal variation in *TYR* expression (right half of the table).

Resp	*Expl*	*F*	*p*	*Param*	*value*	*SE*	*df*	*t*	*p*
TYR	*month*	3.35	0.34	*Intercept*	-11.48	0.51	17	-22.67	0.00
blue	*plate-random*	0.03	0.87	*Mar*	1.02	0.65	17	1.56	0.16
				Apr	1.06	0.75	17	1.42	0.20
				May	0.54	1.34	17	0.40	0.70
TYR	*month*	2.41	0.49	*Intercept*	-11.11	0.72	18	-15.43	0.00
fin	*plate-random*	0.19	0.66	*Mar*	0.72	0.97	18	0.74	0.49
				Apr	1.26	0.88	18	1.43	0.21
				May	0.90	0.97	18	0.93	0.39

6.3.4 Association of measures of pigmentation with skin lesions

Chapter three showed that cytoplasmic vacuolation and intracellular oedema were both inversely predicted by melanocyte counts. Similar results were seen when looking at the association between the presence of these lesions and melanin abundance (Table 6.10; Fig 6.10). Indeed, when the abundance of melanin was high, levels of oedema and vacuolation were low (Table 6.10; Fig 6.10). The same inverse relationship was observed between levels of *TYR* expression and oedema (Table 6.11; Fig 6.10). Individual melanocyte counts and melanin were directly associated with apoptosis (Table 6.10; Fig 6.10).

Table 6.10. Deletion tests (Fisher; left half of the table) used to obtain the estimated values of the final model describing correlation between melanin abundance and microscopic lesions (right half of the table). The upper half of the table shows the analyses conducted on samples for which there were no data on measures of apoptosis (n = 104) and the lower half shows those conducted including measures of apoptosis (level 2 and 3, see section 3.2.2.4 in Chapter three) (n = 31).

Resp	***Expl***	***F***	***p***	***Param***	***value***	***SE***	***df***	***t***	***p***
Melanin	*oed:vac*	3.82	**0.01**	*Intercept*	49.87	4.66	94	10.70	0.00
	vac	na*	na*	*oed*	-34.89	6.72	94	-5.20	**<0.0001**
	oed	na*	na*	*vac-level1*	-9.96	5.00	94	-1.99	**0.05**
	species	20.61	**<0.0001**	*vac-level2*	-8.93	4.60	94	-1.94	**0.05**
				vac-level3	-17.96	6.06	94	-2.96	**0.004**
				fin	15.70	2.59	94	6.07	**<0.0001**
				sperm	-0.53	2.81	94	-0.19	0.85
				oed:vac-1	17.92	7.85	94	2.28	**0.02**
				oed:vac-2	20.22	7.39	94	2.74	**<0.01**
				oed:vac-3	26.85	8.01	94	3.35	**0.001**
Melanin	*oed:vac*	0.64	0.60	*Intercept*	35.67	3.96	27	9.02	0.00
	vac	0.47	0.70	*oed*	-12.86	3.58	27	-3.60	**0.001**
	species	3.40	**0.05**	*apo-level 3*	7.88	3.78	27	2.08	**0.05**
	apo	4.34	**0.05**	*fin*	8.49	4.50	27	1.89	0.07
	oed	12.95	**0.001**	*sperm*	-2.29	4.10	27	-0.56	0.58

*na : not applicable

Table 6.11. Deletion tests (Fisher; left half of the table) used to obtain the estimated values of the final model describing correlation between *TYR* expression and microscopic lesions (right half of the table). Oed = oedema, vac = vacuolation. The upper half of the table shows the analyses conducted on samples for which there were no data on measures of apoptosis (n = 50) and the lower half shows those conducted including measures of apoptosis (level 2 and 3, see section 3.2.2.4 in Chapter three) (n = 19).

Resp	***Expl***	***LRT***	***p***	***Param***	***value***	***SE***	***df***	***t***	***p***
TYR	*oed:vac*	1.50	0.68	*Intercept*	-9.64	0.31	35	-31.45	0.00
	vac	3.73	0.29	*oed*	-1.19	0.32	35	-3.76	**<0.001**
	species	4.87	0.09						
	oed	12.11	**0.001**						
	plate-random	4.42	**0.04**						
TYR	*vac*	4.67	0.20						
	apo	3.27	0.07						
	species	4.39	0.11						
	oed	0.62	0.43						
	plate-random	0.00	1.00						

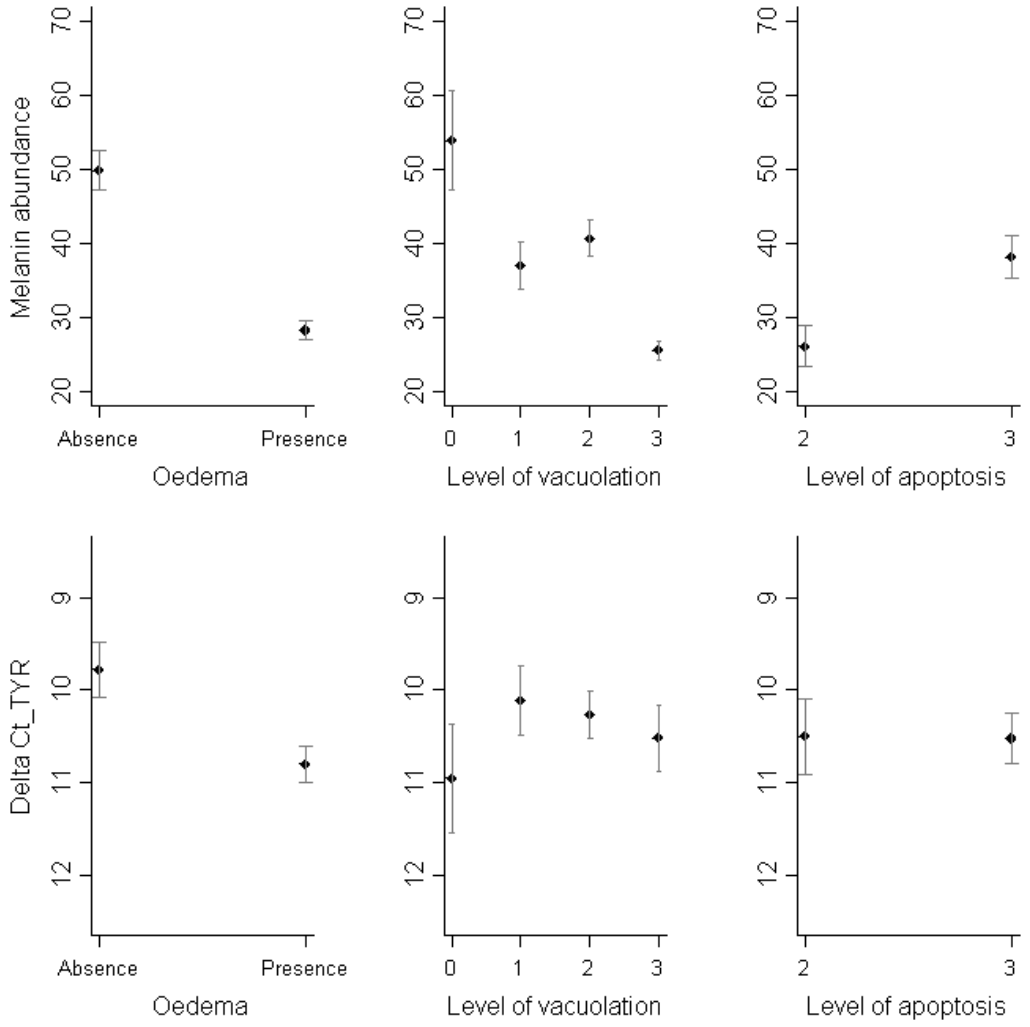

Figure 6.10. Relation between melanin abundance and skin lesions (upper part of the figure) and *TYR* expression and presence of lesions (lower part of the figure). Bars = ± SE.

6.4 Discussion

The characteristic dark brown colour of whale melanin suggests that it is composed mostly of eumelanin, the predominant pigment found in brown and black skin (Ito and Wakamatsu, 2003; Lin and Fisher, 2007). Eumelanin plays a crucial role in photoprotection, while pheomelanin, the yellow-reddish pigment, is thought to be more associated to carcinogenesis following exposure to UVR (Ito and Wakamatsu, 2003; Lin and Fisher, 2007). Melanin was found in all the epidermal layers but was mostly accumulated in the first layers of keratinocytes, where the pigments were

observed forming supranuclear caps over the "sun-exposed" side of the keratinocytes' nuclei. A similar localization of melanin has been described for southern right whale, *Eubalena australis*, integument (Reeb et al., 2007), which also show large and well-developed melanocytes with typical dendritic processes, similar to those observed in the present study. In humans, these phenomena are known to arise as protective responses to UVR exposure (Stierner et al., 1989; Lin and Fisher, 2007). Indeed, one of the first responses of the epidermal pigmentary system when exposed to the sun is the redistribution of melanin via the dendritic process and other mechanisms (Lacour et al., 1992; Costin and Hearing, 2007). Whale melanocytes were distributed along the epidermal ridges, being more concentrated when deeper in the epidermis. Epidermal thickening is known to confer protection against UVR in humans (Bech-Thomsen and Wulf, 1996; Kadekaro et al., 2003; De la Coba et al., 2009). Thus, it is possible that the observed melanocyte distribution together with their thick epidermal layer constitutes whales' photoprotection of melanocytes. Such protection would be essential to avoid oncogenic transformation of affected cells into melanoma, the most lethal type of skin cancer (Kadekaro et al., 2003).

Little is known about constitutive pigmentation in wildlife. Work conducted in humans and laboratory animals has showed that melanin density is dependent on the number of melanocytes and the capacity of melanocytes to produce the pigment granules (Lin and Fisher, 2007). Here, I found that the number of melanocytes significantly predicts melanin abundance, suggesting that whale melanin production relies on the number of melanocytes present in the skin, and consequently, melanocyte number could be considered a reliable measure of pigmentation. However, gene expression analysis confirmed that melanin concentration was also dependent on the transcriptional activity of *TYR*, known to be one of the key players in melanogenesis (Ito and Wakamatsu, 2003; Watabe et al., 2004; Lin and Fisher, 2007).

I also measured levels of *P53* expression (see Chapter five), which under UV radiation stimulates melanocytes to produce melanin (Khlgatian et al., 2002; Oren and Bartek, 2007; Murase et al., 2009). *TYR* expression was directly related to *P53* expression, a result that has been reported for mice, where activation of P53 appears to increase *TYR* transcription and, consequently, skin pigmentation (Khlgatian et al.,

2002). I failed to detect an association between *TYR* expression and melanocyte abundance. This might reflect the fact that regardless of the number of melanocytes present, *P53* will activate melanogenesis, a process that involves *TYR* expression and a subsequent increase in epidermal melanin. Together, these results highlight the complexity of melanogenesis.

Microscopic lesions and mitochondrial DNA damage (see Chapters three and four) were inversely predicted by pigmentation indices, suggesting that increased pigmentation protects the skin from the formation of cytotoxic damage, similar to what occurs in humans (Kadekaro et al., 2003). A positive relationship was found between individual pigmentation indices and apoptosis, strengthening the prior suggestion that darker individuals have a better capacity to remove damaged cells (see Chapter three), a mechanism that has been described for humans and laboratory animals (Yamaguchi et al., 2006; Yamaguchi et al., 2008). Considering the known photoprotective role of skin coloration, it was pertinent to investigate interspecies differences in pigmentation capacity. Fin whales, the darkest species, showed the highest abundance of melanocytes and melanin. Sperm whales presented a higher number of melanocytes than blue whales, the lighter species. However, blue and sperm whales had comparable levels of melanin, suggesting that melanocyte melanin-production capacity is more restricted in sperm whales than in blue whales.

Melanin abundance post UV irradiation has been seen to decrease in mice that over-express *HSP70* (Hoshino et al., 2010). In this sense, it is noteworthy that sperm whales showed the highest level of *HSP70* expression (see Chapter five), as this result could suggest that *HSP70* has an inhibitory effect on melanin production in this species. Paradoxically, sperm whales also had the highest level of *TYR* expression. It might be the case that *HSP70* inhibits melanin synthesis without affecting *TYR* expression (Hoshino et al., 2010). Exploring this possibility in depth is beyond the scope of this thesis, but considering that heat shock proteins are involved with intracellular protein transport (Hightower, 1991), it could be hypothesized that sperm whale *HSP70* regulates melanogenesis by influencing intracellular traffic of TYR protein into melanosomes (Watabe et al., 2004). A second, non-exclusive explanation for the comparatively reduced melanin of sperm whales that overexpress *TYR* could be post-transcriptional regulation (Watabe et al., 2004).

Although it was not possible to investigate temporal variations in individual pigmentation throughout a season, I was able to examine population-level variation (each whale being only sampled once in their lifetime, see Chapter two for details). Blue whale melanocyte abundance increased significantly through the season. This was particularly interesting because the trend mimicked the temporal increase in UVR recorded in the study area within the Gulf of California (see Chapter two). Chronic exposure to UVR can provoke a 4-fold increase in human melanocyte density (Yamaguchi et al., 2007), an observation that could help explain the results observed in this study. However, fin whales did not vary their melanocyte abundance in time. When initially low, human melanocyte density markedly increases in number following short periods of intensive UV irradiation compared to individuals that have an initial high number of melanocytes (Stierner et al., 1989). My results appear to suggest that cetaceans experience similar UVR-induced proliferation of melanocytes.

UV-induced tanning has been well described in humans and laboratory animals (Kadekaro et al., 2003; Costin and Hearing, 2007; Lin and Fisher, 2007), although very few studies have been conducted in wildlife, examples being freshwater zooplankton (Hansson, 2000), fishes (Adachi et al., 2005) and scalloped hammerhead sharks (Lowe and Goodman-Lowe, 1996). My results show that the blue whale population increases melanin concentration as the season progresses, suggesting tanning ability. This trend was not observed for the comparatively darker fin whales. It is possible that "basal" levels of melanin in this species are sufficient to counteract harmful effects of seasonally-increasing UVR levels within the Gulf of California. Another, non exclusive, explanation might involve the migratory behaviour of blue whales. While fin whales are considered a resident population in the Gulf of California (Bérubé et al., 2002), blue whales migrate annually from higher latitudes to the Gulf of California (Calambokidis et al., 2009), where levels and intensity of UVR are superior (Ilyas, 2007). This sudden exposure to higher levels of UVR might induce a tanning response which is not observed in the resident fin whale. It is tempting to interpret these results as evidence environmental adaptation of blue whales.

6.5 Conclusions

In this chapter, I demonstrated that melanin concentration depends on the quantity of melanocytes present in whale epidermis but also on the activity of the tyrosinase gene, known to be one of the key players in melanogenesis. The tumour protein *P53* gene appears to play a role in cetacean melanogenesis, although more studies are needed to understand the gene's precise function in melanogenesis. This chapter also strengthens the prior suggestion that darker individuals are better protected against UVR exposure as I found that skin lesions and apoptotic cells were predicted by pigmentation indices. Finally, I found that blue whales are able to tan in response to seasonal increases in UVR levels. In conclusion, this chapter has provided evidence of a photoprotective role of cetacean skin pigmentation and, taken together, suggest an evolutionary advantage of darker pigmentation in whales.

CHAPTER 7: General discussion

This thesis describes a multifaceted approach to investigate the effects of exposure to solar ultraviolet radiation (UVR) on cetacean skin as well as the mechanisms used by cetaceans in response to such effects. This chapter highlights and discusses the main findings obtained throughout the thesis and considers their implication for cetaceans' health. Some directions for potential future investigation are proposed.

8.1 Effects of solar exposure and response pathways in cetaceans

Due to their life history and physiological constraints, cetaceans are unable to avoid continuous exposure to UVR (Acevedo-Whitehouse and Duffus, 2009). Currently, despite marked reductions in the amount of ozone loss at the poles, high levels of UVR continue to reach our biosphere (WMO-UNEP, 2011). The aim of this thesis was to investigate the extent of damage caused by natural UVR exposure on cetacean epidermis and to study the mechanisms used by cetaceans as a defence against continuous UVR.

The study focused on three species, the blue whale, the fin whale and the sperm whale, selected due to their distinct skin colour, surface behaviour, and seasonal sympatry in the study area (between January and June). In total, 106 blue-, 55 fin- and 23 sperm whale skin biopsies were collected in collaboration with the Marine Mammal Ecology Laboratory of CICIMAR-IPN, Mexico (Chapter two, section 2.2). Working with wildlife, particularly in remote areas such as the marine environment, can be quite challenging. This is mainly due to the difficulty of approaching the animals, above all when large and marine-bound, as are cetaceans. In this light, the 184 skin biopsies collected for this study represent a large sample size, not only for studies on free-ranging cetaceans, but also more generally for studies on wild large mammals (Bissonnette, 1999). In addition, the numbers of samples collected are representative of the species' populations within the Gulf of California,

corresponding to 15 – 36 % of the latest population estimates (Carreta et al. 2009; details in Chapter one, section 1.5.2.1).

Using a combination of pathological and molecular techniques, I identified macroscopic and microscopic lesions in cetacean epidermis (Chapter three), optimized a molecular method to detect and quantify UVR-induced mitochondrial DNA photoproducts (Chapter four), investigated the genotoxic stress response pathways used by cetaceans to counteract the harmful effects of UVR (Chapter five), and finally, explored the role that cetacean skin pigmentation has in shaping protection against UVR (Chapter six).

Photographic and histological analyses of cetacean epidermis (Chapter three, section 3.3.1) revealed a range of abnormalities ranging from gross blisters, intracellular oedema, cytoplasmic vacuolation, glycogen deposition and microvesicles to leukocyte infiltration, all considered typical of acute sunburn (Nakaseko et al., 2003; Ohkawara et al., 1972). The blisters were recorded in a standardized area drawn using a reference unit taken as the length of the base of the dorsal fin for blue and fin whales and the height of the dorsal fin for sperm whales (Chapter three, section 3.2.1.1). The use of a standardized area for counting lesions in cetaceans is unique, as prior studies have counted lesions on the entire dorsal surface exposed (see Bearzi et al., 2009; Brownell et al., 2008; Hamilton and Marx, 2005). Evidently, it could be argued that by defining the abovementioned counting area there will be a bias in lesion counts based on the size of the whale. However, very few individuals presented more than one blister in the defined area and statistical analyses were run using binomial counts (absence or presence; sections 3.3.1.2 and 3.3). I tried to reduce other sources of error by accounting for potential interspecies differences in the size of the defined area by using the height of the dorsal fin in sperm whales instead of the base. Although this method might still be biased to some extent, it was the only feasible technique that could be used based on the data available.

Other biomarkers characteristic of exposure to UVR that were detected in this study were apoptotic cells (Chapter three, section 3.3.1), also known as "sunburn cells" (De la Coba et al., 2009; Nakaseko et al., 2003). Furthermore, evidence of sun-

induced lesions was not only identified at the cellular level but also at the molecular level, as I inferred UVR-induced mitochondrial DNA photoproducts using quantitative real-time PCR (Chapter four, section 4.3.2). I also analysed the expression of genes known to be involved in UVR-induced genotoxic stress pathways of vertebrates (Chapter five). The genes selected included the gene that encodes heat shock protein 70 (*HSP70*), considered an early and sensitive indicator of UVR-induced skin damage (De la Coba et al., 2009), and the gene that encodes KIN17 protein (*KIN*), a DNA maintenance protein involved in DNA damage induced-cellular response in humans (Angulo 2005; Masson et al., 2003; Biard et al., 2002). Overexpression of the tumour protein 53 gene (*P53*) was also demonstrated. In humans, this gene is involved in different response pathways such as cell cycle arrest, DNA repair and, when damage is non-repairable, apoptosis (Amundson et al., 1998; Bhana and Lloyd, 2008; Ikehata et al., 2010). Finally, it was common to observe melanocytes with dendritic expansions and melanin pigments accumulated in the first layers of keratinocytes, where they formed supranuclear caps over the "sun-exposed" side of the nuclei (Chapter six, section 6.3.1). In humans, such phenomena arise as protective responses following UVR exposure (Kobayashi et al., 1998; Tadokoro et al., 2003). Taken together, these diverse threads of evidence indicate that UVR-induced damage in cetaceans is widespread and significant. One of the few free-living studied species known to be affected by UVR exposure are amphibians. To date, embryonic, developmental and physiological abnormalities such as oedema and retinal damage have been recorded in more than 30 species of frogs, toads and salamanders (reviewed in Blaustein et al., 2003). Marine invertebrates, such as sea urchins and fishes have also shown to suffer UVR-induced damage (reviewed in: Dahms and Lee, 2010). My results prove that even cetaceans, which due to their life history are constantly exposed to the sun, can experience UVR-induced damage, and that such damage may be limited by physiological traits, such as variations in pigmentation and expression of repair pathways. It is likely that other marine or terrestrial species such as walruses, which are restricted to land during breeding, nursing, moulting and resting (Fay, 1982), might be similarly affected by sun exposure, and it would be of interest to characterize their response and repair mechanisms.

In this study I not only detected evidence of sun-induced alterations and counteractive responses of cetacean skin but also demonstrated that such changes and responses vary amongst species. Notably, fin whales, the most pigmented of the three study species, had the lowest prevalence of blisters and microscopic abnormalities (Chapter three, section 3.3.2). When investigating the correlation between lesion prevalence and individual skin pigmentation indices across species, I found that pigmentation inversely predicted microscopic lesions including cytoplasmic vacuolation, intracellular oedema and also accumulation of mtDNA photoproducts (Chapter three, four and six). Analogous correlations between lesions and pigmentation are commonly observed in humans. I found a positive relationship between pigmentation and apoptotic cells, suggesting that darker whales are better able to remove potentially precancerous UVR-damaged cells via melanin-mediated apoptosis, and it appears that whale sensitivity to UVR decreases with increasing pigmentation, both processes well described in humans (Del Bino et al., 2006; Yamaguchi et al., 2008). Together, my results suggest that skin pigmentation in whales is the result of selection for providing protection from UVR.

The photoprotective role of pigmentation has been described in freshwater zooplankton (Hansson, 2000), fishes (Adachi et al., 2005) and hammerhead sharks (Lowe and Goodman-Lowe, 1996), but to the best of my knowledge this is the first time that it has been shown for cetaceans. Some evidence supports my findings. For instance, geographical variation in cetacean pigmentation has been recorded in Southern right whales, *Eubalena australis* and humpback whales, *Megaptera novaeangliae* (Rosenbaum et al., 1995; Schaeff et al., 1999) and there is evidence that in right whales dorsal skin gradually darkens with age (Schaeff et al., 1999). In addition, genetic variation within conserved regions of *MC1R* gene has been found in a number of cetacean species, and the functional implications of such variations have been proposed in terms of colouration (Ayoub et al. 2009). Reconstructing the evolutionary history of cetacean skin colour would be challenging as it is possible that, as occurs in humans (Jablonski and Chaplin, 2010), skin pigmentation has changed more than once during cetacean evolution. Besides, although there is paleontological evidence suggesting that the close relative of the direct ancestor of whales was a terrestrial carnivore mammal the size of a wolf called Pakicetus

(Thewissen et al, 2009), fossil analysis makes it difficult to know whether it had hair and its colour remains a mystery.

Interestingly, although average melanocyte counts were greater in sperm whales than in blue whales, the prevalence of blisters and microscopic abnormalities was similar for both species (Chapter three, section 3.3.2). This finding is likely to reflect their markedly dissimilar sea-surfacing behaviours. Between foraging dives, sperm whales remain approximately five times longer at the surface than blue and fin whales (Croll et al., 2001), and during socialization, sperm whales can remain at the surface for up to six hours at a time (Whitehead, 2003), increasing their time of exposure to damaging UVR. These distinct behaviours could also explain the comparatively higher expression levels of *HSP70* and *KIN* that were observed in sperm whale skin (Chapter five, section 5.3.2.2). As *KIN* and *HSP70* genes are known to play a central role in cell and DNA protection against UV-light (Biard et al., 2002; Biard et al., 1997; Calini et al., 2003; Kannouche et al., 2000; Masson et al., 2003; Simon et al., 1995), the recorded levels of expression of these genes suggest that sperm whales activate genotoxic stress molecular pathways that involve overexpression of *HSP70* and *KIN* in response to long and persistent exposure to UVR. In humans and laboratory animals, levels of expression of repair genes such as *HSP70* and *KIN* increase in a time-dependent manner following UV irradiation (De la Coba et al., 2009; Masson et al., 2003), and up-regulation of *HSP70* and *KIN* can be observed between 6h and 8h following UV irradiation (De la Coba et al., 2009; Masson et al., 2003). In this sense, it is likely that the relative overexpression of *HSP70* and *KIN* in the cetacean samples analysed reflects acute exposure to UVR.

When accounting for interspecies differences, I found that transcription levels of *P53* and *HSP70* described a curve between February and May, peaking in March/April (Chapter five, section 5.3.2.4). These trends mimicked the temporal variation in UVR observed between February and April in the Gulf of California (Chapter two, section 2.5), suggesting that overexpression of repair genes occurs in a dose-dependent manner as observed in humans and laboratory animals (De la Coba et al., 2009; Masson et al., 2003) It is possible that the comparatively lower levels of expression recorded in May are due to acclimatization to UVR exposure, which

halted its increase in April (Chapter two, section 2.5). This phenomenon has been described in humans, whose sensitivity to sunburn decreases with increasing frequency and duration of solar exposure (Sayre et al., 1981).

Another relevant response pathway activated by exposure to the sun is the production of melanin (Lin and Fisher, 2007). In cetaceans, melanin concentration was not exclusively dependent on the quantity of melanocytes, but also on *TYR* and *P53* expression, both of which are involved in melanogenesis (Chapter six, section 6.3.4) (Oren and Bartek, 2007; Schuch and Menck, 2010). Surprisingly, regardless of interspecies differences in melanocyte abundance, melanin concentration was similar between sperm and blue whales (Chapter six, section 6.3.2), suggesting that the former are limited in their capacity to produce melanin. It is also possible that the high level of *HSP70* recorded in sperm whales have an inhibitory effect on melanin production as has been observed in mice that overexpress *HSP70* (Hoshino et al., 2010).

It was not possible to investigate temporal variation in pigmentation in the same individuals throughout a season, most whales being sampled once during the study (Chapter two, section 2.2). Thus, I examined variation at a population level. Following the seasonal increase in UV radiation that reached the Gulf of California (Chapter two, section 2.5), blue whales increased their concentration of melanocytes and melanin pigments (Chapter six, section 6.3.2), suggesting a capacity to modulate the level of pigmentation. This trend was not observed for the comparatively darker fin whale. It is possible that fin whale constitutive skin pigmentation is sufficient to counteract the harmful effect of UVR. Indeed, fin whales showed the lowest prevalence of sunburn lesions compared to blue and sperm whales (Chapter three, section 3.3.2). Another explanation for the observed differences in the capacity to modulate pigmentation might entail the distinct migratory behaviour of blue and fin whales. While fin whales reside year long in the Gulf of California (Bérubé et al., 2002), blue whales migrate annually from higher latitude to lower latitude (Calambokidis et al., 2009), where levels and intensity of UVR are greater (Ilyas, 2007). Consequently, when blue whales arrive at the Gulf of California they are exposed suddenly to relatively higher levels of UVR. It is possible that the higher

prevalence of skin lesions at the beginning of the season reflects the time needed for UVR acclimatisation to occur (Armstrong and Kricker, 2001; Sayre et al., 1981), as melanocyte concentration and melanin pigment increased gradually throughout the season. On the whole, the observed trends suggest that blue whales are able to "tan" as a response to increasing levels of seasonal UVR, constituting an interesting environmental adaptation.

8.2 Cetacean health in the context of global environmental changes

Understanding the impact of global environmental changes on wildlife health has become a priority (Acevedo-Whitehouse and Duffus, 2009; Burek et al., 2008). Such impacts are difficult to assess, particularly for species found in remote or inaccessible environments, such as the oceans. In the marine environment, cetaceans are considered "sentinels of the oceans" health (Moore, 2008). Indeed, due to their top-predator position in the web-food chain, cetaceans are sensitive to any alteration that occurs lower in the chain, such as decrease in prey abundance, presence of pathogens or pollutants (Hoekstra et al., 2003; Moore, 2008). Besides, due to their long life expectancy and their large distribution range spanning all latitudes (Wandrey, 1997), cetaceans reflect ecological variation across large spatial and long temporal scales (Moore, 2008). Therefore, evaluating the effect that environmental changes can exert on cetacean health is of high importance not only from a species conservation perspective but also for monitoring the entire marine ecosystem.

A current significant threat to the marine ecosystem is the high level of solar ultraviolet radiation that continues to reach our biosphere (Hader et al., 2007), a situation that is not expected to change for several decades (McKenzie et al., 2007; Solomon, 2004). Although the Montreal Protocol, which in 1987 banned the use of ozone depleting substances, has been central to decelerating the loss of ozone (Newman and McKenzie, 2011; WMO-UNEP, 2011), substances released during the nineties continue to destroy the ozone today due to their long atmospheric half-life (Solomon, 2004). Predictive models show that ozone over the Southern Hemisphere will recover near 2050 at mid latitudes. However, such predictions are more difficult

to make for the Northern Hemisphere due to uncertainties regarding future ozone levels in the Arctic (WMO-UNEP, 2011). This is because the ozone in the Arctic is predicted to be more sensitive to climate change than the Antarctic as the continuing accumulation of green house gases might lead to changes in stratospheric temperatures and circulation that, in turn, could have important consequences for the ozone column in mid-latitudes (WMO-UNEP, 2011). In this light, it is evident that there is a great deal of uncertainty about future UVR levels, particularly since they are not only dependent on the ozone thickness but also on other factors including changes in cloud coverage, surface reflectivity, and accumulation of other ozone-depleting substances such as sulphur dioxide and nitrogen dioxide (WMO-UNEP, 2011).

As high levels of UVR will continue to reach our biosphere and, as demonstrated here, can negatively affect cetaceans, considering solar UVR exposure to be a stressor for cetacean populations might be warranted. Cetaceans likely to be most affected are species with light pigmentation (e.g. blue whales, belugas or river dolphins) and those that tend to remain at the sea surface for longer (e.g. sperm whales). In this study, I demonstrated that these cetaceans appear to share the same molecular-repair pathways or melanogenesis-induction pathways as humans, which suggests that the ancestral origin of these mechanisms has a deep phylogenetic rooting. However, these protective mechanisms are likely to exert a cost in terms of energetic resources (Hessen, 1996) and might pose conflicting selective pressures (Hader et al., 2007), particularly for individuals in poor condition, as occurs, for instance, after long migrations (Burek et al., 2008). Recently, the scientific community has been concerned about the health of marine mammals, whose populations have seemed to deteriorate in the last decade (Gulland and Hall, 2007; Van Bressem et al., 2009). Evidently, as for most pathological processes, it is the combination of species-specific, intrinsic and environmental factors which will help to determine marine mammal sensitivity to UVR exposure (Fig. 7.1). This leads us to question whether exposure to solar radiation could have long term impacts, such as the development of skin cancer, for particularly sensitive species, in turn compromising the health of their populations.

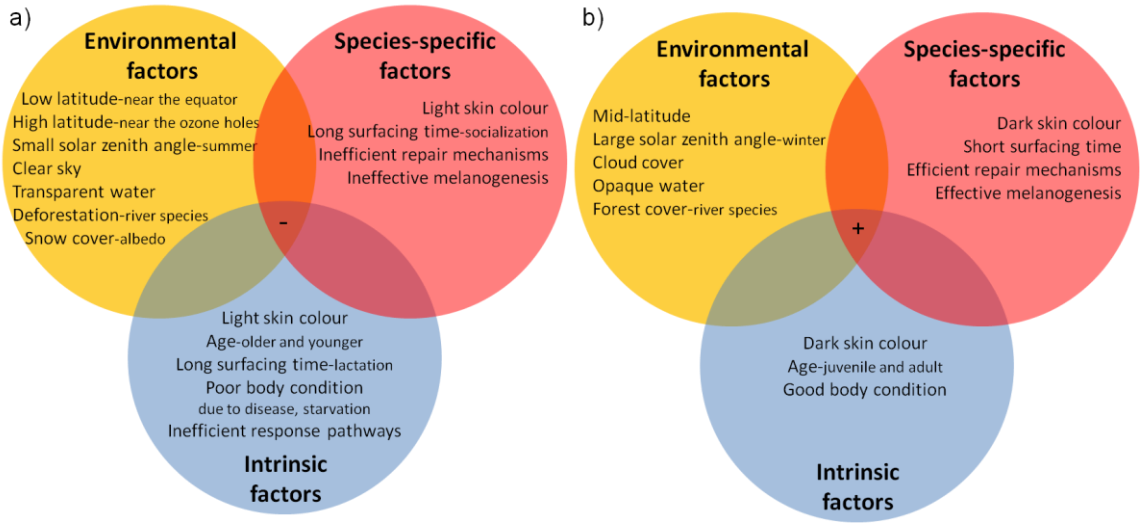

Figure 7.1. Combination of environmental, species-specific and intrinsic factors likely to influence marine mammal sensitivity to UVR exposure. a) Disadvantageous factors b) Advantageous factors.

Skin cancer is one of the most serious long-term consequences of excessive sun exposure (Armstrong and Kricker, 2001; De Gruijl et al., 2003). However, to date only one potential case of sun-induced skin cancer, squamous cell carcinoma, has been reported for cetaceans (Martineau et al., 2002). I failed to find evidence of skin cancer in any of the 142 whale samples examined. In humans, occurrence of skin cancer results from a combination of different factors such as ethnic origin, habits of sun exposure, history of sunburn and capacity to repair DNA damages (Armstrong and Kricker, 2001), which as schematized in figure 7.1, might increase the risk of cancer in whales, although on their own none these factors are likely to cause skin cancer. Recently, it has been proposed that cancer in large whales may be more common but less lethal than in small animals (Caulin and Maley, 2011; Nagy et al., 2007). Up to date this prediction has been not substantiated with empirical evidence. However, the general deterioration of environmental quality, including increased levels of persistent pollutants (e.g. high levels of polycyclic aromatic hydrocarbons, Martineau et al. 2002), unrelenting stress (Acevedo-Whitehouse and Duffus 2009) and higher levels of UV irradiance, might lead to higher cases of cancer in cetaceans in the future.

8.3 Future directions

There are several questions derived from the current study which would be worthwhile pursuing in the future. First, it might be possible to address specifically whether whales are likely to develop skin cancer by investigating UVR-induced specific mutations in genes involved in DNA repair such as the gene coding for tumour protein P53 (Daya-Grosjean et al., 1995; Nakazawa et al., 1994; Rass and Reichrath, 2008). *P53* mutations such as C-T and CC-TT transitions, considered signature mutations for UVR-induced damage (Nakazawa et al., 1994; Schuch and Menck, 2010), appear when photoproducts such as cyclobutane pyrimidine dimers and pyrimidine [6, 4] pyrimidone fail to be repaired (Schuch and Menck, 2010; Tornaletti and Pfeifer, 1996). To detect these mutations it would be necessary to sequence the entire *P53* gene in cetacean species with dissimilar sensitivity to UVR. A potentially more informative but technically more demanding possibility would be to generate cetacean epidermal cell cultures (Yu et al., 2005) and study the mutations produced after different doses of UV irradiation (Nakazawa et al., 1994). These mutations could then be screened using high resolution melting (Erali and Wittwer, 2010; Krypuy et al., 2007), a method based on simple PCR amplification with fluorescent dye intercalated with double-stranded DNA (Erali and Wittwer, 2010). Furthermore, efforts to scan for evidence of skin cancer in stranded animals might shed light on the prevalence of skin cancer in wild cetaceans.

This study identified the likely evolutionary significance of whale pigmentation. However, it would be interesting to broaden these findings in terms of mechanisms of photoprotection. Based on the results observed here, it is tempting to speculate that selection might operate on pigmentation. One approach to further study the evolutionary role of whale pigmentation would be to assess the variability of genes involved in shaping skin colour, such as the tyrosinase gene (*TYR*) and the gene encoding the Agouti signalling protein (Agouti) (Manceau et al., 2011; Steiner et al., 2007). In particular, investigating the variability of the melanocortin-1-receptor gene (*MC1R*) in blue whales might help explain the evident variability in skin colour patterns that exists in this species (Rana et al 1999; Sturm et al 2001). Furthermore, it would be possible to investigate whether pigmentation of cetaceans is darker near the

equator and lighter towards the poles for widely distributed species, as is well known for human populations (Jablonski and Chaplin, 2010). For this, access to high quality and long term photo-archives would be indispensable.

While the present study offers firm evidence that a previously ignored stressor can affect whales, further research is indispensable to investigate whether solar radiation can compromise the long term survival and reproduction of their populations. Such a study, combined with robust atmospheric data on ozone thickness and regional UVR levels, could be integrated in a model to investigate cetaceans' plasticity to environmental effectors. To orientate the research, areas of highest UVR threat (risk mapping) combined with cetacean species distributions and regions of excessive UVR exposure could be defined.

8.4 Conclusions

My study not only offers evidence that whales can sunburn, tan and resolve sun-induced damage, but also that these sun-induced alterations or adjustments vary amongst species. Interspecific variation in sun exposure sensitivity was explained by species dissimilarity in skin colour and sun exposure duration, two factors known to increase the risk of acute sunburn in humans. Individual skin pigmentation inversely predicts cellular and molecular lesions and directly predicts apoptotic cells, suggesting that darker pigmentation protects cetaceans from sun irradiation and plays a role in the elimination of potentially precancerous cells, as is known to occur in humans. While cetacean skin pigmentation has only been discussed in term of predator avoidance, my results underscore a potential photoprotective role likely to be shaped by natural selection. From a more practical perspective, the permanent threat posed by high levels of solar UVR that continue to reach our biosphere warrants considering UVR exposure as a stressor for cetacean populations, particularly for those with light skin such as belugas and blue whales. As a whole, my research has opened a new field of research in marine mammals, one that is both interesting and that may help management plans and conservation efforts.

REFERENCES

Abramoff, M.D., P.J. Magelhaes, and S.J. Ram. 2004. Image Processing with Image J. *Biophotonics International*. 11:36-42.

Acevedo-Whitehouse, K., and A.L.J. Duffus. 2009. Effects of environmental change on wildlife health. *Philosophical Transactions of the Royal Society B: Biological Sciences*. 364:3429-3438.

Adachi, K., K. Kato, K. Wakamatsu, S. Ito, K. Ishimaru, T. Hirata, O. Murata, and H. Kumai. 2005. The histological analysis, colorimetric evaluation, and chemical quantification of melanin content in 'suntanned' fish. *Pigment Cell Research*. 18: 465-468.

Al-Baker, E.A., M. Oshin, C.J. Hutchison, and I.R. Kill. 2005. Analysis of UV-induced damage and repair in young and senescent human dermal fibroblasts using the comet assay. *Mechanisms of Ageing and Development*. 126:664-672.

Amundson, S.A., T.G. Myers, and A.J. Fornace, Jr. 1998. Roles for p53 in growth arrest and apoptosis: putting on the brakes after genotoxic stress. *Oncogene*. 17:3287-3299.

Ananthaswamy, H.N. 1997. Ultraviolet light as a carcinogen. *In* Chemical Carcinogens and Anticarcinogens. Vol. 12. G.T. Bowden and S.M. Fischer, editors, Oxford. 255-279.

Andersen, C.L., J.L. Jensen, and T.F. Orntoft. 2004. Normalization of real-time quantitative reverse transcription-PCR data: a model-based variance estimation approach to identify genes suited for normalization, applied to bladder and colon cancer data sets. *Cancer Research*. 64:5245-5250.

Andrady, A.L., P.J. Aucamp, A.F. Bais, C.L. Ballare, L.O. Bjorn, J.F. Bornman, M.M. Caldwell, A.P. Cullen, F.R. de Gruijl, D.J. Erickson, 3rd, S.D. Flint, D.P. Hader, H.S. Hamid, M. Ilyas, G. Kulandaivelu, H.D. Kumar, R.L. McKenzie, J. Longstreth, R.M. Lucas, F.P. Noonan, M. Norval, N.D. Paul, R.C. Smith, K.R. Soloman, B. Sulzberger, Y. Takizawa, X. Tang, A. Torikai, J.C. van der Leun, S.R. Wilson, R.C. Worrest, and R.G. Zepp. 2007. Environmental effects of ozone depletion: 2006 assessment: interactions of

ozone depletion and climate change. *Photochemical & Photobiological Sciences.* 6:212-217.

Angulo, J.F., P. Mauffrey, G. Pinon-Lataillade, L. Miccoli, and D.S.F. Biard. 2005. Putative roles of kin17, a mammalian protein binding curved DNA, in transcription and replication. *In* DNA Conformation and Transcription. T. Ohyama, editor. Landes biosciences, New York.

Armstrong, B.K., and A. Kricker. 2001. The epidemiology of UV induced skin cancer. *Journal of Photochemistry and Photobiology B.* 63:8-18.

Ayoub, N.A., M.R. McGowen, C. Clark, M.S. Springer, and J. Gatesy. 2009. Evolution and phylogenetic utility of the melanocortin-1 receptor gene (MC1R) in Cetartiodactyla. *Molecular Phylogenetics and Evolution*. 52:550-557.

Balogh, A., G. Paragh, Jr., A. Juhasz, T. Kobling, D. Torocsik, E. Miko, V. Varga, G. Emri, I. Horkay, B. Scholtz, and E. Remenyik. 2008. Reference genes for quantitative real time PCR in UVB irradiated keratinocytes. *Journal of Photochemistry and Photobiology B.* 93:133-139.

Barcelo, J.A., and J. Calkins. 1980. The kinetics of avoidance of simulated solar UV radiation by two arthropods. *Biophysical Journal*. 32:921-929.

Barsh, G.S. 2003. What controls variation in human skin color? *PLoS Biology*. 1: 19-22.

Baruch, R., N. Avishai, and C. Rabinowitz. 2005. UV incites diverse levels of DNA breaks in different cellular compartments of a branching coral species. *The Journal of Experimental Biology*. 208:843-848.

Bearzi, M., S. Rapoport, J. Chau, and C. Saylan. 2009. Skin Lesions and Physical Deformities of Coastal and Offshore Common Bottlenose Dolphins (*Tursiops truncatus*) in Santa Monica Bay and Adjacent Areas, California. *AMBIO: A Journal of the Human Environment***.** 38:66-71.

Bech-Thomsen, N., and H.C. Wulf. 1996. Photoprotection due to pigmentation and epidermal thickness after repeated exposure to ultraviolet light and psoralen plus ultraviolet A therapy. *Photodermatology, Photoimmunology & Photomedicine*.11:213-218.

Berube, M., and P. Palsboll. 1996. Identification of sex in cetaceans by multiplexing with three ZFX and ZFY specific primers. *Molecular Ecology*. 5:283-287.

Bérubé, M., J. Urbán-Ramírez , A.E. Dizon, R.L. Brownell, and P.J. Palsbøll. 2002. Genetic identification of a small and highly isolated population of fin whales (*Balaenoptera physalus*) in the Sea of Cortez, Mexico. *Conservation Genetics.* 3:183–190.

Betti, C., and M. Nigro. 1996. The Comet assay for the evaluation of the genetic hazard of pollutants in cetaceans: Preliminary results on the genotoxic effects of methyl-mercury on the bottle-nosed dolphin (*Tursiops truncatus*) lymphocytes in vitro. *Marine Pollution Bulletin*. 32:545-548.

Bhana, S., and D.R. Lloyd. 2008. The role of p53 in DNA damage-mediated cytotoxicity overrides its ability to regulate nucleotide excision repair in human fibroblasts. *Mutagenesis*. 23:43-50.

Biard, D.S., L. Miccoli, E. Despras, Y. Frobert, C. Creminon, and J.F. Angulo. 2002. Ionizing radiation triggers chromatin-bound kin17 complex formation in human cells. *The Journal of Biological Chemistry*. 277:19156-19165.

Biard, D.S., Y. Saintigny, M. Maratrat, F. Paris, M. Martin, and J.F. Angulo. 1997. Enhanced expression of the Kin17 protein immediately after low doses of ionizing radiation. *Radiation Research*. 147:442-450.

Birch-Machin, M.A. 2000. Mitochondria and skin disease. *Clinical and Experimental Dermatology*. 25:141-146.

Birch-Machin, M.A., and H. Swalwell. 2010. How mitochondria record the effects of UV exposure and oxidative stress using human skin as a model tissue. *Mutagenesis*. 25:101-107.

Birch-Machin, M.A., M. Tindall, R. Turner, F. Haldane, and J.L. Rees. 1998. Mitochondrial DNA deletions in human skin reflect photo-rather than chronologic aging. *Journal of Investigative Dermatology*. 110:149-152.

Bischitz, P.G., and R.S. Snell. 1959. A study of the melanocytes and melanin in the skin of the male guinea-pig. *Journal of Anatomy*. 93:233-245.

Bissonnette, J.A. 1999. Small sample size problems in wildlife ecology: a contingent analytical approach. *Wildlife Biology*. 5:65-71.

Blaustein, A.R., J.M. Kiesecker, D.P. Chivers, D.G. Hokit, A. Marco, L.K. Belden, and A. Hatch. 1998. Effects of Ultraviolet Radiation on Amphibians: Field Experiments. *American Zoologist*. 38:799-812.

Blaustein, A.R., J.M. Romansic, J.M. Kiesecker, and A.C. Hatch. 2003. Ultraviolet radiation, toxic chemicals and amphibian population declines. *Diversity and distributions*. 9:123-140.

Brenner, M., and V.J. Hearing. 2008. The protective role of melanin against UV damage in human skin. *Photochemistry and Photobiology*. 84:539-549.

Brownell, R.L., C.A. Carlson, B.G. Vernazzani, and E. Cabrera. 2008. Skin lesions on blue whales off southern Chile: Possible conservation implications? *In* International Whaling Commission, Santiago, Chile.

Burek, K.A., F.M.D. Gulland, and T.M. O'Hara. 2008. Effects of climate change on arctic marine mammal health. *Ecological Applications*. 18:126-134.

Burren, R., C. Scaletta, E. Frenk, R.G. Panizzon, and L.A. Applegate. 1998. Sunlight and carcinogenesis : Expression of p53 and pyrimidine dimers in human skin following UVA I, UVA I + II and solar simulating radiations. *International Journal of Cancer* 76:201-206.

Calambokidis, J., J. Barlow, J.K.B. Ford, T.E. Chandler, and A.B. Douglas. 2009. Insights into the population structure of blue whales in the Eastern North Pacific from recent sightings and photographic identification. *Marine Mammal Science.* 25:816-832.

Calini, V., C. Urani, and M. Camatini. 2003. Overexpression of HSP70 is induced by ionizing radiation in C3H 10T1/2 cells and protects from DNA damage. *Toxicology in Vitro*. 17:561-566.

Carretta, J.V., K.A. Forney, M.S. Lowry, J. Barlow, J. Baker, D. Johnston, B. Hanson, M.M. Muto, D. Lynch, and L. Carswell. 2009. U.S. Pacific Marine Mammal Stock Assessments: 2008. *U.S. Department of Commerce, NOAA Technical Memorandum NMFS-SWFSC-434*:316pp.

Caulin, A.F., and C.C. Maley. 2011. Peto's Paradox: evolution's prescription for cancer prevention. *Trends in Ecology & Evolution*. 26:175-182.

Chang, Y.M., J.H. Barrett, D.T. Bishop, B.K. Armstrong, V. Bataille, W. Bergman, M. Berwick, P.M. Bracci, J.M. Elwood, M.S. Ernstoff, R.P. Gallagher, A.C. Green, N.A. Gruis, E.A. Holly, C. Ingvar, P.A. Kanetsky, M.R. Karagas, T.K. Lee, L. Le Marchand, R.M. Mackie, H. Olsson, A. Osterlind, T.R. Rebbeck, P. Sasieni, V. Siskind, A.J. Swerdlow, L. Titus-Ernstoff, M.S. Zens, and J.A. Newton-Bishop. 2009. Sun exposure and melanoma risk at different latitudes:

a pooled analysis of 5700 cases and 7216 controls. *International Journal of Epidemiology*. 38:814-830.

Chipchase, M.D., and D.W. Melton. 2002. The formation of UV-induced chromosome aberrations involves ERCC1 and XPF but not other nucleotide excision repair genes. *DNA Repair*. 1:335-340.

Cockell, C.S., and J. Knowland. 1999. Ultraviolet radiation screening compounds. *Biologial reviews of the Cambridge Philosophical Society*. 74:311-345.

Costin, G.-E., and V.J. Hearing. 2007. Human skin pigmentation: melanocytes modulate skin color in response to stress. *FASEB Journal*. 21:976-994.

Crawley, M.J. 2007. The R Book. Wiley, Chichester. 950 pp.

Croll, D.A., A. Acevedo-Gutiérrez, B.R. Tershy, and J. Urbán-Ramírez 2001. The diving behavior of blue and fin whales: is dive duration shorter than expected based on oxygen stores? *Comparative Biochemistry and Physiology*. 129:797–809.

D'Errico, M., T. Lemma, A. Calcagnile, L.P. De Santis, and E. Dogliotti. 2007. Cell type and DNA damage specific response of human skin cells to environmental agents. *Mutation Research*. 614:37–47.

Dahms, H.U., and J.S. Lee. 2010. UV radiation in marine ectotherms: molecular effects and responses. *Aquatic Toxicology*. 97:3-14.

Daya-Grosjean, L., N. Dumaz, and A. Sarasin. 1995. The specificity of p53 mutation spectra in sunlight induced human cancers. *Journal of Photochemistry and Photobiology B.* 28:115-124.

De Cock, J.G., A. Van Hoffen, J. Wijnands, G. Molenaar, P.H. Lohman, and J.C. Eeken. 1992. Repair of UV-induced (6-4)photoproducts measured in individual genes in the Drosophila embryonic Kc cell line. *Nucleic Acids Research*. 20:4789-4793.

De Gruijl , F.R. 1997. Health Effects from Solar UV Radiation. *Radiation Protection Dosimetry*. 72:177-196.

De Gruijl, F.R., J. Longstreth, M. Norval, A.P. Cullen, H. Slaper, M.L. Kripke, Y. Takizawa, and J.C. Van der Leun. 2003. Health effects from stratospheric ozone depletion and interactions with climate change. *Photochemical & Photobiological Sciences.* 2:16-28.

De la Coba, F., J. Aguilera, M.V. De Galvez, M. Alvarez, E. Gallego, F.L. Figueroa, and E. Herrera. 2009. Prevention of the ultraviolet effects on clinical and histopathological changes, as well as the heat shock protein-70 expression in mouse skin by topical application of algal UV-absorbing compounds. *Journal of Dermatological Science*. 55:161-169.

Decome, L., M. De Méo, A. Geffard, O. Doucet, G. Duménil, and A. Botta. 2005. Evaluation of photolyase (Photosome®) repair activity in human keratinocytes after a single dose of ultraviolet B irradiation using the comet assay. *Journal of Photochemistry and Photobiology B*. 79:101–108.

Del Bino, S., J. Sok, E. Bessac, and F. Bernerd. 2006. Relationship between skin response to ultraviolet exposure and skin color type. *Pigment Cell Research*. 19: 606-614.

Diaz, A., S. Carro, L. Santiago, J. Estevez, C. Guevara, M. Blanco, L. Sanchez, N. Lopez, D. Cruz, R. Lopez, E.B. Cuetara, and J.L. Fuentes. 2009. Estimates of DNA strand breakage in bottlenose dolphin (*Tursiops truncatus*) leukocytes measured with the Comet and DNA diffusion assays. *Genetics and Molecular Biology*. 32:367-372.

El-Zein, R.A., D.A. Hastings-Smith, M.M. Ammenheuser, M. Treinen-Moslen, F.M. Gulland, and J.B. Ward, Jr. 2006. Evaluation of two different biomarkers for use in the assessment of toxic chemical exposure in California sea lions (*Zalophus californianus*). *Marine Pollution Bulletin*. 52:108-113.

Erali, M., and C.T. Wittwer. 2010. High resolution melting analysis for gene scanning. *Methods*. 50:250-261.

Farman, J.C., B.G. Gardiner, and J.D. Shanklin. 1985. Large losses of total ozone in Antarctica reveal seasonal ClOx/NOx interaction. *Nature*. 315:207-210.

Fay, F.H. 1982. Ecology and biology of the Pacific walrus, *Odobenus rosmarus divergens*. US Dept Interior, Fish and Wildlife Service, Washington, DC.

Finkel, T., and N.J. Holbrook. 2000. Oxidants, oxidative stress and the biology of ageing. *Nature*. 408:239-247.

Flach, L., M.F. Van Bressem, J.C. Reyes, M. Echegaray, S. Siciliano, M. Santos, F. Viddi, E. Crespo, J. Klaich, I. Moreno, N.R. Emin-Lima, F. Felix, and K. Van Waerebeek. 2008. Miscellaneous skin lesions of unknown aetiology in

cetaceans from South America. *In* International Whaling Commission, Santiago, Chile.

Fourie, A.M., T.R. Hupp, D.P. Lane, B.-C. Sang, M.S. Barbosa, J.F. Sambrook, and M.-J.H. Gething. 1997. HSP70 Binding Sites in the Tumor Suppressor Protein p53. *Journal of Biological Chemistry*. 272:19471-19479.

Gallagher, R.P., and T.K. Lee. 2006. Adverse effects of ultraviolet radiation: a brief review. *Progress in Biophysics and Molecular Biology*. 92:119-131.

Garcia, O., I. Romero, J.E. González, and T. Mandina. 2007. Measurements of DNA damage on silver stained comets using free Internet software. *Mutation Research*. 627:186-190.

Gendron, D. 2002. Ecología poblacional de la ballena azul, *Balaenoptera musculus*, de la Península de Baja California. PhD thesis. Centro de Investigación Científica y Educación Superior de Ensenada, México.112pp.

Geraci, J.R., D.J. St Aubin, and B.D. Hicks. 1986. Anatomy and Physiology. The epidermis of odontocetes:a view from within. *In* Research on Dolphins. M.M. Bryden and R. Harrison, editors. Clarendon Press, Oxford. 3-21.

Gies, P.H., C.R. Roy, S. Toomey, and A. McLennan. 1998. Protection against solar ultraviolet radiation. *Mutation Research*. 422:15-22.

Giglia-Mari, G., and A. Sarasin. 2003. TP53 mutations in human skin cancers. *Human Mutation*. 21:217-228.

Gulland, F.M.D., and A.J. Hall. 2007. Is marine mammal health deteriorating? Trends in the global reporting of marine mammal disease. *EcoHealth*. 4:1335-1150.

Hader, D.P., H.D. Kumar, R.C. Smith, and R.C. Worrest. 2007. Effects of solar UV radiation on aquatic ecosystems and interactions with climate change. *Photochemical & Photobiological Sciences*. 6: 267–285.

Halliday, G.M., M. Norval, S.N. Byrne, X.X. Huang, and P. Wolf. 2008. The effects of sunlight on the skin. *Drug Discovery Today: Disease Mechanisms*. 5:e201-e209.

Hamilton, P.K., and M.K. Marx. 2005. Skin lesions on North Atlantic right whales: categories, prevalence and change in occurrence in the 1990s. *Diseases of Aquatic Organisms*. 68:71-82.

Hammond, P.S. 1990. Capturing whales on film-estimating cetacean population parameters from individual recognition data. *Mammal Review*. 20:17-22.

Han, B.A., L.B. Kats, R.C. Pommerening, R.P. Ferrer, M. Murry-Ewers, and A.R. Blaustein. 2007. Behavioral Avoidance of Ultraviolet-B Radiation by Two Species of Neotropical Poison-Dart Frogs. *Biotropica*. 39:433-435.

Hansson, L.A. 2000. Induced pigmentation in zooplankton: a trade-off between threats from predation and ultraviolet radiation. *Proceedings of the Royal Society B: Biological Sciences.* 267:2327-2331.

Hartmann, A., E. Agurell, C. Beevers, S. Brendler-Schwaab, B. Burlinson, P. Clay, A. Collins, A. Smith, G. Speit, V. Thybaud, and C.C. Tice. 2003. Recommendations for conducting the in vivo alkaline comet assay. *Mutagenesis*. 18:45-51.

Haywood, R.M., M. Lee, and C. Linge. 2006. Synthetic melanin is a model for soluble natural eumelanin in UVA-photosensitised superoxide production. *Journal of Photochemistry and Photobiology*. 82:224-235.

Hearing, V.J., and T.M. Ekel. 1976. Mammalian tyrosinase. A comparison of tyrosine hydroxylation and melanin formation. *Biochemistry Journal*. 157:549-557.

Heleskia, C.H., and I. Murtazashvili. 2010. Daytime shelter-seeking behavior in domestic horses. *Journal of Veterinary Behavior*. 5:276-282.

Helmbrecht, K., E. Zeise, and L. Rensing. 2000. Chaperones in cell cycle regulation and mitogenic signal transduction: a review. *Cell Proliferation*. 33:341-365.

Helton, E.S., and X. Chen. 2007. p53 modulation of the DNA damage response. *Journal of Celullar Biochemistry*. 100:883-896.

Hessen, D.O. 1996. Competitive trade-off strategies in Arctic *Daphia* linked to melanism and UV-B stress. *Polar Biology*. 16:573-579.

Hightower, L.E. 1991. Heat shock, stress proteins, chaperones, and proteotoxicity. *Cell*. 66:191-197.

Hoekstra, P.F., T.M. O'Hara, A.T. Fisk, K. Borga, K.R. Solomon, and D.C. Muir. 2003. Trophic transfer of persistent organochlorine contaminants (OCs) within an Arctic marine food web from the southern Beaufort-Chukchi Seas. *Environmental Pollution*. 124:509-522.

Hollstein, M., D. Sidransky, B. Vogelstein, and C. Harris. 1991. p53 mutations in human cancers. *Science*. 253:49-53.

Hoshino, T., M. Matsuda, Y. Yamashita, M. Takehara, M. Fukuya, K. Mineda, D. Maji, H. Ihn, H. Adachi, G. Sobue, Y. Funasaka, and T. Mizushima. 2010. Suppression of Melanin Production by Expression of HSP70. *Journal of Biological Chemistry*. 285:13254-13263.

Ierardi, J.L., A. Mancia, J. McMillan, M.L. Lundqvist, T.A. Romano, J.P. Wise Sr, G.W. Warr, and R.W. Chapman. 2009. Sampling the skin transcriptome of the North Atlantic right whale. *Comparative Biochemistry and Physiology Part D: Genomics and Proteomics*. 4:154-158.

Ihaka, R., and R. Gentleman. 1996. R: A Language for Data Analysis and Graphics. *Journal of Computational and Graphical Statistics*. 5:299-314.

Ikehata, H., R. Okuyama, E. Ogawa, S. Nakamura, A. Usami, T. Mori, K. Tanaka, S. Aiba, and T. Ono. 2010. Influences of p53 deficiency on the apoptotic response, DNA damage removal and mutagenesis in UVB-exposed mouse skin. *Mutagenesis*. 25:397-405.

Ilyas, M. 2007. Climate augmentation of erythemal UV-B radiation dose damage in the tropics and global change. *Current Science*. 93:1604-1608.

Ishii, Y., T. Kimura, S. Itagaki, and K. Doi. 1997. The skin injury induced by high energy dose of ultraviolet in hairless descendants of Mexican hairless dogs. *Histology and Histopathology*. 12:383-389.

Ito, S., and K. Wakamatsu. 2003. Quantitative analysis of eumelanin and pheomelanin in humans, mice, and other animals: a comparative review. *Pigment Cell Research*. 16:523-531.

Jablonski, N.G., and G. Chaplin. 2010. Human skin pigmentation as an adaptation to UV radiation. *Proceedings of the National Academy of Sciences of the United States of America*. 107:8962-8968.

Jakupciak, J.P., W. Wang, M.E. Markowitz, D. Ally, M. Coble, S. Srivastava, A. Maitra, P.E. Barker, D. Sidransky, and C.D. O'Connell. 2005. Mitochondrial DNA as a cancer biomarker. *The Journal of Molecular Diagnostics*. 7:258-267.

Jaquet, N., and D. Gendron. 2002. Distribution and relative abundance of sperm whales in relation to key environmental features, squid landings and the

distribution of other cetacean species in the Gulf of California, Mexico. *Marine Biology.* 141:591-601.

Jean, S., C. Bideau, L. Bellon, G. Halimi, M. De Meo, T. Orsiere, G. Dumenil, J.L. Berge-Lefranc, and A. Botta. 2001. The expression of genes induced in melanocytes by exposure to 365-nm UVA: study by cDNA arrays and real-time quantitative RT-PCR. *Biochimica et Biophysica Acta.* 1522:89-96.

Jensen, K.A., and M.J. Smerdon. 1990. DNA repair within nucleosome cores of UV-irradiated human cells. *Biochemistry*. 29:4773-4782.

Kadekaro, A.L., R.J. Kavanagh, K. Wakamatsu, S. Ito, M.A. Pipitone, and Z.A. Abdel-Malek. 2003. Cutaneous photobiology. The melanocyte vs. the sun: who will win the final round? *Pigment Cell Research*. 16:434-447.

Kannouche, P., and J.F. Angulo. 1999. Overexpression of kin17 protein disrupts nuclear morphology and inhibits the growth of mammalian cells. *Journal of Cell Science*. 112:3215-3224.

Kannouche, P., P. Mauffrey, G. Pinon-Lataillade, M.G. Mattei, A. Sarasin, L. Daya-Grosjean, and J.F. Angulo. 2000. Molecular cloning and characterization of the human KIN17 cDNA encoding a component of the UVC response that is conserved among metazoans. *Carcinogenesis*. 21:1701-1710.

Karentz, D., and I. Bosch. 2001. Influence of ozone-related increases in ultraviolet radiation on antarctic marine organisms. *American Zoologist*. 41:3-16.

Karentz, D., F.S. McEuen, M.C. Land, and W.C. Dunlap. 1991. Survey of mycosporine-like amino acid compounds in Antarctic marine organisms: Potential protection from ultraviolet exposure. *Marine Biology.* 108:157-166.

Khlgatian, M.K., I.M. Hadshiew, P. Asawanonda, M. Yaar, M.S. Eller, M. Fujita, D.A. Norris, and B.A. Gilchrest. 2002. Tyrosinase gene expression is regulated by p53. *The Journal of Investigative Dermatology*. 118:126-132.

Kiesecker, J.M., A.R. Blaustein, and L.K. Belden. 2001. Complex causes of amphibian population declines. *Nature*. 410:681-684.

Kobayashi, N., A. Nakagawa, T. Muramatsu, Y. Yamashina, T. Shirai, M.W. Hashimoto, Y. Ishigaki, T. Ohnishi, and T. Mori. 1998. Supranuclear Melanin Caps Reduce Ultraviolet Induced DNA Photoproducts in Human Epidermis. *The Journal of Investigative Dermatology*. 110:806-810.

Koņca, K., A. Lankoff, A. Banasik, H. Lisowska, T. Kuszewski, S**.** Góźdź**,** Z. Koza, and A. Wojcik. 2003. A cross platform public domain PC image analysis program for the comet assay. *Mutation Research*. 534:15-20.

Kouwenberg, J.H.M., H.I. Browman, J.J. Cullen, R.F. Davis, J.-F. St-Pierre, and J.A. Runge. 1999. Biological weighting of ultraviolet (280-400 nm) induced mortality in marine zooplankton and fish. I. Atlantic cod (*Gadus morhua*) eggs. *Marine Biology.* 134:269-284.

Krypuy, M., A.A. Ahmed, D. Etemadmoghadam, S.J. Hyland, A. DeFazio, S.B. Fox, J.D. Brenton, D.D. Bowtell, and A. Dobrovic. 2007. High resolution melting for mutation scanning of TP53 exons 5-8. *BMC Cancer*. 7:168.

Kucab, J.E., D.H. Phillips, and V.M. Arlt. 2010. Linking environmental carcinogen exposure to TP53 mutations in human tumours using the human TP53 knock-in (Hupki) mouse model. *FEBS Journal.* 277:2567-2583.

Lacour, J.P., P.R. Gordon, M. Eller, J. Bhawan, and B.A. Gilchrest. 1992. Cytoskeletal events underlying dendrite formation by cultured pigment cells. *Journal of Cellular Physiology*. 151:287–299.

Land, E.J., and P.A. Riley. 2000. Spontaneous redox reactions of dopaquinone and the balance between the eumelanic and phaeomelanic pathways. *Pigment Cell Research.* 13:273-277.

Latonen, L., and M. Laiho. 2005. Cellular UV damage responses--functions of tumor suppressor p53. *Biochimica et Biophysica Acta.* 1755:71-89.

Lee, R.F., and S. Steinert. 2003. Use of the single cell gel electrophoresis/comet assay for detecting DNA damage in aquatic (marine and freshwater) animals. *Mutation Research*. 544:43-64.

Lemus-Deschamps, L., I. Galindo, R. Solano, A.T. Elizalde, and J. Fonseca. 2002. Diagnosis of clear sky ultraviolet radiation for Mexico. *Atmosfera*. 15:165-171.

Li, Y., L. Zou, Q. Li, B. Haibe-Kains, R. Tian, Y. Li, C. Desmedt, C. Sotiriou, Z. Szallasi, J.D. Iglehart, A.L. Richardson, and Z.C. Wang. 2010. Amplification of LAPTM4B and YWHAZ contributes to chemotherapy resistance and recurrence of breast cancer. *Nature Medicine*. 16:214-218.

Lightner, J.K. 2008. Genetics of Coat Color I:The Melanocortin 1 Receptor (MC1R). *Answers Research Journal*. 1:109–116.

Lin, C.S., L.S. Wang, C.M. Tsai, and Y.H. Wei. 2008. Low copy number and low oxidative damage of mitochondrial DNA are associated with tumor progression in lung cancer tissues after neoadjuvant chemotherapy. *Interactive CardioVascular Thoracic Surgery*. 7:954-958.

Lin, J.Y., and D.E. Fisher. 2007. Melanocyte biology and skin pigmentation. *Nature*. 445:843-850.

Lindahl, T., and R.D. Wood. 1999. Quality control by DNA repair. *Science*. 286:1897-1905.

Lluch-Cota, S.E., E.A. Aragón-Noriega, F. Arreguín-Sánchez, D. Aurioles-Gamboa, J.J. Bautista-Romero, R.C. Brusca, R. Cervantes-Duarte, R. Cortés-Altamirano, P. Del-Monte-Luna, A. Esquivel-Herrera, G. Fernández, M.E. Hendrickx, S. Hernández-Vázquez, H. Herrera-Cervantes, M.L. Kahru, M., D. Lluch-Belda, D.B. Lluch-Cota, J. López-Martínez, S.G. Marinone, M.O. Nevárez-Martínez, S. Ortega-García, E. Palacios-Castro, A. Parés-Sierra, G. Ponce-Díaz, M. Ramírez-Rodríguez, C.A. Salinas-Zavala, R.A. Schwartzlose, and A.P. Sierra-Beltrán. 2007. The Gulf of California: Review of ecosystem status and sustainability challenges. *Progress in Oceanography*. 73:1-26.

Lo, H.L., S. Nakajima, L. Ma, B. Walter, A. Yasui, D.W. Ethell, and L.B. Owen. 2005. Differential biologic effects of CPD and 6-4PP UV-induced DNA damage on the induction of apoptosis and cell-cycle arrest. *BMC Cancer*. 5:135.

Lowe, C., and G. Goodman-Lowe. 1996. Suntanning in hammerhead sharks. *Nature*. 383:677.

MacIntyre, N. 2001. Unmasking antigens for immunohistochemistry. *British Journal of Biomedical Science*. 58:190-196.

Malloy, K.D., M.A. Holman, D. Mitchell, and H.W. Detrich, 3rd. 1997. Solar UVB-induced DNA damage and photoenzymatic DNA repair in antarctic zooplankton. *Proceedings of the National Academy of Sciences of the United States of America*. 94:1258-1263.

Manceau, M., V.S. Domingues, R. Mallarino, and H.E. Hoekstra. 2011. The developmental role of agouti in color pattern evolution. *Sciences*. 331:1062-1065.

Marco, A., M. Lizana, A. Alvarez, and A.R. Blaustein. 2001. Egg-wrapping behaviour protects newt embryos from UV radiation. *Animal Behaviour*. 61:639-644.

Martens, W.J.M., M.G.J. Den Elzen, H. Slaper, P.J.M. Koken, and B.A.T. Willems. 1996. The impact of ozone depletion on skin cancer incidence: An assessment of the Netherlands and Autralia. *Environmental Modeling and Assessment.* 1:229-240.

Martineau, D., K. Lemberger, A. Dallaire, P. Labelle, T.P. Lipscomb, P. Michel, and I. Mikaelian. 2002. Cancer in Wildlife, a Case Study: Beluga from the St. Lawrence Estuary, Québec, Canada. *Environmental Health Perspectives*. 110: 285-292.

Masson, C., F. Menaa, G. Pinon-Lataillade, Y. Frobert, S. Chevillard, J.P. Radicella, A. Sarasin, and J.F. Angulo. 2003. Global genome repair is required to activate KIN17, a UVC-responsive gene involved in DNA replication. *Proceedings of the National Academy of Sciences of the United States of America*. 100:616-621.

Matsuda, M., T. Hoshino, Y. Yamashita, K.-i. Tanaka, D. Maji, K. Sato, H. Adachi, G. Sobue, H. Ihn, Y. Funasaka, and T. Mizushima. 2010. Prevention of UVB Radiation-induced Epidermal Damage by Expression of Heat Shock Protein 70. *Journal of Biological Chemistry*. 285:5848-5858.

Matts, P.J., and B. Fink. 2010. Chronic sun damage and the perception of age, health and attractiveness. *Photochemical & Photobiological Sciences.* 9:421-431.

McKenzie, R.L., P.J. Aucamp, A.F. Bais, L.O. Bjorn, and M. Ilyas. 2007. Changes in biologically-active ultraviolet radiation reaching the Earth's surface. *Photochemical & Photobiological Sciences.* 6:218-231.

Meyer, J.N. QPCR: a tool for analysis of mitochondrial and nuclear DNA damage in ecotoxicology. 2010. *Ecotoxicology*. 19:804-811.

Miccoli, L., I. Frouin, O. Novac, D. Di Paola, F. Harper, M. Zannis-Hadjopoulos, G. Maga, D.S. Biard, and J.F. Angulo. 2005. The human stress-activated protein kin17 belongs to the multiprotein DNA replication complex and associates in vivo with mammalian replication origins. *Molecular and Cellular Biology*. 25:3814-3830.

Moore, S.E. 2008. Marine mammals as ecosystem sentinels. *Journal of Mammalogy*. 89:534-540.

Murase, D., A. Hachiya, Y. Amano, A. Ohuchi, T. Kitahara, and Y. Takema. 2009. The essential role of p53 in hyperpigmentation of the skin via regulation of paracrine melanogenic cytokine receptor signaling. *The Journal of Biological Chemistry*. 284:4343-4353.

Nagy, J.D., E.M. Victor, and J.H. Cropper. 2007. Why don't all whales have cancer? A novel hypothesis resolving Peto's paradox. *Integrative and Comparative Biology*. 47:317-328.

Nakanishi, M., H. Niida, H. Murakami, and M. Shimada. 2009. DNA damage responses in skin biology--implications in tumor prevention and aging acceleration. *Journal of Dermatological Science.* 56:76-81.

Nakaseko, H., M. Kobayashi, Y. Akita, Y. Tamada, and Y. Matsumoto. 2003. Histological changes and involvement of apoptosis after photodynamic therapy for actinic keratoses. *British Journal of Dermatology.* 148:122-127.

Nakazawa, H., D. English, P.L. Randell, K. Nakazawa, N. Martel, B.K. Armstrong, and H. Yamasaki. 1994. UV and skin cancer: specific p53 gene mutation in normal skin as a biologically relevant exposure measurement. *Proceedings of the National Academy of Sciences of the United States of America*. 91:360-364.

Newman, P.A., and R. McKenzie. 2011. UV impacts avoided by the Montreal Protocol. *Photochemical & Photobiological Sciences.* In Press.

Nghiem, D.X., N. Kazimi, D.L. Mitchell, A.A. Vink, H.N. Ananthaswamy, M.L. Kripke, and S.E. Ullrich. 2002. Mechanisms underlying the suppression of established immune responses by ultraviolet radiation. *The Journal of Investigative Dermatology*. 119: 600-608.

Noonan, F.P., J. Dudek, G. Merlino, and E.C. De Fabo. 2003. Animal models of melanoma: an HGF/SF transgenic mouse model may facilitate experimental access to UV initiating events. *Pigment Cell Research*. 16:16-25.

Oetting, W.S. 2000. The tyrosinase gene and oculocutaneous albinism type 1 (OCA1): A model for understanding the molecular biology of melanin formation. *Pigment Cell Research*. 13:320-325.

Ohkawara, A., K. Halprin, and V. Levine. 1972. Glycogen metabolism following ultraviolet irradiation. *The Journal of Investigative Dermatology*. 59:264-268.

Olive, P.L., and J.P. Banath. 2006. The comet assay: a method to measure DNA damage in individual cells. *Nature Protocols*. 1:23-29.

Olive, P.L., R.E. Durand, S.M. Jackson, J.C. Le Riche, C. Luo, R. Ma, D.B. McLaren, C. Aquino-Parsons, T.A. Thomson, and T. Trotter. 1999. The comet assay in clinical practice. *Acta Oncologica*. 38:839-844.

Oren, M., and J. Bartek. 2007. The sunny side of p53. *Cell*. 128:826-828.

Ortega Ortiz, C.D. 2009. Aspecto de la dinamica poblacional de la ballena azul (*Balaenoptera musculus*) del Pacifico Noreste. PhD Thesis. Instituto Politecnico Nacional-Centro Interdisciplinario de Ciencias Marinas, La Paz. 215pp.

Pattison, D.I., and M.J. Davies. 2006. Actions of ultraviolet light on cellular structures. *EXS*. 96:131-157.

Peterson, C.L., and J. Côté. 2004. Cellular machineries for chromosomal DNA repair. *Genes and development*. 18:602-616.

Pfaffl, M.W., A. Tichopad, C. Prgomet, and T.P. Neuvians. 2004. Determination of stable housekeeping genes, differentially regulated target genes and sample integrity: BestKeeper – Excel-based tool using pair-wise correlations. *Biotechnology Letters*. 26:509-515.

Pinheiro, J., D. Bates, S. DebRoy, D. Sarkar, and RCoreteam. 2008. nlme: Linear and Nonlinear Mixed Effects Models. *In* R package version 3.1-89.

Porter, P.C., D.R. Clark, L.D. McDaniel, G.W. McGregor, and C.J. States. 2006. Telomerase-immortalized human fibroblasts retain UV-induced mutagenesis and p53-mediated DNA damage responses *DNA Repair*. 5:61-70.

Rana, B.K., D. Hewett-Emmett, L. Jin, B.H. Chang, N. Sambuughin, M. Lin, S. Watkins, M. Bamshad, L.B. Jorde, M. Ramsay, T. Jenkins, and W.H. Li. 1999. High polymorphism at the human melanocortin 1 receptor locus. *Genetics*. 151:1547-1557.

Rass, K., and J. Reichrath. 2008. UV damage and DNA repair in malignant melanoma and nonmelanoma skin cancer. *Advances in Experimental Medicine and Biology*. 624:162-178.

R Development Core Team. 2008. R: A Language and Environment for Statistical Computing. *In* Computing RFfS, editor, Vienna, Austria.

Reeb, D., P.B. Best, and S.H. Kidson. 2007. Structure of the integument of southern right whales, Eubalaena australis. *The Anatomical Record*. 290:596-613.

Rhode, S.C., M. Pawlowski, and R. Tollrian. 2001. The impact of ultraviolet radiation on the vertical distribution of zooplankton of the genus Daphnia. *Nature*. 412:69-72.

Riemer, U., M.D. Lamare, and B.M. Peake. 2007. Temporal concentrations of sunscreen compounds (Mycosporine-like Amino Acids) in phytoplankton and in the New Zealand krill, Nyctiphanes australis G.O. Sars. *Journal of Plankton Research*. 29:1077-1086.

Rosenbaum, H.C., P.J. Clapham, J. Allen, M. Nicole-Jenner, C. Jenner, L. Florez-Gonzalez, J. Urban, P. Ladron, K. Mori, M. Yamaguchi, and C.S. Baker. 1995. Geographic variation in ventral fluke pigmentation of humpback whale (*Megaptera novaeangliae*) populations worldwide. *Marine Ecology Progress Series*. 124:1-7.

Rouzaud, F., G.E. Costin, Y. Yamaguchi, J.C. Valencia, W.F. Berens, K.G. Chen, T. Hoashi, M. Bohm, Z.A. Abdel-Malek, and V.J. Hearing. 2006. Regulation of constitutive and UVR-induced skin pigmentation by melanocortin 1 receptor isoforms. *The FASEB Journal*. 20:1927-1929.

Rozen, S., and H. Skaletsky. 2000. Primer3 on the WWW for general users and for biologist programmers. *Methods in Molecular Biology*. 132:365-386.

Ruppert, D., M.P. Wand, and R.J. Carroll. 2003. Semiparametric Regression. Cambridge University Press, Cambridge. 416pp.

Saikawa, Y., K. Hashimoto, M. Nakata, M. Yoshihara, K. Nagai, M. Ida, and T. Komiya. 2004. Pigment chemistry: The red sweat of the hippopotamus. *Nature*. 429:363-363.

Sambrook, J., E.F. Fritch, and T. Maniatis. 1989. Molecular Cloning, a laboratory manual, 2nd edition. Cold Spring Harbor Laboratory Press, Cold Spring Harbor, New York.

Sayre, R.M., D.L. Desrochers, C.J. Wilson, and E. Marlowe. 1981. Skin type, minimal erythema dose (MED), and sunlight acclimatization. *Journal of the American Academy of Dermatology*. 5:439-443.

Schaeff, C.M., P.B. Best, V.J. Rowntree, R. Payne, C. Jarvis, and V.A. Portway. 1999. Dorsal skin color patterns among southern right whales (*Eubalaena australis*): genetic basis and evolutionary significance. *Journal of Heredity*. 90:464-471.

Schmittgen, T.D., and K.J. Livak. 2008. Analyzing real-time PCR data by the comparative CT method. *Nature Protocols*. 3:1101-1108.

Schuch, A.P., and C.F. Menck. 2010. The genotoxic effects of DNA lesions induced by artificial UV-radiation and sunlight. *Journal of Photochemistry and Photobiology B.* 99:111-116.

Sears, R., and J. Calambokidis. 2002. Update COSEWIC status report on the blue whale *Balaenoptera musculus* in Canada. *In* COSEWIC assessment and update status report on the blue whale *Balaenoptera in musculus* in Canada. Comittee on the status of endangered wildlife in Canada, Otawa. 1-32.

Simon, M.M., A. Reikerstorfer, A. Schwarz, C. Krone, T.A. Luger, M. Jaattela, and T. Schwarz. 1995. Heat shock protein 70 overexpression affects the response to ultraviolet light in murine fibroblasts. Evidence for increased cell viability and suppression of cytokine release. *The Journal of Clinical Investigation.* 95:926-933.

Solomon, S. 2004. The hole truth. *Nature*. 427:289-291.

Solomon, S., R.W. Portmann, and D.W. Thompson. 2007. Contrasts between Antarctic and Arctic ozone depletion. *Proceedings of the National Academy of Sciences of the United States of America.* 104:445-449.

Sommaruga, R., K. Whitehead, J.M. Shick, and C.S. Lobban. 2006. Mycosporine-like amino acids in the zooxanthella-ciliate symbiosis Maristentor dinoferus. *Protist*. 157:185-191.

Spinsanti, G., C. Panti, E. Lazzeri, L. Marsili, S. Casini, F. Frati, and C. Fossi. 2006. Selection of reference genes for quantitative RT-PCR studies in striped dolphin (*Stenella coeruleoalba*) skin biopsies. *BMC: Molecular Biology.* 19:7:32.

Spradbrow, P.B., J.L. Samuel, W.R. Kelly, and A.L. Wood. 1987. Skin cancer and papillomaviruses in cattle. *Journal of Comparative Pathology.* 97:469-479.

Stangl, S., M. Gehrmann, J. Riegger, K. Kuhs, I. Riederer, W. Sievert, K. Hube, R. Mocikat, R. Dressel, E. Kremmer, A.G. Pockley, L. Friedrich, L. Vigh, A.

Skerra, and G. Multhoff. 2011. Targeting membrane heat-shock protein 70 (Hsp70) on tumors by cmHsp70.1 antibody. *Proceedings of the National Academy of Sciences of the United States of America*. 108:733-738.

Steele, B.K., C. Meyers, and M.A. Ozbun. 2002. Variable expression of some "housekeeping" genes during human keratinocyte differentiation. *Analytical Biochemistry*. 307:341-347.

Steiner, C.C., J.N. Weber, and H.E. Hoekstra. 2007. Adaptive variation in beach mice produced by two interacting pigmentation genes. *PLoS Biol*. 5:1-10.

Stevens, M., and S. Merilaita. 2009. Animal camouflage: current issues and new perspectives. *Philosophical Transactions of the Royal Society B: Biological Sciences*. 364:423-427.

Stierner, U., I. Rosdahl, A. Augustsson, and B. Kagedal. 1989. UVB irradiation induces melanocyte increase in both exposed and shielded human skin. *The Journal of Investigative Dermatology*. 92:561-564.

Stuart-Fox, D., and A. Moussalli. 2009. Camouflage, communication and thermoregulation: lessons from colour changing organisms. *Philosophical Transactions of the Royal Society B: Biological Sciences*. 364:463-470.

Sturm, R.A., R.D. Teasdale, and N.F. Box. 2001. Human pigmentation genes: identification, structure and consequences of polymorphic variation. *Gene*. 277:49-62.

Susin, S.A., N. Zamzami, and G. Kroemer. 1998. Mitochondria as regulators of apoptosis: doubt no more. *Biochimica et Biophysica Acta*. 1366:151-165.

Taddei, F., V. Scarcelli, G. Frenzilli, and M. Nigro. 2001. Genotoxic Hazard of Pollutants in Cetaceans: DNA Damage and Repair Evaluated in the Bottlenose Dolphin (*Tursiops truncatus*) by the Comet Assay. *Marine Pollution Bulletin*. 42:324-328.

Tadokoro, T., N. Kobayashi, B.Z. Zmudzka, S. Ito, K. Wakamatsu, Y. Yamaguchi, K.S. Korossy, S.A. Miller, J.Z. Beer, and V.J. Hearing. 2003. UV-induced DNA damage and melanin content in human skin differing in racial/ethnic origin. *The FASEB Journal*. 17:1177-1179.

Takeuchi, S., W. Zhang, K. Wakamatsu, S. Ito, V.J. Hearing, K.H. Kraemer, and D.E. Brash. 2004. Melanin acts as a potent UVB photosensitizer to cause an

atypical mode of cell death in murine skin. *Proceedings of the National Academy of Sciences of the United States of America*. 101:15076-15081.

Taylor, C.F. 2009. Mutation scanning using high-resolution melting. *Biochemical Society Transactions*. 37:433-437.

Taylor, S., M. Wakem, G. Dijkman, M. Alsarraj, and M. Nguyen. 2010. A practical approach to RT-qPCR-Publishing data that conform to the MIQE guidelines. *Methods*. 50:S1-S5.

Tedetti, M., and R. Sempere. 2006. Penetration of ultraviolet radiation in the marine environment. A review. *Photochemistry and Photobiology*. 82:389-397.

Teloni, V., J.P. Mark, M.J.O. Patrick, and M.T. Peter. 2008. Shallow food for deep divers : Dynamic foraging behavior of male sperm whales in a high latitude habitat. *Journal of Experimental Marine Biology and Ecology*. 354:119–131.

Thewissen, J.G.M., L.N. Cooper, J.C. George, and S. Bajpai. 2009. From Land to Water: the Origin of Whales, Dolphins, and Porpoises. *Evolution: Education and Outreach*. 2:272–288.

Tice, R.R., E. Agurell, D. Anderson, B. Burlinson, A. Hartmann, H. Kobayashi, Y. Miyamae, E. Rojas, J.C. Ryu, and Y.F. Sasaki. 2000. Single cell gel/comet assay: guidelines for in vitro and in vivo genetic toxicology testing. *Environmental and Molecular Mutagenesis*. 35:206-221.

Todo, T., H. Ryo, K. Yamamoto, H. Toh, T. Inui, H. Ayaki, T. Nomura, and M. Ikenaga. 1996. Similarity among the Drosophila (6-4)photolyase, a human photolyase homolog, and the DNA photolyase-blue-light photoreceptor family. *Science*. 272:109-112.

Tornaletti, S., and G.P. Pfeifer. 1996. UV damage and repair mechanisms in mammalian cells. *Bioessays*. 18:221-228.

UNEP-DTIE, and GRID-Arendal. 2007. Vital Ozone Graphics.

Van Bressem, M.F., J.A. Raga, G. Di Guardo, P.D. Jepson, P.J. Duignan, U. Siebert, T. Barrett, M.C. Santos, I.B. Moreno, S. Siciliano, A. Aguilar, and K. Van Waerebeek. 2009. Emerging infectious diseases in cetaceans worldwide and the possible role of environmental stressors. *Diseases of Aquatic Organisms*. 86:143-157.

Van Bressem, M.F., K. Van Waerebeek, F.J. Aznar, J.A. Raga, P.D. Jepson, P. Duignan, R. Deaville, L. Flach, F. Viddi, J.R. Baker, A.P. Di Beneditto, M.

Echegaray, T. Genovo, J. Reyes, F. Felix, R. Gaspar, R. Ramos, V. Peddemors, G.P. Sanino, and U. Siebert. 2009. Epidemiological pattern of tattoo skin disease: a potential general health indicator for cetaceans. *Diseases of Aquatic Organisms.* 85:225-237.

Vandesompele, J., K. De Preter, F. Pattyn, B. Poppe, N. Van Roy, A. De Paepe, and F. Speleman. 2002. Accurate normalization of real-time quantitative RT-PCR data by geometric averaging of multiple internal control genes. *Genome Biology*. 3: research0034.1–research0034.11.

Vernet, M., S.B. Diaz, H.A. Fuenzalida, C. Camilion, C.R. Booth, S. Cabrera, C. Casiccia, G. Deferrari, C. Lovengreen, A. Paladini, J. Pedroni, A. Rosales, and H.E. Zagarese. 2009. Quality of UVR exposure for different biological systems along a latitudinal gradient. *Photochemical & Photobiological Sciences.* 8:1329-1345.

Wandrey, R. 1997. Guide des mammifères marins du monde. Delachaux et Niestlé, Neufchâtel. 284 pp.

Watabe, H., J.C. Valencia, K. Yasumoto, T. Kushimoto, H. Ando, J. Muller, W.D. Vieira, M. Mizoguchi, E. Appella, and V.J. Hearing. 2004. Regulation of tyrosinase processing and trafficking by organellar pH and by proteasome activity. *The Journal of Biological Chemistry.* 279:7971-7981.

Webb, A.R. 2006. Who, what, where and when-influences on cutaneous vitamin D synthesis. *Progress in Biophysics and Molecular Biology*. 92:17-25.

Wheeler, D.S., K.E. Dunsmore, A.G. Denenberg, L. Muething, S.E. Poynter, and H.R. Wong. 2011. Biological activity of truncated C-terminus human heat shock protein 72. *Immunology Letters.* 135:173-179.

Whitehead, H. 2002. Estimates of the current global population size and historical trajectory for sperm whales. *Marine Ecology Progress Series.* 242:295-304.

Whitehead, H. 2003. Sperm whales: social evolution in the ocean. The University of Chicago Press, Chicago. 431 pp.

Whitehead, H., M. Dillon, S. Dufault, L. Weilgart, and J. Wright. 1998. Non-geographically based population structure of South Pacific sperm whales: dialects, fluke-markings and genetics. *Journal of Animal Ecology*. 67:142-151.

Wilson, B., H. Arnold, G. Bearzi, C.M. Fortuna, R. Gaspar, S. Ingram, C. Liret, S. Pribanic, A.J. Read, V. Ridoux, K. Schneider, K.W. Urian, R.S. Wells, C. Wood, P.M. Thompson, and P.S. Hammond. 1999. Epidermal diseases in bottlenose dolphins: impacts of natural and anthropogenic factors. *Proceedings of the Royal Society B: Biological Sciences.* 266:1077-1083.

WMO-UNEP. 2011. Scientific Assessment of Ozone Depletion: 2010, Global Ozone Research and Monitoring Project. *In* World Meteorological Organization, Geneva, Switzerland.

Yamaguchi, Y., J. Beer, and V. Hearing. 2008. Melanin mediated apoptosis of epidermal cells damaged by ultraviolet radiation: factors influencing the incidence of skin cancer. *Archives of Dermatological Research.* 300:43-50.

Yamaguchi, Y., M. Brenner, and V.J. Hearing. 2007. The Regulation of Skin Pigmentation. *Journal of Biological Chemistry*. 282:27557-27561.

Yamaguchi, Y., K. Takahashi, B.Z. Zmudzka, A. Kornhauser, S.A. Miller, T. Tadokoro, W. Berens, J.Z. Beer, and V.J. Hearing. 2006. Human skin responses to UV radiation: pigment in the upper epidermis protects against DNA damage in the lower epidermis and facilitates apoptosis. The *FASEB Journal*. 20:1486-1488.

Yoshida, H., T. Matsui, N. Hosokawa, R.J. Kaufman, K. Nagata, and K. Mori. 2003. A time-dependent phase shift in the mammalian unfolded protein response. *Developmental Cell.* 4:265-271.

You, Y.H., D.H. Lee, J.H. Yoon, S. Nakajima, A. Yasui, and G.P. Pfeifer. 2001. Cyclobutane pyrimidine dimers are responsible for the vast majority of mutations induced by UVB irradiation in mammalian cells. *The Journal of Biological Chemistry.* 276:44688-44694.

Yu, J., M.S. Kindy, B.C. Ellis, J.E. Baatz, M. Peden-Adams, T.J. Ellingham, D.J. Wolff, P.A. Fair, and S. Gattoni-Celli. 2005. Establishment of epidermal cell lines derived from the skin of the Atlantic bottlenose dolphin (*Tursiops truncatus*). *The Anatomical Record. Part A, Discoveries in Molecular, Cellular, and Evolutionary Biology.* 287:1246-1255.

Zhou, B.B., and S.J. Elledge. 2000. The DNA damage response: putting checkpoints in perspective. *Nature*. 408:433-439.

Zittermann, A., and J.F. Gummert. 2010. Sun, vitamin D, and cardiovascular disease. *Journal of Photochemistry and Photobiology B.* 101:124-129.

Zuur, A., E. Ieno, N. Walker, A. Saveliev, and G. Smith. 2009. Mixed effects models and extensions in ecology with R. Springer, New York. 574 pp.

Zylicz, M., F.W. King, and A. Wawrzynow. 2001. Hsp70 interactions with the p53 tumour suppressor protein. *The EMBO Journal.* 20:4634-463.

Appendix 2.1. General materials and methods

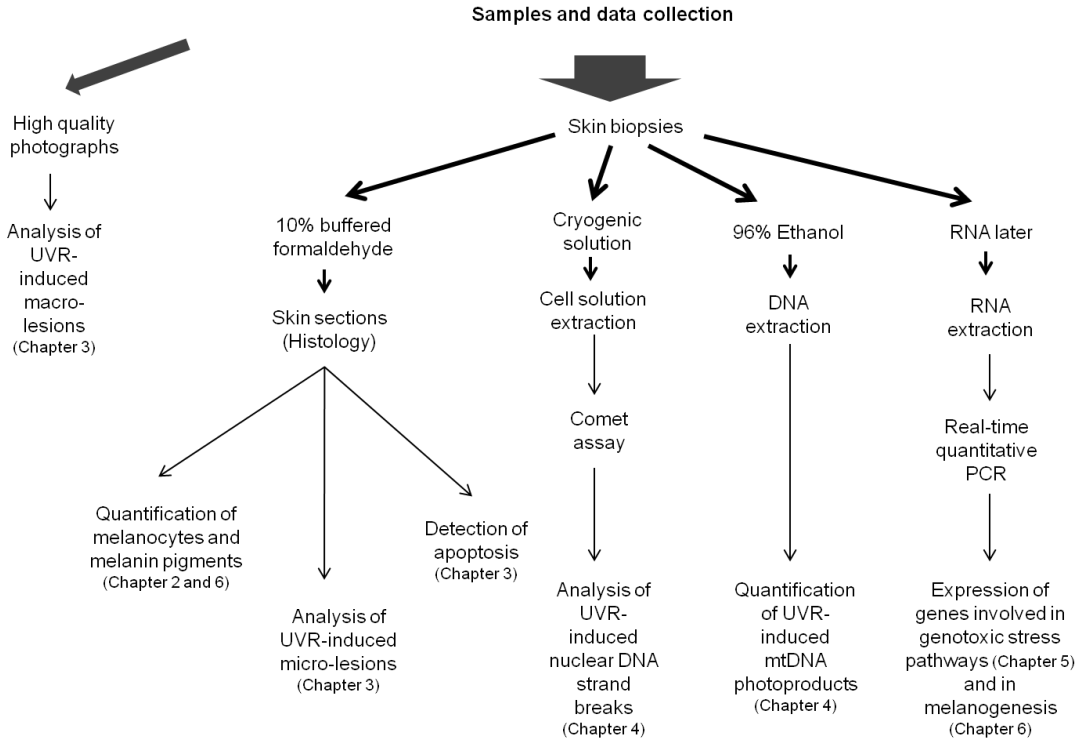

Appendix 3.1. Manuscript

PROCEEDINGS OF THE ROYAL SOCIETY B

FirstCite e-publishing

Proc. R. Soc. B
doi:10.1098/rspb.2010.1903
Published online

Acute sun damage and photoprotective responses in whales

Laura M. Martinez-Levasseur[1,2], Diane Gendron[3], Rob J. Knell[2], Edel A. O'Toole[4], Manuraj Singh[4] and Karina Acevedo-Whitehouse[1,5,*]

[1]*Institute of Zoology, Regent's Park, London NW1 4RY, UK*
[2]*School of Biological and Chemical Sciences, Queen Mary University of London, Mile End Road, London E1 4NS, UK*
[3]*Centro Interdisciplinario de Ciencias Marinas, Instituto Politécnico Nacional, Av. IPN s/n, Playa Palo de Sta Rita, La Paz, BCS C.P. 23000, México*
[4]*Centre for Cutaneous Research, Blizard Institute of Cell and Molecular Science, Barts and the London School of Medicine and Dentistry, Queen Mary University of London, London E1 2AT, UK*
[5]*Facultad de Ciencias Naturales, Universidad Autónoma de Querétaro, 76230, Querétaro, México*

Rising levels of ultraviolet radiation (UVR) secondary to ozone depletion are an issue of concern for public health. Skin cancers and intraepidermal dysplasia are increasingly observed in individuals that undergo chronic or excessive sun exposure. Such alterations of skin integrity and function are well established for humans and laboratory animals, but remain unexplored for mammalian wildlife. However, effects are unlikely to be negligible, particularly for species such as whales, whose anatomical or life-history traits force them to experience continuous sun exposure. We conducted photographic and histological surveys of three seasonally sympatric whale species to investigate sunburn and photoprotection. We find that lesions commonly associated with acute severe sun damage in humans are widespread and that individuals with fewer melanocytes have more lesions and less apoptotic cells. This suggests that the pathways used to limit and resolve UVR-induced damage in humans are shared by whales and that darker pigmentation is advantageous to them. Furthermore, lesions increased significantly in time, as would be expected under increasing UV irradiance. Apoptosis and melanocyte proliferation mirror this trend, suggesting that whales are capable of quick photoprotective responses. We conclude that the thinning ozone layer may pose a risk to the health of whales and other vulnerable wildlife.

Keywords: apoptosis; ozone depletion; photoprotection; pigmentation; skin lesions; whales

1. INTRODUCTION

Since the 20th century, worldwide mounting levels of solar ultraviolet radiation (UVR) consequential to ozone depletion [1–3] have generated concern owing to their health implications [4–5]. Across all latitudes, cases of skin cancers and intraepidermal dysplasia are being increasingly reported in humans who are chronically or excessively exposed to UVR [4–6]. Despite UVR-induced alterations of skin integrity and function being well established for humans and laboratory animals [4], similar studies on wild mammals are virtually non-existent [7]. However, effects are unlikely to be negligible, particularly for species such as cetaceans, which by anatomical (e.g. lack of fur, feathers or keratinized plates) or life-history constraints (e.g. obligate air-breathing physiology, lactation or socialization at the sea surface) are unable to avoid continuous exposure to UVR [8,9]. Interestingly, in recent years, reports of cetacean skin lesions have multiplied [10,11]. The aetiology of some of the skin conditions that show distinct patterns have already been characterized (e.g. lobomycosis, caused by the fungus *Lacazia loboi* [12], and poxvirus tattoo skin disease [13]), but many other types of lesion (e.g. blistering lesions) have not [14]. It is possible that these lesions are linked to mounting levels of UVR, since for each percentage of stratospheric ozone lost, erythema-inducing (skin-damaging) radiation increases by 1.2 per cent [1].

Studies in humans and laboratory animals have shown that lighter-skinned individuals are more sensitive to UVR than those with darker skin [15,16], whose risk of developing skin cancer is 10- to 100-fold lower [17]. When controlling for differences in skin pigmentation, longer periods of exposure to the sun influence severity of skin damage [4]. If this knowledge were extrapolated to cetaceans, one would expect cetaceans with paler skin pigmentation and those spending longer periods at the sea surface to be more severely exposed and develop more blistering skin lesions. In addition, as a result of mounting levels of UVR, an increment in skin lesions over time would also be expected.

We tested these predictions by examining skin lesions in three seasonally sympatric cetacean species (blue, fin and sperm whales) from the Gulf of California, a region

* Author for correspondence (karina.acevedo-whitehouse@ioz.ac.uk).

Electronic supplementary material is available at http://dx.doi.org/10.1098/rspb.2010.1903 or via http://rspb.royalsocietypublishing.org.

Received 3 September 2010
Accepted 18 October 2010

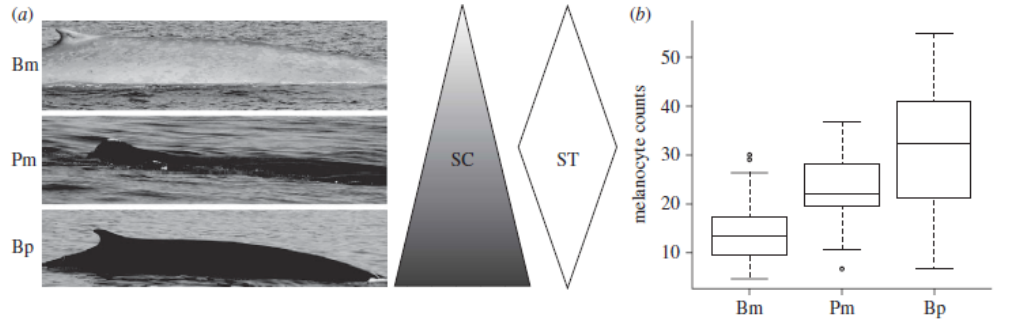

Figure 1. (*a*) Differences in skin colour (SC) and time spent at the surface (ST) among blue (Bm), sperm (Pm) and fin whales (Bp). (*b*) Melanocyte counts in blue (Bm, $n = 63$), sperm (Pm, $n = 17$) and fin whales (Bp, $n = 46$).

situated near tropical latitudes, where skin cancer radiation dosages are five times higher than in mid-latitude zones [18]. Marked differences in skin pigmentation among these species, as well as distinct surface behaviours (figure 1*a*), made it possible to investigate the potential photoprotective role of cetacean skin pigmentation and the importance of sun exposure length for lesion development. We performed gross analysis of skin sections using high-quality photographs, and microscopic analysis that involved routine and specialized staining to detect apoptotic cells [17,19]. We find widespread evidence of epidermal damage commonly associated with acute and severe sunburn in the three species, and demonstrate that whales with more melanocytes have fewer lesions and more apoptotic cells. Interestingly, apoptosis and melanocyte proliferation increase in time, suggesting quick photoprotective responses.

2. MATERIAL AND METHODS

(a) *Sample collection*

Cetacean surveys were conducted in the Gulf of California (Mexico) between January and June (2007–2009). High-quality photographs were obtained using a digital camera (Canon EOS20) and skin biopsies were collected with a 7 mm stainless steel dart from blue whales, *Balaenoptera musculus* ($n = 98$ and 71, respectively), fin whales, *Balaenoptera physalus* ($n = 34$ and 50), and sperm whales, *Physeter macrocephalus* ($n = 24$ and 21; details in electronic supplementary material, table S1). Epidermal samples were preserved in 10 per cent buffered formalin. Each whale was photo-identified and catalogued based on skin patterns and scars on the back and dorsal fin [20] and the ventral side of the flukes [21]. In each season recaptured individuals were excluded from the analyses, the first capture being the one included. Minimum age was calculated from the first year each whale was observed in the Gulf of California. We excluded new individuals (minimum age = 1) from the age-related analyses ($n = 58$).

(b) *Analysis of gross lesions*

Occurrence, prevalence (%) and intensity (number of lesions/individual) of gross lesions were determined in a previously defined area using high-quality photographs (see the electronic supplementary material). Photos were included only when the whale's flank was perpendicular to the camera and focus was sharp. To ensure consistency, all photographs were analysed by a single person at the end of the final sampling season.

(c) *Histology*

Skin sections were stained with haematoxylin and eosin (H&E). Accumulation of glycogen was confirmed with periodic acid schiff (PAS) and diastase-resistant (DPAS) stains [22]. Four categories were defined for cytoplasmic vacuolation, from zero (absence) to three (severe; see electronic supplementary material, figure S1*a–c*). Apoptosis was examined in a subset of 43 individuals using the terminal deoxynucleotidyl transferase-mediated deoxyuridine triphosphate-biotine nick end labelling method (TUNEL) that detects DNA double-strand breaks typical of final stages of apoptosis [17,19,23]. A semi-quantitative measure of apoptotic cells was used as indicated above (level 0 to 2 = none to few localized apoptotic cells, level 3 = many and widely distributed apoptotic cells; see electronic supplementary material, figure S1*d–f*). Melanocytes (M = number of melanocytes per 100 arbitrary units), which were used as a surrogate measure of skin pigmentation, were counted within a standardized area (details in the electronic supplementary material). To avoid bias, all slides were examined at the end of the final sampling season.

(d) *Statistical methods*

Interspecies differences in lesion prevalence were examined with Fisher's exact tests. ANOVA and non-parametric Kruskall–Wallis tests were used to compare melanocyte counts between years and lesion intensity among species, respectively. Generalized linear models (GLMs) were constructed to investigate interspecies differences in melanocyte counts and epidermal lesions, and temporal trends in lesion prevalence. When explanatory variables were bimodal responses, error structure was defined accordingly. Analyses were conducted in R [24].

3. RESULTS AND DISCUSSION

Melanocyte counts varied significantly between species, being lowest for blue whales (14.1 M $\pm$ 0.77) and highest for fin whales (30.8 M $\pm$ 1.71; Kruskall–Wallis, $\chi^2 = 54.1$, d.f. = 2, $p = 1.8 \times 10^{-12}$; figure 1*b*). Gross lesions observed were predator bite marks (19% overall prevalence) and blister-type lesions (hereafter blisters; 28% overall prevalence). Histological analysis revealed a range of abnormalities, including intracellular oedema,

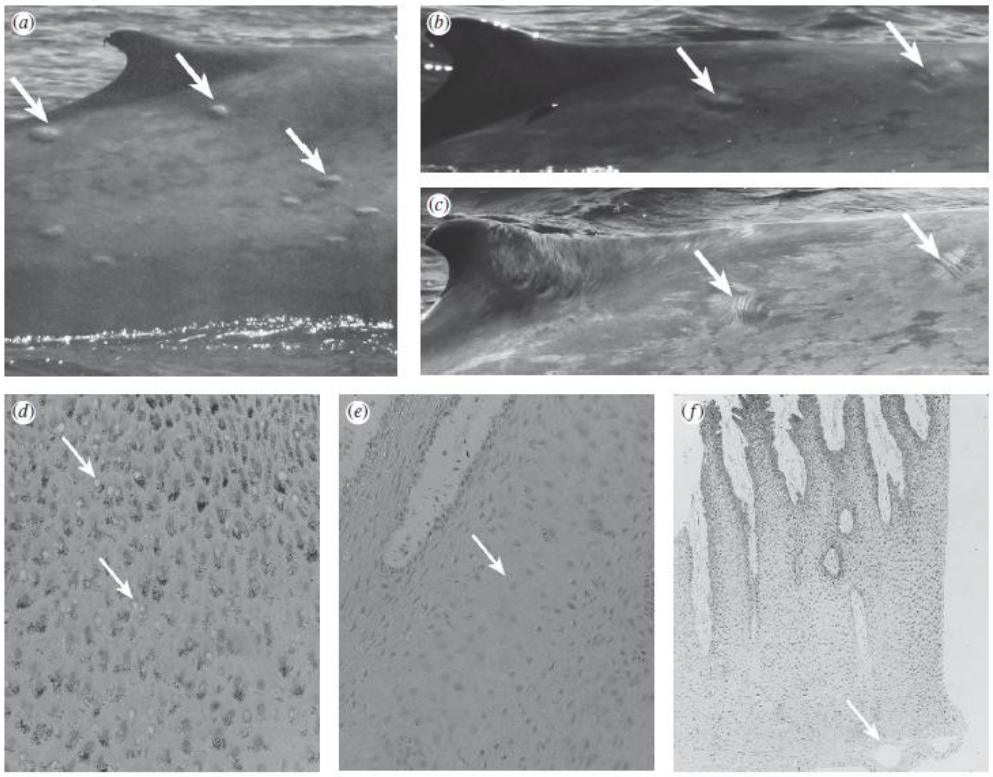

Figure 2. Typical images of skin lesions. (*a*) Gross blistering on the dorsal surface of a blue whale, (*b*) bite marks on the dorsal surface of a blue whale seen as oval-shaped lesions with a sunken perimeter, (*c*) bite marks seen as parallel rakings, (*d*) cytoplasmic vacuolation (400×), (*e*) intracellular oedema (250×) and (*f*) microvesicles (50×). Lesions are indicated by arrows.

cytoplasmic vacuolation, glycogen deposition, microvesicles and leucocyte infiltration (figure 2), all considered characteristic of sunburn and generally observed 24 h after UVR exposure [19,22]. Basal dendritic melanocytes and basal and suprabasal perinuclear melanin pigments (supranuclear caps) were common findings. These phenomena arise as protective responses following UVR exposure in humans [25,26].

As predicted under the assumption that pigmentation plays a significant photoprotective role [16], the prevalence of blisters and microscopic abnormalities differed between species, being lowest for fin whales, the darkest species (figure 3). Moreover, for each species, melanocyte counts inversely predicted cytoplasmic vacuolation and intracellular oedema ($p < 0.02$ for all responses; full model details in electronic supplementary material, table S2), providing further evidence of photoprotection in cetaceans. Interestingly, despite having different average melanocyte counts, the prevalence of blisters and microscopic abnormalities was equal for blue and sperm whales (figure 3). This finding might reflect dissimilar sea-surfacing behaviours. Sperm whales spend approximately 7–10 min breathing at the surface between foraging dives, whereas both blue and fin whales tend to surface for less than 2 min at a time [27]. Moreover, although all species remain at the surface while resting, sperm whales also aggregate virtually all the daylight hours at the surface during socialization, in periods of up to 6 h at a time [21]. A fitted GLM showed that the length of sun exposure (i.e. surface time) predicted epidermal lesions, although skin pigmentation remained the most important explanatory factor for all lesions examined (full model details in electronic supplementary material, table S3*a*).

Another non-exclusive explanation for the higher prevalence of lesions observed in blue whales when compared with fin whales could relate to differences in migration patterns. This is because UVR (and consequently skin cancer radiation dosage) varies across latitudes, being five times higher at lower latitudes when compared with mid-latitudes [18]. Across Mexico, UVR is high during most of the year, and the UV index at clear sky values (a measure of the potential human exposure to UVR) is normally 6 (high) to 15 (extreme) [28]. Thus, blue whales from the northeast pacific population that migrate annually from the feeding areas between Alaska and California [29] to the Gulf of California, where some remain for at least two months (normally arriving in January/February and leaving in April/May) [30], are abruptly exposed to higher UVR. Conversely, fin whales are year-round residents of the Gulf of California [31] and thus constantly exposed to high UVR. If, as occurs in humans, sun-induced damage is most critical when first exposed to higher levels of UVR, it is possible that the observed variations in lesions,

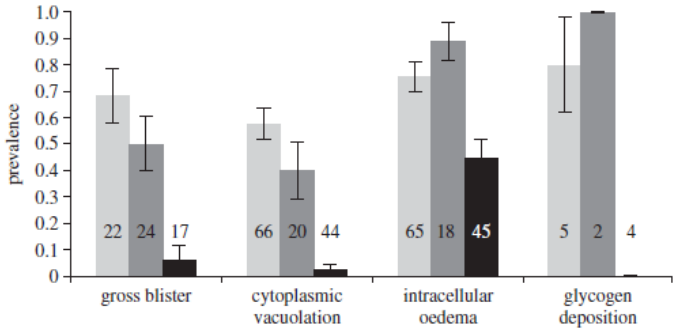

Figure 3. Prevalence of gross blisters and microscopic epidermal abnormalities in blue whales (pale grey bars), sperm whales (dark grey bars) and fin whales (black bars). Sample sizes are indicated in the figure. Bars = ±s.e.m.

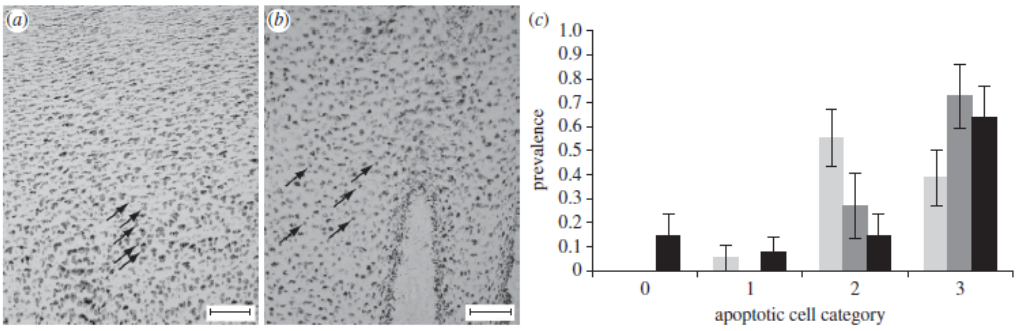

Figure 4. Presence of apoptotic cells (AC) in skin sections. (*a*) TUNEL-stained fin whale skin showing AC (round-stained nucleus indicated by arrows) throughout the epidermis (category 3 AC; bar = 100 µm). (*b*) TUNEL-stained sperm whale skin with category 2 AC (bar = 100 µm). Melanin pigments are seen as black granular material. (*c*) Prevalence and categories of AC in blue whales (pale grey bars, $n = 18$), sperm whales (dark grey bars, $n = 11$) and fin whales (black bars, $n = 14$). Bars = ±s.e.m.

melanocytes and apoptotic cells between species reflect differences in migration. Interestingly, blue whales sampled at the beginning of each sampling season had a higher prevalence of microscopic lesions than those sampled at the end of each sampling season (LR = 37.99, d.f. = 1, $p = 0.04$; see electronic supplementary material, table S4 and figure S2), suggesting that some acclimatization might occur, as happens in humans [32].

Exposure to UVR produces numerous effects on keratinocytes, including the formation of 'sunburn cells': keratinocytes showing eosinophilic cytoplasm with or without remnants of shrunken and condensed nuclei [17,19]. These are apoptotic cells resulting from UV-induced DNA damage [17]. Highly pigmented skin is better able to prevent damage and remove potentially precancerous UVR-damaged cells via melanin-mediated apoptosis [15]. Thus, whales with more pigmentation would be expected to have higher epidermal apoptosis rates than less-pigmented whales. We found that sunburn cells were present in nearly all (95%) of the skin sections and in more than half (56%) of all whales; these cells were distributed throughout the epidermis (figure 4), including the basal layer. Such high levels and widespread distribution of apoptotic cells are uncommon in clinically healthy mouse skin, and are associated with acute responses to UVR exposure, which peak between 24 and 48 h [33]. When investigating the association between individual melanocyte counts and apoptosis, a positive relationship was found for all species (full GLM and model details in electronic supplementary material, table S3*b*), implying that darker pigmentation confers an advantage for the elimination of UVR-induced damage in whales. Geographical variation in pigmentation has been described for southern right whales, *Eubalena australis* [34], and humpback whales, *Megaptera novaeangliae* [35], and there is evidence that dorsal skin gradually darkens with age in right whales [34]. To our knowledge, the evolutionary significance of whale skin pigmentation patterns has not been discussed in terms of photoprotection, but it is tempting to speculate, based on our findings, that selection might operate at this level.

As a consequence of the global reduction in the stratospheric ozone layer, levels of UVR have augmented, leading to higher rates of acute lesions and skin cancer in humans [4]. If whale skin is affected by exposure to growing levels of UVR, a higher prevalence of lesions over time would be expected. When testing this hypothesis for blue whales, the species for which we had data and samples spanning a 3 year period, we found that

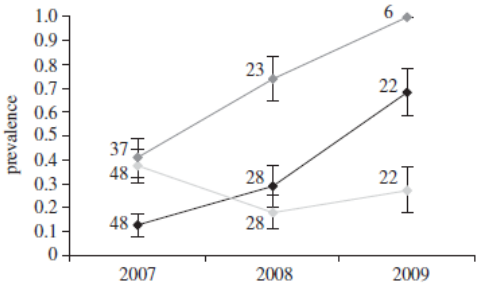

Figure 5. Temporal changes in the prevalence of blue whale skin lesions (blisters, black line; bite marks, pale grey line; cytoplasmic vacuolation, dark grey line). Sample sizes are indicated in the figure. Bars = ±s.e.m.

while bite marks remained unchanged (GLM: LR = 110.33, d.f. = 2, $p = 0.18$), the prevalence of blisters rose significantly over time (GLM: LR = 90.50, d.f. = 2, $p = 5.24 \times 10^{-5}$; figure 5), being markedly higher in 2009. A similar (but statistically insignificant) trend was observed for cytoplasmic vacuolation (GLM: LR = 5.44, d.f. = 2, $p = 0.07$; figure 5). Despite the short time frame, our results would suggest that, as predicted, heightened exposure to UVR secondary to global [1–3] and regional [36,37] ozone depletion is leading to more skin damage in whales. It is worth mentioning that we found no evidence that the population is ageing (GLM: LR = 32.16, d.f. = 2, $p = 0.31$), suggesting that the observed results do not reflect an age-related decrease in repair mechanisms [38]. The obvious question to arise from our results is: if whales are historically adapted to daily UVR exposure, are their photoprotection and damage-repair mechanisms able to respond to increasing average radiation? When addressing this question we found that blue whale epidermal apoptotic cells and melanocytes also expanded in time (GLM: LR = 16.00, d.f. = 2, $p = 0.04$; ANOVA: $F = 4.33$, d.f. = 2, $p = 0.02$), a trend that also occurred in fin whales, the darkest species studied (GLM: LR = 5.00, d.f. = 1, $p = 3.6 \times 10^{-3}$; ANOVA: $F = 11.20$, d.f. = 2, $p = 1.74 \times 10^{-4}$). If, as occurs in humans and laboratory animals, exposure to UVR increases the number of melanocytes [25], stimulates the synthesis of melanin and leads to augmented apoptosis [17], it is possible that our results indicate quick responses to increasing irradiation. Testing this hypothesis in more depth was beyond the scope of our study, but quantifying the expression of genes involved in melanin production and DNA damage repair might help address this question in the future.

Taken together, our results show that whales exhibit lesions typical of acute UVR exposure, suggesting that the thinning ozone layer poses a significant and rising threat to the health of our oceans' whales. Considering that UVR is expected to increase 4 per cent in the tropics and up to 20 per cent in the poles [39], more studies are needed to fully understand the consequences of UVR-induced damage and the evolutionary significance of cetacean pigmentation.

Members of the Cetacean Ecology Laboratory (CICIMAR) greatly assisted us during fieldwork. We are grateful to Hal Whitehead for allowing us to participate in his sperm whale research expedition, and to Prof. Cerio for his assistance with PAS/DPAS staining. Robert Brownell, William Amos and Paul Jepson provided valuable comments that greatly improved our manuscript. L.M. is funded by a NERC Studentship (NE/F00818X/1). This work was partially funded by a Royal Society Grant (2005/R2) awarded to K.A. and by the Instituto Politécnico Nacional. Samples were collected under permits SGPA/DGVS/00506/08, SGPA/DGVS/09760/08 and SGPA/DGVS/08021/06 issued by SEMARNAT.

REFERENCES

1 McKenzie, R. L., Aucamp, P. J., Bais, A. F., Bjorn, L. O. & Ilyas, M. 2007 Changes in biologically-active ultraviolet radiation reaching the Earth's surface. *Photochem. Photobiol. Sci.* **6**, 218–231. (doi:10.1039/B700017K)
2 Li, F., Stolarski, R. S. & Newman, P. A. 2009 Stratospheric ozone in the post-CFC era. *Atmos. Chem. Phys.* **9**, 2207–2213. (doi:10.5194/acp-9-2207-2009)
3 Dameris, M. 2009 Depletion of the ozone layer in the 21st century. *Angew. Chem. Int. Ed.* **49**, 489–491. (doi:10.1002/anie.200906334)
4 De Gruijl, F. R., Longstreth, J., Norval, M., Cullen, A. P., Slaper, H., Kripke, M. L., Takizawa, Y. & Van der Leun, J. C. 2003 Health effects from stratospheric ozone depletion and interactions with climate change. *Photochem. Photobiol. Sci.* **2**, 16–28. (doi:10.1039/b211156j)
5 Gallagher, R. P. & Lee, T. K. 2006 Adverse effects of ultraviolet radiation: a brief review. *Prog. Biophys. Mol. Biol.* **92**, 119–131. (doi:10.1016/j.pbiomolbio.2006.02.011)
6 Chang, Y. M. *et al.* 2009 Sun exposure and melanoma risk at different latitudes: a pooled analysis of 5700 cases and 7216 controls. *Int. J. Epidemiol.* **38**, 814–830. (doi:10.1093/ije/dyp166)
7 Karentz, D. & Bosch, I. 2001 Influence of ozone-related increases in ultraviolet radiation on antarctic marine organisms. *Am. Zool.* **41**, 3–16. (doi:10.1093/icb/41.1.3)
8 Geraci, J. R., St Aubin, D. J. & Hicks, B. D. 1986 Anatomy and physiology. The epidermis of odontocetes: a view from within. In *Research on dolphins* (eds M. M. Bryden & R. Harrison), pp. 3–21. Oxford, UK: Clarendon Press.
9 Acevedo-Whitehouse, K. & Duffus, A. L. J. 2009 Effects of environmental change on wildlife health. *Phil. Trans. R. Soc. B* **364**, 3429–3438. (doi:10.1098/rstb.2009.0128)
10 Wilson, B. *et al.* 1999 Epidermal diseases in bottlenose dolphins: impacts of natural and anthropogenic factors. *Proc. R. Soc. Lond. B* **266**, 1077–1083. (doi:10.1098/rspb.1999.0746)
11 Van Bressem, M. F. *et al.* 2009 Emerging infectious diseases in cetaceans worldwide and the possible role of environmental stressors. *Dis. Aquat. Organ.* **86**, 143–157. (doi:10.3354/dao02101)
12 Taborda, P. R., Taborda, V. A. & McGinnis, M. R. 1999 *Lacazia loboi* gen. nov., comb. nov., the etiologic agent of lobomycosis. *J. Clin. Microbiol.* **37**, 2031–2033.
13 Van Bressem, M. F. *et al.* 2009 Epidemiological pattern of tattoo skin disease: a potential general health indicator for cetaceans. *Dis. Aquat. Organ.* **85**, 225–237. (doi:10.3354/dao02080)
14 Flach, L. *et al.* 2008 Miscellaneous skin lesions of unknown aetiology in cetaceans from South America. Paper SC/60/DW4 presented to the International Whaling Commission Scientific Meeting, Santiago, Chile.
15 Yamaguchi, Y., Beer, J. & Hearing, V. 2008 Melanin mediated apoptosis of epidermal cells damaged by ultraviolet radiation: factors influencing the incidence of skin cancer. *Arch. Dermatol. Res.* **300**, 43–50. (doi:10.1007/s00403-007-0807-0)

16 Lin, J. Y. & Fisher, D. E. 2007 Melanocyte biology and skin pigmentation. *Nature* **445**, 843–850. (doi:10.1038/nature05660)
17 Takeuchi, S., Zhang, W., Wakamatsu, K., Ito, S., Hearing, V. J., Kraemer, K. H. & Brash, D. E. 2004 Melanin acts as a potent UVB photosensitizer to cause an atypical mode of cell death in murine skin. *Proc. Natl Acad. Sci. USA* **101**, 15 076–15 081. (doi:10.1073/pnas.0403994101)
18 Ilyas, M. 2007 Climate augmentation of erythemal UV-B radiation dose damage in the tropics and global change. *Curr. Sci.* **93**, 1604–1608.
19 Nakaseko, H., Kobayashi, M., Akita, Y., Tamada, Y. & Matsumoto, Y. 2003 Histological changes and involvement of apoptosis after photodynamic therapy for actinic keratoses. *Bri. J. Dermatol.* **148**, 122–127. (doi:10.1046/j.1365-2133.2003.04898.x)
20 Hammond, P. S. 1990 Capturing whales on film: estimating cetacean population parameters from individual recognition data. *Mammal Rev.* **20**, 17–22. (doi:10.1111/j.1365-2907.1990.tb00099.x)
21 Whitehead, H. 2003 Sperm whale behavior and vocalizations. In *Sperm whales: social evolution in the ocean*, pp. 133–205. Chicago, IL: The University of Chicago Press.
22 Ohkawara, A., Halprin, K. & Levine, V. 1972 Glycogen metabolism following ultraviolet irradiation. *J. Invest. Dermatol.* **59**, 264–268. (doi:10.1111/1523-1747.ep12627285)
23 Kawagishi, N., Hashimoto, Y., Takahashi, H., Ishida-Yamamoto, A. & Iizuka, H. 1998 Epidermal cell kinetics of pig skin in vivo following UVB irradiation: apoptosis induced by UVB is enhanced in hyperproliferative skin condition. *J. Dermatol. Sci.* **18**, 43–53. (doi:10.1016/S0923-1811(98)00024-3)
24 Ihaka, R. & Gentleman, R. 1996 R: a language for data analysis and graphics. *J. Comput. Graph Stat.* **5**, 299–314. (doi:10.1234/12345678)
25 Stierner, U., Rosdahl, I., Augustsson, A. & Kagedal, B. 1989 UVB irradiation induces melanocyte increase in both exposed and shielded human skin. *J. Invest. Dermatol.* **92**, 561–564. (doi:10.1111/1523-1747.ep12709572)
26 Kobayashi, N., Nakagawa, A., Muramatsu, T., Yamashina, Y., Shirai, T., Hashimoto, M. W., Ishigaki, Y., Ohnishi, T. & Mori, T. 1998 Supranuclear melanin caps reduce ultraviolet induced DNA photoproducts in human epidermis. *J. Invest. Dermatol.* **110**, 806–810. (doi:10.1046/j.1523-1747.1998.00178.x)
27 Croll, D. A., Acevedo-Gutiérrez, A., Tershy, B. R. & Urbán-Ramírez, J. 2001 The diving behavior of blue and fin whales: is dive duration shorter than expected based on oxygen stores? *Comp. Biochem. Physiol.* **129**, 797–809. (doi:10.1016/S1095-6433(01)00348-8)
28 Lemus-Deschamps, L., Galindo, I., Solano, R., Elizalde, A. T. & Fonseca, J. 2002 Diagnosis of clear sky ultraviolet radiation for Mexico. *Atmosfera* **15**, 165–171.
29 Calambokidis, J., Barlow, J., Ford, J. K. B., Chandler, T. E. & Douglas, A. B. 2009 Insights into the population structure of blue whales in the eastern North Pacific from recent sightings and photographic identification. *Mar. Mammal Sci.* **25**, 816–832. (doi:10.1111/j.1748-7692.2009.00298)
30 Gendron, D. 2002 Ecología poblacional de la ballena azul, *Balaenoptera musculus*, de la Península de Baja California. PhD thesis, Centro de Investigación Científica y Educación Superior de Ensenada, Mexico.
31 Bérubé, M., Urbán-Ramírez, J., Dizon, A. E., Brownell, R. L. & Palsbøll, P. J. 2002 Genetic identification of a small and highly isolated population of fin whales (*Balaenoptera physalus*) in the Sea of Cortez, Mexico. *Conserv. Genet.* **3**, 183–190. (doi:10.1234/12345678)
32 Sayre, R. M., Desrochers, D. L., Wilson, C. J. & Marlowe, E. 1981 Skin type, minimal erythema dose (MED), and sunlight acclimatization. *J. Am. Acad. Dermatol.* **5**, 439–443. (doi:10.1016/S0190-9622(81)70106-3)
33 De la Coba, F., Aguilera, J., De Galvez, M. V., Alvarez, M., Gallego, E., Figueroa, F. L. & Herrera, E. 2009 Prevention of the ultraviolet effects on clinical and histopathological changes, as well as the heat shock protein-70 expression in mouse skin by topical application of algal UV-absorbing compounds. *J. Dermatol. Sci.* **55**, 161–169. (doi:10.1016/j.jdermsci.2009.06.004)
34 Schaeff, C. M., Best, P. B., Rowntree, V. J., Payne, R., Jarvis, C. & Portway, V. A. 1999 Dorsal skin color patterns among southern right whales (*Eubalaena australis*): genetic basis and evolutionary significance. *J. Hered.* **90**, 464–471. (doi:10.1093/jhered/90.4.464)
35 Rosenbaum, H. C. *et al.* 1995 Geographic variation in ventral fluke pigmentation of humpback whale (*Megaptera novaeangliae*) populations worldwide. *Mar. Ecol. Prog. Ser.* **124**, 1–7. (doi:10.3354/meps124001)
36 Kane, R. P. 2009 Ozone depletion, worst not yet over. *Indian J. Radio Space Phys.* **38**, 313–316.
37 Feng, W., Chipperfield, M. P., Davies, S., von der Gathen, P., Kyrö, E., Volk, C. M., Ulanovsky, A. & Belyaev, G. 2007 Large chemical ozone loss in 2004/2005 Arctic winter/spring. *Geophys. Res. Lett.* **34**, L09803. (doi:10.1029/2006GL029098)
38 Matts, P. J. & Fink, B. 2010 Chronic sun damage and the perception of age, health and attractiveness. *Photochem. Photobiol. Sci.* **9**, 421–431. (doi:10.1039/b9pp00166b)
39 Hegglin, M. I. & Shepherd, T. G. 2009 Large climate-induced changes in ultraviolet index and stratosphere-to-troposphere ozone flux. *Nat. Geosci.* **2**, 687–691. (doi:10.1038/ngeo604)

Appendix 4.1. Comet Assay protocol

All reagents were prepared with sterile deionised water. The key steps of the protocol were conducted in the dark to avoid further damage to the DNA samples. Comet slides were prepared by covering them with a thin layer of 1% agarose (prepared with distilled water). For that, slides were dipped in agarose solution (liquefied by heating) and, after removing the agarose from the back of the slides with a tissue, were dried at room temperature.

To prepare the control samples of human blood cell solution, 2.5 µl of blood obtained by finger puncture were mixed with 75 µl of low melting point (LMA) agarose (1% LMA agarose prepared in 1X PBS, boiled and then maintained at 37°C) and immediately deposited on a pre-warmed slide (at 37°C). A glass cover slide was added carefully and slides were placed at 4°C for 10 min. After removing the cover slide, a positive control was prepared. For that, each gel was incubated with 100 µl of 3.8mM H_2O_2 at 4°C for 10 min. The slide was then washed with distilled water.

To prepare the whale keratinocyte solution, individual skin samples (27mm³) were first cleaned with PBS-1X and cut in small fragments. Then those were incubated in trypsin solution (0.25 % trypsin, 1mM EDTA-4Na) at 4ºC during 12 h. The samples were immersed in 500 µl of fresh trypsin solution and placed in a rotor at 37ºC for 45 min. The reaction was stopped by adding 500 µl of cell culture medium (Recovery™Cell Culture Freezing Medium). The solution was centrifuged at 250 G for 1 min and the supernatant was collected. The cell solution was mixed with 0.4 % trypan blue (V/V) and the viability of the cells was determined in a hemocytometer. Finally, 7.5 µl of the keratinocyte solution obtained mixed with 75 µl of LMA agarose and were prepared as indicated in the paragraph above. After removing the cover slide, a third layer of LMA agarose (100 µl) was added and the gel was covered with a large (24 X 32) cover slide before incubating at 4°C for 10min.

All slides were placed in a Coplin jar containing pre-chilled lysis solution # 1 (2.5 M NaCl, 10 mM Tris Base, 100 mM EDTA pH 10, 1 % sodium lauryl sarcosinate, adjusted to pH 10 with NaOH). Prior to lysis 1 % Triton X-100 and 10 % DMSO

were added) and incubated at 4 °C all night. The keratinocytes were washed with 1X PBS and lysed a second time by covering with 100 µl of lysis solution # 2 (100 mM NaCl, 10 mM Tris-Cl, 25 mM EDTA pH 8, 0.5 % SDS, 0.1 mg/ml proteinase K) and incubating at 37°C for 2 h. The slides were placed at 4 °C for 10 min and incubated in lysis solution # 1 at 4 ºC during 30 min.

Alkaline unwinding was performed in an alkaline electrophoresis solution (0.3 NaOH, 1mM EDTA) at 4 ºC, during 40 min in the dark. Electrophoresis was run during 40 min at 0.8 V/cm and 300 mA. To neutralize the reaction, slides were washed three times with distilled water, three times with deionised water and placed for 5 min in a 70 % ethanol solution before drying at room temperature.

Dry slides were placed vertically in a Coplin jar containing fixation solution (15 % trichloroacetic acid, 5 % zinc sulphate, 5 % glicerol) and were left for 10 min at room temperature in the dark. Slides were then washed twice in deionised water and dried at air temperature before re-hydrating with deionised water at 4 °C for 5 min and placing them in a freshly-prepared silver staining solution (0.04 % ammonium nitrate, 0.04 % silver nitrate, 0.09 % tungstosilicic acid, 0.05 % formaldehyde and 1.78 % Na_2CO_3). The level of staining was controlled by microscopic examination of the slides. Slides were washed three times with deionised water and the reaction was stopped by incubating the slides in a 1 % acetic acid solution for 5 min. Finally the slides were washed three times with deionised water and dried at air temperature before examination under the microscope.

Appendix 5.1. Gene expression protocol

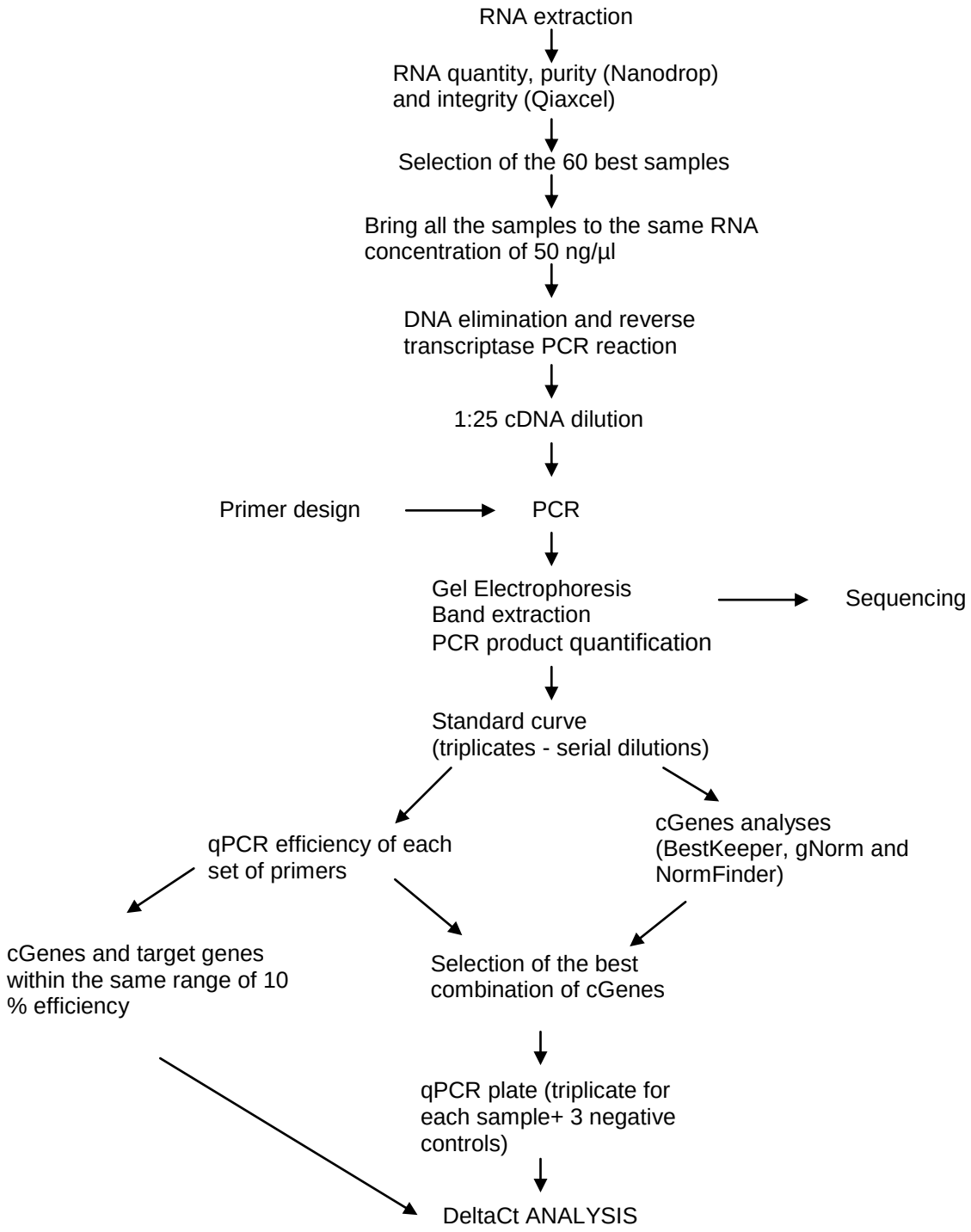

Appendix 5.2. Summary of the data used for gene expression analyses

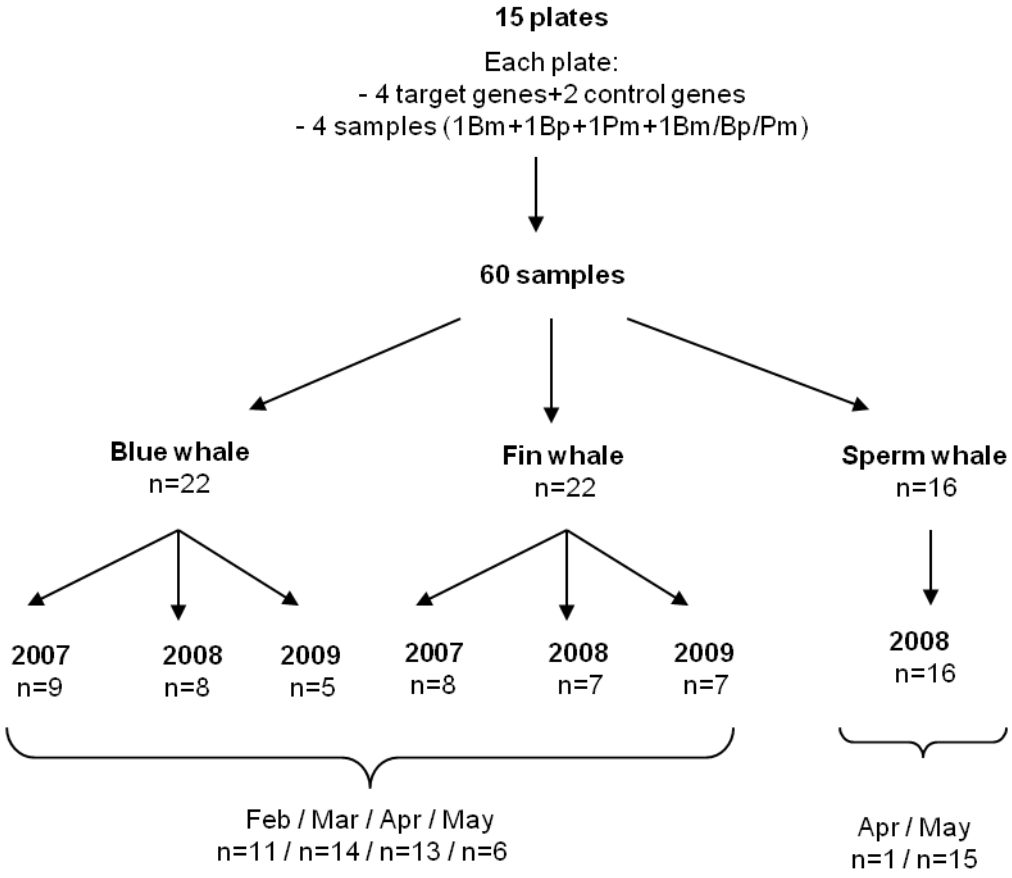

The four target genes are the genes coding for HSP70, P53, KIN and TYR. The two control genes are the genes coding for RPS18 and RPL4. Each experiment includes four samples, one of each species (one blue whale = 1Bm, one fin whale = 1Bp, one sperm whale = 1Pm and a repeated species (corresponding to one of the three species = 1Bm/Bp/Pm). Note that sperm whales have only been sampled in April/May 2008. Samples sizes (n) are indicated in the figure.

Appendix 5.3. RNA integrity using the QIAxcel system

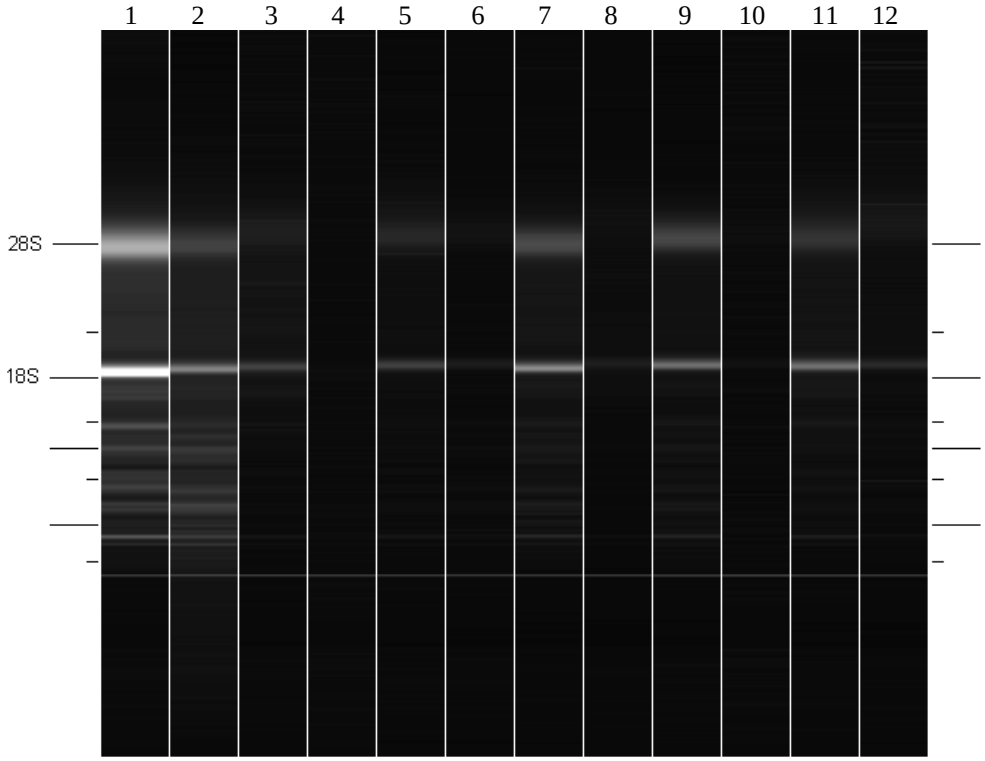

Intact RNA subunits 28S and 18S were observed (wells 1, 2, 3, 5, 7, 9, 11 and 12) in an automated capillarity-electrophoresis system, the QIAxcel system (Qiagen,UK).

Appendix 5.4. qPCR dissociation curves

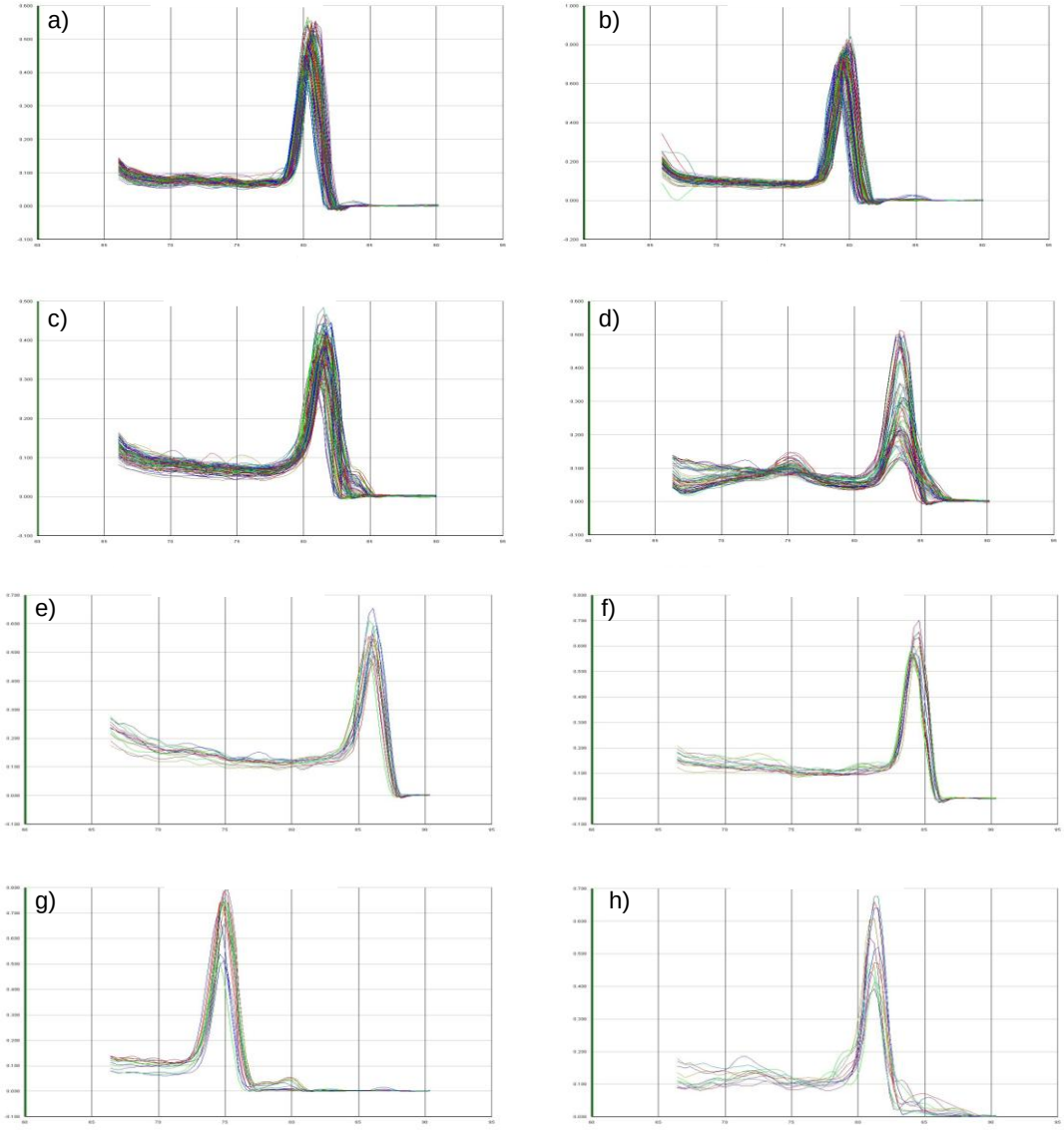

Dissociation curves of the genes a) *S18*, b) *RPL4*, c) *PGK1* d) *SDHA* e) *HSP70*, f) *P53*, g) *KIN*, and h) *TYR* showing unique amplification.

Appendix 5.5. Gene sequences

The following sequences correspond to the gene segments used for gene expression analyses. Forward and reverse primers are underlined.

RPS18
CAATTAAGGGTGTGGGGCGAAGATATGCTCATGTGGTGTTGAGGAAAGCAGACA
TCGACCTCACCAAGAGGGCAGGAGAGCTCACTGAGGATGAGGTGGAACGTGTG
ATCACCATTATGCAGAATCCACGCCAATACAAGA

RPL4
CAGACCTTAGCAGAATCTTGAAAAGCCCAGAGATCCAAAGAGCCCTCCGAGCAC
CACGCAAGAAGATTCATCGCAGAGTCCTGAAGAAGAATCCACTGAAAAACCTG
AGAATCATGTTGAAGCTAAACCCATATGCAAAGACCATGCGCCGGAACACCATT
CTTCGCCAGG

SDHA
TGTTTCCCACCAGGTCACACACTGTCGCAGCCCAGGGAGGGATCAACGCCGCCC
TGGGGAACATGGAGGAGGACAACTGGAGGTGGCACTTCTACGACACCGTGAAG
GGCTCCGACTGG

PGK1
ACAATGGAGCCAAGTCAGTTGTTCTTATGAGCCACCTGGGCCGGCCTGATGGTG
TCCCCATGCCTGACAAGTACTCCTTGCAGCCAGTTGCTGTAGAACTCAAATCTCT
GCTGGGCAAGGATGTTTTGTTCTTGAAGGACTGCGTG

P53F2R3
CTCACCATCATCACACTGGAAGACTCCAGTGGTAATCTGCTGGGACGGAACAGC
TTTGAGGTGCGTGTTTGTGCCTGTCCTGGGAGAGACCGCCGCACAGAGGAAGAA
AATTTCCGCAAGAAGGGGCAGTCTGGCCCTGAGCCGCCTCCTGGGAGCGCTAAG
CGAGCACTGCCTA

HSP70
GTCAAGCACGGTGTTCTGTGGGTTCAGCGCCACCTGGTTCTTGGCCGCGTCGCCG
ATGAGCCGCTCGGTGTCCGTGAAGGCCACGTAGCTGGGGGTGGTGCGGTTGCCC
TGATCGTTGGCGATGATCTCTACTTTGCCGTG

KINF3R5
TGCTGGCTTCAGAAAATCCTCAGCAGTTTATGGATTATTTTCAGAGGAAT
CCGAAATGACTTTCTAGAACTTCTCAGGAGACGCTTTGGAACCAAGAG

TYRF10R8
GCATCCTTCTTCTCCTCTTGGCAGGTCATCTGCAGCCAATTGGAGGAGTA
CAACAGCCGTCACGCTTTATGCAATGGGACGTCCGAGGGACCGATACTG
CGCAATCCTGGAAACCACGACAAAGC

Appendix 5.6. Primer details

Gene encoding	Primer	Sequence 5'- 3'	Size	GC	Tm	Amp	Eff	R^2
Ribosomal protein S18	S18-f	CAATTAAGGGTGTGGGGCGAAG	22	54.5	62.1	141	99.0	1.000
	S18-r	TCTTGTATTGGCGTGGATTCTGC	22	47.8	60.6			
Succinate dehydrogenase	SDHA-f	TGTTTCCCACCAGGTCACACAC	22	54.5	62.1	119	93.4	0.991
	SDHA-r	CCAGTCGGAGCCCTTCACG	19	68.4	63.1			
Phosphoglycerate kinase 1	PGK1-f	ACAATGGAGCCAAGTCAG	18	50.0	53.7	146	91.9	0.998
	PGK1-r	CACGCAGTCCTTCAAGAAC	19	52.6	56.7			
Ribosomal protein L4	RPL4-f	CAGACCTTAGCAGAATCTTGAAAAGC	26	42.3	61.6	171	92.0	0.998
	RPL4-r	CCTGGCGAAGAATGGTGTTCC	21	57.1	61.8			
Heat shock protein 70	HSP70-f	GTCAAGCACGGTGTTCTGTG	20	55.0	59.4	141	101.2	0.999
	HSP70-r	CACGGCAAAGTAGAGATCATCG	22	50.0	60.3			
Tumour protein 53	P53-f2	CTCACCATCATCACACTGGA	20	50.0	57.3	175	94.2	0.998
	P53-r3	TAGGCAGTGCTCGCTTAGC	19	57.9	58.8			
KIN17	KIN-f3	TGCTGGCTTCAGAAAATCC	19	47.4	54.5	98	92.3	0.997
	KIN-r5	CTCTTGGTTCCAAAGCGTCTC	21	52.4	59.8			
Tyrosinase	TYR-f10	GCATCCTTCTTCTCCTCTTGG	21	52.4	59.8	125	93.5	0.991
	TYR-r8	GCTTTGTCGTGGTTTCCAGG	20	55.0	59.4			

f = forward; r = reverse; Size of the primer in nucleotides; GC = percentage of GC in the primers; Tm corresponds to the theoretical primers melting temperature; Amp = Amplicon length in nucleotides. R^2 corresponds to the linear correlation coefficient of the standard curve obtained by plotting the logarithm of the quantity of gene expression versus the threshold cycle (Ct). The slope of the curve was used to calculate the amplification efficiency (in %) for each pair of primers (Eff = $(10^{1/-slope}-1)*100$). The efficiency of the target and internal control genes were within the range of the accepted 10 % of each other to use the Delta Ct method (Schmittgen and Livak, 2008).